GEORGIA INSTITUTE OF TECHNOLOGY
OFFICE OF CONTRACT ADMINISTRATION
SPONSORED PROJECT INITIATION

Date: 1/7/81

Project Title: Development of an Analytical Technique for the Optimization of Jet Engine Inlet and Duct Acoustic Lines

Project No: E-16-685

Project Director: Ben T. Zinn and W. L. Meyer

Sponsor: NASA, Langley Research Center; Hampton, VA

Agreement Period: From 3/1/81 Until 2/28/82 (Perf. & Report)

Type Agreement: Grant No. NAG1-133 dated 12/10/80

Amount:		
	$30,712	NASA
	1,203	E-16-351 (Cost-sharing)
	$31,915	

Reports Required: Semi-Annual Status, Final Technical

Sponsor Contact Person (s):

Technical Matters

Dr. Harold C. Lester
ANRD
NASA - Langley Research Center
Hampton, VA 23665
PHONE:804/827-2617

Contractual Matters
(thru OCA)

Mrs. A. S. Reed or
Mr. C. L. Crowder, Jr.
NASA - Langley Research Center
Hampton, VA 23665
PHONE:804/827-2536

Defense Priority Rating: N/A

Assigned to: Aerospace Engineering (School/Laboratory)

COPIES TO:

Project Director
Division Chief (EES)
School/Laboratory Director
Dean/Director—EES
Accounting Office
Procurement Office
Security Coordinator (OCA)
Reports Coordinator (OCA)

Library, Technical Reports Section
EES Information Office
EES Reports & Procedures
Project File (OCA)
Project Code (GTRI)
Other: C. E. Smith

GEORGIA INSTITUTE OF TECHNOLOGY — OFFICE OF CONTRACT ADMINISTRATION

SPONSORED PROJECT TERMINATION SHEET

Date 6/15/82

Project Title: Development of an Analytical Technique for the Optimization of Jet Engine Inlet and Duct Acoustic Lines

Project No: E-16-685

Project Director: Ben T. Zinn and W. L. Meyer

Sponsor: NASA, Langley Research Center; Hampton, VA

Effective Termination Date: 4/30/82

Clearance of Accounting Charges: 4/30/82

Grant/Contract Closeout Actions Remaining:

- [ ] Final Invoice and Closing Documents
- [x] Final Fiscal Report (SF 272)
- [x] Final Report of Inventions
- [ ] Govt. Property Inventory & Related Certificate
- [ ] Classified Material Certificate
- [ ] Other ____________________

Assigned to: Aerospace Engineering (School/Laboratory)

COPIES TO:

Administrative Coordinator
Research Property Management
Accounting
Procurement/EES Supply Services
Research Security Services
~~Reports Coordinator (OCA)~~
Legal Services (OCA)
Library
EES Public Relations (2)
Computer Input
Project File
Other ____________________

FORM OCA 10:781

E16685

NASA LANGLEY SEMI-ANNUAL STATUS REPORT
NAG 1–133 (3/1/81 – 8/31/81)

DEVELOPMENT OF AN ANALYTICAL TECHNIQUE FOR THE OPTIMIZATION OF JET ENGINE AND DUCT ACOUSTIC LINERS

By

Ben T. Zinn

and

William L. Meyer

GEORGIA INSTITUTE OF TECHNOLOGY

A UNIT OF THE UNIVERSITY SYSTEM OF GEORGIA

SCHOOL OF AEROSPACE ENGINEERING

ATLANTA, GEORGIA 30332

1981

NASA LANGLEY SEMI-ANNUAL STATUS REPORT
NAG 1-133 (3/1/81 - 8/31/81)

DEVELOPMENT OF AN ANALYTICAL TECHNIQUE FOR THE OPTIMIZATION OF JET ENGINE AND DUCT ACOUSTIC LINERS

BY

Ben T. Zinn

and

William L. Meyer

SCHOOL OF AEROSPACE ENGINEERING
GEORGIA INSTITUTE OF TECHNOLOGY
ATLANTA, GA 30332

ABSTRACT

This report summarizes the work performed during the first six months of the NASA LANGLEY research program (Grant Number NAG 1-133) entitled "Development of an Analytical Technique for the Optimization of Jet Engine and Duct Acoustic Liners". Contained in this report is a brief summary of the development of the special integral representation of the external solutions of the Helmholtz equation which forms the basis for the analytical method developed under this contract. A detailed description of the new analytical technique for the generation of the optimum acoustic admittance for an arbitrary axisymmetric body is also presented along with some numerical procedures and some preliminary results for a straight duct.

TABLE OF CONTENTS

I	INTRODUCTION	1
II	BACKGROUND	2
III	THE ANALYTICAL METHOD	8
IV	NUMERICAL PROCEDURES	16
V	SOME PRELIMINARY RESULTS	18
VI	AN ALTERNATIVE FORMULATION	21
VII	CHECK CASES	23
VIII	SUMMARY	24
IX	REFERENCES	25

I. INTRODUCTION

The object of this research project is the development of an analytical technique which is capable of generating an optimum admittance distribution for a duct liner for maximum sound suppression. This analytical technique should yield this optimum distribution without iteration or the need for the calculation of many separate solutions. It is based upon a special integral representation of the external solutions of the Helmholtz equation previously developed here at Georgia Tech. The particulars of this method are presented in Section II.

The new analytical method itself is presented in Section III and some of the numerical procedures used in implementing the method are presented in Section IV. Briefly, the method entails the use of simple source solutions on the admittance surface of the body which are summed, using the linear superposition theorem for solutions of linear equations, to generate a general solution over the liner surface of the body. This general solution, is then substituted into the power equation and subsequently optimized with respect to the complex coupling constants, used in the linear superposition for the general solution, for maximum power lost to the liner surface.

The independent simple source solutions required for this method can be gotten by only solving the problem once due to the special form that the integral equation technique assumes when certain classes of simple boundary conditions are applied. This is gone into in more detail in Section IV which deals with numerical procedures.

II. BACKGROUND

In previous research conducted for the Air Force Office of Scientific Research[1,2] a special integral representation of the external solutions of the Helmholtz equation

$$\nabla^2\varphi + k^2\varphi = 0 \tag{1}$$

where k is the wave number and φ is the acoustic potential, was developed.[3] This integral formulation is special because unlike the straight forward formulation of the problem[4] it can generate unique solutions at all wave numbers. In subsequent research, the formulation and computer codes were specialized for axisymmetric bodies[5] but retained the capability of generating solutions for tangential acoustic modes greater than zero. It is this cylindrically symmetric formulation of the acoustic radiation problem that is used in this research. For the sake of completeness and to help define some of the nomenclature used in subsequent sections, the highlights of this development are presented below.

The classical integral representation of the external solutions of the Helmholtz equation is presented below[4] where S represents the surface of the body, the point Q is on the body, the point P lies outside the body, $\frac{\partial}{\partial n_q}$ represents the normal derivative $\nabla_q \cdot \vec{n}_q$ (where $\vec{n}_q$ is the unit outward normal to the body at the point Q), and G(P,Q) is any fundamental solution of the Helmholtz equation which satisfies the Sommerfeld radiation conditions at infinity.

$$\int\!\!\int_S \left\{ \varphi(Q) \frac{\partial G(P,Q)}{\partial n_q} - G(P,Q) \frac{\partial \varphi(Q)}{\partial n_q} \right\} dS_q = 4\pi\varphi(P) \tag{2}$$

The simplist form that G(P,Q) can take for this problem is the free space Green's function which is

$$G(P,Q) = \frac{e^{ikr(P,Q)}}{r(P,Q)} \tag{3}$$

where r(P,Q) represents the distance between the points P and Q (See Fig. 1.).

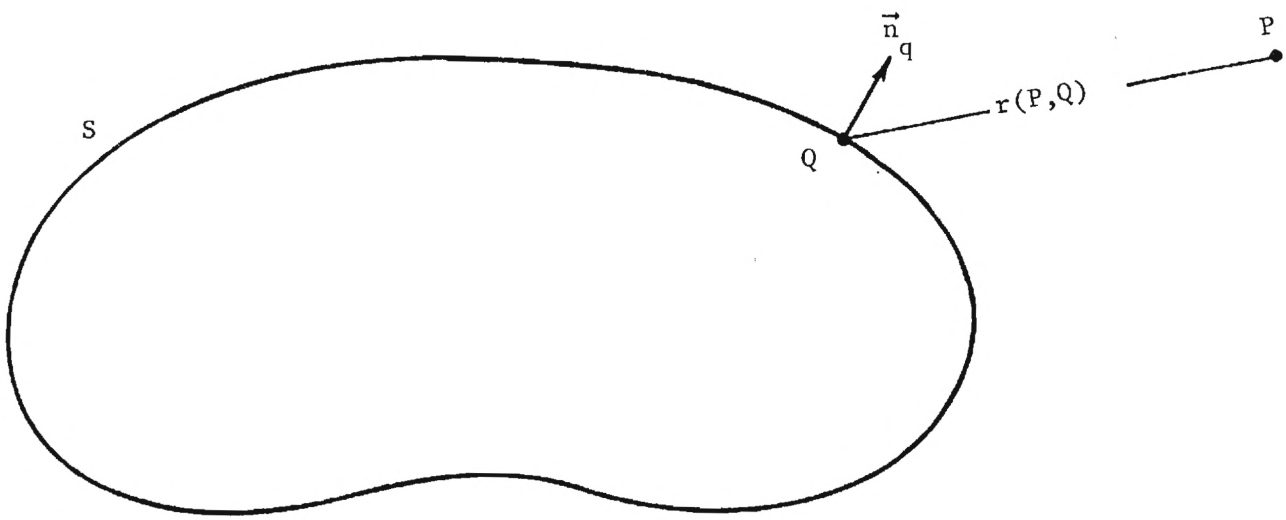

Figure 1. Body showing Q and P points and the distance between them r(P,Q).

From Eqn. (2) it follows that if the acoustic potential φ and the normal acoustic velocity $\frac{\partial\varphi}{\partial n}$ are known on the surface of the body, (i.e., at the Q points) then the acoustic potential may be calculated anywhere in the field outside the body (i.e., at any P point). A similar equation can be developed for the normal acoustic velocity with an arbitrary normal specified in the field and is presented below.

$$\iint_S \left\{ \varphi(Q) \frac{\partial^2 G(P,Q)}{\partial n_p \, \partial n_q} - \frac{\partial G(P,Q)}{\partial n_p} \frac{\partial\varphi(Q)}{\partial n_q} \right\} dS_q = 4\pi \frac{\partial\varphi(P)}{\partial n_p} \tag{4}$$

Thus, if the acoustic quantities are known on the body, they may be calculated anywhere in the field.

To obtain the acoustic quantitites on the surface of the body, equations must be developed that contain only surface quantities. To do this, we let the field point P approach the surface of the body; then, taking the proper limits we obtain

$$\iint_S \left\{ \varphi(Q) \frac{\partial G(P,Q)}{\partial n_q} - G(P,Q) \frac{\partial \varphi(Q)}{\partial n_q} \right\} dS_q = 2\pi\varphi(P) \tag{5}$$

from Eqn. (2). With the proper boundary conditions (i.e., φ, $\partial\varphi/\partial n$ or $Y = \frac{\partial \varphi}{\partial n} / \varphi$) known at each point on the surface of the body Eqn. (5) may be solved for the unknown acoustic quantities. From here on, Y shall be referred to as the effective acoustic admittance; also, it is related to the specific acoustic admittance β by the relationship

$$Y = - ik\beta \tag{6}$$

where β is defined with an inward normal and Y is defined with an outward normal.

The problem with Eqn. (5) is that it does not yield unique solutions for all wave numbers. This can be traced to the internal acoustic eigenvalue problem which when formulated in the same way is governed by an equation similar to Eqn. (5) except that the sign of the R. H. S. is negative. This being the case, it is found that Eqn. (5) does not yield unique solutions at the eigenvalues (i.e., resonant wave numbers) of the internal acoustic problem. Various methods have been proposed in the literature for overcoming this problem[5-8] however, all of these methods have their problems. This is discussed in detail in Ref. 3.

To overcome this uniqueness problem, the method of Burton and Miller[8] was used as a starting point. They were able to solve external radiation problems in two dimensions; however, the extension to three dimensions required some new mathematical identities before it could be made to work as the 3-D formulation contained a strongly singular integral. Briefly, the method consisted of solving a sum of equations (i.e., Eqn. (5) and the surface analog of Eqn. (4)) coupled with a complex coupling constant α .

$$\iint_S \left\{ \varphi(Q) \frac{\partial G(P,Q)}{\partial n_q} - \frac{\partial \varphi(Q)}{\partial n_q} G(P,Q) \right\} dS_q$$

$$+ \alpha \iint_S \left\{ \varphi(Q) \frac{\partial^2 G(P,Q)}{\partial n_p \, \partial n_q} - \frac{\partial \varphi(Q)}{\partial n_q} \frac{\partial G(P,Q)}{\partial n_p} \right\} dS_q$$

$$= 2\pi \left\{ \varphi(P) + \alpha \frac{\partial \varphi(P)}{\partial n_p} \right\} \tag{7}$$

Burton and Miller were able to show that Eqn. (7) always had the unique, correct solution if α were chosen properly; specifically:

$$\begin{aligned} &\text{Im } (\alpha) \neq 0 \text{ when k is real or imaginary} \\ &\text{Im } (\alpha) = 0 \text{ when k is a complex number} \end{aligned} \tag{8}$$

The problem arises in three dimensions that the first term of the second integral is strongly singular and cannot be directly integrated; that is:

$$\iint_S \varphi(Q) \frac{\partial^2 G(P,Q)}{\partial n_p \, \partial n_q} \, dS_q \rightarrow \mathcal{O}\left(\frac{1}{r(P,Q)} \right) \tag{9}$$

which is singular as $Q \rightarrow P$ on the surface of the body.

Stallybrass[9] was able to show that this integral is equivalent to

$$\begin{aligned} &\iint_S \varphi(Q) \; (n_p \cdot n_q) \; \nabla_p \cdot \nabla_q \; G(P,Q) \; dS_q \\ &+ \iint_S \varphi(Q) \; (n_p \times n_q) \cdot (\nabla_p \times \nabla_q \; G(P,Q)) \; dS_q \\ &- \iint_S \varphi(Q) \; n_q \cdot \left\{ \nabla_q \times (n_p \times \nabla_p \; G(P,Q)) \right\} dS_q \end{aligned} \tag{10}$$

and that the last term, which contains the singular component of the integral in Eqn. (9), can be represented as

$$\iint_S (n_q \times \nabla_q \varphi(Q)) \circ (n_p \times \nabla_p G(P,Q))\, dS_q \tag{11}$$

which is regular. Although the singular integral has been regularized, this form is not suitable for numerical calculations as it contains tangential derivatives of the acoustic potential on the surface of the body.

After some manipulation, it can be shown that this integral (See Eqn. (11).) can be rewritten as

$$\iint_S \left\{ \varphi(Q) - \varphi(P) \right\} n_q \cdot \nabla_q \times (n_p \times \nabla_p G(P,Q))\, dS_q \tag{12}$$

which presents no computational difficulties. Thus, the singular integral has been shown to have a regular representation which can be easily integrated numerically. The remaining practical problem was now the specification of a reasonable value for α subject to the constraints in Eqn. (8). Since no analytical method of determining the value of α could be found, its specification is the result of computational considerations. Specifically, it can be shown that the most significant term of the first integral in Eqn. (7) is proportional to the wave number k and that the most significant term of the second integral increases as k^2. So to keep the two integrals in Eqn. (7) in balance numerically as the wave number is increased, the complex coupling constant α is chosen to be

$$\alpha = i/k \tag{13}$$

It is shown in Ref. 10 though the use of many examples, that this is indeed the optimum value of α from a computational point of view.

Having developed the general three dimensional equations, the specialization of these equations for axisymmetric bodies is straight forward[10] and therefore will not be repeated here. Efficient computer codes have been written for the solution of these equations and the results of these computer codes have been compared with both theoretical "exact" solutions in Ref. 10 and with experimental results in Ref. 11. In both cases, very good agreement was observed.

III. THE ANALYTICAL METHOD

The object of this research project is the development of an analytical method and attendant computer programs for the determination of the optimum admittance distribution of a liner for maximum sound suppression for a specific body and acoustic excitation without iteration. This method will contain two advances over previous methods[12] for finding the optimum admittance for liners: 1) this new method will not require iteration in order to generate the optimum solution of the problem and 2) the optimum solution generated will yield a pointwise continuous distribution of admittance values which should demonstrate better sound suppression than optimum constant or segmented liners. To generate the point source solutions necessary for this method to work, the cylindrically symmetric form of the theory developed in the previous section[10] is used as most bodies of interest (e. g. jet engine inlets and straight circular ducts) are axisymmetric. This will be gone into in greater detail in subsequent sections.

Since the objective of this research is to minimize the energy radiated from a body under specific acoustic excitation through the use of an acoustic liner, the problem can be turned around so that the objective is to maximize the acoustic energy absorbed by the liner. Contained in the problem statement are the implicit assumptions that: 1) the placement of the liner is fixed; 2) the specific acoustic excitation is fixed by the assumption of a distribution of acoustic potential (i.e., the same as the specification of the acoustic pressure), and 3) the liner can be represented by an acoustic admittance (i.e.,it is a surface of local reaction).[13] This being the case, the acoustic energy absorbed by the liner can be represented as

$$E = - \int\int_{S_\ell} \bar{\bar{\rho c}}\; k\; Y^I \left|\varphi\right|^2 dS \qquad (14)$$

where the subscript ℓ refers to the liner surface and the superscript I denotes the "imaginary part of." Using the definition $Y = \dfrac{\frac{\partial\varphi}{\partial n}}{\varphi}$ (See Eqn. (6).) this can be written as

$$E \propto \iint_{S_\ell} \left\{ \frac{\partial\varphi}{\partial n}^R \varphi^I - \frac{\partial\varphi}{\partial n}^I \varphi^R \right\} dS \tag{15}$$

where the superscript R denotes the "real part of" and all values are assumed to be R. M. S.

The analytical optimization procedure entails the maximization of E as defined in Eqn. (15) where the acoustic quantities are represented in terms of a general solution consisting of a combination of simple source solutions on the surface of the body. The development of this general solution is presented below wherein the body of interest is assumed to have three distinct regions on its surface (See Fig. 2.).

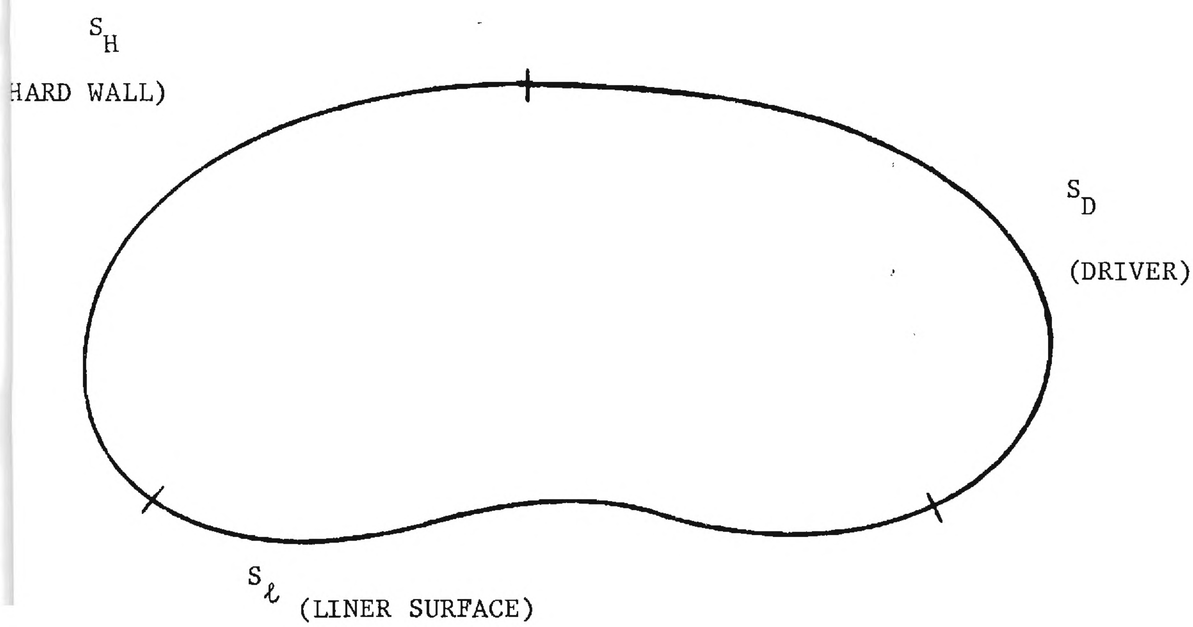

Figure 2. The three distinct types of regions on the body.

These regions do not necessarily have to be contiguous however for the sake of clarity they are presented as such here.

To form the general solution we first must consider the effect of the driver surface (s). To do this we solve for the acoustic quantities on the surface of the body subject to the boundary conditions

$$
\begin{aligned}
\varphi(Q) &= \tilde{\varphi}_D(Q) && \text{on } S_D \\
\frac{\partial\varphi}{\partial n}(Q) &= 0 && \text{on } S_H \text{ and } S_\ell
\end{aligned}
\tag{16}
$$

where $\tilde{\varphi}_D(Q)$ is some specified function of the acoustic potential on the driver. Solving this problem we obtain the driver solution; that is:

$$
\begin{aligned}
&\frac{\partial\varphi_D}{\partial n}(Q) && \text{on } S_D \\
&\varphi_D(Q) && \text{on } S_H \text{ and } S_\ell
\end{aligned}
\tag{17}
$$

Next, the liner surface (s) is divided up into N finite regions as in Fig. 3.

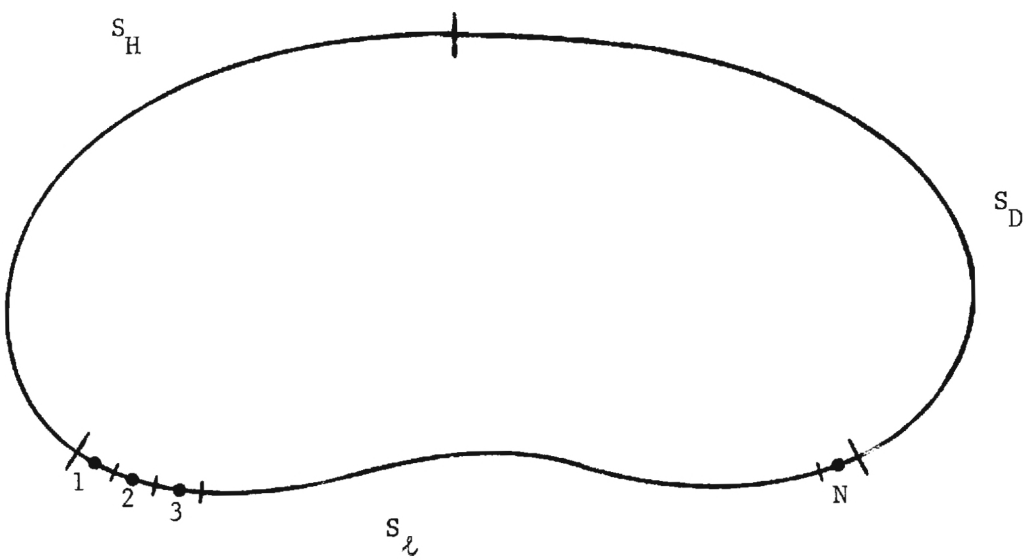

Figure 3. Liner surface divided into N finite regions.

Then N independent solutions are generated which represent the effect of N simple acoustic velocity sources on the liner using the boundary conditions given below.

$$\left.\begin{array}{ll} \varphi(Q) = 0 & \text{on } S_D \\ \frac{\partial\varphi}{\partial n}(Q) = 0 & \text{on } S_H \\ \left.\begin{array}{l} \frac{\partial\varphi}{\partial n}(Q_j) = 1 \quad j = 1,\ldots,N \\ \frac{\partial\varphi}{\partial n}(Q_i) = 0 \quad i \neq j \end{array}\right\} & \text{on } S_\ell \end{array}\right. \tag{18}$$

The N solutions thus generated are given by

$$\begin{array}{ll} \frac{\partial\varphi}{\partial n}{}_j(Q) & \text{on } S_D \\ \varphi_j(Q) & \text{on } S_H \\ \varphi_j(Q) & \text{on } S_\ell \end{array} \tag{19}$$

If we now sum these solutions multiplied by some arbitrary coupling constants designated by a_j, which we can do as the problem is linear, we generate a general solution which has the form

$$\left.\begin{array}{l} \varphi(Q) = \tilde{\varphi}(Q) \\ \frac{\partial\varphi}{\partial n}(Q) = \frac{\partial\varphi_D}{\partial n}(Q) + \sum_{j=1}^{N} a_j \frac{\partial\varphi_j}{\partial n}(Q) \end{array}\right. \quad \text{on } S_D \tag{20}$$

$$\left.\begin{array}{l} \varphi(Q) = \varphi_D(Q) + \sum_{j=1}^{N} a_j\, \varphi_j(Q) \\ \frac{\partial\varphi}{\partial n}(Q) = 0 \end{array}\right. \quad \text{on } S_H \tag{21}$$

$$\varphi(Q) = \varphi_D(Q) + \sum_{j=1}^{N} a_j \varphi_j(Q)$$

$$\frac{\partial\varphi}{\partial n}(Q_j) = a_j \qquad j = 1,\ldots,N \qquad \text{on } S_\ell \tag{22}$$

$$\frac{\partial\varphi}{\partial n}(Q_j) = 0 \qquad i \neq j$$

It will be noted here that the above solution has some interesting properties in that the acoustic potential on the driver surface (See Eqn. (20).) and the normal acoustic velocity on the hard walled surface (See Eqn. (21).) are not dependent upon the choice of the coupling constants a_j. Also, strictly speaking all possible values of the effective admittance Y are not possible on the liner surface. To demonstrate this, let us look at the point j = 1 on the liner surface where

$$Y(Q_1) = \frac{\partial\varphi(Q_1)}{\partial n} \Big/ \varphi(Q_1) = \frac{a_1}{\varphi_D(Q_1) + \sum_{i=1}^{N} a_i \varphi_i(Q_1)} \tag{23}$$

Solving for a_1, we obtain

$$a_1 = \frac{Y(Q_1) \sum_{i=2}^{N} a_i \varphi_i(Q_1)}{1 - Y(Q_1)\varphi_1(Q_1)} \tag{24}$$

where it can be seen that if we want $Y(Q_1) = \frac{1}{\varphi_1(Q_1)}$ we must have $a_1 \rightarrow \infty$. Thus, we cannot generate the solution where the effective admittance $Y(Q_j) = \frac{1}{\varphi_j(Q_j)}$ with finite values for the complex coupling constants a_j.

If we now substitute the expressions for the acoustic quantities on the liner surface (See Eqn. (22).) into the equation for the power lost to the admittance surface Eqn. (15) and treat the surface integral as a sum we obtain

$$\sum_{j=1}^{N} \left\{ a_j^R \left[\varphi_D^I (Q_j) + \sum_{i=1}^{N} \left[a_i^R \varphi_i^I (Q_j) + a_i^I \varphi_i^R (Q_j) \right] \right] \right.$$

$$\left. - a_j^I \left[\varphi_D^R (Q_j) + \sum_{i=1}^{N} \left[a_i^R \varphi_i^R (Q_j) - a_i^I \varphi_i^I (Q_j) \right] \right] \right\} \Delta s_\ell (Q_j) \tag{25}$$

If we now want to maximize the power lost to the admittance surface with respect to the real and imaginary parts of the complex coupling constants we must take the derivatives of Eqn. (25) with respect to the constants:

$$\frac{\partial}{\partial a_j^R} \left\{ \text{Eqn. (25)} \right\} = 0$$

$$j = 1, \ldots, N \tag{26}$$

$$\frac{\partial}{\partial a_j^I} \left\{ \text{Eqn. (25)} \right\} = 0$$

and set them equal to zero. Doing this we get

$$\left\{ \varphi_D^I (Q_j) + \sum_{i=1}^{N} \left[a_i^R \varphi_i^I (Q_j) + a_i^I \varphi_i^R (Q_j) \right] \right\} \Delta s_\ell (Q_j)$$

$$+ \sum_{i=1}^{N} \left[a_i^R \varphi_j^I (Q_i) - a_i^I \varphi_j^R (Q_i) \right] \Delta s_\ell (Q_i) = 0$$

$$j = 1, \ldots, N \tag{27}$$

$$\left\{ - \varphi_D^R (Q_j) - \sum_{i=1}^{N} \left[a_i^R \varphi_i^R (Q_j) - a_i^I \varphi_i^I (Q_j) \right] \right\} \Delta s_\ell (Q_j)$$

$$+ \sum_{i=1}^{N} \left[a_i^R \varphi_j^R (Q_i) + a_i^I \varphi_j^I (Q_i) \right] \Big\} \Delta s_\ell (Q_i) = 0$$

which upon rearrangement becomes:

$$\sum_{i=1}^{N} \left[a_i^R \varphi_i^I (Q_j) + a_i^I \varphi_i^R (Q_j) \right] \Delta s_\ell (Q_j)$$

$$+ \sum_{i=1}^{N} \left[a_i^R \varphi_j^I (Q_i) - a_i^I \varphi_j^I (Q_i) \right] \Delta s_\ell (Q_i) = - \varphi_D^I (Q_j) \Delta s_\ell (Q_j)$$

$$j = 1, \ldots, N \qquad (28)$$

$$- \sum_{i=1}^{N} \left[a_i^R \varphi_i^R (Q_j) - a_i^I \varphi_i^I (Q_j) \right] \Delta s_\ell (Q_j)$$

$$+ \sum_{i=1}^{N} \left[a_i^R \varphi_j^R (Q_j) + a_i^I \varphi_j^I (Q_i) \right] \Delta s_\ell (Q_i) = \varphi_D^R (Q_j) \Delta s_\ell (Q_j)$$

If we now define the complex conjugates of the original variables as:

$$\begin{aligned} \hat{a}_j &= a_j^R - i a_j^I \\ \hat{\varphi}_j &= \varphi_j^R - i \varphi_j^I \\ \hat{\varphi}_D &= \varphi_D^R - i \varphi_D^I \end{aligned} \qquad (29)$$

the two sets of real equations in Eqn. (28) can be reformulated as one complex set of equations given by

$$- \sum_{i=1}^{N} \left[\hat{a}_i \hat{\varphi}_i (Q_j) \right] \Delta S_{\ell} (q_j) + \sum_{i=1}^{N} \left[\hat{a}_i \varphi_j (Q_i) \right] \Delta S_{\ell} (Q_i) \tag{30}$$

$$= \hat{\varphi}_D (Q_j) \, \Delta S_{\ell} (Q_j) \qquad j = 1, \ldots, N$$

where the $\hat{a}_j$ are now the unknowns. As can be seen, Eqn. (30) represents N complex equations in N complex unknowns and can therefore be solved by straight forward numerical means. Once the optimum values of the complex coupling constants are calculated, the optimum surface distributions of the acoustic quantities may be found through the use of Eqns. (20) - (22). Then the power radiated to the field may be found using Eqns. (2) and (4) to calculate the acoustic quantities in the field on an imaginary sphere surrounding the body and then using Eqn. (14) to calculate the power.

IV. NUMERICAL PROCEDURES

The method outlined in the previous section requires not only the generation of a driver solution for the body of interest but also the generation of many simple source solutions on the admittance surface. If each of these solutions had to be generated separately, the present method would be no more attractive from a computational stand point than the method of Ref. 12 where many separate solutions are also necessary to find the optimum conditions. Thus, a way had to be found to generate the required source solutions efficiently.

The main computational advantage of the present method can only be realized when the method is coupled with the integral solution technique set forth in the Section II. In solving Eqn. (7) for the surface quantities, the coefficients of the unknowns are placed in a matrix while the knowns (i.e., the boundary conditions) are collected into an inhomogeneous vector. Thus, each simple source solution requires the solution of a liner set of equations.

If the boundary conditions are chosen correctly, only the inhomogeneous vector changes and therefore the matrix of coefficients for the unknowns only has to be inverted once. A special matrix solving routine was then written to take advantage of this which solves a system of linear equations with multiple inhomogeneous vectors very efficiently. This being the case, the multiple simple source solutions and the driver solution necessary for the optimization method can be generated all at once using little more computing time than it takes to calculate the driver solution alone.

One of the potential problems that had to be checked for was if the integral solution technique was capable of generating simple source solutions. Normally when Eqn. (7) is discretized the non-zero boundary conditions (e.g., the potential on the driver surface) are specified on a number of successive points on the body. Since relatively large errors have been found to exist where boundary conditions change abruptly when using the integral solution procedure, it was of concern that accurate source solutions might not be gotten using this method. This was checked by first generating a number of simple source solutions on a body and summing them, using the linear superposition principle, and then comparing this result with one generated specifying all the points on the body together. Excellent agreement was found between the two solutions generated in this way which was considered to be justification that accurate simple source solutions could indeed be calculated using the integral equation techniques

Once the computer program is written to generate the independent solutions necessary for the optimization procedure, the generation of the optimum admittance distribution on the body is straight forward. Substituting the independent solutions into Eqn. (30) another system of linear, complex equations is generated which can be solved by straight forward Gaussian elimination for the complex coupling constants (i.e., the a_j's) Having done this, the optimum admittance on the liner surface can be directly calculated from Eqn. (22).

V. SOME PRELIMINARY RESULTS

The test body being used for verification of the method is a straight duct with a rounded lip, an external wall thickness of 0.15a where a is the non-dimensional distance (i.e., the radius at the driver plane) and an L/a of 2.0 where L is the length of the duct (See Fig. 4.). Also, the liner surface is considered to run from a/2 to 3a/2 on the inner wall of the duct and the duct is terminated by an ellipse whose ratio of major to minor axis is 2.0. For the test case, plane wave input is assumed with an acoustic mode of M = (0,0) and a non-dimensional wave number of ka = 1.0. It will be noted here that this simple case is being used as a test case only and that more complicated cases, that is a true inlet shape at a higher wave number with a more complicated modal input, can easily be run without changing the computer codes; only the input files need to be changed.

For the numerical calculations, the straight duct is broken into 92 separate line segments along the body: 20 of these are on the driver and 25 are on the admittance surface. Also, in carrying out the numerical integrations necessary in the tangential direction (recall that a cylindrically symmetric formulation of the problem is used) a 32 point Gauss-Legendre formula is used.

Using the Georgia Tech CDC-CYBER 70/74, the generation of the driver solution and the 25 independent source solutions on the admittance surface required only 3 minutes of computing time. This compares favorably with the time required to calculate one single solution using the same body and number of points which takes ~ 2½ minutes. Once these have been gotten the next program requires only 30 seconds to calculate the complex coupling constants and the optimum solution.

The hard wall (or driver) solution radiates a power of P = 1.91 out of the duct where the power is calculated at the driver plane using

$$P = \iint_{S_D} \left(\frac{\partial \varphi^I}{\partial n} \varphi^R - \frac{\partial \varphi^R}{\partial n} \varphi^I \right)(ka)\,dS_D \tag{31}$$

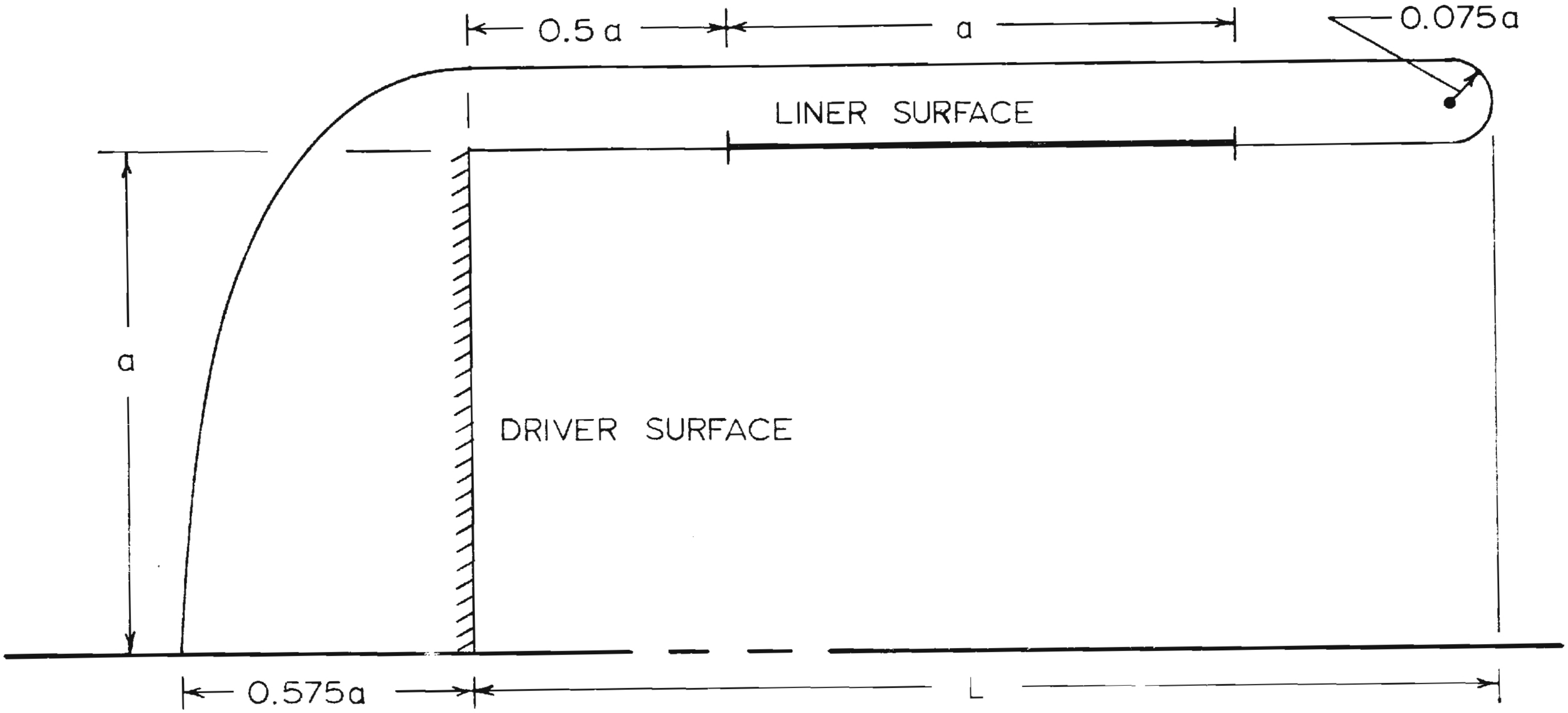

Figure 4. Straight Duct Geometry (L/a = 2.0).

where it will be noted that the wave number dependence has been kept (although in the present case ka = 1.0). This number should be used for comparison purposes.

The optimum admittance calculation for this case yielded a power lost to the admittance surface of P = 143.44. To get the power lost to the admittance surface Eqn. (31) was used except that the integration was performed over the admittance surface. To obtain the power radiated out of the duct, the power out of the driver plane must be recalculated as changing the admittance surface from a hard wall to an admittance distribution changes the driver. Doing this, it was found that the power out of the driver rose to P = 287.96 so that the power out of the duct was increased from P = 1.91 in the hard walled case to P = 144.52. As can be seen, this is not what we had hoped for but upon review it is exactly what we asked for; that is, find the solution (i.e., the admittance distribution on the liner surface) which yields the greatest power lost to the liner surface.

The above results show that just maximizing the power lost to the admittance surface does not necessarily minimize the power out of the duct. This is thought to be the result of the fact that the effect of the liner on the driver was not taken into account in the present formulation. This being the case, a reformulation of the problem has been accomplished which takes into account the effect the admittance on the liner surface has on the power output of the driver. This alternative formulation is presented in the next section.

VI. AN ALTERNATIVE FORMULATION

In the original formulation of the problem, the effect of changing the admittance on the liner surface on the power output of the driver was not taken into account. Since subsequent calculations have shown that the admittance on the liner surface can significantly effect the power output of the driver, an alternative formulation of the problem has been developed which includes the driver surface in the power calculation. In short this new formulation seeks to minimize the power out of the combination of the driver and admittance surfaces rather than simply maximizing the power lost to the liner surface. This formulation should yield the minimum power out of the duct rather than the maximum power lost to the admittance surface.

If we develop an equation for the power radiated out of the driver surface (similar to Eqn. (25) for the liner surface) we obtain

$$\sum_{j=K}^{M} \Big\{ \Big[\frac{\partial \varphi_D^R(Q_j)}{\partial n} + \sum_{i=1}^{N} \Big[a_i^R \frac{\partial \varphi_i^R(Q_j)}{\partial n} - a_i^I \frac{\partial \varphi_i^I(Q_j)}{\partial n} \Big] \Big] \varphi_D^I(Q_j)$$

$$- \Big[\frac{\partial \varphi_D^I(Q_j)}{\partial n} + \sum_{i=1}^{N} \Big[a_i^R \frac{\partial \varphi_i^I(Q_j)}{\partial n} + a_i^I \frac{\partial \varphi_i^R(Q_j)}{\partial n} \Big] \Big] \varphi_D^R(Q_j) \Big\} \Delta S_D(Q_j) \qquad (32)$$

from Eqns. (15) and (20) where K and M are the beginning and ending points on the driver surface (recall the admittance surface goes from 1 to N). Carrying out the operation of Eqn. (26) on Eqn. (32) we obtain in complex notation

$$- \sum_{j=K}^{M} \Big\{ \frac{\partial \varphi_i(Q_j)}{\partial n} \hat{\varphi}_D(Q_j) \Big\} \Delta S_D(Q_j) = 0 \qquad i = 1,\ldots,N \qquad (33)$$

Adding this to Eqn. (30) we obtain

$$- \sum_{i=1}^{N} \left[\hat{a}_i \, \hat{\varphi}_i (Q_j) \right] \Delta s_{\ell} (Q_j) + \sum_{i=1}^{N} \left[\hat{a}_i \, \varphi_j \, (Q_i) \right] \Delta s_{\ell} (Q_i)$$

$$= \hat{\varphi}_D \, (Q_j) \, \Delta s_{\ell} \, (Q_j) + \sum_{i=K}^{M} \frac{\partial \varphi_j (Q_i)}{\varphi n} \, \hat{\varphi}_D \, (Q_i) \, \Delta s_D (Q_i) \qquad (34)$$

$$j = 1, \ldots, N$$

which a set of N simultaneous linear equations for the $\hat{a}_j$'s. This reformulation of the problem is now being programmed.

VII. CHECK CASES

In order to check the results of the new method optimum constant liner results are necessary for the specific geometrys and wave numbers used in this study. To obtain these results, computer programs have been written and checked out which calculate the power radiated from an axisymmetric body with an acoustic liner. These programs are based on the integral equation technique presented in Section II and will employ the method of Ref. 12 which entails the calculation of many separate solutions. The optimum constant liner admittance will be calculated for each body and for each modal input (i. e., at each wave number) for which the optimum admittance calculation is run.

VIII. SUMMARY

During the first six months of this research project, the computer programs were written and checked out which are necessary to implement the new analytical method for the calculation of the optimum liner admittance for sound suppression in a duct. This analytical method was designed to maximize the power lost to the admittance surface which it accomplished very well. Unfortunately, since the effect of the liners admittance on the power output of the driver was not considered, this scheme did not optimize for the minimum power out of the duct. In fact, the sound power out of the duct was increased drastically over the hard walled case. Thus, a new theoretical method was developed which is designed to minimize he power out of the duct by considering both the power output of the driver and the power loss to the admittance surface. The computer programs are currently being modified to handle the extra terms this method requires.

To generate the required optimum admittace check cases, computer programs have been written and checked out which can calculate the power output of a duct under specific excitation conditions with a liner surface in the duct. These programs are currently being run to find the optimum constant admittance for sound suppression for each configuration of interest.

IX. REFERENCES

1) Zinn, B. T., Meyer, W. L. and Bell, W. A., "Noise Suppression in Jet Inlets," AFOSR Interim Scientific Report, AFOSR TR-78-0696, Contract No. F49620-77-C-0066, February 1978.

2) Zinn, B. T., Meyer, W. L. and Bell, W. A., "Noise Suppression in Jet Inlets," AFOSR Annual Technical Report, AFOSR TR-79-0614, Contract No. F49620-77-C-0066, February 1979.

3) Meyer, W. L., Bell, W. A., Stallybrass, M. P. and Zinn, B. T., "Boundary Integral Solutions of Three Dimensional Acoustic Radiation Problems, "Journal of Sound and Vibration, Vol. 59, No. 2, July 1978.

4) Burton, A. J., "The Solution of Helmholtz' Equation is Exterior Domains Using Integral Equations," NPL Report NAC 30, National Physical Laboratory, Teddington, Middlesex, January 1973.

5) Chertock, G., "Sound from Vibrating Surfaces," Journal of the Acoustical Society of America, No. 36, pp. 1305-1312, 1964.

6) Schenck, H. A., "Improved Integral Formulation for Radiation Problems," Journal of the Acoustical Society of America, No. 44, pp. 41-58, 1968.

7) Ursell, F., "On the Exterior Problems of Acoustics," Proceedings of the Cambridge Philosophical Society, No. 74, pp. 117-125, 1973.

8) Burton, A. J. and Miller, G. F., "The Application of Integral Equation Methods to the Numerical Solution of Some Exterior Boundary Value Problems," Proceedings of the Royal Society of London, A. 323, pp. 201-210, 1971.

9) Stallybrass, M. P., "On a Pointwise Variational Principle for the Approximate Solution of Linear Boundary Value Problems," Journal of Mathematics and Mechanics, No. 16, pp. 1247-1286, 1967.

10) Meyer, W. L., Bell, W. A., Stallybrass, M. P. and Zinn, B. T., "Prediction of the Sound Field Radiated from Axisymmetric Surfaces," Journal of the Acoustical Society of America, Vol. 63, No. 2, pp. 631-638, March 1979.

11) Meyer, W. L., Daniel, B. R. and Zinn, B. T., "Acoustic Radiation from Axisymmetric Ducts: A Comparison of Theory and Experiment," AIAA Paper No. 80-0097, presented at the AIAA 18th Aerospace Sciences Meeting, Pasadena, California, January 14-16, 1980.

12) Motsinger, R.E., Kraft, R.E. and Zwick, J.W., "Design of Optimum Acoustic Treatment for Rectangular Ducts with Flow," ASME Paper 76-GT-113, March 1976.

13) Morse, P. M. and Ingard, K. U., Theoretical Acoustics, McGraw-Hill, New York, 1969.

E-16-653

NASA LANGLEY FINAL TECHNICAL REPORT
NAG 1-133 (3/1/81 - 2/28/82)

DEVELOPMENT OF ANALYTICAL TECHNIQUE FOR THE OPTIMIZATION OF JET ENGINE AND DUCT ACOUSTIC LINERS

By
Ben T. Zinn
and
William L. Meyer

GEORGIA INSTITUTE OF TECHNOLOGY
A UNIT OF THE UNIVERSITY SYSTEM OF GEORGIA
SCHOOL OF AEROSPACE ENGINEERING
ATLANTA, GEORGIA 30332

1982

NASA LANGLEY FINAL TECHNICAL REPORT

NAG 1-133 (3/1/81 - 2/28/82)

DEVELOPMENT OF AN ANALYTICAL TECHNIQUE FOR THE OPTIMIZATION OF JET ENGINE AND DUCT ACOUSTIC LINERS

BY

Ben T. Zinn

and

William L. Meyer

SCHOOL OF AEROSPACE ENGINEERING

GEORGIA INSTITUTE OF TECHNOLOGY

Atlanta, GA 30332

ABSTRACT

This report summarizes the work performed during the NASA LANGLEY research program entitled "Development of an Analytical Technique for the Optimization of Jet Engine and Duct Acoustic Liners." This research program ran for one year (3/1/81-2/28/82) and carries the NASA number NAG 1-133. Detailed results of the work performed during the first six months of this contract are presented in the NASA LANGLEY SEMI-ANNUAL STATUS REPORT (3/1/81-8/31/81) for NAG 1-133 and thus will not be repeated here in its entirety.

During the past six months, a new method was developed for the calculation of optimum constant admittance solutions for the minimization of the sound radiated from an arbitrary axisymmetric body. This method utilizes both the integral equation technique used in the calculation of the optimum non-constant admittance liners and the independent solutions generated as a by product of these calculations. The results generated by both these methods are presented for three duct geometries: (1) a straight duct; (2) the QCSEE inlet; and (3) the QCSEE inlet less its centerbody.

TABLE OF CONTENTS

I.	Introduction	1
II.	Calculation of Optimum Constant Admittance Liners	4
III.	Some General Comments	13
IV.	Numerical Considerations	14
V.	Results	16
VI.	Summary and Conclusions	20
VII.	References	22
VIII.	Tables	23
IX.	Figures	41

I. INTRODUCTION

The object of this research program was the development of an analytical technique for the determination of the optimum admittance distribution along the wall of an axisymmetric duct for the minimization of sound radiated from the duct given a specific source of acoustic radiation in the duct. The results of this method were to be checked against calculations performed for constant admittance liners to see if better results could be obtained with the new method. Finally, a parametric study was to be done, based on wave number, for at least two geometries in which the optimum constant and distributed admittance liners were to be calculated.

The formulation of the problem which has been used in the parametric study is presented in detail in Chapter IV of the previous six month status report for this grant (See Reference 1.). This being the case, the precise mathematical formulation of the method will not be repeated. Instead, only a brief overview of the method will be presented here.

The method itself is based upon a special integral formulation of the external solutions of the Helmholtz equation. The basic formulation of the governing equations for three dimensions is given in great detail in Reference 2. This formulation can be specialized for axisymmetric bodies[3] and it is this form of the equations which is used in this study.

These integral equations govern the acoustic quantities on the surface of the body and take into account the Sommerfeld radiation conditions at infinity in the field so that only outgoing, decaying solutions are considered. To solve these equations, the surface of the body is discretized into many small areas and since the problem is elliptic in nature a boundary condition is applied over each small area. The boundary condition specified may be either the acoustic potential which is directly related to the acoustic pressure, the normal acoustic velocity, or a ratio of these two quantities referred to as the effective acoustic admittance at each point.

When this is done, a system of linear equations can be developed in which the acoustic potential or the normal acoustic velocity is the unknown at each point on the body depending on which boundary condition is specified there. The boundary conditions themselves contribute to the inhomogeneous term in each equation and in some cases the diagonal term of the matrix.

Since the resulting equations are linear, the solutions may be superimposed. Also, if the boundary conditions are chosen appropriately they do not effect the matrix coefficients, only the inhomogeneous vector terms. It is these two characteristics of this formulation which are exploited in both the calculation of the optimum varying admittance for a duct and the optimum constant admittance.

Normally to find the optimum constant admittance for a duct, a parametric study must be done in which the real and imaginary parts of the admittance of the liner are varied. Usually, this means that a complete, separate solution must be generated for each admittance value; however, a method has been developed which utilizes the same independent solutions on the admittance surface which were generated for the calculation of the optimum varying admittance solution. This new method greatly reduces the amount of computing time required for the generation of constant admittance solutions and is presented in detail in the following section of this report.

Having developed both the theory and the computer codes for the generation of both optimum constant and varying admittance liners for general finite axisymmetric ducts, a parametric study was performed on three separate duct geometries. The three duct geometries are: (1) a straight duct with a rounded lip; (2) the NASA QCSEE inlet of Reference 4; and (3) the NASA QCSEE inlet less its centerbody. The results of this parametric study are presented at six wave numbers for each geometry at which both the constant and varying optimum admittance liners are calculated for both constant acoustic potential and constant normal acoustic velocity drivers.

II. CALCULATION OF OPTIMUM CONSTANT ADMITTANCE LINERS

In this section, we will briefly go over the generation of the independent solutions on the surface of the body. Then, the development of constant admittance solutions will be discussed in detail. Since the development of the special integral formulation of the external solutions of the Helmholtz equation is given in References 1-3, only the final form of the equations will be presented here. It will be noted that although this form of the equations has been specialized for axisymmetric geometries, that any cylindrically symmetric acoustic mode may be calculated.

Firstly, let us define the geometrical variables that we will use on a surface of revolution. In Fig. 1, the coordinate system employed on the body S is given (ρ , Z,Θ) along with an outward normal from the body, $\vec{n}$, and an element of area on the surface of the body, $\rho \, ds d\Theta$. The variable s is the distance along the generating line of the surface of revolution and is assumed to go from o at one end of the body to ℓ at the other.

We now assume that the acoustic potential on the surface of a body of revolution can be written as

$$\Phi(\rho, Z, \Theta) = \phi(s) \cos(m\Theta)$$

and similarly that the normal acoustic velotìcy on the surface of the body can be written as

$$\frac{\partial \Phi(\rho, Z, \Theta)}{\partial \vec{n}} = V(s) \cos(m\,\Theta)$$

In doing this we have incurred no loss in generality. Since all of the equations are linear, any acoustic radiation pattern may be generated as a sum of these simple, cylindrically symmetric patterns. Also, the variable m is commonly referred to as the tangential acoustic mode number.

In order to write the equation in compact form we now define three sets of functions:

Influence functions:

$$I_1(r_{pq}) = 2\int_0^{\pi} G(P, Q)\cos(m\Theta_q)\, d\Theta_q \tag{3}$$

$$I_2(r_{pq}) = 2\alpha\int_0^{\pi} \frac{\partial G(P, Q)}{\partial \vec{n}_p}\cos(m\Theta_q)\, d\Theta_q$$

Kernel Functions:

$$K_1(r_{pq}) = 2\int_0^{\pi} \frac{\partial G(P, Q)}{\partial \vec{n}_q}\cos(m\Theta_q)\, d\Theta_q$$

$$K_2(r_{pq}) = 2\alpha\int_0^{\pi} \frac{\partial^2 G(P, Q)}{\partial \vec{n}_p\,\partial \vec{n}_q}\cos(m\Theta_q)\, d\Theta_q, \qquad \Theta_q \neq \Theta_p \tag{4}$$

Forcing functions:

$$F_1(r_{pq}) = 2\alpha\int_0^{\pi} G(P,Q)\,(ik)^2(\vec{n}_p\cdot\vec{n}_q)\, d\Theta_q$$

$$F_2(r_{pq}) = 2\alpha\int_0^{\pi} \frac{\partial^2 G(P,Q)}{\partial \vec{n}_p\,\partial \vec{n}_q}\, d\Theta_q, \qquad \Theta_q \neq \Theta_p \tag{5}$$

where r_{pq} is the distance between points P and Q and $\vec{n}_p$ and $\vec{n}_q$ are the outward normals from the points P and Q, respectively (See Fig. 2.). Also, G(P,Q) is the free space Green's function

$$G(P,Q) = \frac{e^{ikr_{pq}}}{r_{pq}} \tag{6}$$

where k is the wave number and α is the complex coupling constant for this particular formulation which is found to be

$$\alpha = i/k \tag{7}$$

It will be noted that in evaluating K_2 and F_2 the point at which $\Theta_p = \Theta_q$ is excluded from the integration as it constitutes a strong sigularity.

Using the above definitions and equations, the special integral formulation of the external solutions of the Helmholtz equation may be written as

$$\begin{aligned} &\int_o^{\ell} \phi(s_q)\left[K_1(r_{pq}) + K_2(r_{pq})\right] \rho_q \, ds_q \\ &- \phi(s_p)\int_o^{\ell} \left[F_1(r_{pq}) + F_2(r_{pq})\right] \rho_q \, ds_q \\ &- \int_o^{\ell} V(s_q)\left[I_1(r_{pq}) + I_2(r_{pq})\right] \rho_q \, ds_q \\ &= 2\pi\left[\phi(s_p) + \alpha V(s_p)\right] \end{aligned} \tag{8}$$

In this particular formulation of the problem the s and θ coordinate directions have been uncoupled so that the solution of the problem has been reduced to the evaluation of line integrals on the surface of the body.

Equation (8) represents a relationship between the acoustic pressure and normal acoustic velocity at any given point on a body (i.e., point P) to all of the values everywhere else on the body (i.e., at the Q points). If this equation is applied at each point on the body, along with the boundary condition at each point, a system of linear algebraic equations is obtained for the unknown variables at each point on the body. Thus, if there are N points on the body, a system of N complex equations in N complex unknowns is developed.

In the numerical integration of the functions (See Eqns. (3)-(5).) a Gauss-Legendre integration formula is used. For the integration in the s direction, a simple two point integration is employed such that the point P is never actually equal to any of the integration points (i.e., the Q points). Also, when the body is divided into N points in the s direction, both the acoustic potential ϕ and the normal acoustic velocity V are assumed to be constant over each element even though there are two integration points per element.

For the development of the independent solutions on the surface of the body let us assume that the body is divided into three distinct regions as in Fig. 3. These regions do not necessarily have to be contiguous however, for the sake of clarity they are presented as such here. The first solution which we must consider is the driver solution. To calculate it we must solve for the acoustic quantities on the surface of the body subject to the boundary conditions

$$\begin{aligned} \phi(Q) &= \tilde{\phi}_D(Q) \qquad \text{on } S_D \\ V(Q) &= 0 \qquad \text{on } S_H \text{ and } S_L \end{aligned} \tag{9}$$

where $\tilde{\phi}_D$ (Q) is some specified function of the acoustic potential on the driver. Solving this problem, we obtain the driver solution

$$\begin{aligned} &V_D(Q) && \text{on } S_D \\ &\phi_D(Q) && \text{on } S_H \text{ and } S_L \end{aligned} \tag{10}$$

Next, the liner surface(s) is divided up into M finite regions as in Fig. 4. Then M independent solutions are generated which represent the effect of M simple acoustic velocity sources on the liner using the boundary conditions given below

$$\begin{aligned} &\phi\,(Q) = 0 \ \text{ on } S_D \\ &V(Q) = 0 \text{ on } S_H \\ &\left.\begin{aligned} &V(Q_j) = 1 \qquad j = 1, \ldots, M \\ &V(Q_i) = 0 \qquad i \neq j \end{aligned}\right\} \text{ on } S_L \end{aligned} \tag{11}$$

The M solutions thus generated are given by

$$
\begin{aligned}
&V_j\,(Q) && \text{on } S_D \\
&\phi_j\,(Q) && \text{on } S_H \\
&\phi_j\,(Q) && \text{on } S_L
\end{aligned}
\qquad (12)
$$

If we now sum these solutions multiplied by some arbitrary coupling constants designated by a_j, which we can do as the problem is linear,we generate a general solution which has the form

$$
\begin{aligned}
&\phi\,(Q) = \tilde{\phi}\,(Q) \\
&V(Q) = V_D\,(Q) + \sum_{j=1}^{M} a_j\,V_j\,(Q) \qquad \text{on } S_D
\end{aligned}
\qquad (13)
$$

$$
\begin{aligned}
&\phi\,(Q) = \phi_D(Q) + \sum_{j=1}^{M} a_j\phi_j\,(Q) \\
& \qquad\qquad\qquad\qquad \text{on } S_H \\
&V(Q) = 0
\end{aligned}
\qquad (14)
$$

$$
\begin{aligned}
&\phi\,(Q) = \phi_D\,(Q) + \sum_{j=1}^{M} a_j\,\phi_j\,(Q) \\
&V(Q_j) = a_j \qquad j=1,\ldots,M \qquad \text{on } S_L \\
&V(Q_j) = 0 \qquad i \neq j
\end{aligned}
\qquad (15)
$$

It will be noted here that the above solution has some interesting properties in that the acoustic potential on the driver surface (See Eqn. (13).) and the normal acoustic velocity on the hard walled surface (See Eqn. (14).) are not dependent upon the choice of the coupling constants a_j.

In this study we are interested in the effective acoustic admittance Y which is defined as

$$Y = \frac{\partial \Phi}{\partial \vec{n}} \Big/ \Phi = \frac{V}{\phi} \tag{16}$$

This being the case, we can now represent the effective acoustic admittance at any point on the admittance surface as

$$Y(Q_j) = \frac{a_j}{\phi_D (Q_j) + \sum_{i=1}^{M} a_i \phi_i (Q_j)} \tag{17}$$

If we now specify that the effective acoustic admittance at all points on the admittance surface is to be the complex number C we obtain

$$\sum_{i=1}^{M} a_i \phi_i (Q_j) - \frac{1}{C} a_j = \phi_D (Q_j), \tag{18}$$

$$j = 1, \ldots, M$$

which represents a system of M linear complex equations for the M complex coupling constants, a_j. Using this method many constant admittance solutions can be generated very economically once the independent solutions on the surface of the body are known. Since the independent solutions have already been calculated for the generation of the optimum varying admittance, a relatively small amount of extra computing time is required for the determination of the optimum constant admittance solution.

To find the optimum constant admittance solution for a specified geometry, driver and wave number, the values of C are chosen in a grid pattern and a solution is generated for each value. Once the surface solution is known it is an easy job to calculate the acoustic power radiated from the driver and the acoustic power lost to the admittance surface using[1,5]

$$E \propto \iint_{S_L} \left[\phi^R(Q)\, v^I(Q) - \phi^I(Q)\, v^R(Q) \right] dS(Q) \tag{19}$$

where E is the acoustic energy radiated out of a surface and the superscripts R and I refer to the "real and imaginary part of", respectively. When the solution having the minimum radiated power is found, the region may be further subdivided to "home in" on the optimal value of the admittance.

It is of interest to note here that strictly speaking all possible values of the effective admittance Y are not possible at each point on the liner surface. To demonstrate this, let us look at the point j=1 on the liner surface where

$$\bar{Y}(Q_1) = \frac{a_1}{\phi_D(Q_1) + \sum_{i=1}^{M} a_i\, \phi_i(Q_1)} \tag{20}$$

Solving for a_1 we obtain

$$a_1 = \frac{Y(Q_1) \sum_{i=2}^{M} a_i \, \phi_i \, (Q_1)}{1 - Y(Q_1) \, \phi_1 \, (Q_1)} \tag{21}$$

where it can be seen that if we want $Y(Q_1) = \frac{1}{\phi_j(Q_j)}$ we must hava $a_1 \rightarrow \infty$. Thus, we cannot generate the solution where the effective admittance $Y(Q_j) = \frac{1}{\phi_j \, (Q_j)}$ with a finite value for the complex coupling constant, a_j.

III. SOME GENERAL COMMENTS

The problem of acoustic radiation from a duct, as formulated for this study, is strictly elliptic so that only one boundary condition may be specified on any part of the body. Thus, either the acoustic potential (i.e., pressure) or the normal acoustic velocity may be specified on the driver but not both. This leads us to an interesting problem when trying to compare the results of this method to any other as other methods utilize the mathematical artifice of a semi-infinite duct.[6] This artifice allows them to keep the driver power and modal input constant while varying the acoustic properties of a liner. This tends to neglect any possible effect the acoustic properties of the liner could have on the amount or modal content of the power coming out of the driver.

In the problem, as formulated for this study, the driver power and more importantly the radial modal output of the driver cannot be fixed as this would overspecify the problem. This being the case, there are two possible optimum constant admittance liners possible, one a relative measure of the percent of the driver power attenuated by the liner and the other an absolute measure of the power coming out of the duct. Both were calculated at each wave number for each geometry and are presented as such (i.e., Relative and Absolute optimum constant admittances). Also, since either the acoustic potential or the normal acoustic velocity could be specified on the driver runs were done with each and are noted as such. For the runs where the normal acoustic velocity is specified on the driver, the acoustic potential is specified on the admittance (i.e., liner) surface and vice versa (See Eqns. (9) and (11).).

IV. NUMERICAL CONSIDERATIONS

The special integral formulation of the external solutions of the Helmholtz equation[2,3] which is used as the basis for all of the calculations done in this study requires a closed body. Thus, all three of the ducts used in this study: the straight duct with the rounded lip; the NASA QCSEE inlet; and, the NASA QCSEE inlet less its centerbody were terminated with a 2:1 ellipse (See Figs. 5-7.). Also, for the three geometries investigated the total height to the inner wall of the duct at the driver plane was normalized to one and the outer wall of the duct was 1.15. All of the ducts have an L/a of 2.0

For the numerical calculations , points were spaced evenly along the inner walls of the ducts with a nominal spacing of 0.05a. On the outer walls of the ducts, the points were systematically spaced at larger and larger intervals as it has been found that the outer walls of ducts and their terminations have little effect on the total power radiated and the radiation pattern in the forward half plane. The total number of points used on the three geometries in the s direction for the calculations performed for this study were: 92 points for the straight duct; 108 points for the NASA QCSEE inlet; and, 100 points for the NASA QCSEE inlet less its centerbody. For the θ integration, a 32-point Gauss-Legendre integration formula was used in all cases.

For all three of the ducts, the admittance surface consisted of 25 points or intervals over which the optimum admittance distributions were to be generated and ran from 0.4a to 1.6a in the Z direction along the inner walls of the ducts.

Thus, a hard wall or driver solution and 25 independent source solutions were calculated for each geometry, wave number and type of driver specified (i.e., potential or velocity).

V. RESULTS

Each of the geometries was run with a plane wave as input on the driver for non-dimensional wave numbers of 1, 2, 3, 5, 7, and 10. That is, in all of the cases run, the tangential mode number was taken as zero. Although a plane wave was input, a plane wave driver did not necessarily result since only one variable could be specified at a time.

The results for all of the straight duct runs are presented in Tables I-VI and in Figs. 8-13. In the Tables, the power radiated out of the driver and the power radiated into the field are tabulated along with their values, for the optimum distributed admittance and for the optimum absolute and relative constant admittances. In all the Tables, the power values are relative as they have been normalized by the power out of the hard walled configuration. Also, each table contains the results for one wave number for both the constant acoustic pressure and normal acoustic velocity drivers.

It will be of interest to note here that for the lower wave numbers, the power out of the driver is negative (i.e., it is damping). This necessarily means that the liner surface is driving since the formulation of the integral equations only allows for the case where there is a net flow of power out of the body (i.e., no incoming waves). If the imaginary part of the effective admittance Y (See Eqn. (16).) is positive, this denotes driving; that is, an active suppressor. The relative optimum constant admittance must always be a damping admittance since it is determined as the smallest ratio of power out of the driver, to the power lost to the admittance surface.

In general, it is found that the lowest power output is obtained from the optimum admittance distribution. Also, the relative constant admittance usually has the highest power output as measured in the field surrounding the duct.

Each Figure constitutes a set of 6 plots for each wave number. The first group of three plots in each set are for the case where a constant acoustic pressure is specified on the driver and the second group is for the case where a constant normal acoustic velocity was specified. The first plot in each group (e.g., Figs. 8a & d), contains a plot of the optimum admittance distribution on the inner wall of the duct from the driver end Z=0.4a (inner), to the open end, Z=1.6a (outer). As can be seen even at the low wave numbers where there are a more than sufficient number of points on the body to generate an accurate solution, the effective admittance distribution is not very smooth. This is because it is a ratio of two functions on the surface of the body which tends to make it less continuous than either generating function. Of course, more points could be taken on the surface of the body to obtain a smoother function for the effective admittance; however, this would not substantially change the overall accuracy of the solution (i.e., the power output). At the higher wave numbers, the solution does become suspect however, and more points should probably have been used for the cases where ka=7 and 10. This should not detract from the overall validity of the method however.

It will be noted that at the lower wave numbers, the distributed admittance found for the minimum power out of the body is totally driving. As the wave number gets higher, the optimum admittance distribution becomes mixed (i.e., some of the liner surface drives and some of it damps) and finally at some of the higher wave numbers, the distributed admittance is almost totally passive. This is probably due to the fact that at the higher wave numbers, the wave structure in the duct becomes more complicated so that interference patterns are more difficult to set up. Since an active suppressor damps out sound through the setting up of interference patterns, these types of suppressors are probably only useful at lower wave numbers where the wave patterns are less complicated. Also, since it is more difficult to set up interference patterns with the constraint of a constant admittance liner, the optimum absolute constant admittance liner transition from driving to damping occurs sooner.

In the second plot in each group of three, is a plot of the absolute power out of the duct as a function of the admittance (constant) on the liner surface which is expressed in dB. The admittance value for which the minimum power out of the duct is obtained is marked with a large dot. Again, these values are tabulated in the tables (See Tables I-VI.).

In the final plot in each group of three, is a plot of the relative power out of the duct as a function of admittance (constant) on the liner which is also expressed in dB. Only negative values of the imaginary part of the admittance are considered in this case as the power out of the duct is referrenced to the power out of the driver. As with the previous plot, the admittance value, for which the minimum percent power is radiated, is marked with a large dot and those values also are tabulated in the Tables.

The results for the QCSEE inlet are presented in Tables VII-XII and in Figs. 14-19. As with the straight duct, the tables contain the results for the six wave numbers run, one wave number per table. The results at a non-dimensional wave number of ka=7.0 for the case where the acoustic potential is specified on the driver are not included since the optimum values for the absolute and relative constant admittances fell outside of the initial search pattern. This pattern ran from -10 to 10 in increments of 1 for both the real and imaginary parts of the admittance. This is not to imply that they couldn't be calculated, just that they were not, since this would have required modification of the computer programs used for all of the other cases run.

As with the straight duct, each figure for this geometry consists of the six plots done for each wave number. As before, the optimum admittance distribution for both the constant acoustic pressure and the constant normal acoustic velocity drivers are presented along with the contour power plots for the constant absolute and relative admittance liners. Again, the optimum values are marked with dots in these plots and are tabulated in the Tables. It will be noted in Fig. 18a and b that these points are not marked since they fell outside the range of the plots.

The results for the QCSEE inlet less its centerbody are presented in Tables XIII-XVIII and in Figs. 20-25. The reason for running the cases for this particular geometry was to see if any trends could be established in going from the straight duct geometry to the full inlet geometry. At the lower wave numbers, the optimum admittance values calculated for it, seem to fall between those for the other two geometries as one would intuitively expect; however, this trend is not maintained at the higher wave numbers.

VI. SUMMARY AND CONCLUSIONS

During the past year, a method was developed for the calculation of optimum distributed admittance duct liners. This method is based upon a special integral representaiton of the external solutions of the Helmholtz equation which is valid (i.e., can be used to generate the correct, unique solutions) at all wave numbers. The equations used had been specialized for axisymmetric geometries but this is not a restriction on the method itself.

As a by-product of this method, a procedure was developed for the identification of optimum constant admittance duct liners. This procedure utilizes solutions already developed for the optimum distributed admittance calculation. At present, it entails the use of a simple search pattern for the optimum constant admittance; however, it is believed that this could be refined if time allowed.

To give some idea of the time involved in calculating these results , some typical computing times are presented below. These runs were done on the Georgia Tech CDC CYBER 760 and the programs are written in Fortran V. For the case where 100 points were used on the body in the s direction, a 32 point Gauss-Legendre integration formula was used in the Θ direction (See Fig. 1.), and there were 25 points on the liner surface, the calculation of the 26 independent solutions required for the optimization procedure took 185 seconds of CPU time. The generation of the optimum distributed admittance then took an additional 10 seconds and the identification of the optimum constant admittances took 390 seconds. As can be seen, the calculation of the constant admittance solutions is slow compared to the calculation of the optimum distributed admittance. The contour plots of the sound radiated for each constant admittance chosen on the liner surface were done with the GPCP (General Purpose Contour Plotting) package which we have available here at Georgia Tech. It was developed originally for plotting contour maps but was found to be very useful in this research program.

In conclusion, an effective, efficient method has been developed for the calculation of both optimum distributed and constant admittance liners for general geometries. It was found through the use of this method that even very similar geometries may have vastly different optimum liners associated with them. Also, it was found that at low wave numbers often the most efficient liners for the reduction of the sound radiated are active and not passive. At the higher wave numbers, the optimum distributed admittances are found to be almost always a combination of both active and passive elements.

REFERENCES

1. Zinn, B.T. and Meyer, W.L., "Development of an Analytical Technique for the Optimization of Jet Engine and Duct Acoustic Liners," NASA Langley Semi-Annual Status Report for grant NAG 1-133, (3/1/81-8/31/81).

2. Meyer, W.L., Bell, W.A., Stallybrass, M.P. and Zinn, B.T., "Boundary Integral Solutions of Three Dimensional Acoustic Radiation Problems," Journal of Sound and Vibration, Vol. 59, No. 2, July 1978, pp. 245-262.

3. Meyer, W.L., Bell, W.A., Stallybrass, M.P. and Zinn, B.T., "Prediction of the Sound Field Radiated from Axisymmetric Surfaces," Journal of the Acoustical Society of America, Vol. 65, No. 3, March 1979, pp. 631-638.

4. Miller, B.A., Dastoli, B.J. and Wesoky, H.L., "Effect of Entry-Lip Design on Aerodynamics and Acoustics of High-Throat-Mach-Number Inlets for the Quiet, Clean, Short-Haul Experimental Engine," NASA TM X-3222, May 1975.

5. Morse, P.M. and Ingard, K.U., Theoretical Acoustics, McGraw-Hill, New York, 1969.

6. Rice, E.J., "Spinning Mode Sound Propagation in Ducts with Acoustic Treatment and Sheared Flow," NASA TM X-71672, March 1975.

TABLE I

STRAIGHT DUCT

Relative power normalized with respect to the hard walled radiated power

ka = 1.0

	Constant Phi on the Driver	Constant Velocity on the Driver
OPTIMUM ADMITTANCE DISTRIBUTION		
POWER OUT OF THE DRIVER	-0.57	-0.67
TOTAL POWER IN FAR FIELD	0.000017	0.000042
ABSOLUTE CONSTANT ADMITTANCE	(-0.18, 4.88i)	(-1.32, 4.60i)
POWER OUT OF THE DRIVER	-0.64	-0.53
TOTAL POWER IN FAR FIELD	0.0014	0.00063
RELATIVE CONSTANT ADMITTANCE	(-1.30, -3.40i)	(-1.34, -3.33i)
POWER OUT OF THE DRIVER	0.87	0.65
TOTAL POWER IN FAR FIELD	0.0015	0.0012

TABLE II

STRAIGHT DUCT

Relative power normalized with respect to the hard walled radiated power

ka = 2.0

	Constant Phi on the Driver	Constant Velocity on the Driver
OPTIMUM ADMITTANCE DISTRIBUTION		
POWER OUT OF THE DRIVER	-0.65	-0.61
TOTAL POWER IN FAR FIELD	0.00012	0.00014
ABSOLUTE CONSTANT ADMITTANCE	(-2.95, 3.05i)	(-2.70, -2.90i)
POWER OUT OF THE DRIVER	-0.89	0.75
TOTAL POWER IN FAR FIELD	0.00034	0.00054
RELATIVE CONSTANT ADMITTANCE	(-2.64, -3.14i)	(-2.65, -3.13i)
POWER OUT OF THE DRIVER	0.91	0.78
TOTAL POWER IN FAR FIELD	0.00088	0.00068

TABLE III

STRAIGHT DUCT

Relative power normalized with respect to the hard walled radiated power

$ka = 3.0$

	Constant Phi on the Driver	Constant Velocity on the Driver
OPTIMUM ADMITTANCE DISTRIBUTION		
POWER OUT OF THE DRIVER	-0.23	-0.016
TOTAL POWER IN FAR FIELD	0.000075	0.00011
ABSOLUTE CONSTANT ADMITTANCE	(-2.71, -2.38i)	(-2.65, -2.33i)
POWER OUT OF THE DRIVER	0.77	0.13
TOTAL POWER IN FAR FIELD	0.00072	0.00014
RELATIVE CONSTANT ADMITTANCE	(-2.70, -2.39i)	(-2.65, -2.32i)
POWER OUT OF THE DRIVER	0.77	0.13
TOTAL POWER IN FAR FIELD	0.00079	0.00013

TABLE IV

STRAIGHT DUCT

Relative power normalized with respect to the hard walled radiated power

ka = 5.0

	Constant Phi on the Driver	Constant Velocity on the Driver
OPTIMUM ADMITTANCE DISTRIBUTION		
POWER OUT OF THE DRIVER	-0.0011	0.0075
TOTAL POWER IN FAR FIELD	0.00084	0.000011
ABSOLUTE CONSTANT ADMITTANCE	(-3.48, -1.66i)	(-4.61, -2.29i)
POWER OUT OF THE DRIVER	1.00	0.043
TOTAL POWER IN FAR FIELD	0.37	0.010
RELATIVE CONSTANT ADMITTANCE	(-4.13, -1.77i)	(-4.44, -2.38i)
POWER OUT OF THE DRIVER	1.06	0.043
TOTAL POWER IN FAR FIELD	0.37	0.010

TABLE V

STRAIGHT DUCT

Relative power normalized with respect to the hard walled radiated power

ka = 7.0

	Constant Phi on the Driver	Constant Velocity on the Driver
OPTIMUM ADMITTANCE DISTRIBUTION		
POWER OUT OF THE DRIVER	0.066	0.014
TOTAL POWER IN FAR FIELD	0.00064	0.054
ABSOLUTE CONSTANT ADMITTANCE	(-5.17, -1.95i)	(-4.72, -0.89i)
POWER OUT OF THE DRIVER	1.29	0.016
TOTAL POWER IN FAR FIELD	0.43	0.0078
RELATIVE CONSTANT ADMITTANCE	(-5.56, -1.30i)	(-3.97, -1.76i)
POWER OUT OF THE DRIVER	1.42	0.019
TOTAL POWER IN FAR FIELD	0.42	0.0086

TABLE VI

STRAIGHT DUCT

Relative power normalized with respect to the hard walled radiated power

ka = 10.0

	Constant Phi on the Driver	Constant Velocity on the Driver
OPTIMUM ADMITTANCE DISTRIBUTION		
POWER OUT OF THE DRIVER	0.050	0.00066
TOTAL POWER IN FAR FIELD	0.0049	0.00016
ABSOLUTE CONSTANT ADMITTANCE	(-5.65, -2.80i)	(-4.89, -2.69i)
POWER OUT OF THE DRIVER	1.02	0.010
TOTAL POWER IN FAR FIELD	0.48	0.0051
RELATIVE CONSTANT ADMITTANCE	(-5.41, -2.75i)	(-5.02, -2.83i)
POWER OUT OF THE DRIVER	1.02	0.010
TOTAL POWER IN FAR FIELD	0.48	0.0051

TABLE VII

NASA QCSEE INLET

Relative power normalized with respect to the hard walled radiated power

ka = 1.0

	Constant Phi on the Driver	Constant Velocity on the Driver
OPTIMUM ADMITTANCE DISTRIBUTION		
POWER OUT OF THE DRIVER	-1.91	-2.45
TOTAL POWER IN FAR FIELD	0.00012	0.00012
ABSOLUTE CONSTANT ADMITTANCE	(-0.64, 4.03i)	(-0.65, 4.11i)
POWER OUT OF THE DRIVER	-1.25	-0.74
TOTAL POWER IN FAR FIELD	0.0015	0.00082
RELATIVE CONSTANT ADMITTANCE	(-0.47, -3.78i)	(-0.53, -3.77i)
POWER OUT OF THE DRIVER	1.27	0.79
TOTAL POWER IN FAR FIELD	0.0019	0.0011

TABLE VIII

NASA QCSEE INLET

Relative power normalized with respect to the hard walled radiated power

ka = 2.0

	Constant Phi on the Driver	Constant Velocity on the Driver
OPTIMUM ADMITTANCE DISTRIBUTION		
POWER OUT OF THE DRIVER	-1.11	-0.70
TOTAL POWER IN FAR FIELD	0.00011	0.000060
ABSOLUTE CONSTANT ADMITTANCE	(-2.99, 3.91i)	(-3.06, 3.58i)
POWER OUT OF THE DRIVER	-0.79	-0.53
TOTAL POWER IN FAR FIELD	0.00074	0.00025
RELATIVE CONSTANT ADMITTANCE	(-2.35, -3.91i)	(-2.36, -3.93i)
POWER OUT OF THE DRIVER	0.82	0.59
TOTAL POWER IN FAR FIELD	0.0013	0.00094

TABLE IX

NASA QCSEE INLET

Relative power normalized with respect to the hard walled radiated power

ka = 3.0

	Constant Phi on the Driver	Constant Velocity on the Driver
OPTIMUM ADMITTANCE DISTRIBUTION		
POWER OUT OF THE DRIVER	-3.69	-0.050
TOTAL POWER IN FAR FIELD	0.0096	0.000049
ABSOLUTE CONSTANT ADMITTANCE	(-3.10, -3.20i)	(-3.00, -3.19i)
POWER OUT OF THE DRIVER	0.69	0.18
TOTAL POWER IN FAR FIELD	0.00045	0.00020
RELATIVE CONSTANT ADMITTANCE	(-3.04, -3.20i)	(-3.05, -3.18i)
POWER OUT OF THE DRIVER	0.69	0.18
TOTAL POWER IN FAR FIELD	0.00061	0.00015

TABLE X

NASA QCSEE INLET

Relative power normalized with respect to the hard walled radiated power

ka = 5.0

	Constant Phi on the Driver	Constant Velocity on the Driver
OPTIMUM ADMITTANCE DISTRIBUTION		
POWER OUT OF THE DRIVER	-0.023	0.00059
TOTAL POWER IN FAR FIELD	0.00040	0.000031
ABSOLUTE CONSTANT ADMITTANCE	(-4.20, -1.80i)	(-4.57, -1.89i)
POWER OUT OF THE DRIVER	0.80	0.040
TOTAL POWER IN FAR FIELD	0.13	0.0065
RELATIVE CONSTANT ADMITTANCE	(-4.26, -1.96i)	(-4.37, -1.87i)
POWER OUT OF THE DRIVER	0.81	0.041
TOTAL POWER IN FAR FIELD	0.13	0.0066

TABLE XI

NASA QCSEE INLET

Relative power normalized with respect to the hard walled radiated power

ka = 7.0

	Constant Phi on the Driver	Constant Velocity on the Driver
OPTIMUM ADMITTANCE DISTRIBUTION		
POWER OUT OF THE DRIVER	0.56	0.0066
TOTAL POWER IN FAR FIELD	0.13	0.00013
ABSOLUTE CONSTANT ADMITTANCE	(-----, -----i)	(-5.42, -2.57i)
POWER OUT OF THE DRIVER	----	0.018
TOTAL POWER IN FAR FIELD	----	0.0022
RELATIVE CONSTANT ADMITTANCE	(-----, -----i)	(-5.28, -2.56i)
POWER OUT OF THE DRIVER	----	0.018
TOTAL POWER IN FAR FIELD	----	0.0022

TABLE XII

NASA QCSEE INLET

Relative power normalized with respect to the hard walled radiated power

ka = 10.0

	Constant Phi on the Driver	Constant Velocity on the Driver
OPTIMUM ADMITTANCE DISTRIBUTION		
POWER OUT OF THE DRIVER	0.29	0.010
TOTAL POWER IN FAR FIELD	0.00075	0.000064
ABSOLUTE CONSTANT ADMITTANCE	(-4.32, -3.83i)	(-4.02, -3.56i)
POWER OUT OF THE DRIVER	0.94	0.010
TOTAL POWER IN FAR FIELD	0.22	0.0026
RELATIVE CONSTANT ADMITTANCE	(-4.27, -3.78i)	(-4.05, -3.60i)
POWER OUT OF THE DRIVER	0.94	0.010
TOTAL POWER IN FAR FIELD	0.22	0.0026

TABLE XIII

QCSEE INLET LESS CENTERBODY

Relative power normalized with respect to the hard walled radiated power

ka = 1.0

	Constant Phi on the Driver	Constant Velocity on the Driver
OPTIMUM ADMITTANCE DISTRIBUTION		
POWER OUT OF THE DRIVER	-1.20	-1.78
TOTAL POWER IN FAR FIELD	0.000025	0.000072
ABSOLUTE CONSTANT ADMITTANCE	(0.81, 4.68i)	(-0.75, 4.72i)
POWER OUT OF THE DRIVER	-1.19	-1.06
TOTAL POWER IN FAR FIELD	0.0021	0.00091
RELATIVE CONSTANT ADMITTANCE	(-0.73, -3.49i)	(-0.79, -3.44i)
POWER OUT OF THE DRIVER	1.71	1.33
TOTAL POWER IN FAR FIELD	0.0029	0.0023

TABLE XIV

QCSEE INLET LESS CENTERBODY

Relative power normalized with respect to the hard walled radiated power

ka = 2.0

	Constant Phi on the Driver	Constant Velocity on the Driver
OPTIMUM ADMITTANCE DISTRIBUTION		
POWER OUT OF THE DRIVER	-0.56	-0.50
TOTAL POWER IN FAR FIELD	0.000044	0.000049
ABSOLUTE CONSTANT ADMITTANCE	(-2.99, 3.73i)	(-2.99, 3.41i)
POWER OUT OF THE DRIVER	-0.74	-0.65
TOTAL POWER IN FAR FIELD	0.00058	0.00025
RELATIVE CONSTANT ADMITTANCE	(-2.42, -3.78i)	(-2.45, -3.79i)
POWER OUT OF THE DRIVER	0.76	0.71
TOTAL POWER IN FAR FIELD	0.0011	0.00093

TABLE XV

QCSEE INLET LESS CENTERBODY

Relative power normalized with respect to the hard walled radiated power

ka = 3.0

	Constant Phi on the Driver	Constant Velocity on the Driver
OPTIMUM ADMITTANCE DISTRIBUTION		
POWER OUT OF THE DRIVER	-0.41	-0.024
TOTAL POWER IN FAR FIELD	0.000084	0.000032
ABSOLUTE CONSTANT ADMITTANCE	(-3.06, 2.94i)	(-2.88, -3.02i)
POWER OUT OF THE DRIVER	-0.67	0.13
TOTAL POWER IN FAR FIELD	0.000087	0.000094
RELATIVE CONSTANT ADMITTANCE	(-2.90, -3.07i)	(-2.91, -2.97i)
POWER OUT OF THE DRIVER	0.69	0.13
TOTAL POWER IN FAR FIELD	0.00047	0.000063

TABLE XVI

QCSEE INLET LESS CENTERBODY

Relative power normalized with respect to the hard walled radiated power

ka = 5.0

	Constant Phi on the Driver	Constant Velocity on the Driver
OPTIMUM ADMITTANCE DISTRIBUTION		
POWER OUT OF THE DRIVER	0.098	0.0069
TOTAL POWER IN FAR FIELD	0.00077	0.0000071
ABSOLUTE CONSTANT ADMITTANCE	(-3.89, -1.65i)	(-3.93, -2.39i)
POWER OUT OF THE DRIVER	0.74	0.044
TOTAL POWER IN FAR FIELD	0.20	0.0042
RELATIVE CONSTANT ADMITTANCE	(-3.87, -1.98i)	(-3.88, -2.24i)
POWER OUT OF THE DRIVER	0.77	0.044
TOTAL POWER IN FAR FIELD	0.21	0.0042

TABLE XVII

QCSEE INLET LESS CENTERBODY

Relative power normalized with respect to the hard walled radiated power

ka = 7.0

	Constant Phi on the Driver	Constant Velocity on the Driver
OPTIMUM ADMITTANCE DISTRIBUTION		
POWER OUT OF THE DRIVER	0.14	0.0091
TOTAL POWER IN FAR FIELD	0.0016	0.00028
ABSOLUTE CONSTANT ADMITTANCE	(-4.77, -2.07i)	(-7.32, -1.67i)
POWER OUT OF THE DRIVER	1.02	0.020
TOTAL POWER IN FAR FIELD	0.29	0.0058
RELATIVE CONSTANT ADMITTANCE	(-4.87, -2.06i)	(-6.84, -1.57i)
POWER OUT OF THE DRIVER	1.02	0.021
TOTAL POWER IN FAR FIELD	0.29	0.0062

TABLE XVIII

QCSEE INLET LESS CENTERBODY

Relative power normalized with respect to the hard walled radiated power

ka = 10.0

	Constant Phi on the Driver	Constant Velocity on the Driver
OPTIMUM ADMITTANCE DISTRIBUTION		
POWER OUT OF THE DRIVER	0.33	0.00060
TOTAL POWER IN FAR FIELD	0.16	0.000060
ABSOLUTE CONSTANT ADMITTANCE	(-5.27, -3.01i)	(-4.38, -3.18i)
POWER OUT OF THE DRIVER	0.97	0.010
TOTAL POWER IN FAR FIELD	0.36	0.0039
RELATIVE CONSTANT ADMITTANCE	(-5.05, -2.91i)	(-4.49, -3.30i)
POWER OUT OF THE DRIVER	0.98	0.010
TOTAL POWER IN FAR FIELD	0.36	0.0039

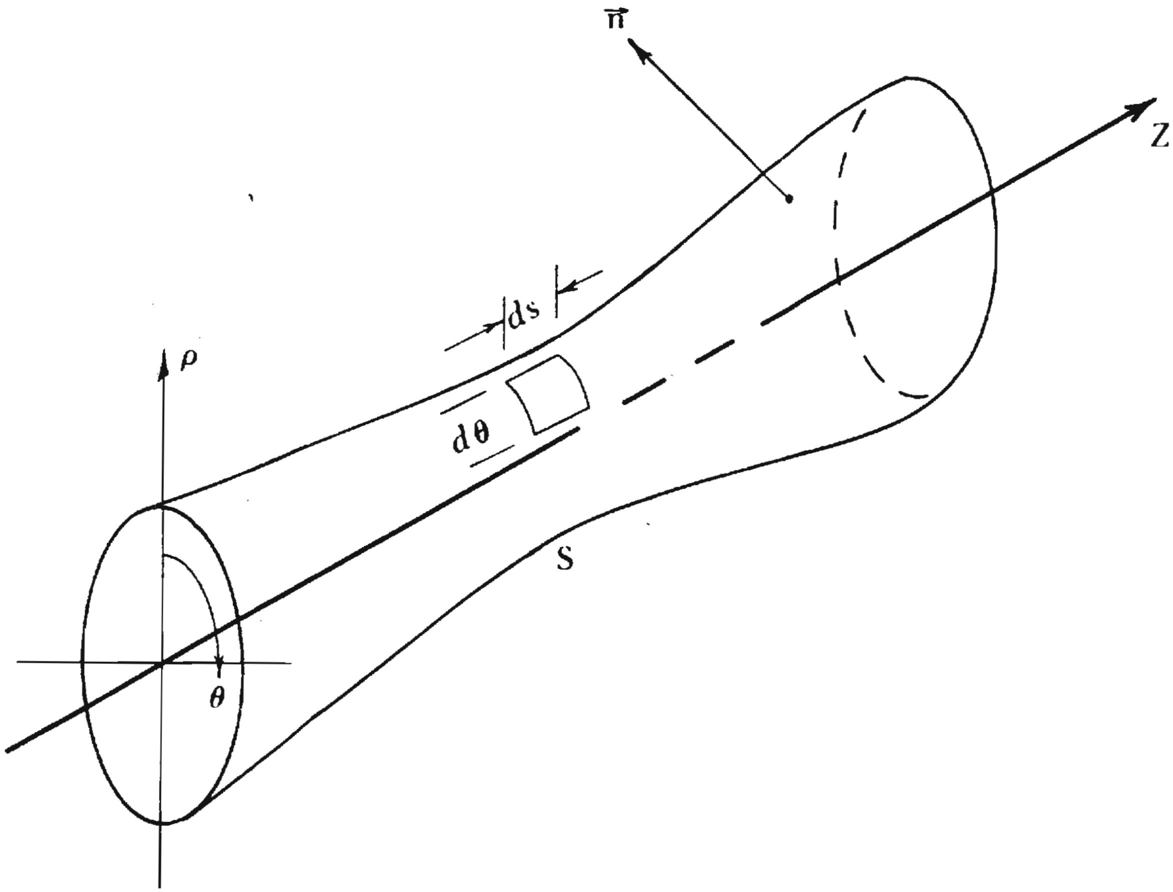

Figure 1. (ρ, Z, Θ) coordinate system for a body of revolution

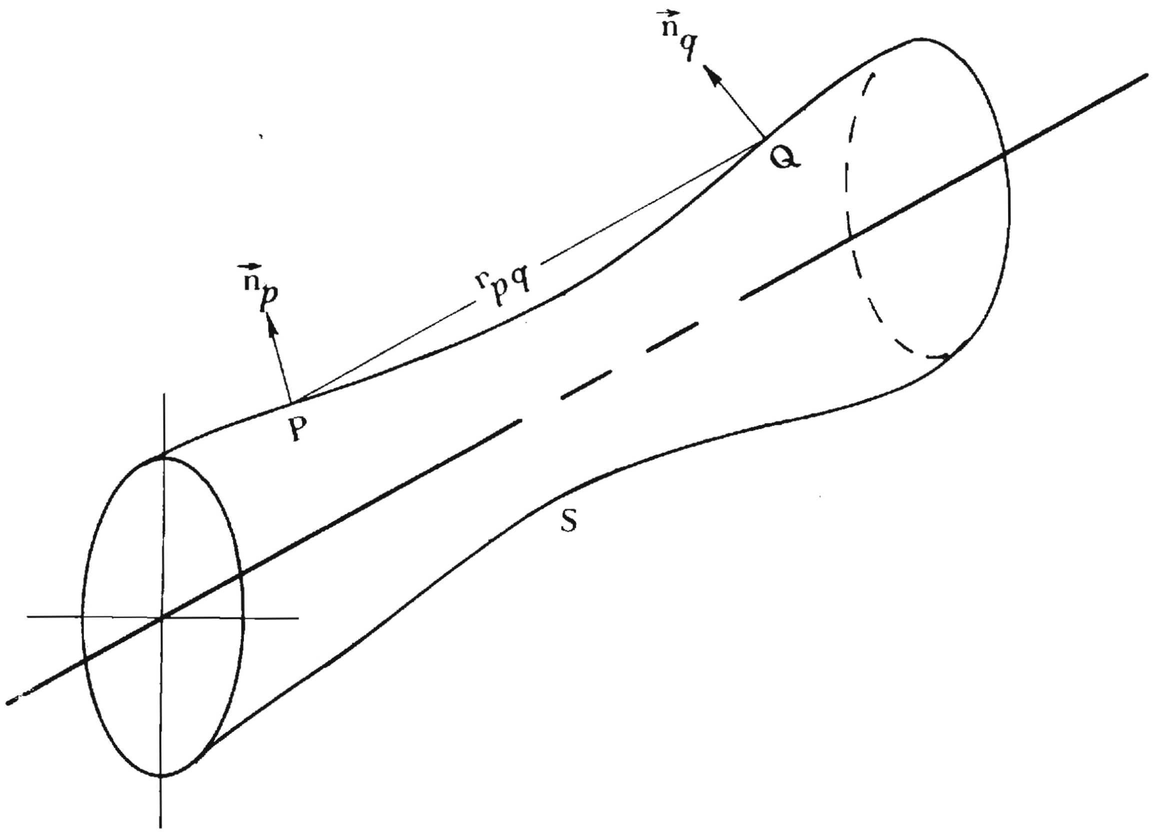

Figure 2. Body S showing P and Q points, the distance between them r_{pq} and their outward normals

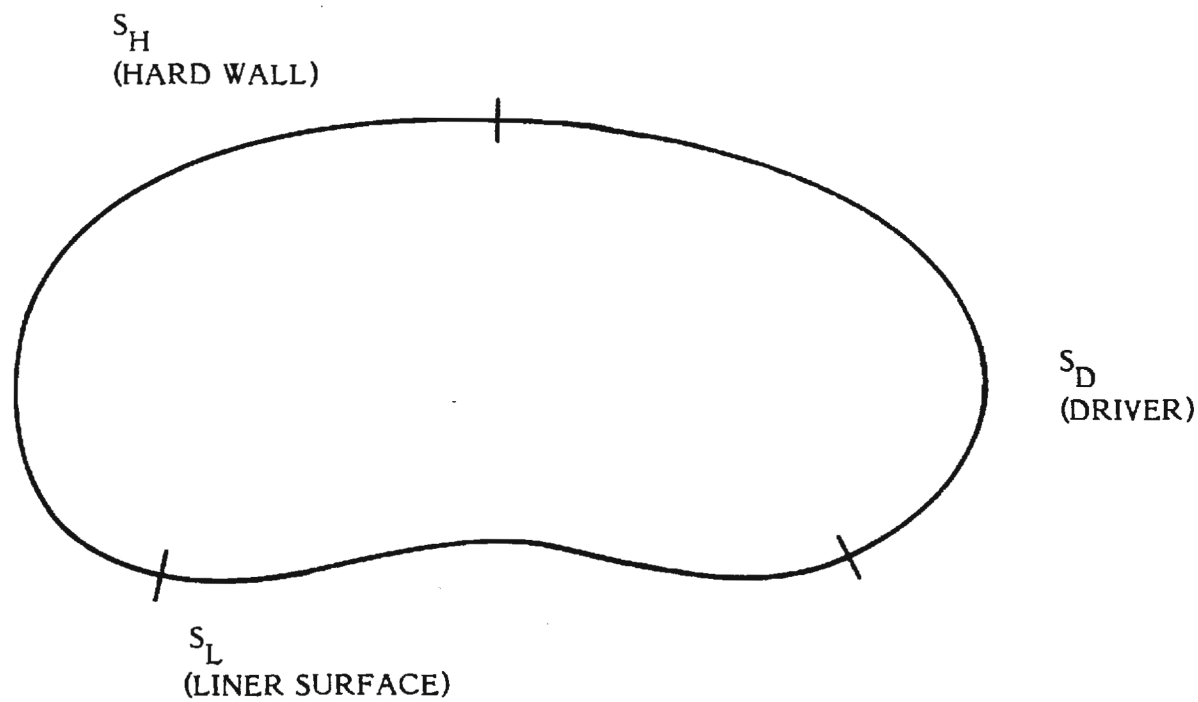

Figure 3. The three types of regions on the body

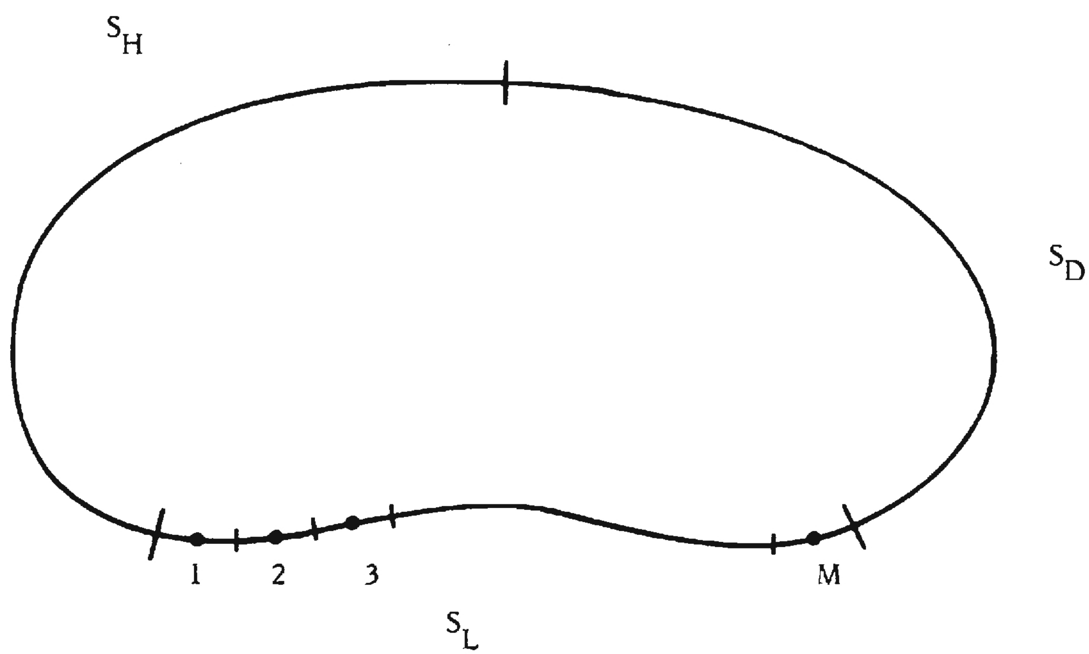

Figure 4. Liner surface divided into M finite regions.

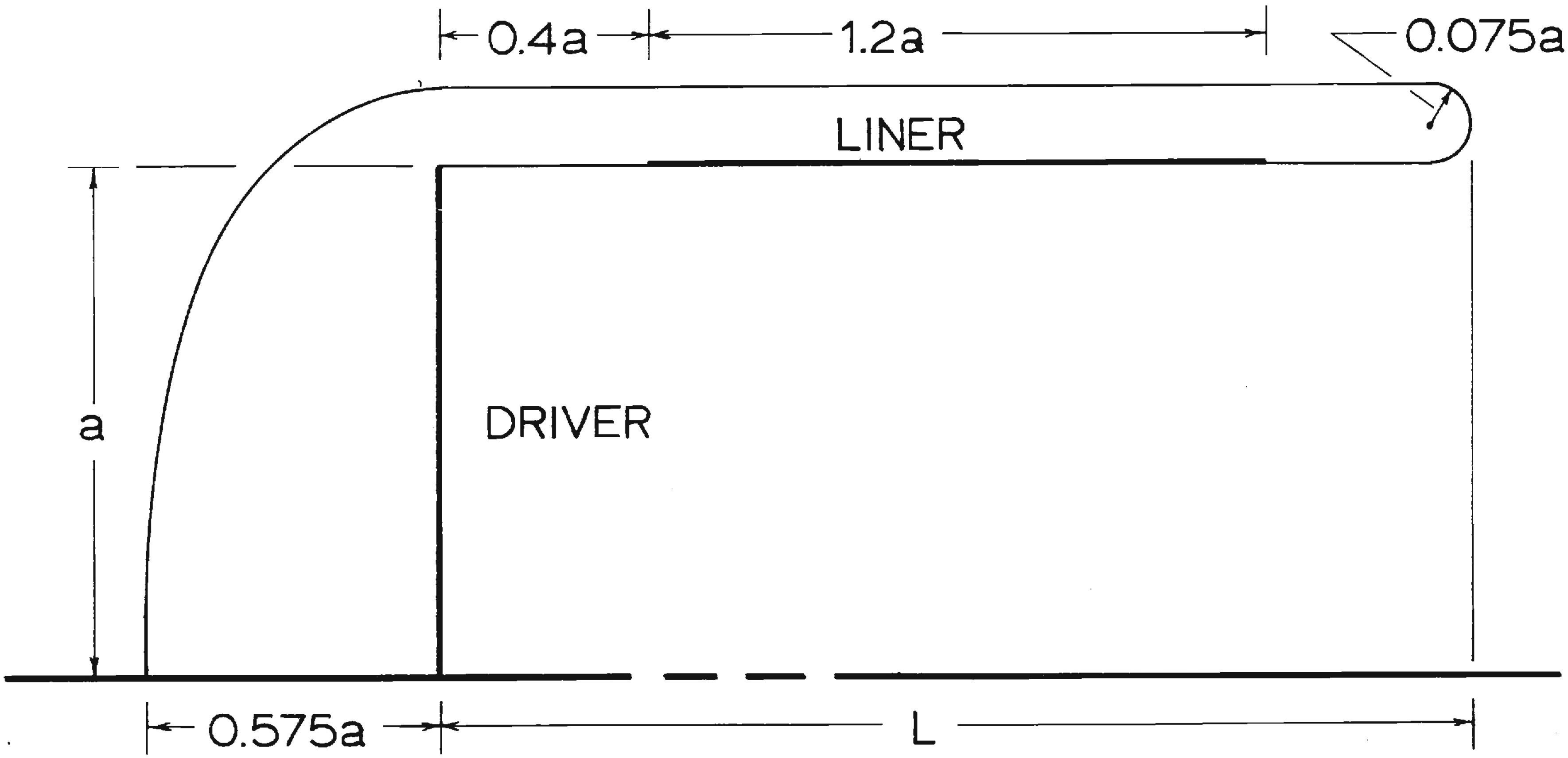

Figure 5. Straight Duct

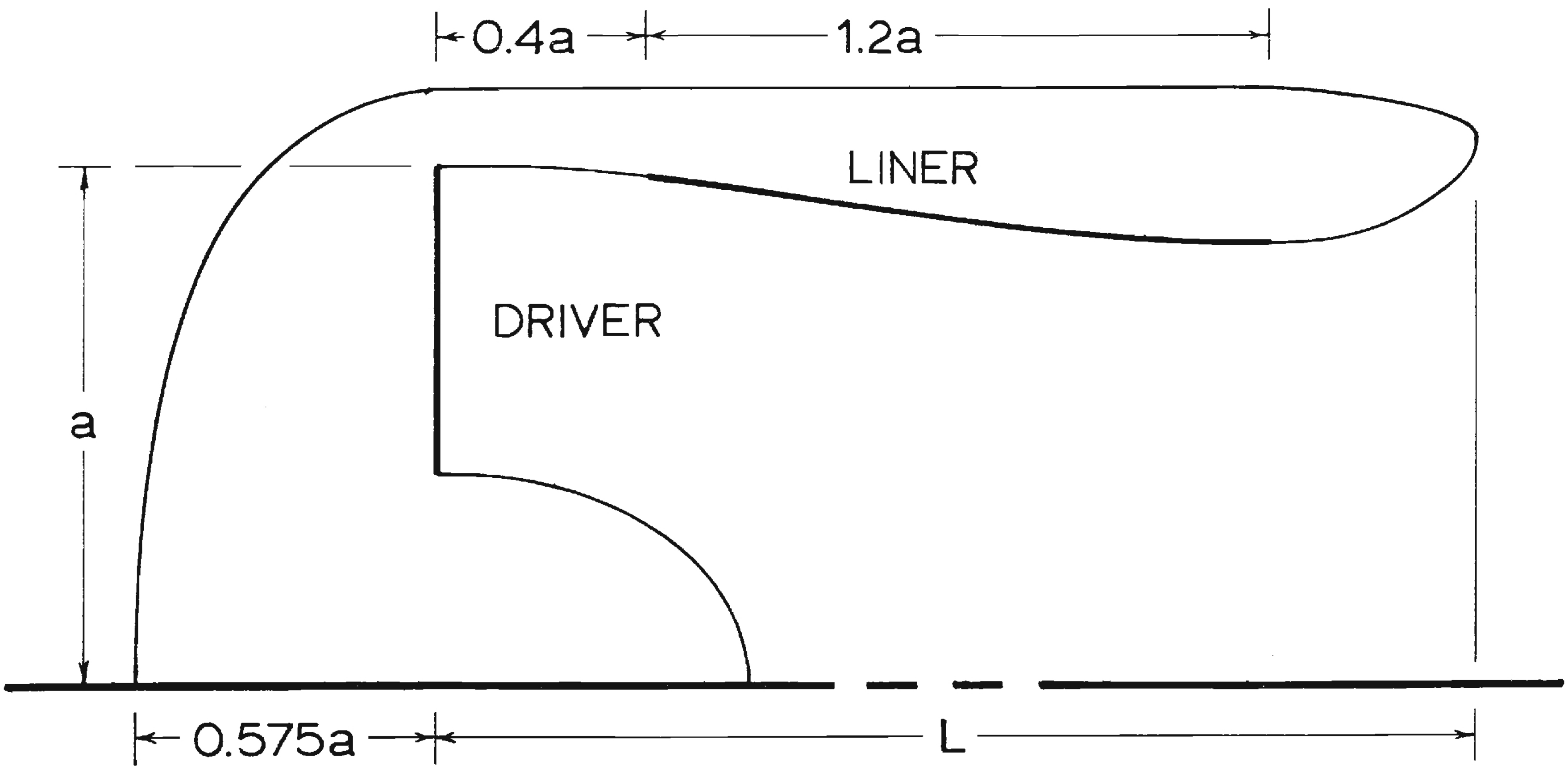

Figure 6. QCSEE Inlet

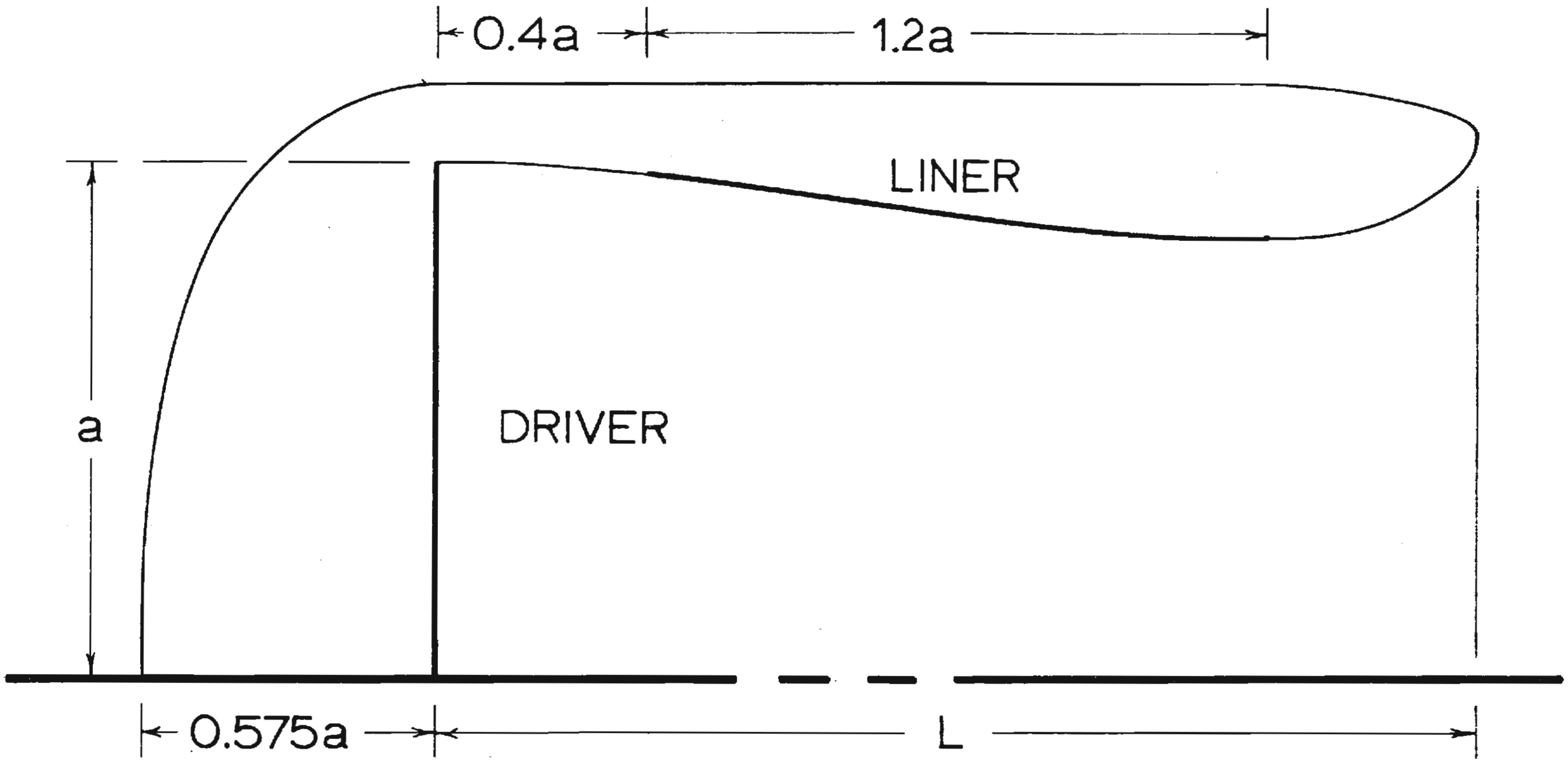

Figure 7. QCSEE inlet less centerbody

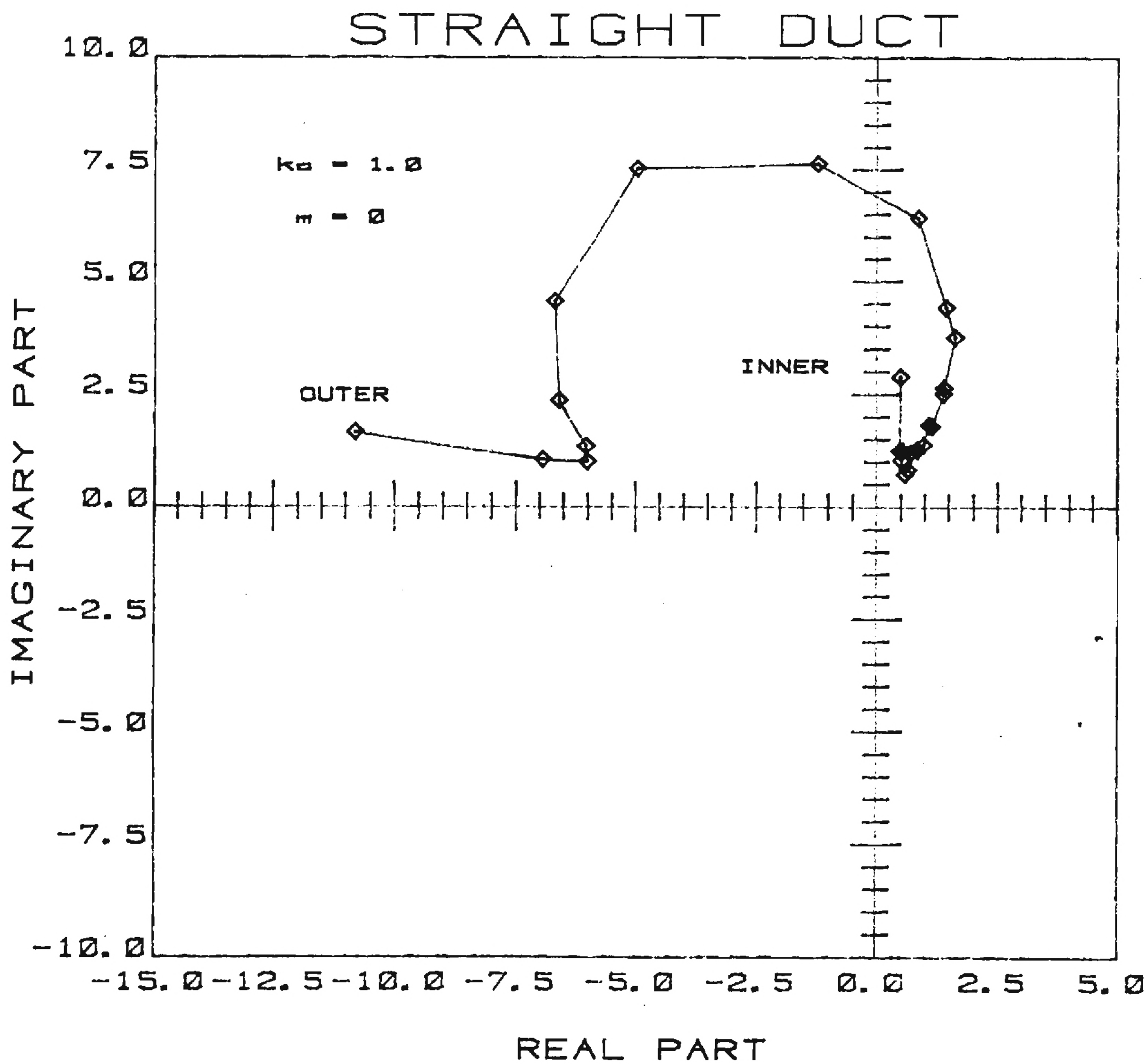

OPTIMUM ADMITTANCE DISTRIBUTION

Constant Phi on the Driver

Figure 8a

STRAIGHT DUCT, KA=1.0, PHI SPECIFIED ON THE DRIVER
(ABSOLUTE POWER)

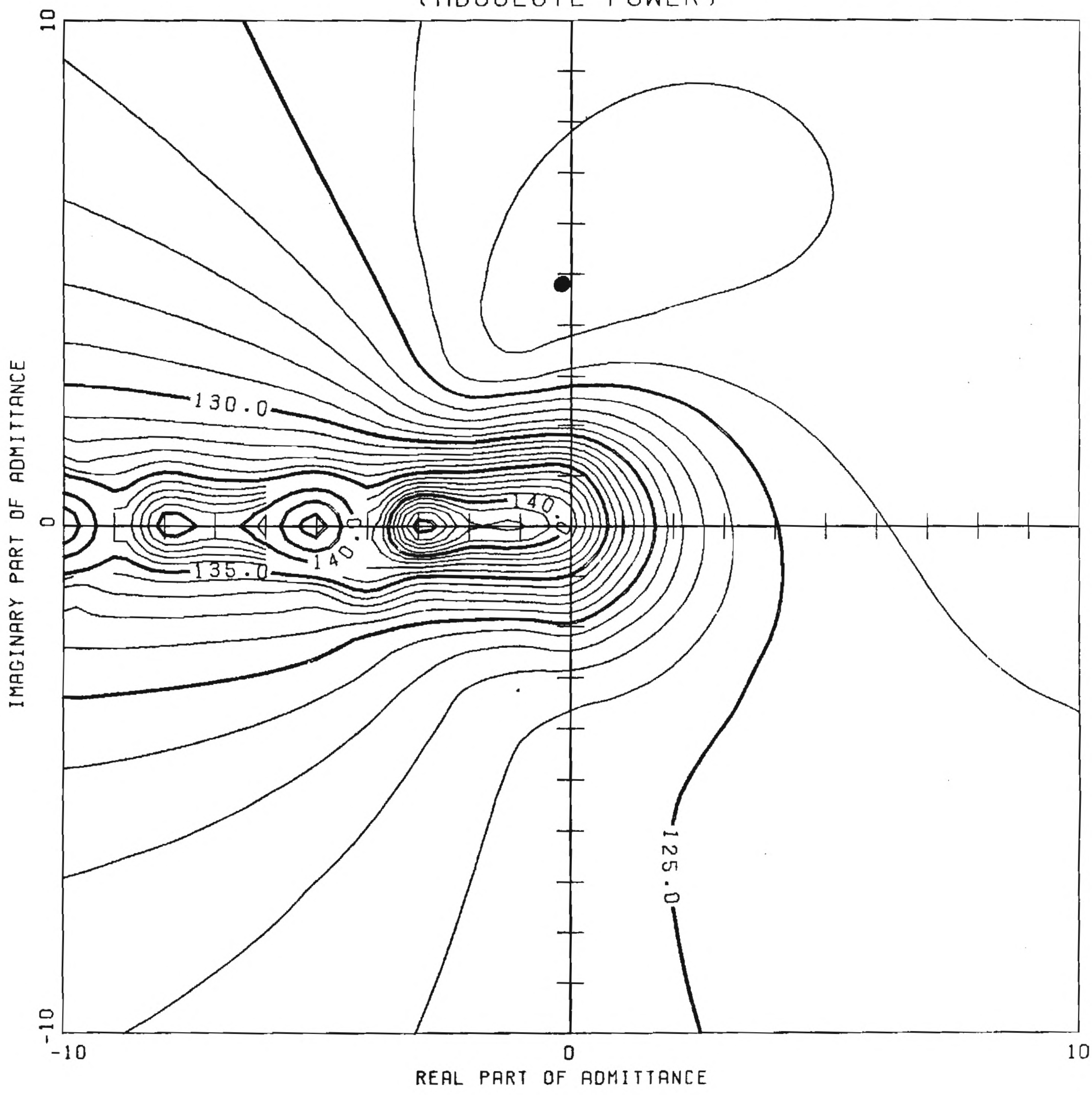

Figure 8b

STRAIGHT DUCT, KA=1.0, PHI SPECIFIED ON THE DRIVER
(RELATIVE POWER)

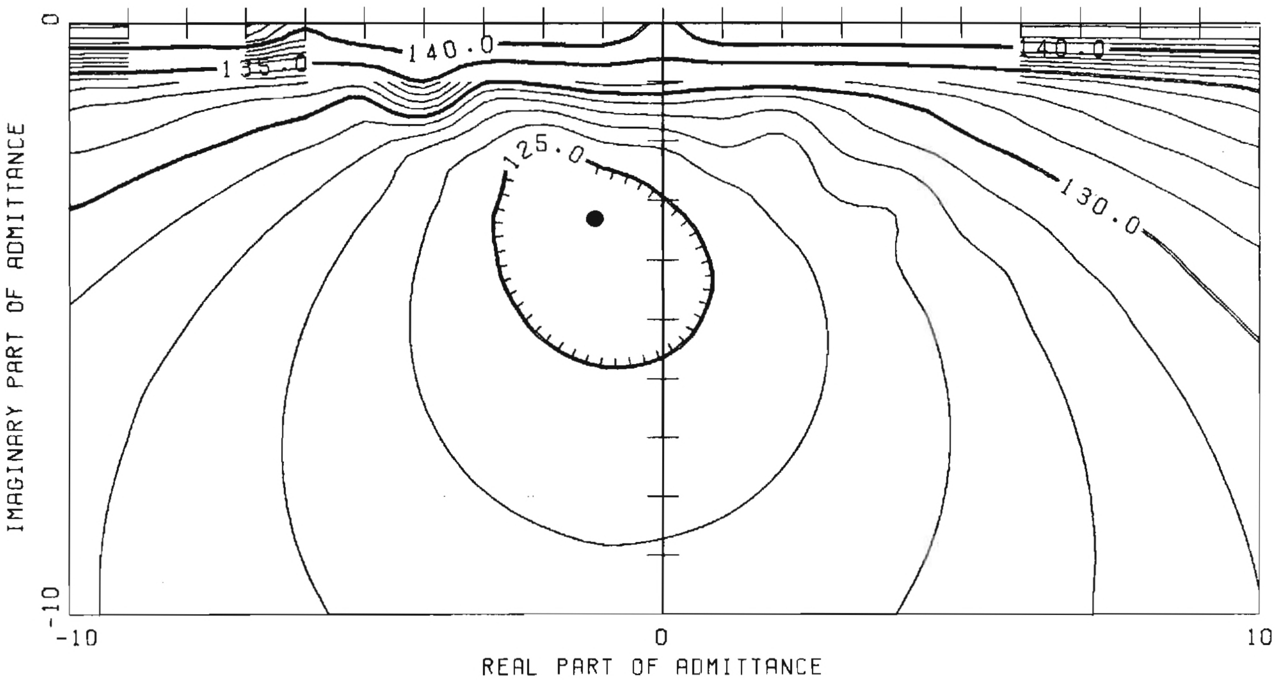

Figure 8c

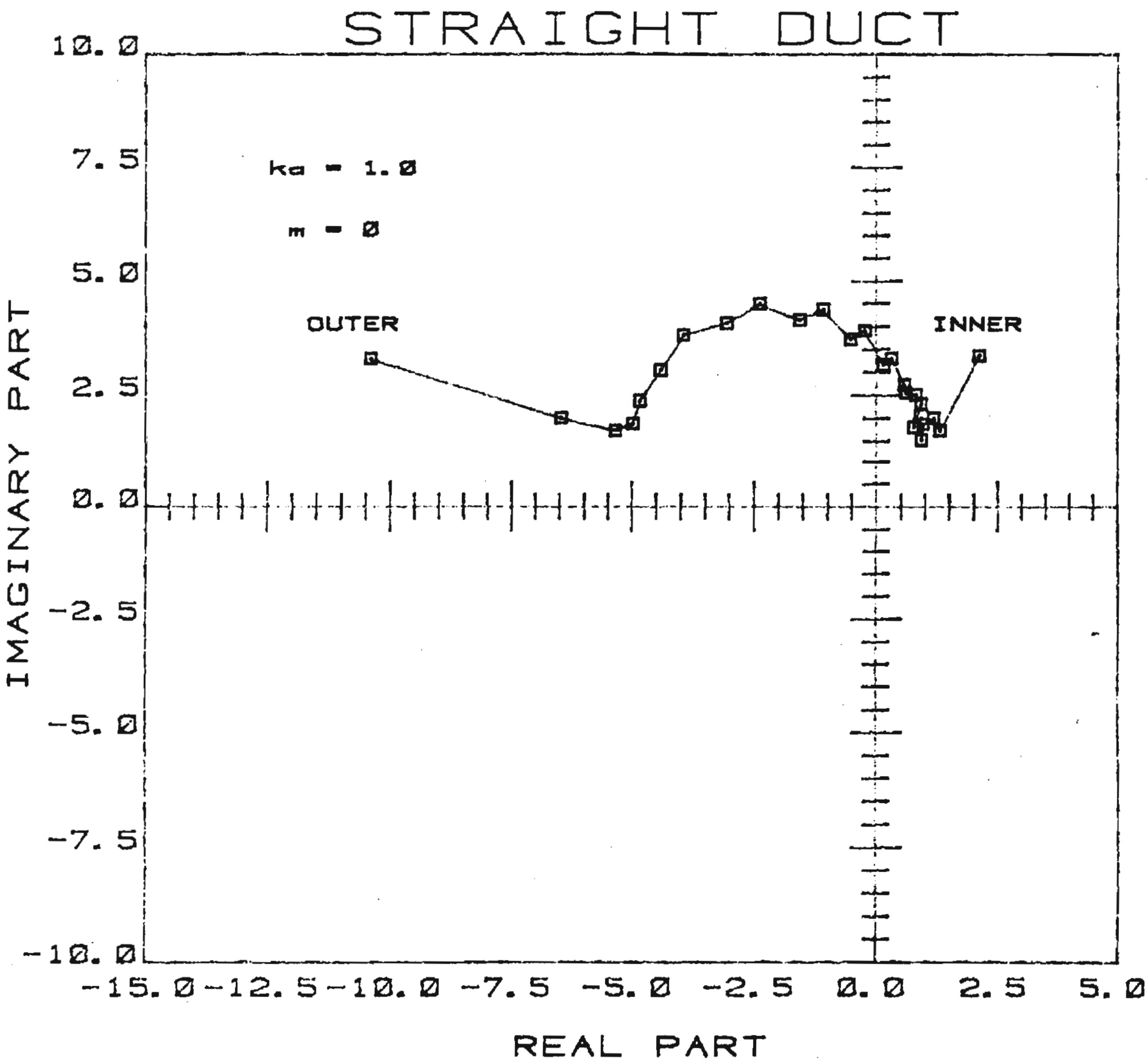

OPTIMUM ADMITTANCE DISTRIBUTION

Constant Velocity on the Driver

Figure 8d

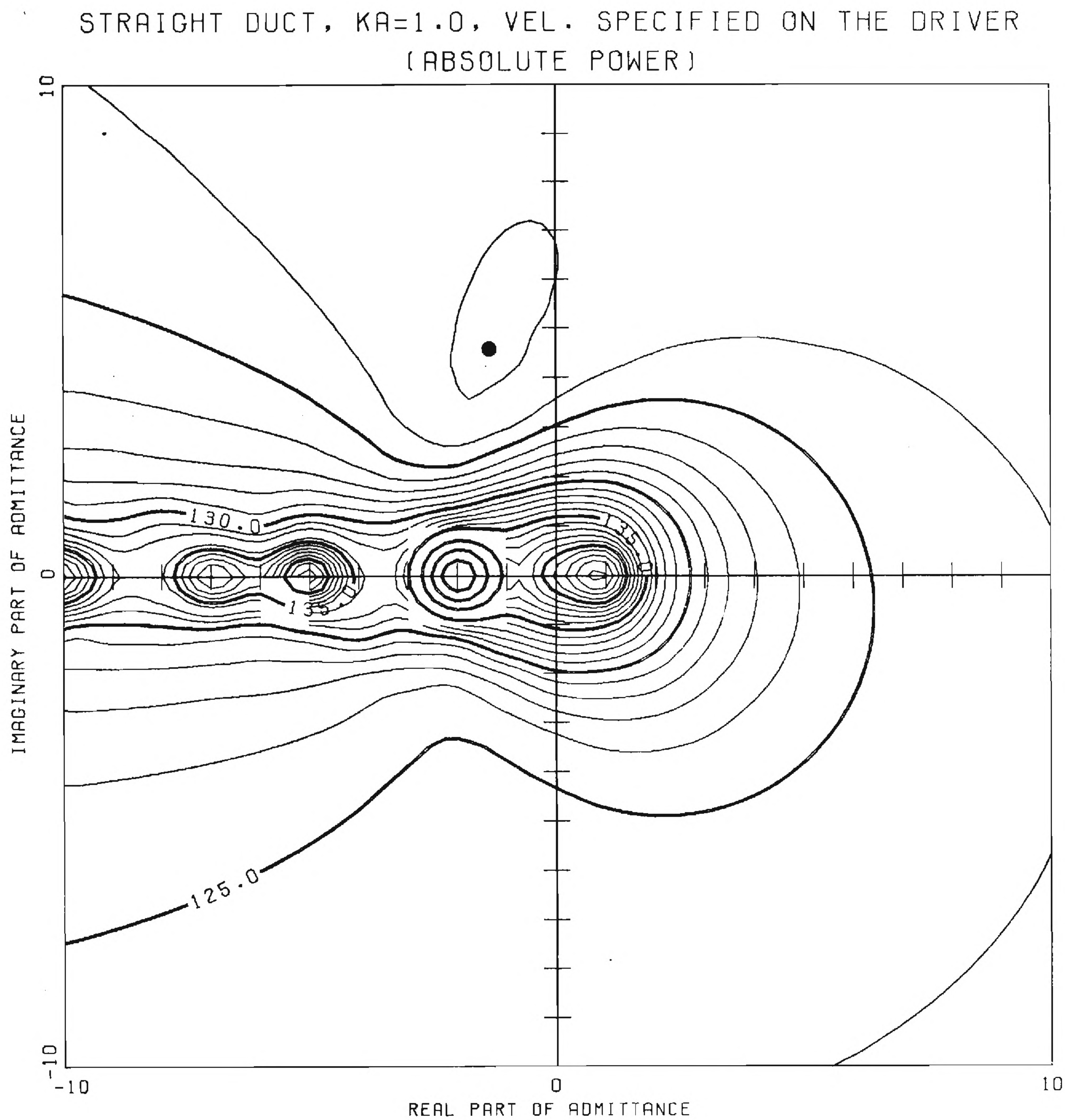
STRAIGHT DUCT, KA=1.0, VEL. SPECIFIED ON THE DRIVER
(ABSOLUTE POWER)
130.0
135.0
135
125.0
10
0
-10
-10
0
10
IMAGINARY PART OF ADMITTANCE
REAL PART OF ADMITTANCE

Figure 8e

STRAIGHT DUCT, KA=1.0, VEL. SPECIFIED ON THE DRIVER
(RELATIVE POWER)

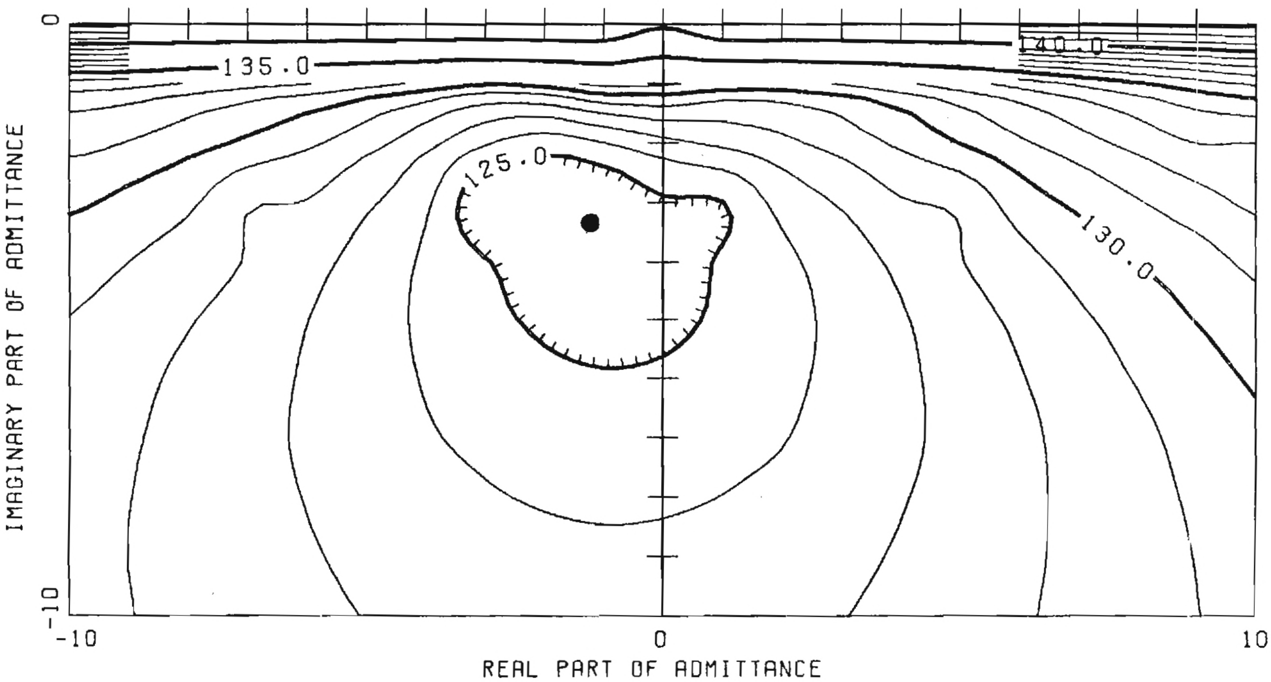

Figure 8f

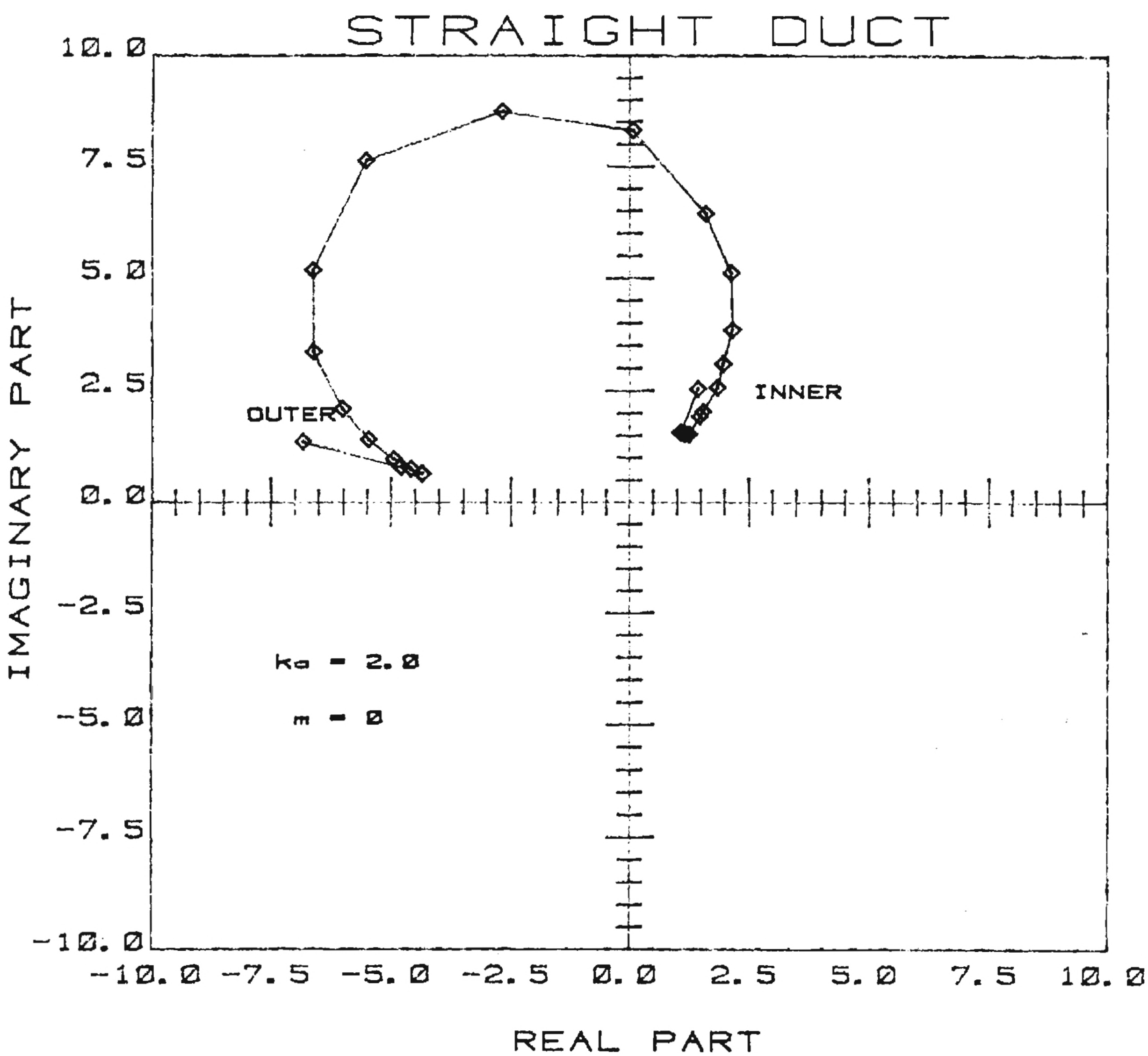

OPTIMUM ADMITTANCE DISTRIBUTION

Constant Phi on the Driver

Figure 9a

STRAIGHT DUCT, KA=2.0, PHI SPECIFIED ON THE DRIVER
(ABSOLUTE POWER)

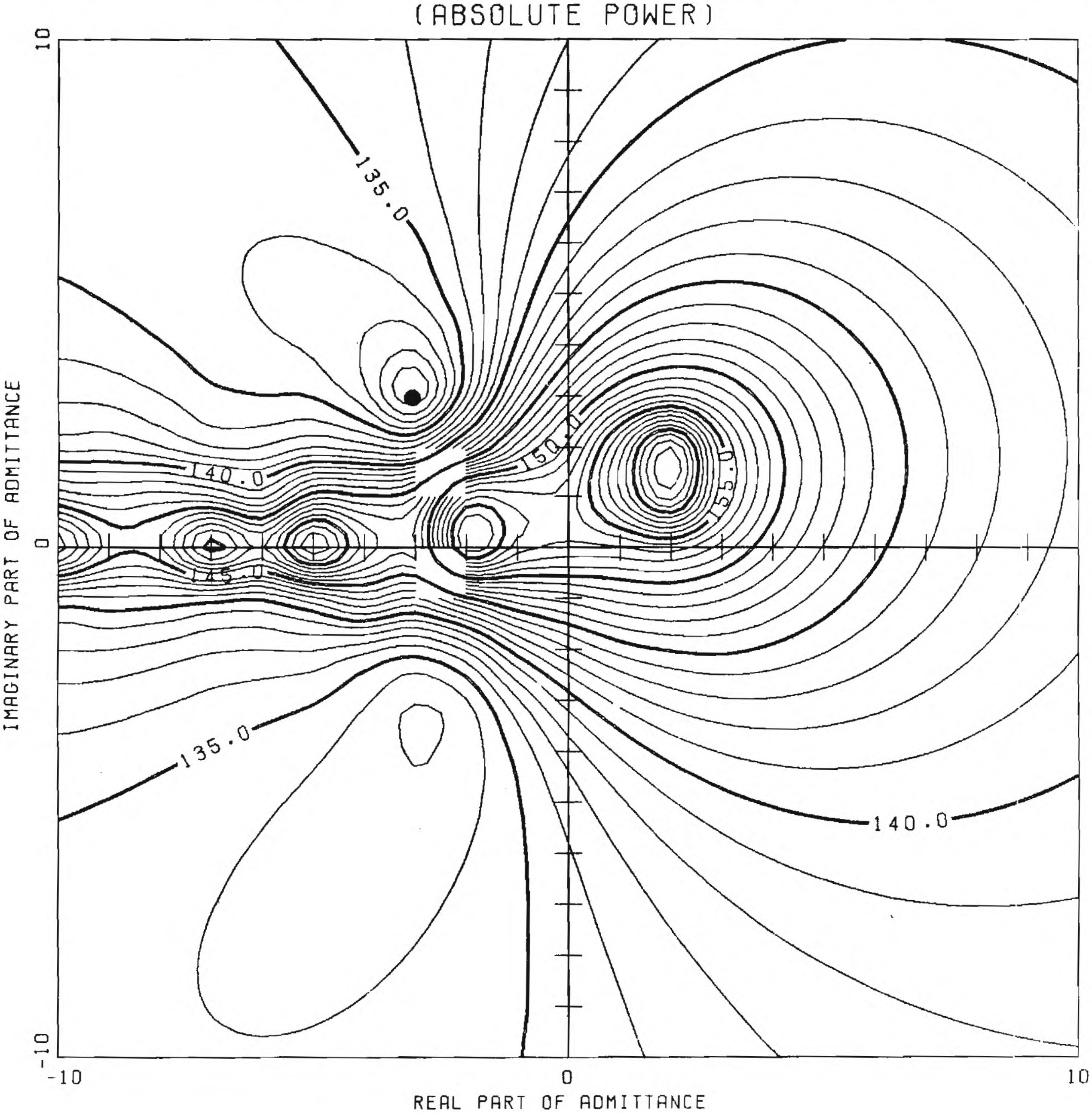

Figure 9b

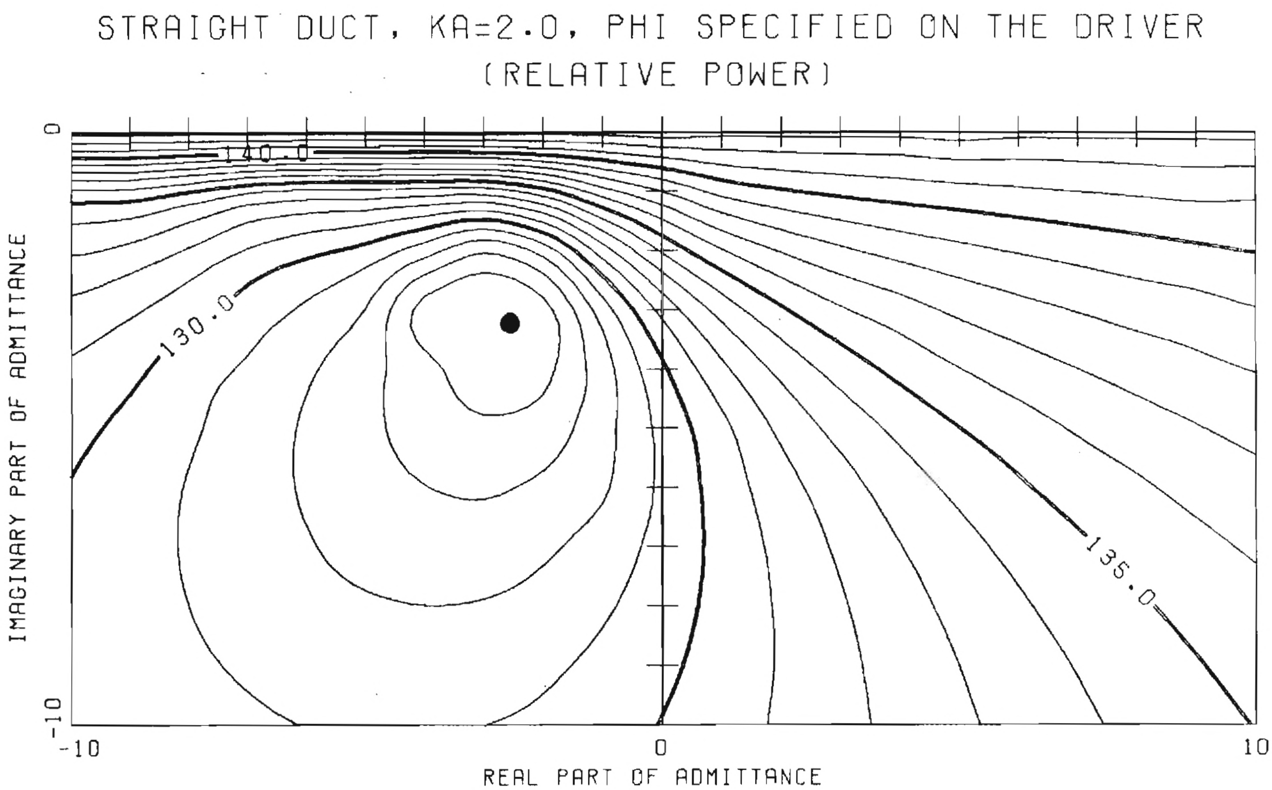
STRAIGHT DUCT, KA=2.0, PHI SPECIFIED ON THE DRIVER
(RELATIVE POWER)
140.0
130.0
135.0
IMAGINARY PART OF ADMITTANCE
0
-10
-10
0
10
REAL PART OF ADMITTANCE

Figure 9c

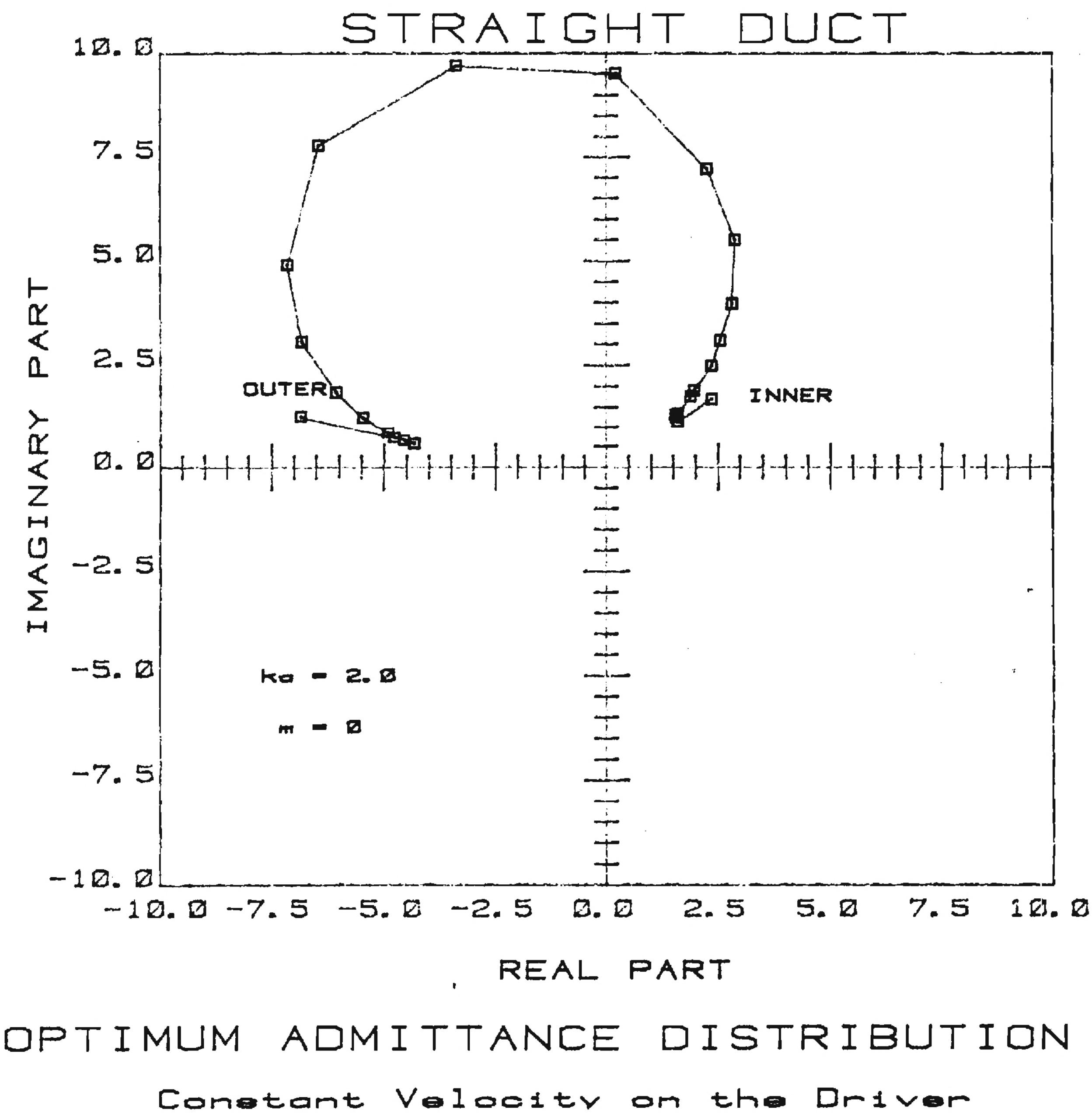
STRAIGHT DUCT
10.0
7.5
5.0
2.5
0.0
-2.5
-5.0
-7.5
-10.0
IMAGINARY PART
OUTER
INNER
ka = 2.0
m = 0
-10.0 -7.5 -5.0 -2.5 0.0 2.5 5.0 7.5 10.0
REAL PART
OPTIMUM ADMITTANCE DISTRIBUTION
Constant Velocity on the Driver

Figure 9d

STRAIGHT DUCT, KA=2.0, VEL. SPECIFIED ON THE DRIVER
(ABSOLUTE POWER)

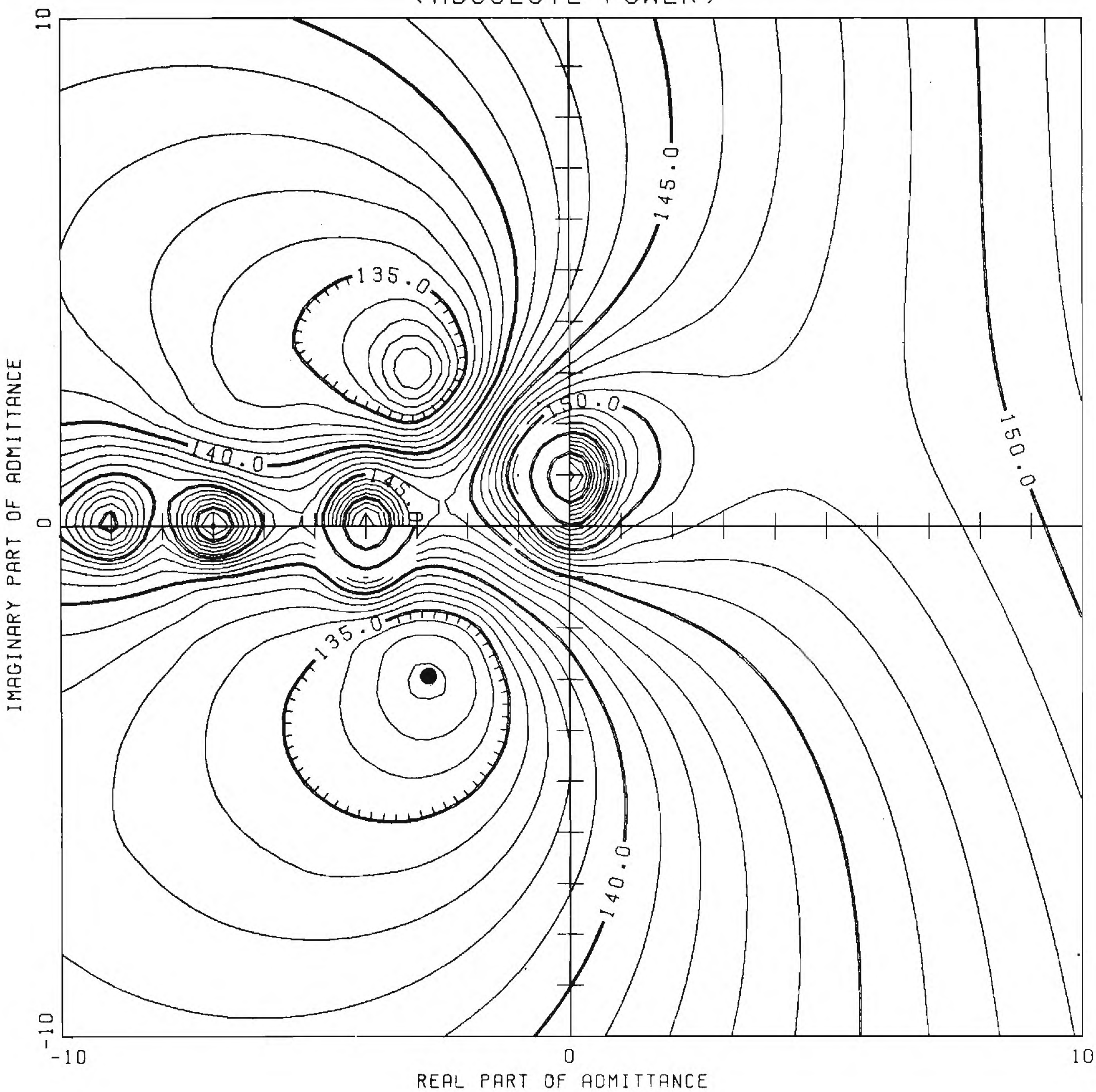

Figure 9e

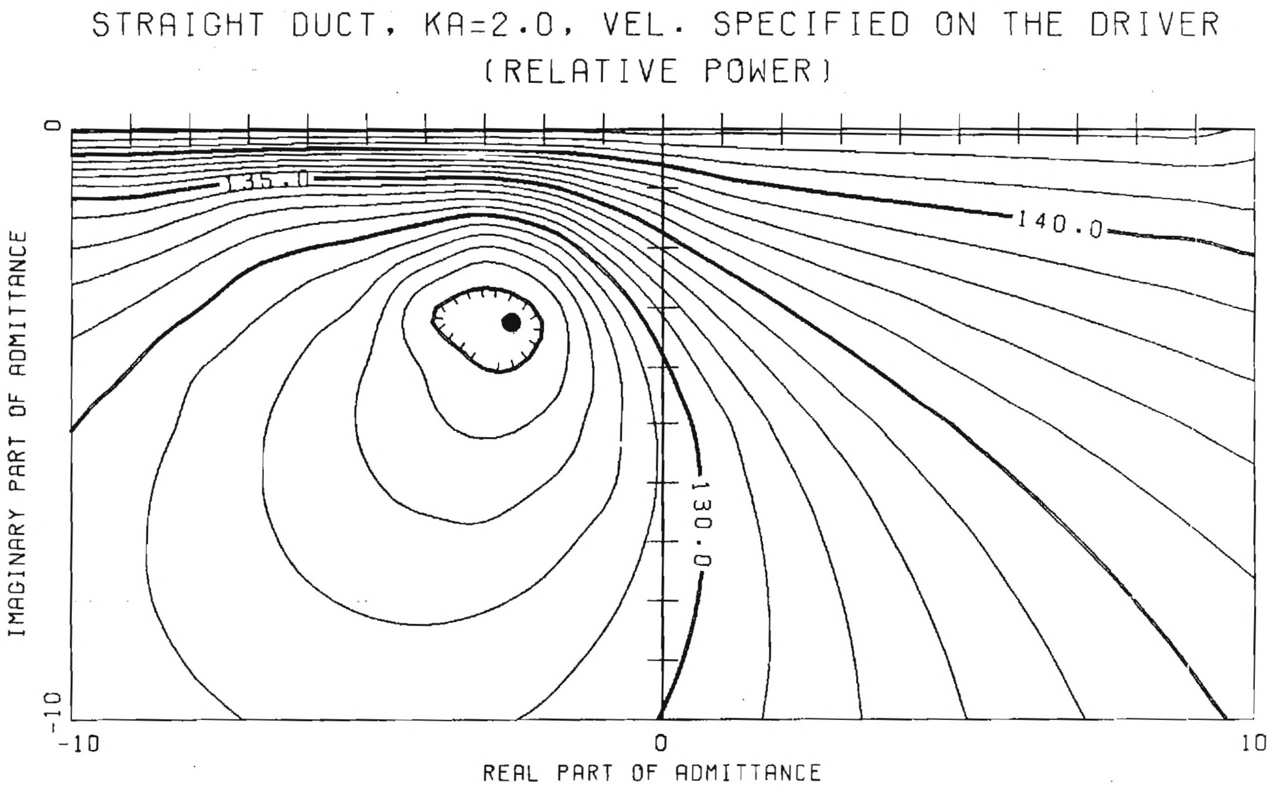
STRAIGHT DUCT, KA=2.0, VEL. SPECIFIED ON THE DRIVER
(RELATIVE POWER)
135.0
140.0
130.0
IMAGINARY PART OF ADMITTANCE
0
-10
-10
0
10
REAL PART OF ADMITTANCE

Figure 9f

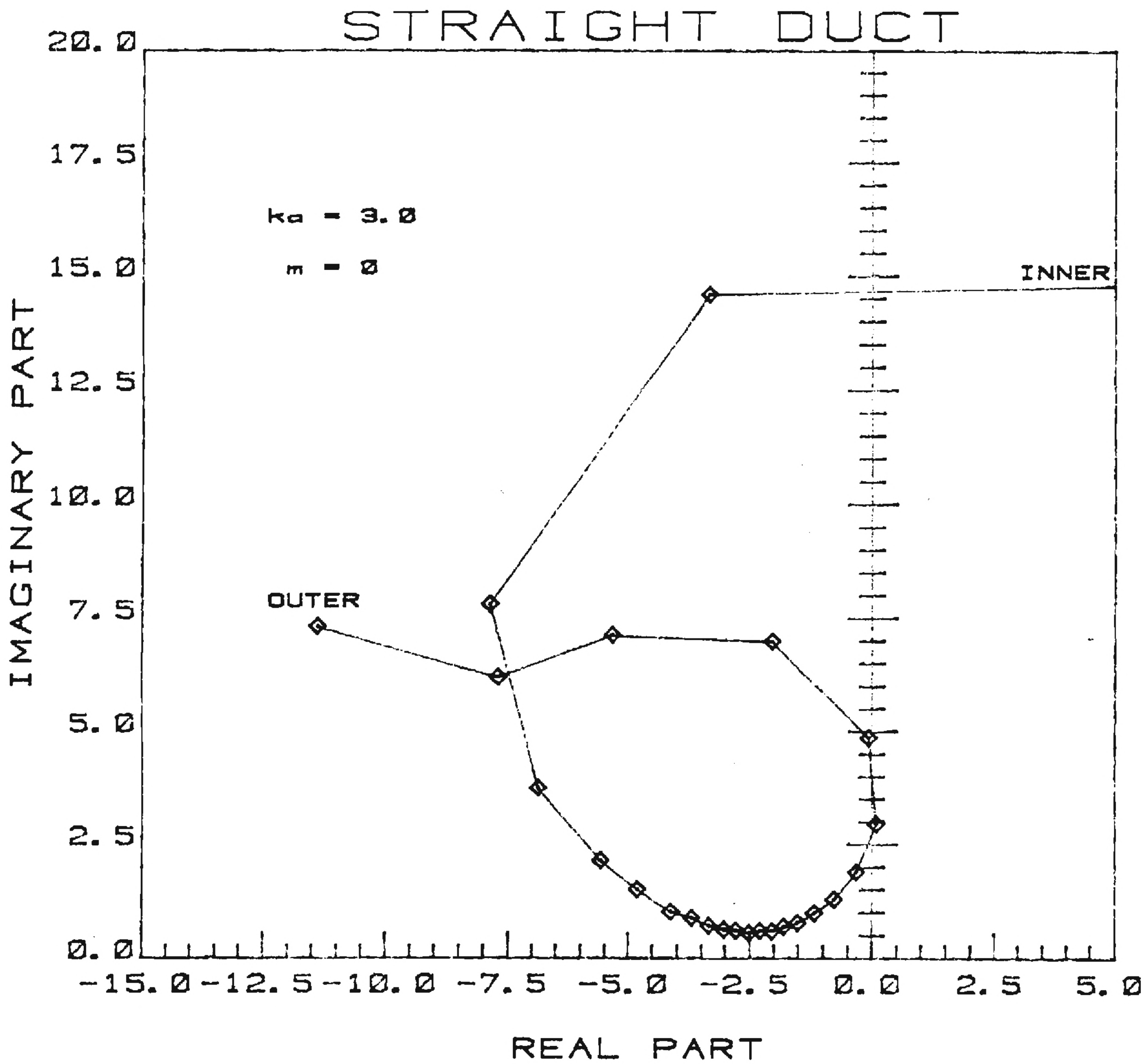

OPTIMUM ADMITTANCE DISTRIBUTION

Constant Phi on the Driver

Figure 10a

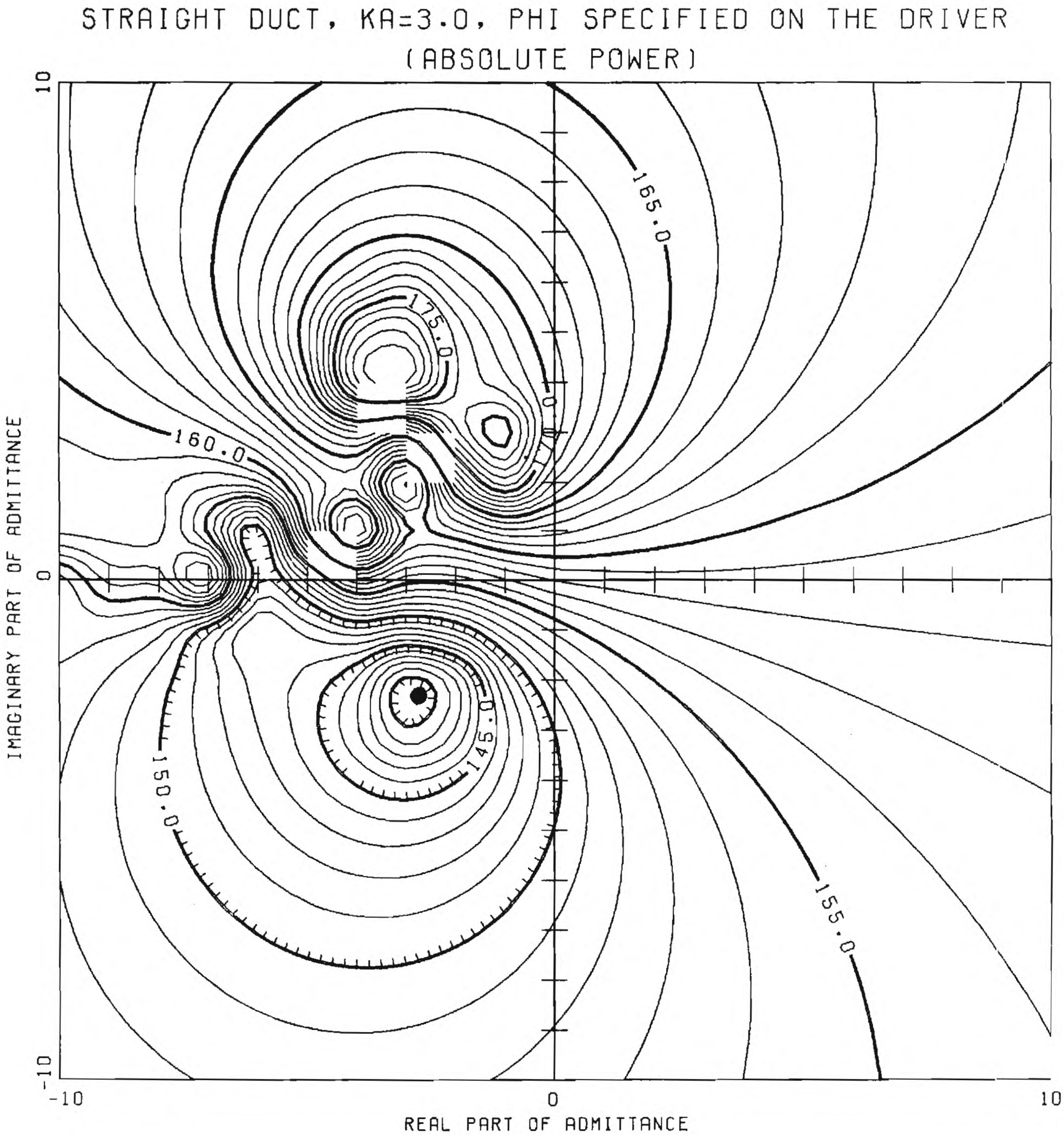

STRAIGHT DUCT, KA=3.0, PHI SPECIFIED ON THE DRIVER
(ABSOLUTE POWER)
IMAGINARY PART OF ADMITTANCE
REAL PART OF ADMITTANCE
10
0
-10
-10
0
10
165.0
175.0
170.0
160.0
145.0
150.0
155.0

Figure 10b

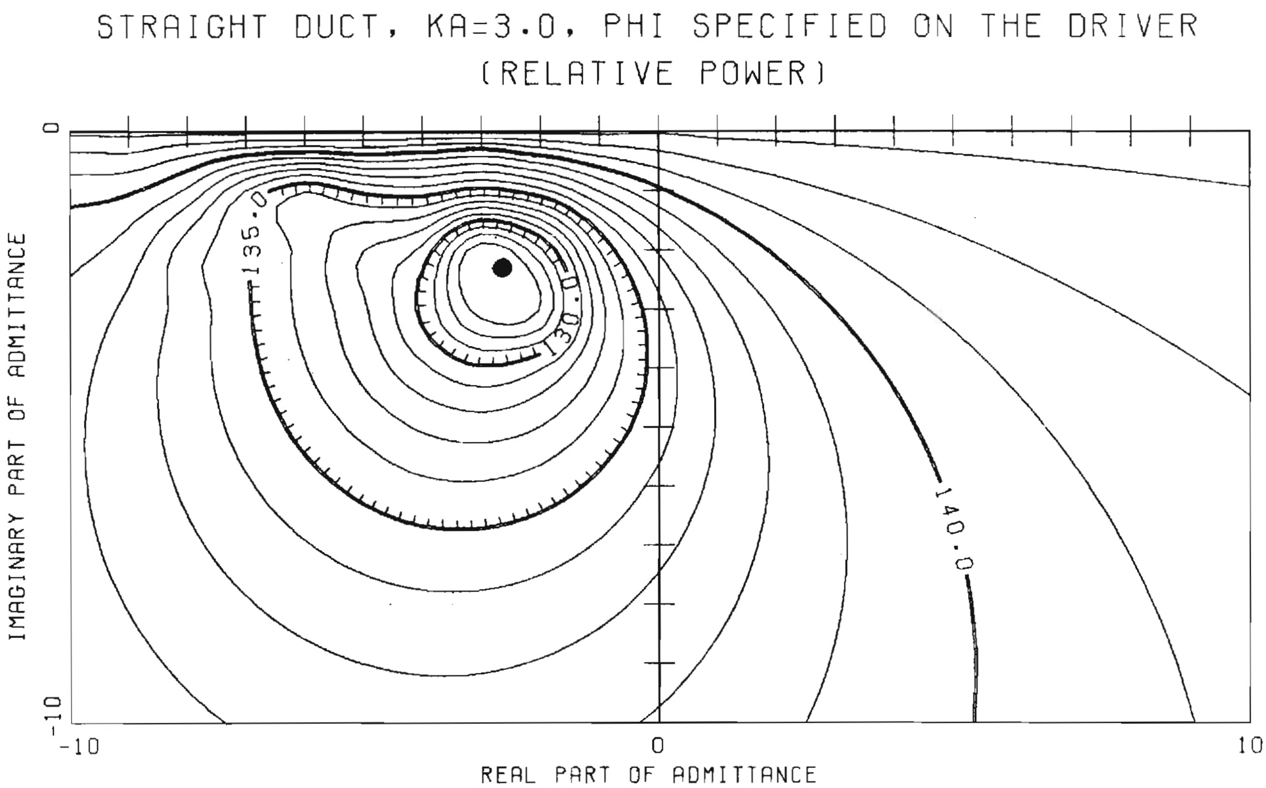

STRAIGHT DUCT, KA=3.0, PHI SPECIFIED ON THE DRIVER
(RELATIVE POWER)
135.0
130.0
140.0
0
-10
IMAGINARY PART OF ADMITTANCE
-10
0
10
REAL PART OF ADMITTANCE

Figure 10c

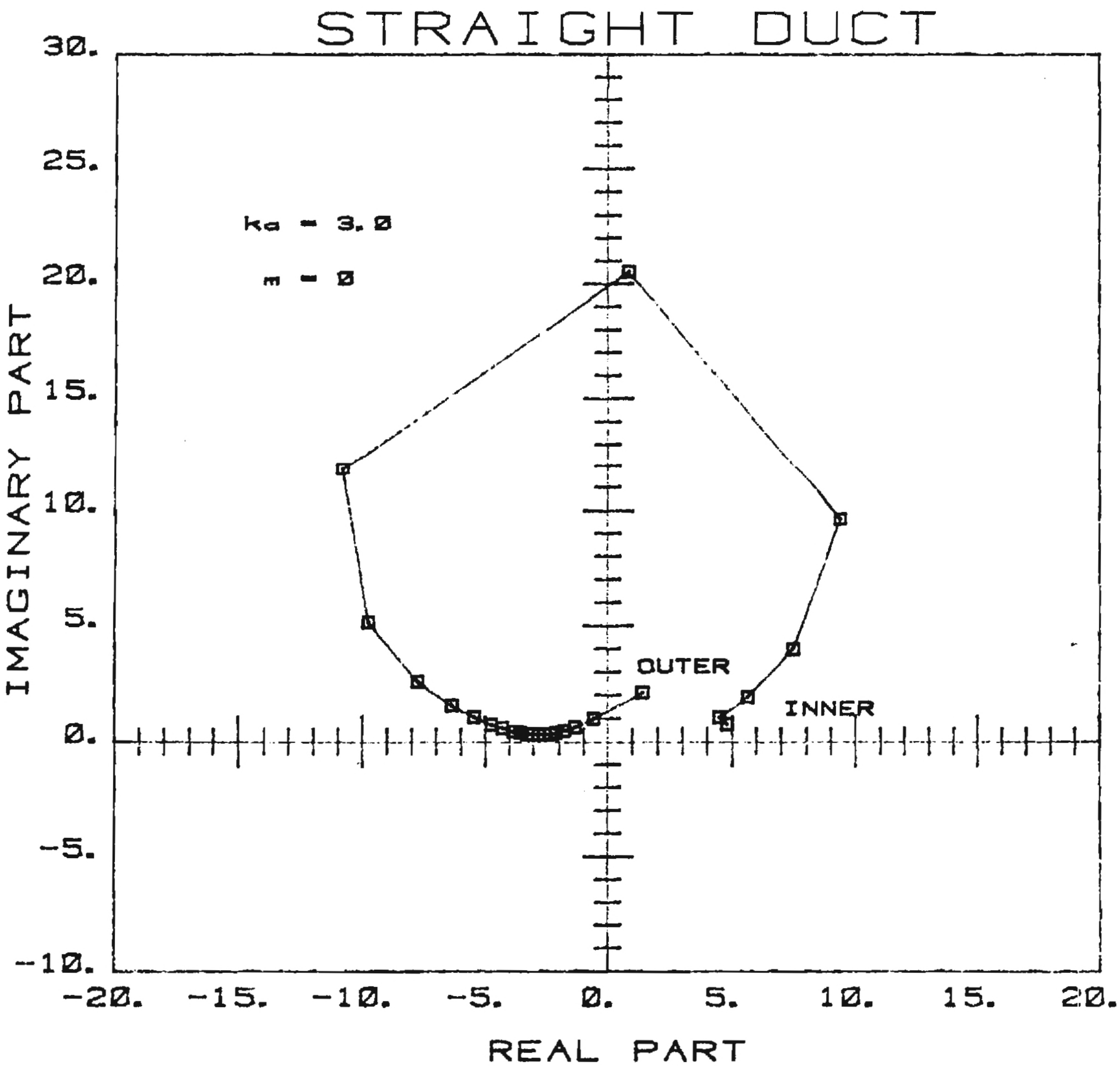

OPTIMUM ADMITTANCE DISTRIBUTION

Constant Velocity on the Driver

Figure 10d

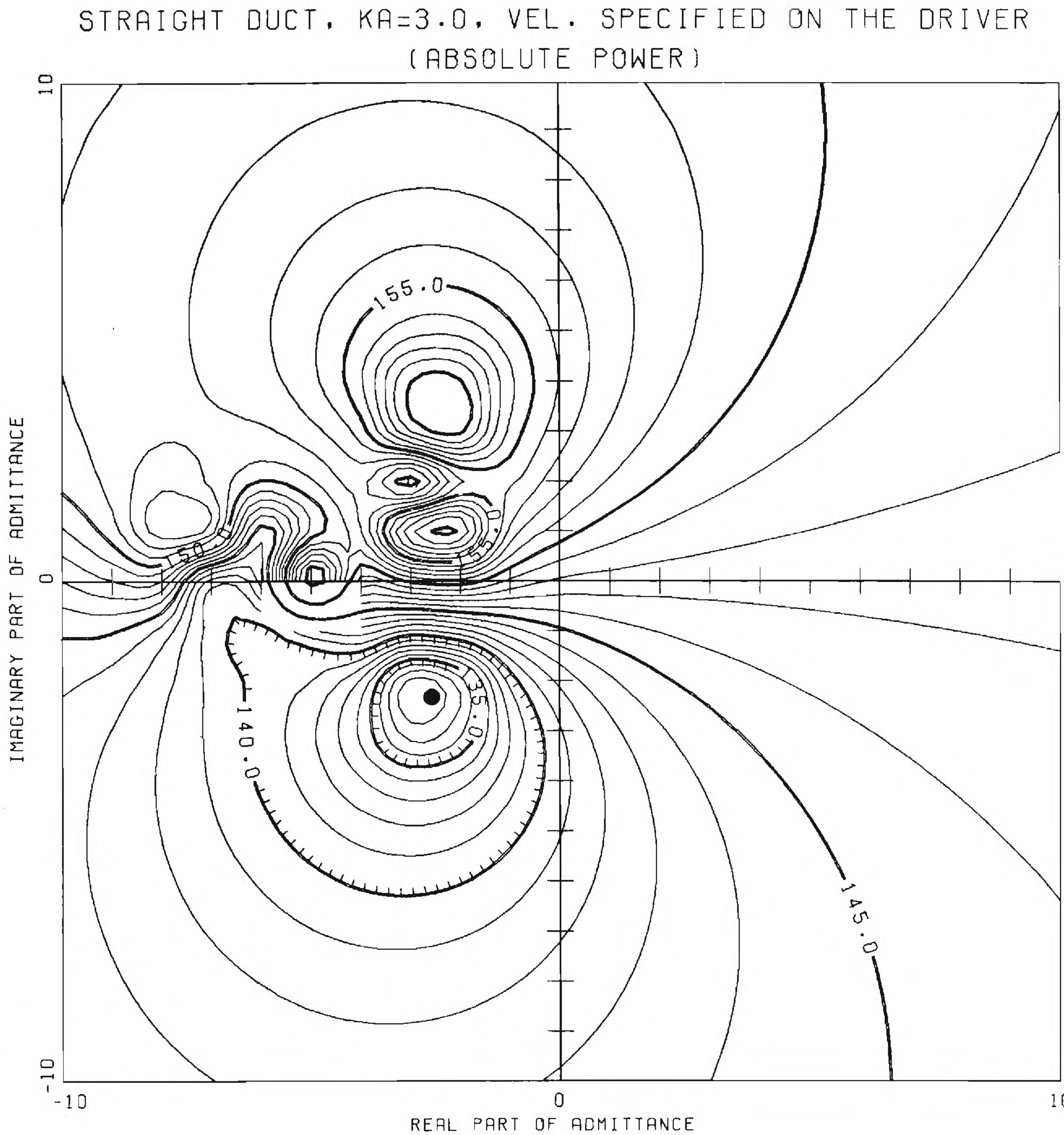
STRAIGHT DUCT, KA=3.0, VEL. SPECIFIED ON THE DRIVER
(ABSOLUTE POWER)
IMAGINARY PART OF ADMITTANCE
10
0
-10
-10
0
10
REAL PART OF ADMITTANCE
155.0
150
155.0
135.0
140.0
145.0

Figure 10e

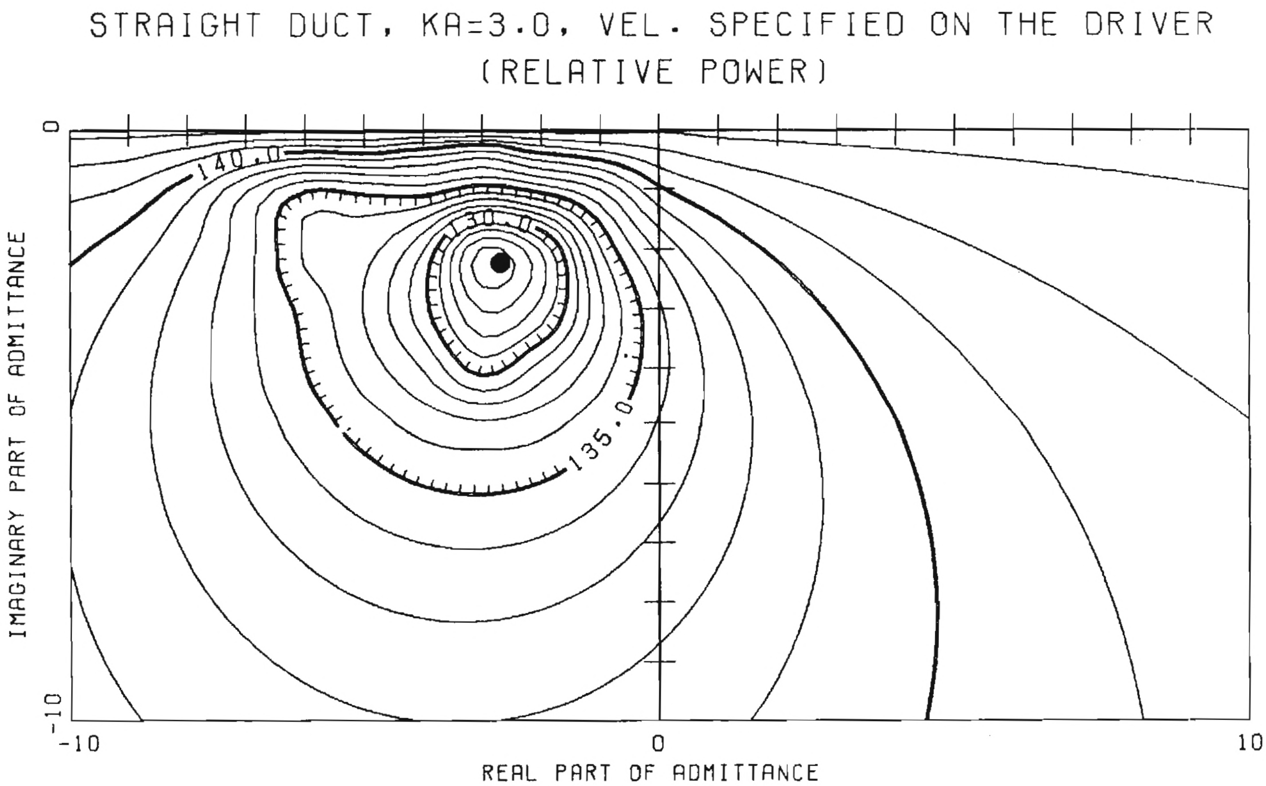
STRAIGHT DUCT, KA=3.0, VEL. SPECIFIED ON THE DRIVER
(RELATIVE POWER)
0
IMAGINARY PART OF ADMITTANCE
-10
140.0
130.0
135.0
-10
0
10
REAL PART OF ADMITTANCE

Figure 10f

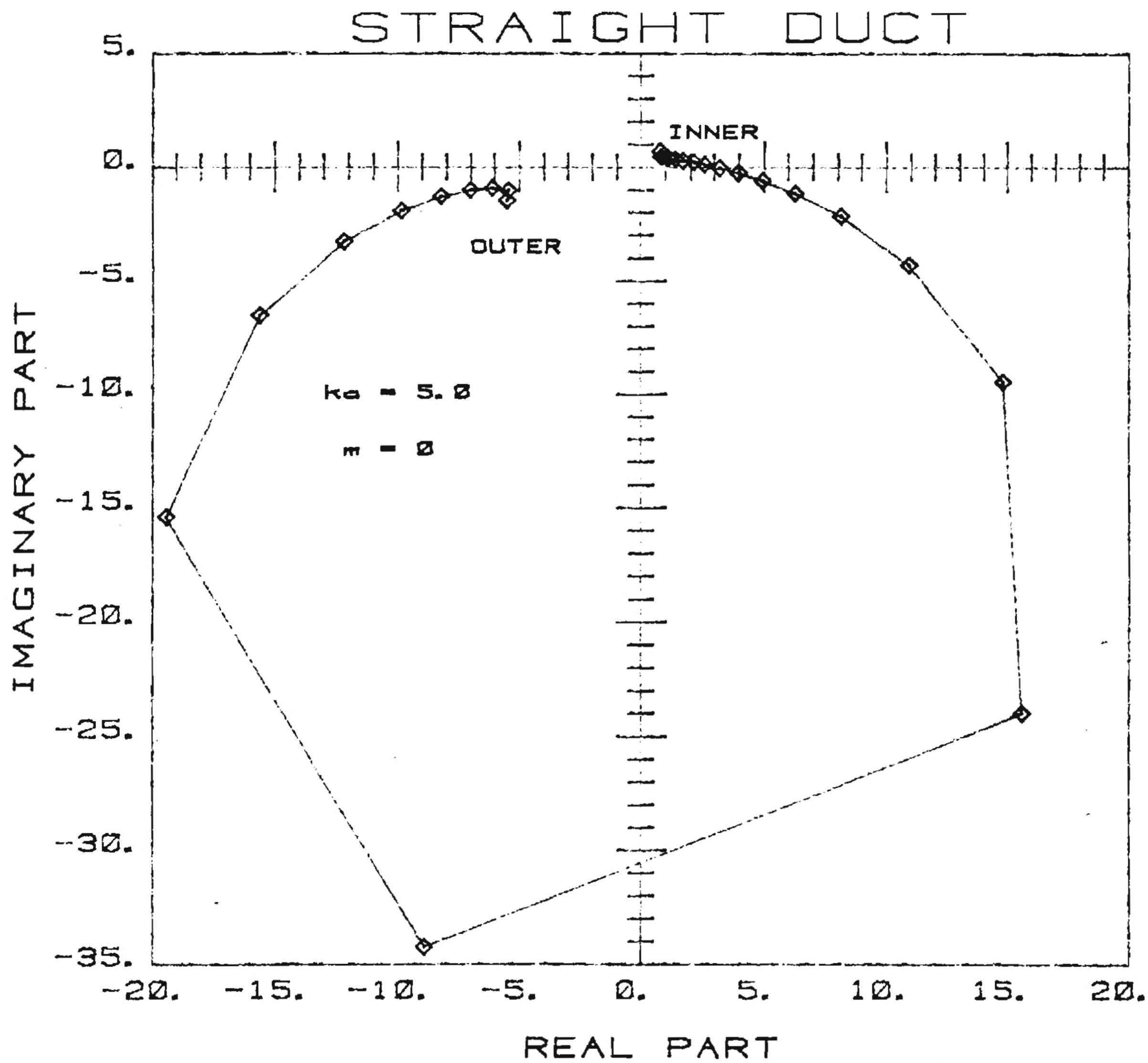

OPTIMUM ADMITTANCE DISTRIBUTION

Constant Phi on the Driver

Figure 11a

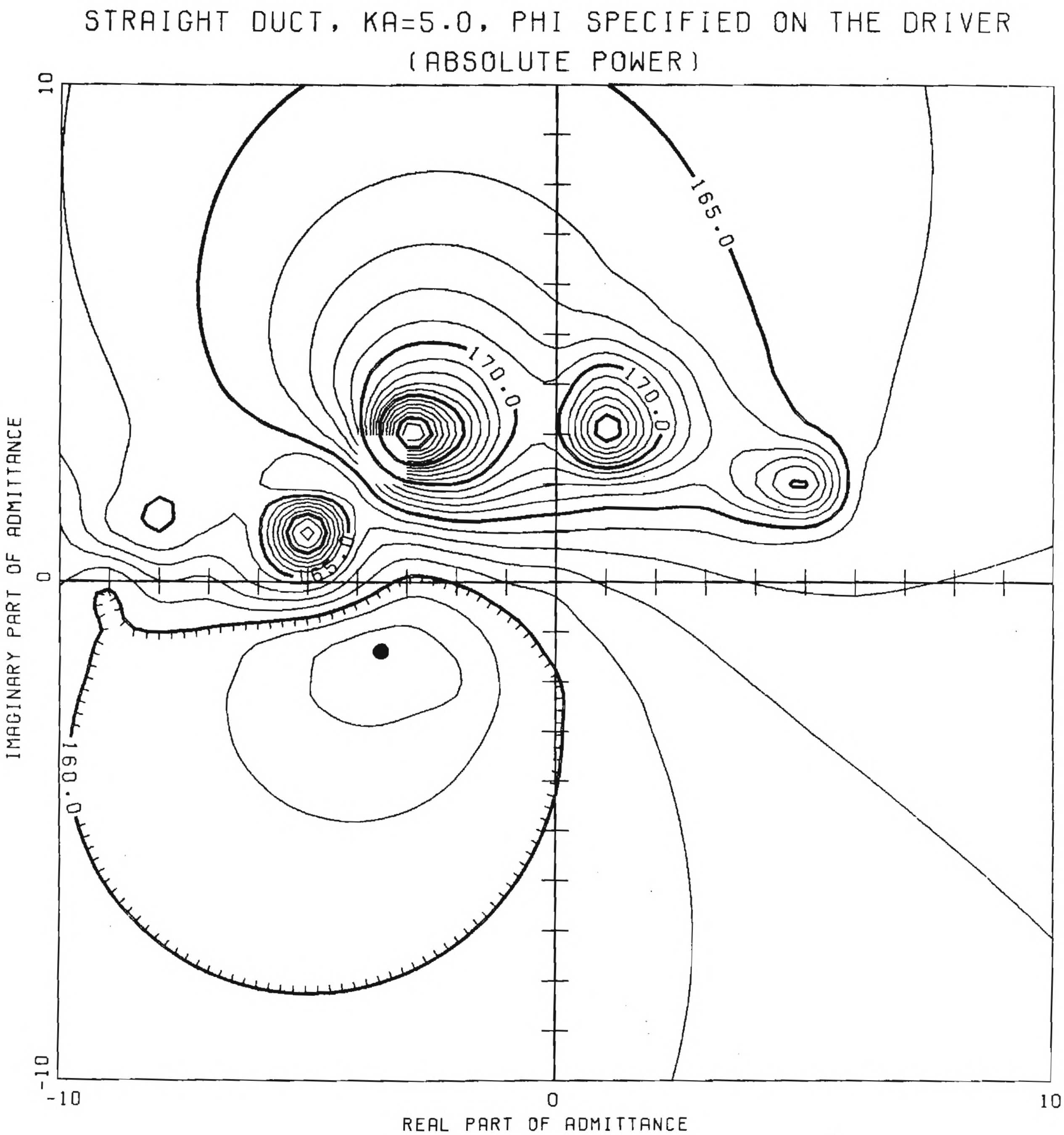
STRAIGHT DUCT, KA=5.0, PHI SPECIFIED ON THE DRIVER
(ABSOLUTE POWER)
10
0
-10
-10
0
10
IMAGINARY PART OF ADMITTANCE
REAL PART OF ADMITTANCE
165.0
170.0
170.0
165.0
160.0

Figure 11b

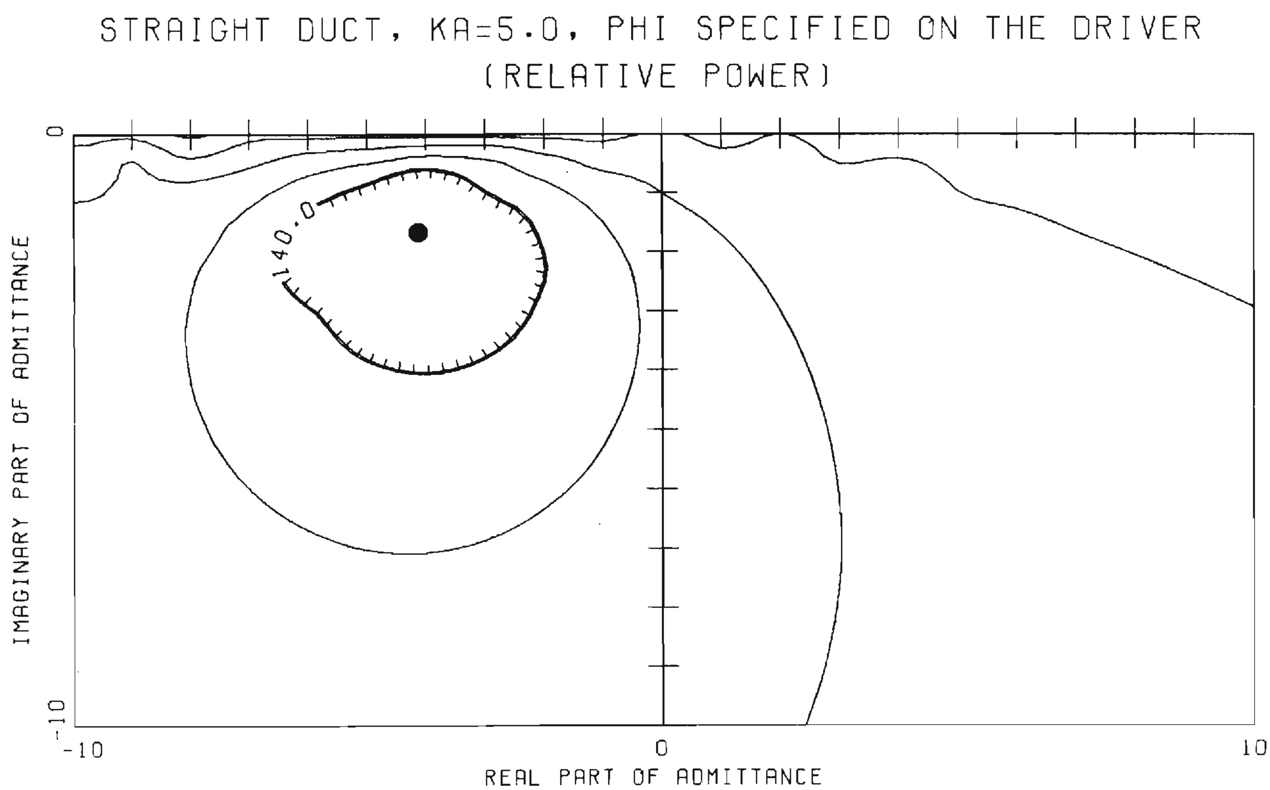

STRAIGHT DUCT, KA=5.0, PHI SPECIFIED ON THE DRIVER
(RELATIVE POWER)
140.0
IMAGINARY PART OF ADMITTANCE
REAL PART OF ADMITTANCE
0
-10
-10
0
10

Figure 11c

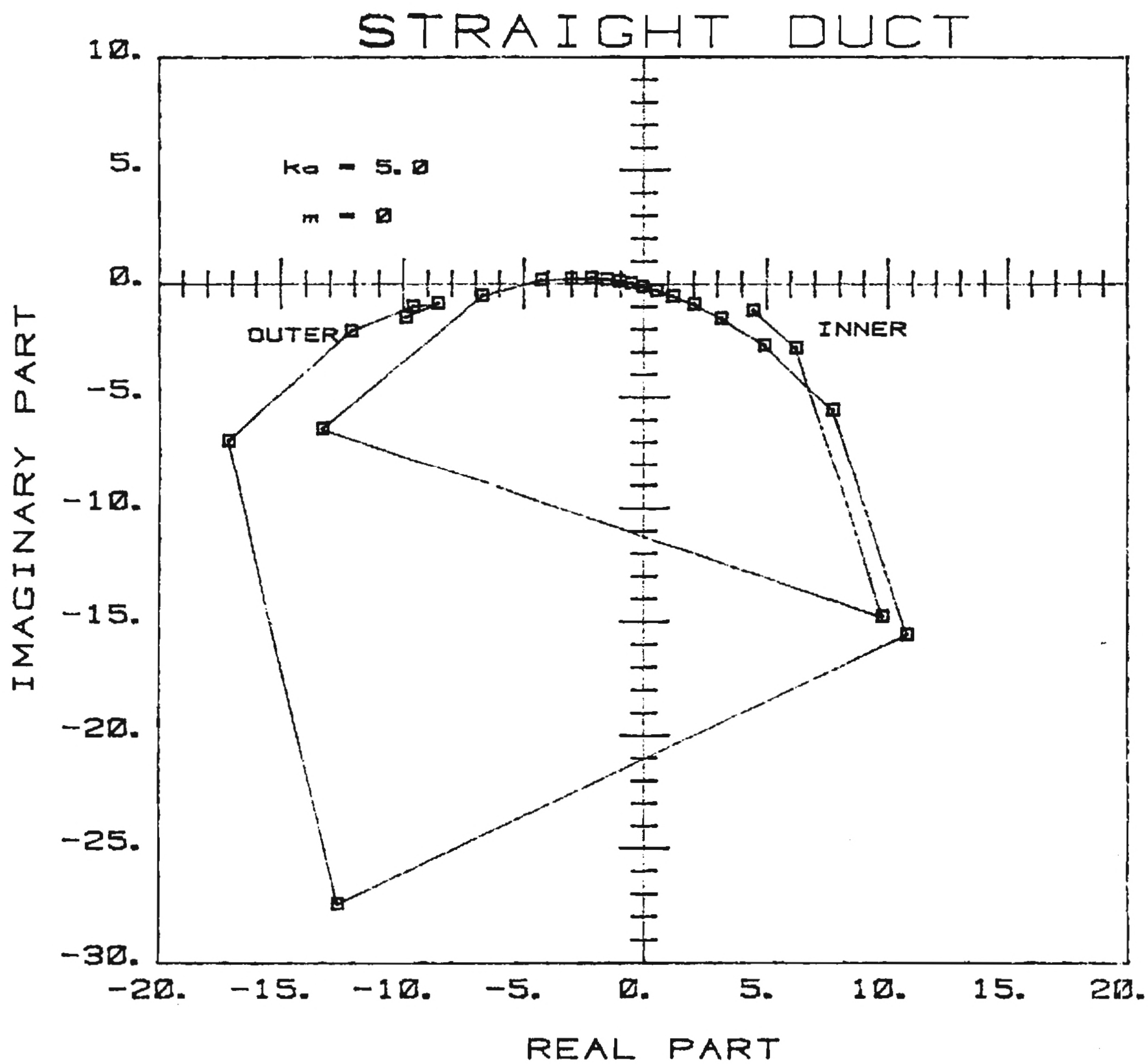

OPTIMUM ADMITTANCE DISTRIBUTION

Constant Velocity on the Driver

Figure 11d

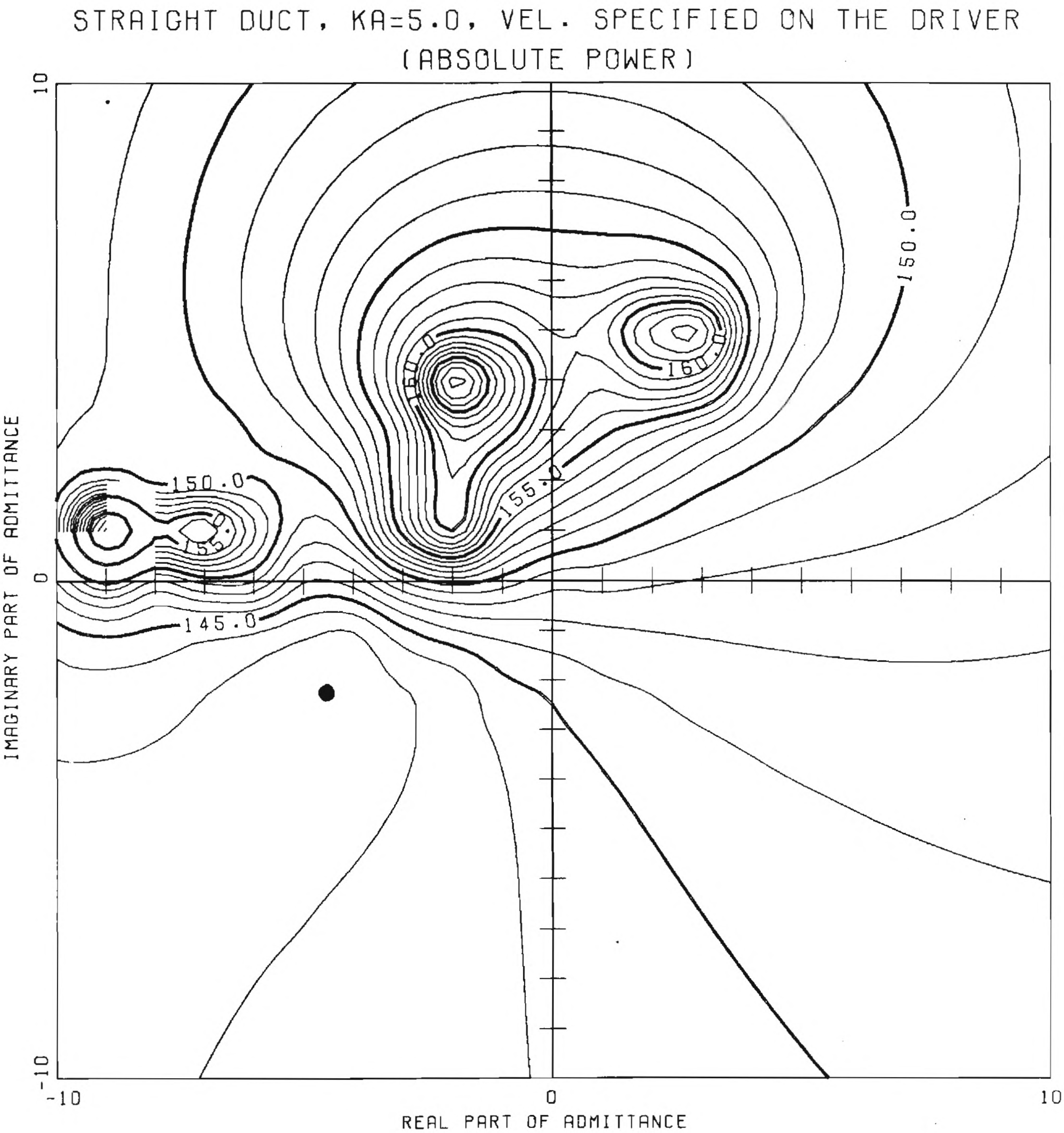
STRAIGHT DUCT, KA=5.0, VEL. SPECIFIED ON THE DRIVER
(ABSOLUTE POWER)
150.0
160
155.0
155
145.0
IMAGINARY PART OF ADMITTANCE
REAL PART OF ADMITTANCE
10
0
-10
10
0
-10

Figure 11e

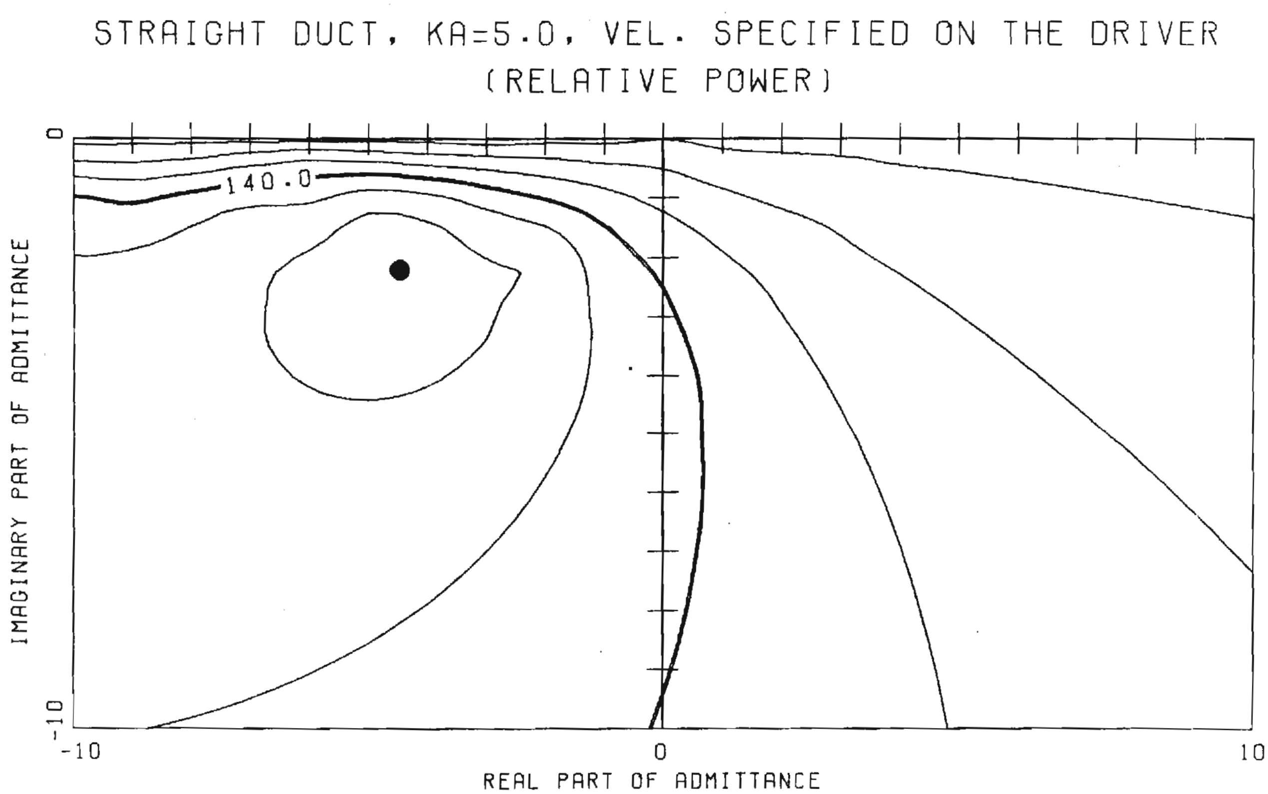
STRAIGHT DUCT, KA=5.0, VEL. SPECIFIED ON THE DRIVER
(RELATIVE POWER)
140.0
IMAGINARY PART OF ADMITTANCE
0
-10
-10
0
10
REAL PART OF ADMITTANCE

Figure 11f

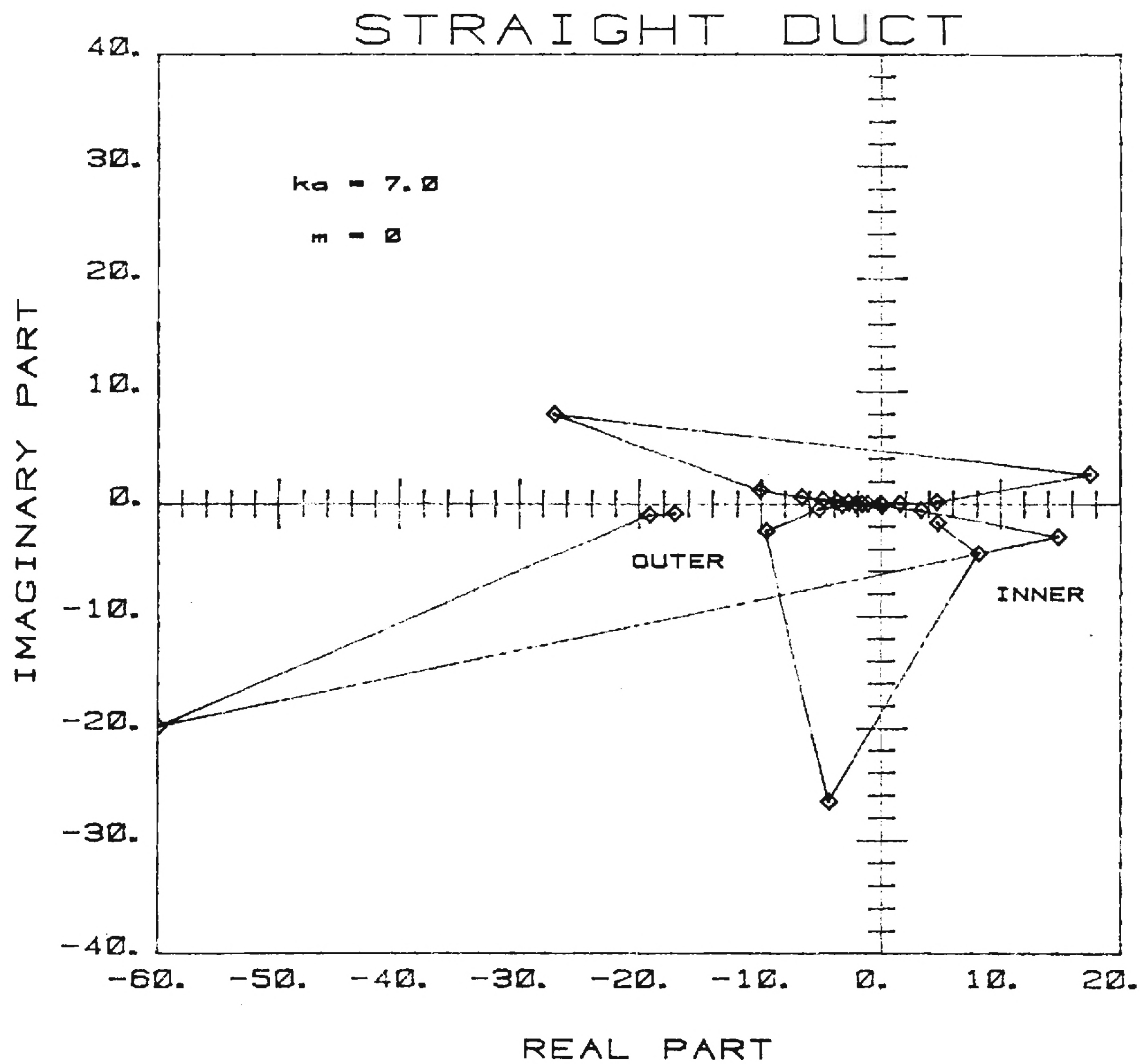

OPTIMUM ADMITTANCE DISTRIBUTION

Constant Phi on the Driver

Figure 12a

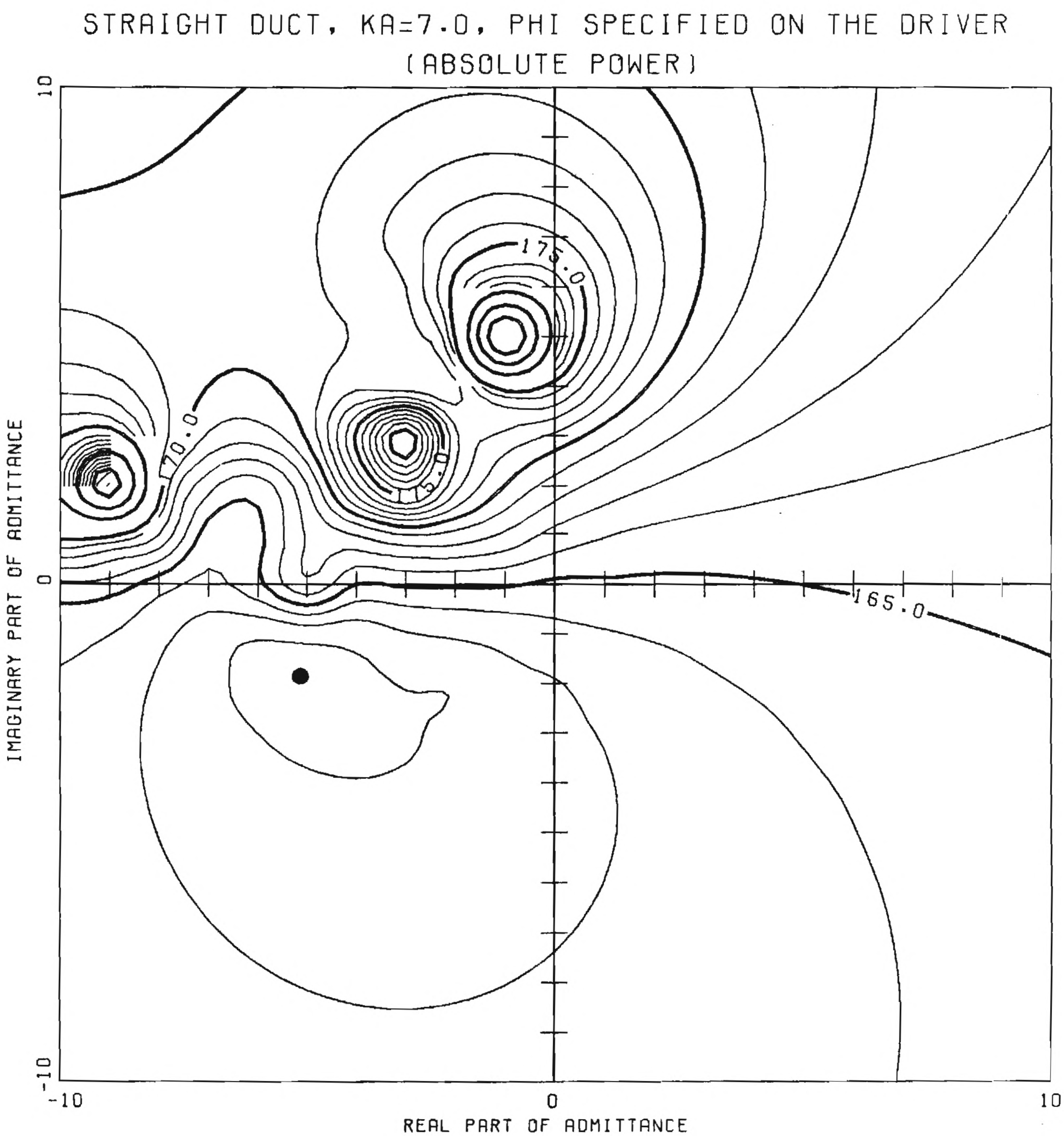

STRAIGHT DUCT, KA=7.0, PHI SPECIFIED ON THE DRIVER
(ABSOLUTE POWER)
175.0
170.0
165.0
10
0
-10
-10
0
10
IMAGINARY PART OF ADMITTANCE
REAL PART OF ADMITTANCE

Figure 12b

STRAIGHT DUCT, KA=7.0, PHI SPECIFIED ON THE DRIVER
(RELATIVE POWER)

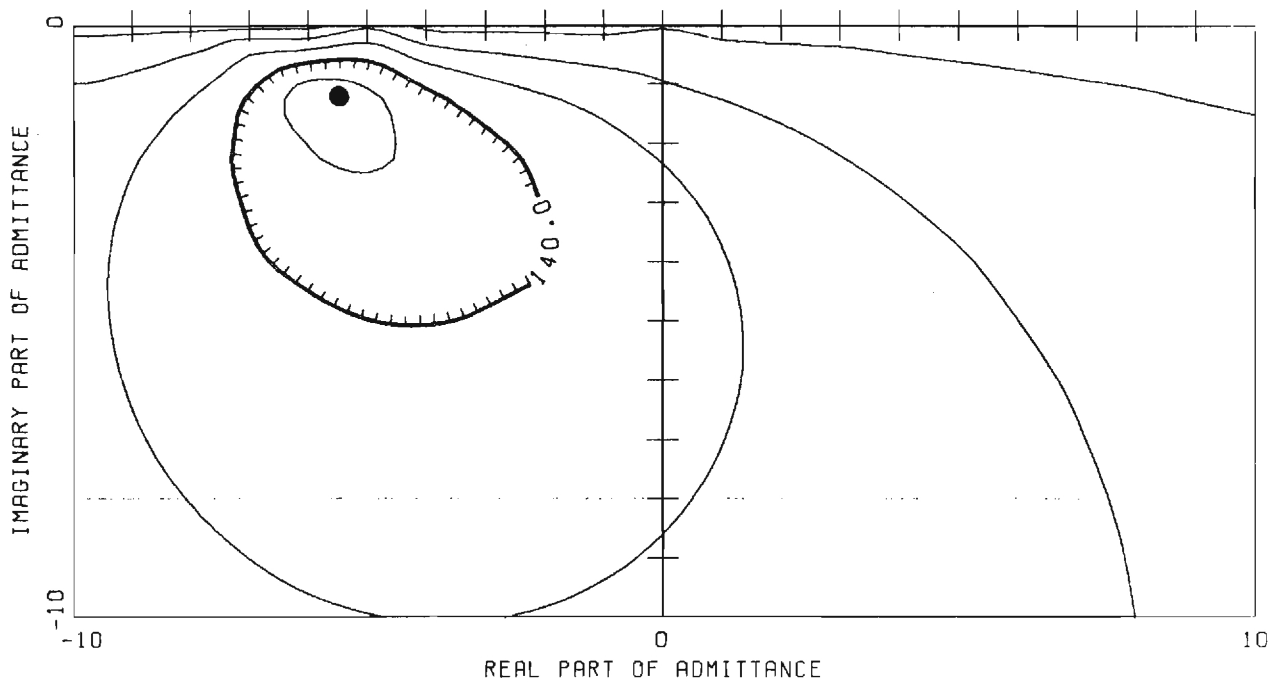

Figure 12c

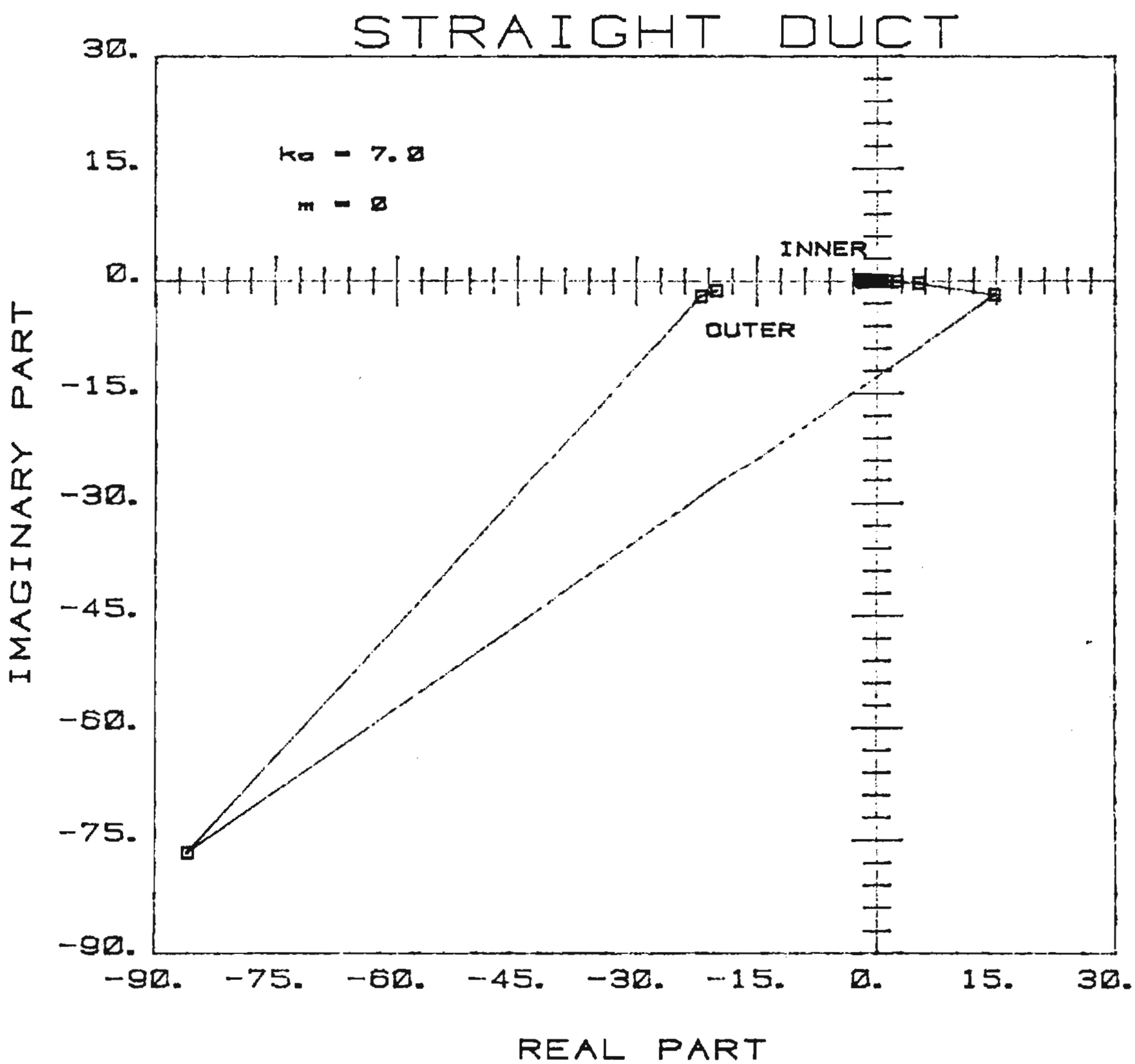

OPTIMUM ADMITTANCE DISTRIBUTION

Constant Velocity on the Driver

Figure 12d

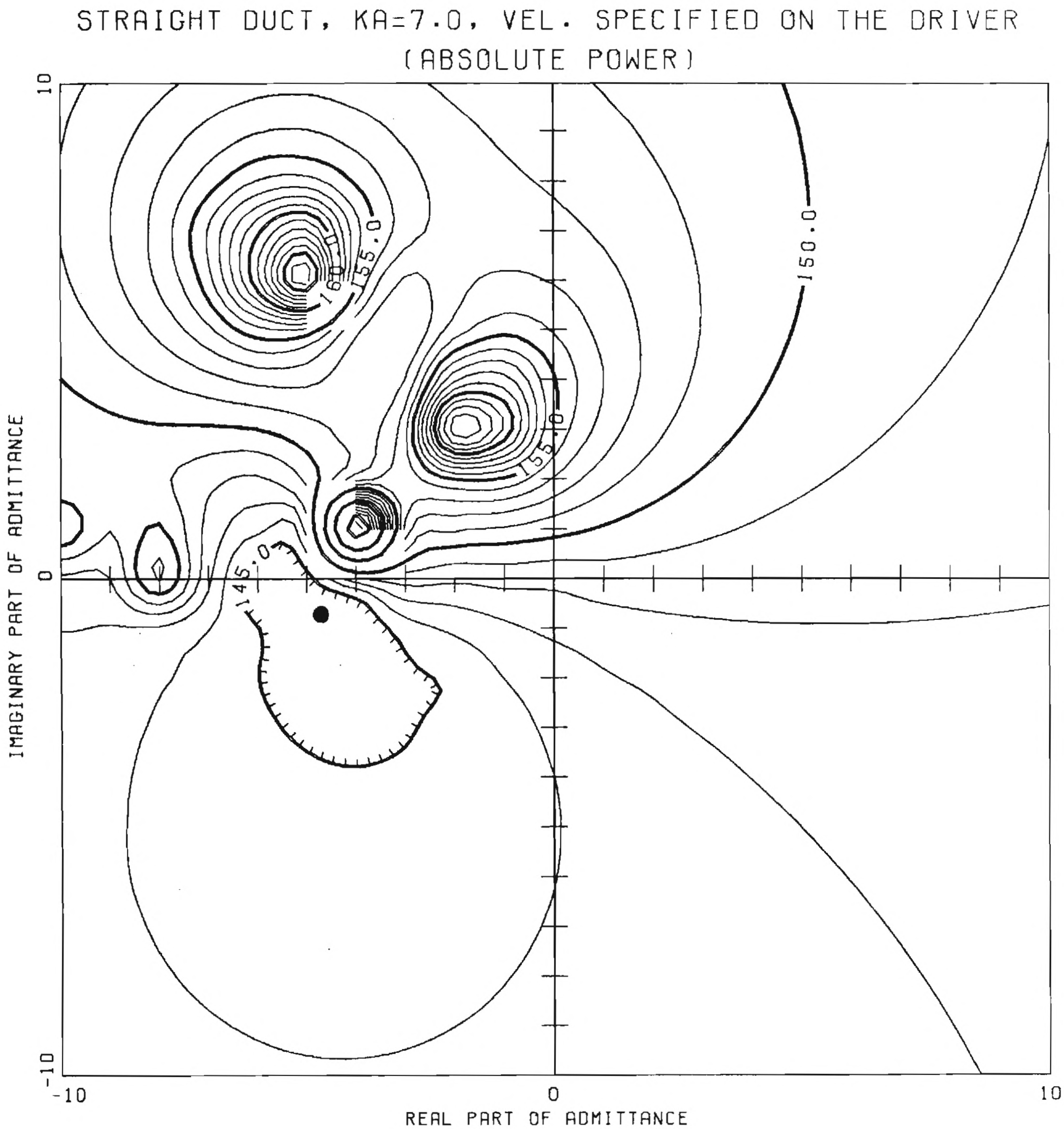
STRAIGHT DUCT, KA=7.0, VEL. SPECIFIED ON THE DRIVER
(ABSOLUTE POWER)
150.0
155.0
160.0
155.0
145.0
10
0
-10
-10
0
10
IMAGINARY PART OF ADMITTANCE
REAL PART OF ADMITTANCE

Figure 12e

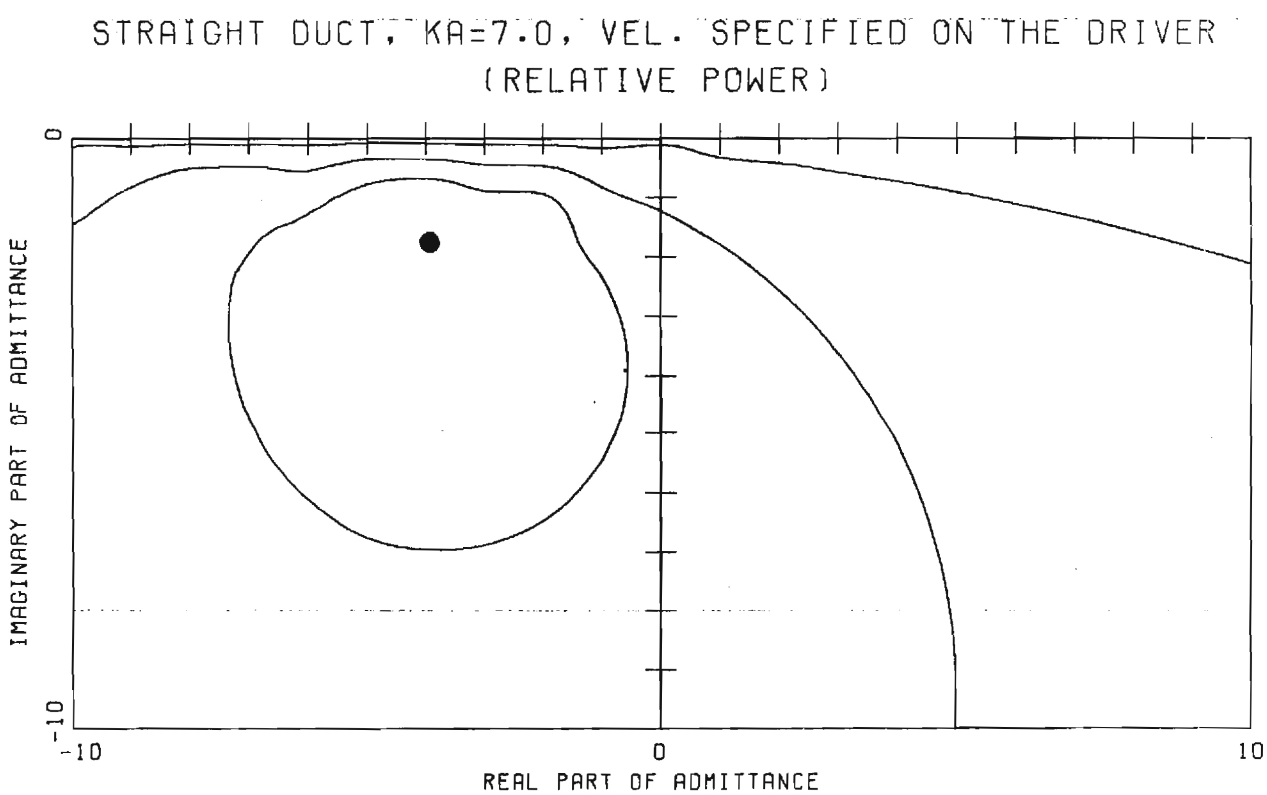

STRAIGHT DUCT, KA=7.0, VEL. SPECIFIED ON THE DRIVER
(RELATIVE POWER)
0
-10
IMAGINARY PART OF ADMITTANCE
-10
0
10
REAL PART OF ADMITTANCE

Figure 12f

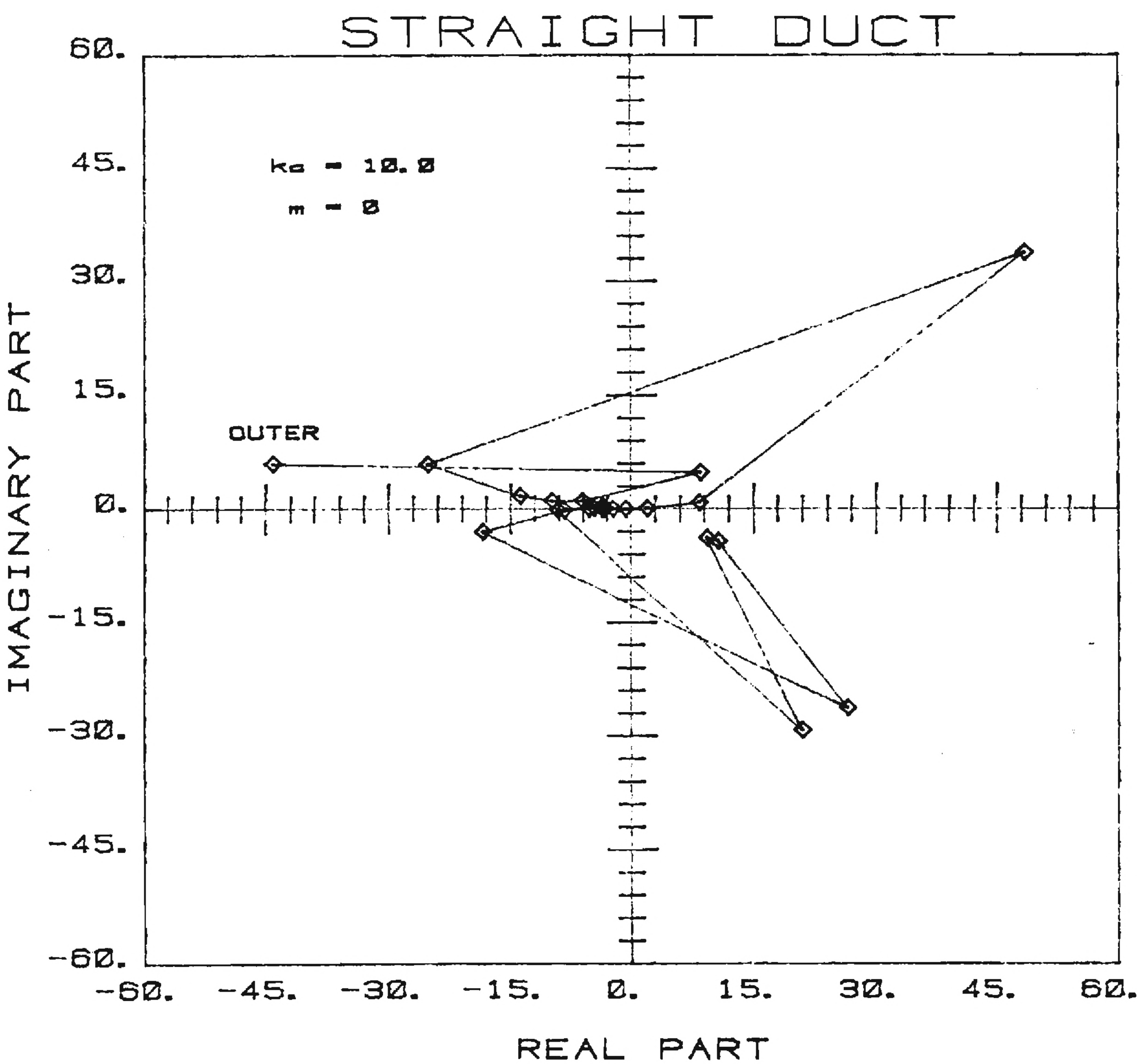

OPTIMUM ADMITTANCE DISTRIBUTION

Constant Phi on the Driver

Figure 13a

STRAIGHT DUCT, KA=10.0, PHI SPECIFIED ON THE DRIVER
(ABSOLUTE POWER)

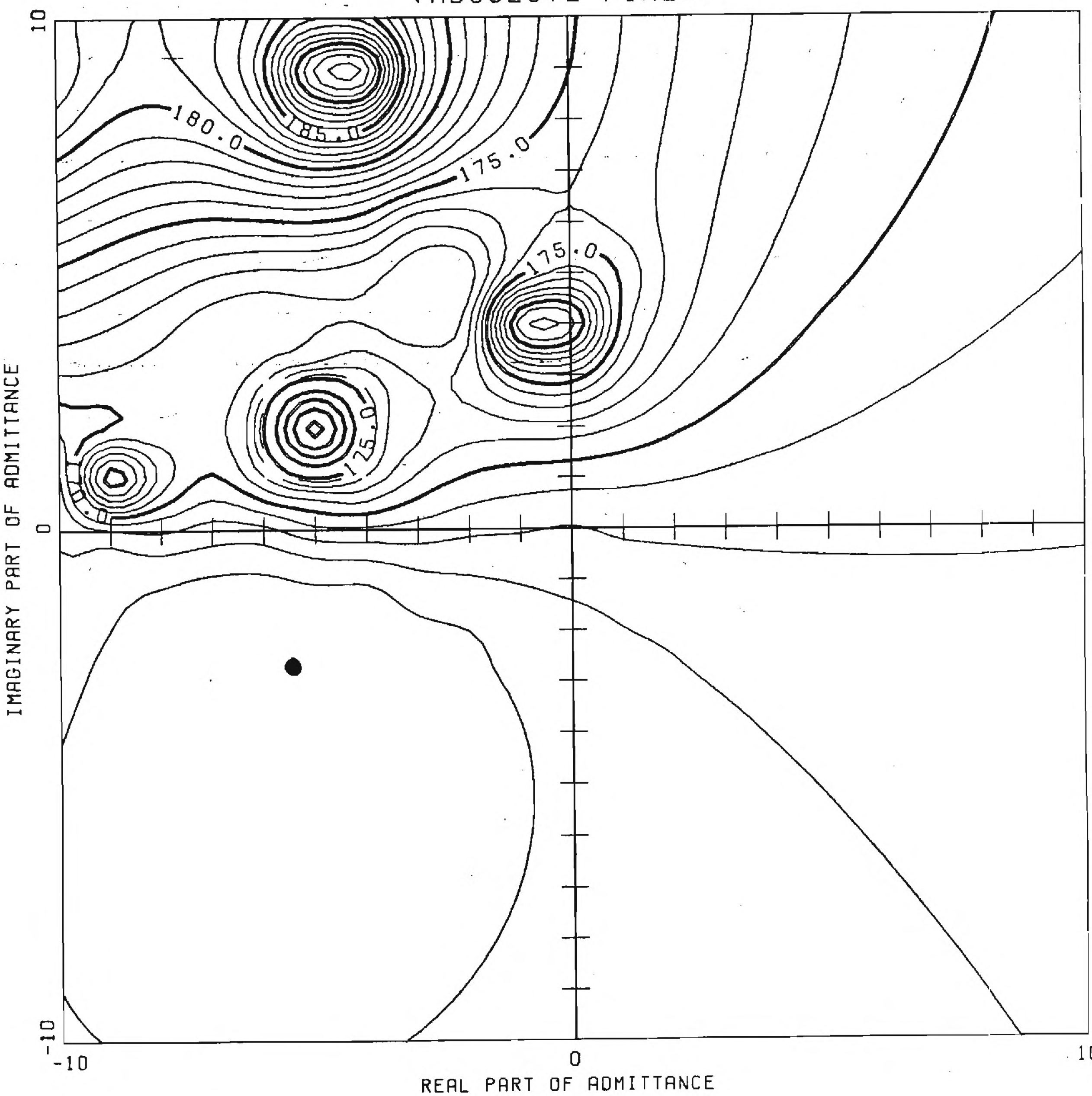

Figure 13b

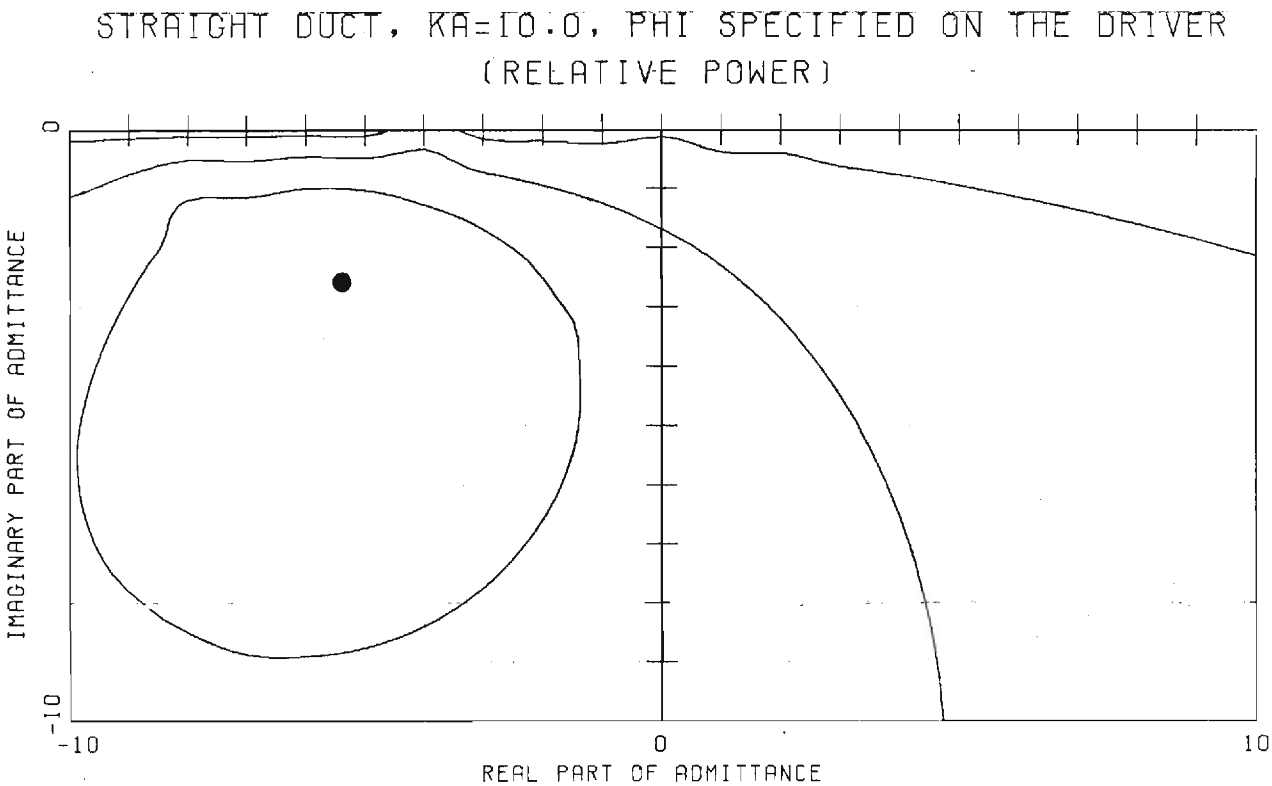
STRAIGHT DUCT, KA=10.0, PHI SPECIFIED ON THE DRIVER
(RELATIVE POWER)
0
-10
IMAGINARY PART OF ADMITTANCE
-10
0
10
REAL PART OF ADMITTANCE

Figure 13c

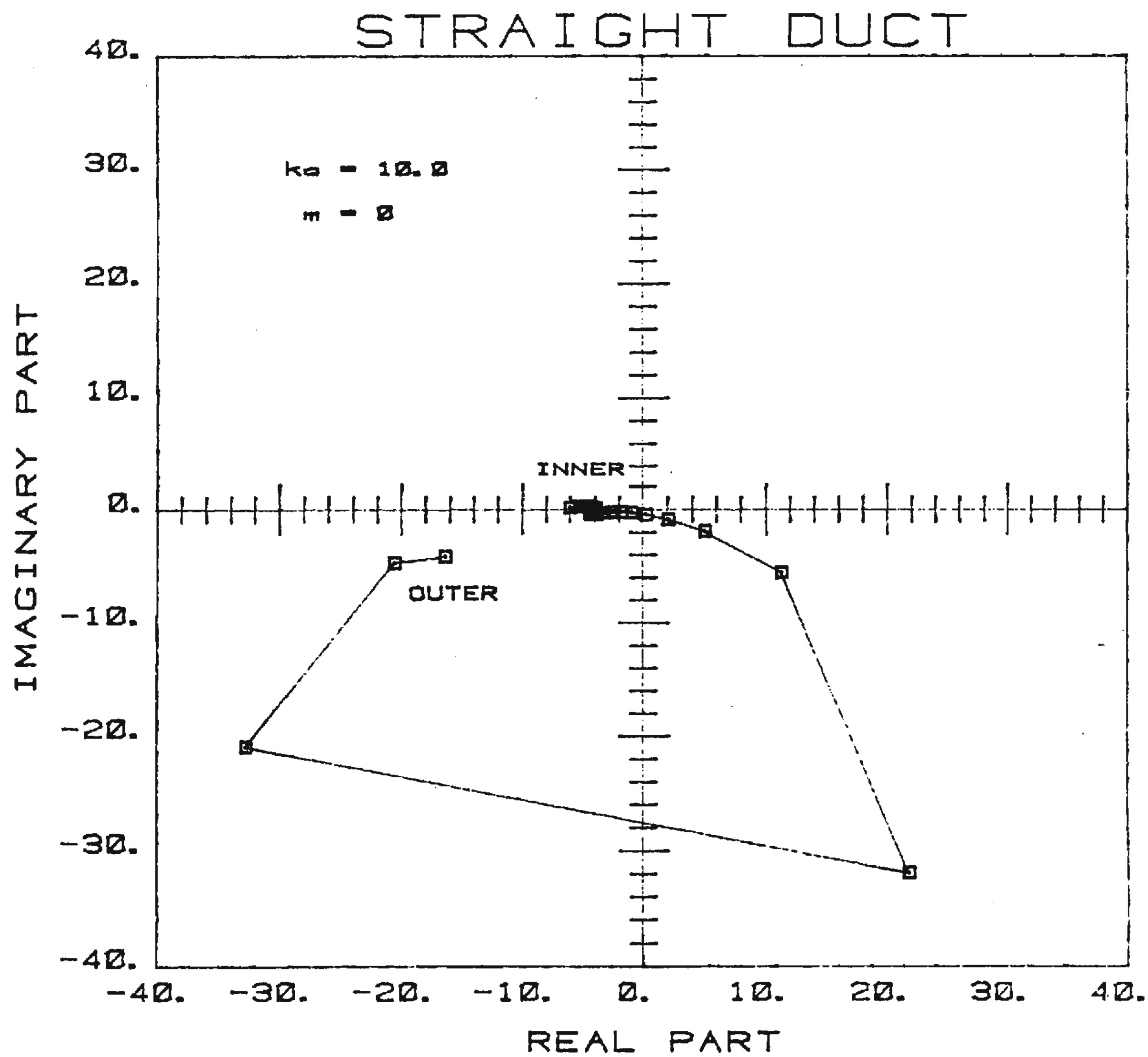

OPTIMUM ADMITTANCE DISTRIBUTION

Constant Velocity on the Driver

Figure 13d

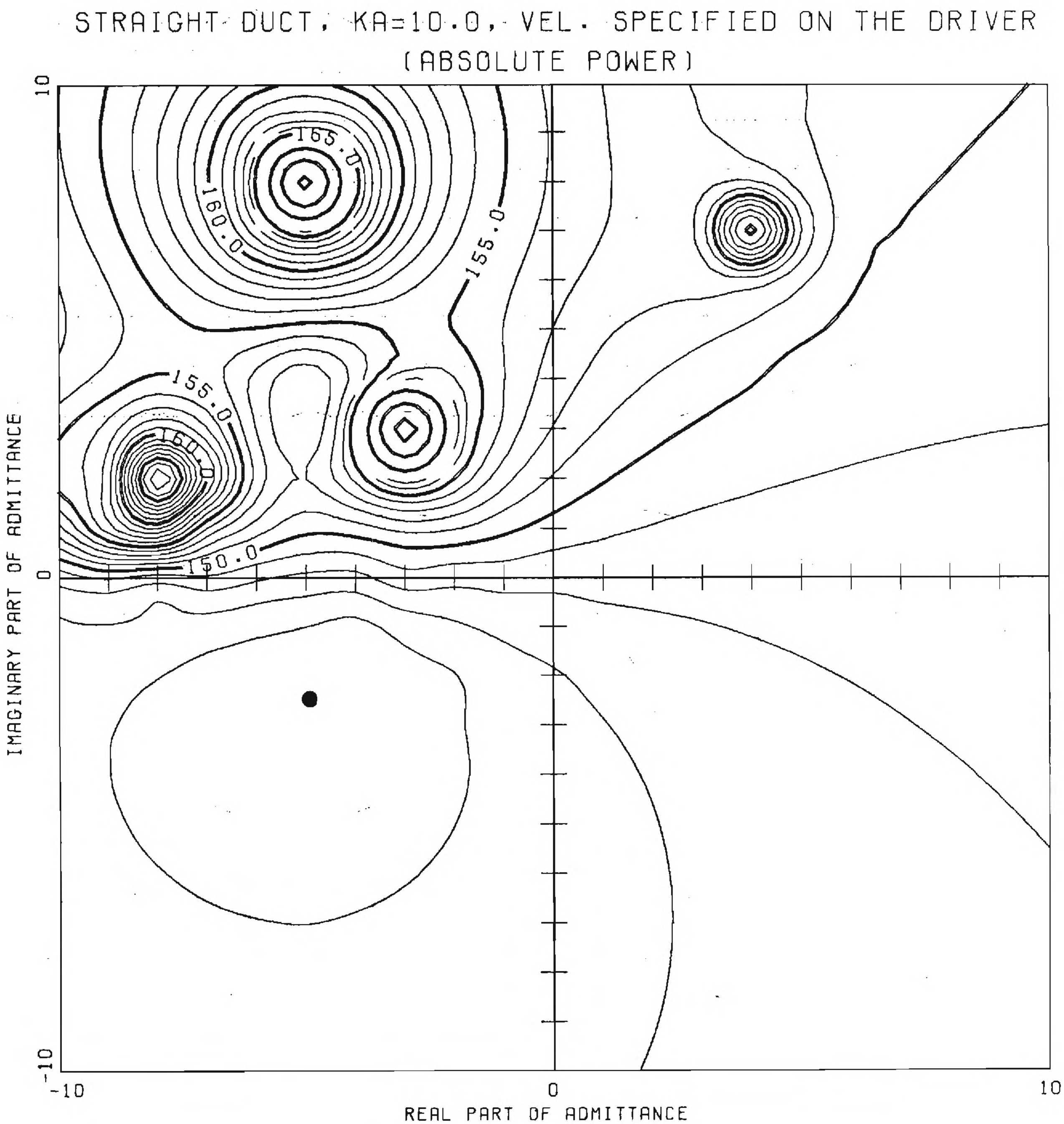
STRAIGHT DUCT, KA=10.0, VEL. SPECIFIED ON THE DRIVER
(ABSOLUTE POWER)
165.0
160.0
155.0
155.0
160.0
150.0
10
0
-10
-10
0
10
IMAGINARY PART OF ADMITTANCE
REAL PART OF ADMITTANCE

Figure 13e

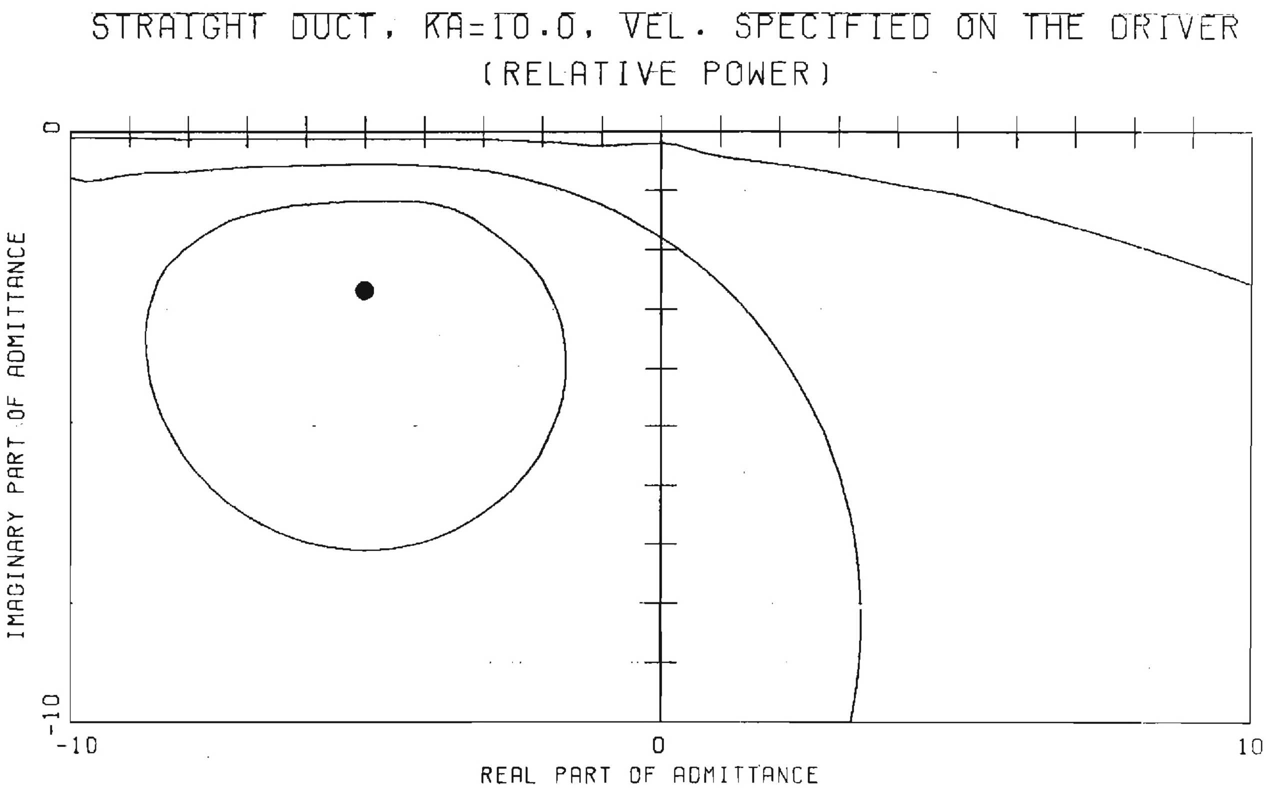
STRAIGHT DUCT, KA=10.0, VEL. SPECIFIED ON THE DRIVER
(RELATIVE POWER)
0
-10
IMAGINARY PART OF ADMITTANCE
-10
0
10
REAL PART OF ADMITTANCE

Figure 13f

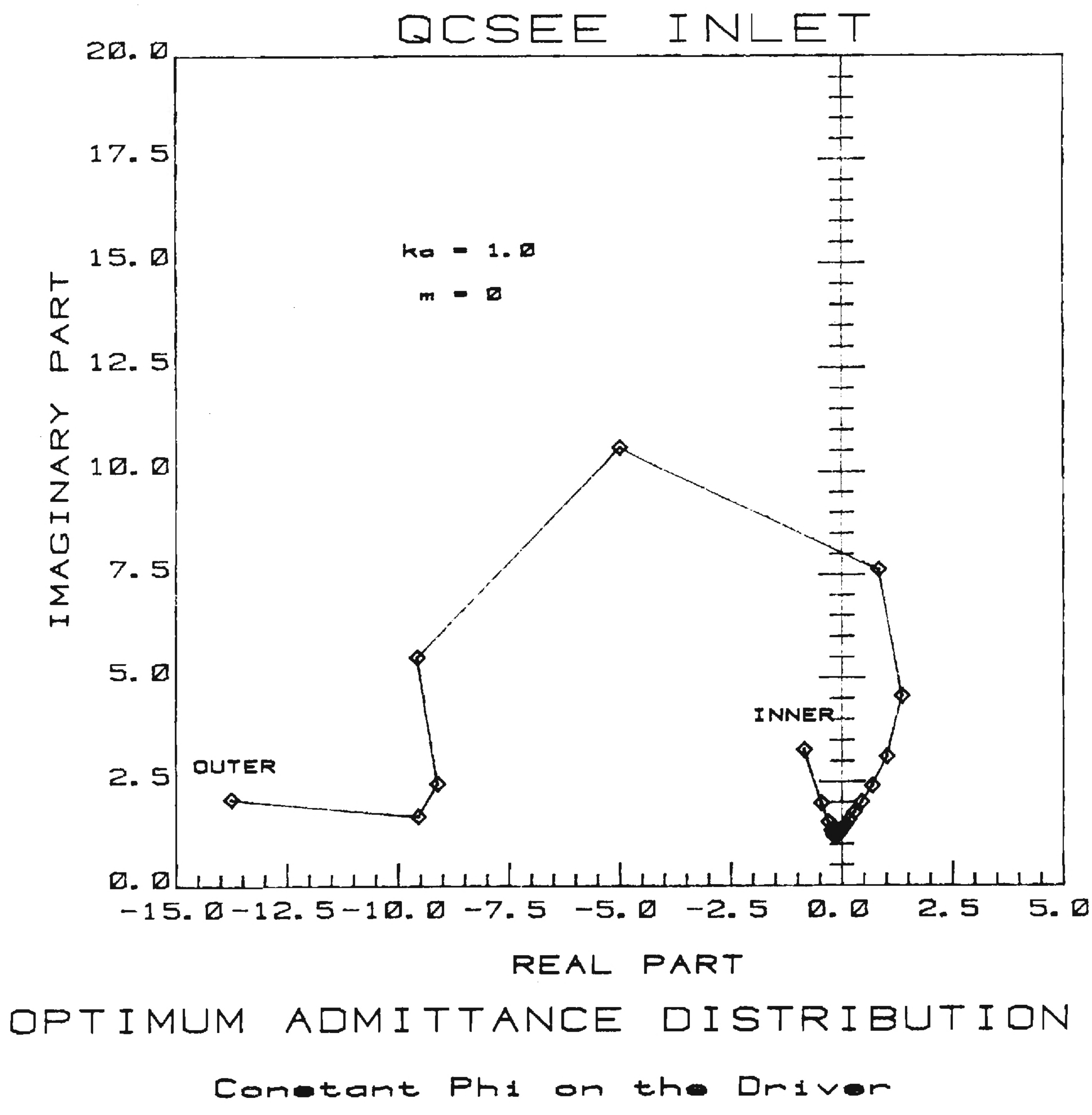
QCSEE INLET
IMAGINARY PART
REAL PART
20.0
17.5
15.0
12.5
10.0
7.5
5.0
2.5
0.0
-15.0
-12.5
-10.0
-7.5
-5.0
-2.5
0.0
2.5
5.0
ka = 1.0
m = 0
OUTER
INNER
OPTIMUM ADMITTANCE DISTRIBUTION
Constant Phi on the Driver

Figure 14a

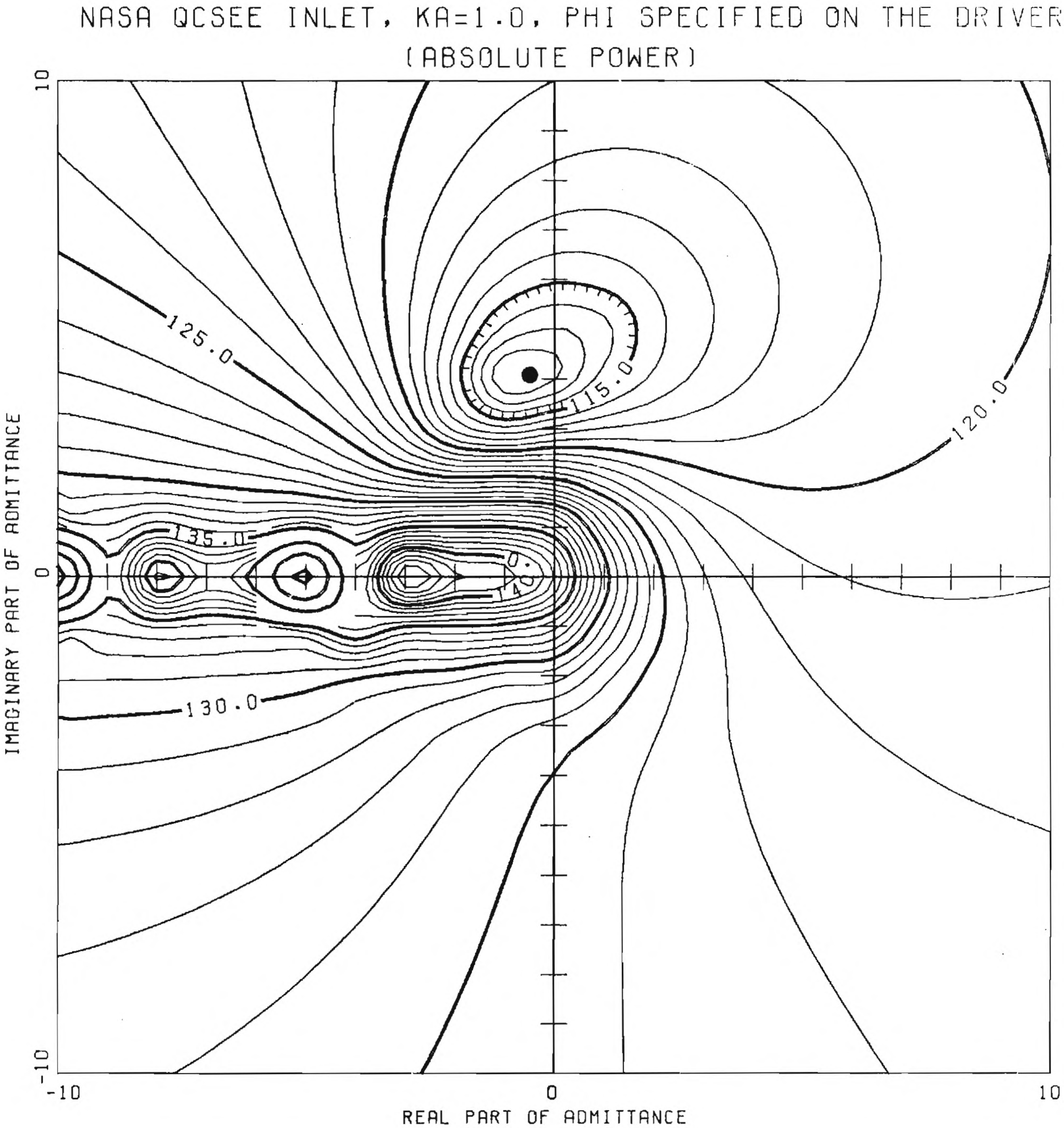
NASA QCSEE INLET, KA=1.0, PHI SPECIFIED ON THE DRIVER
(ABSOLUTE POWER)
10
0
-10
-10
0
10
IMAGINARY PART OF ADMITTANCE
REAL PART OF ADMITTANCE
125.0
115.0
120.0
135.0
130.0

Figure 14b

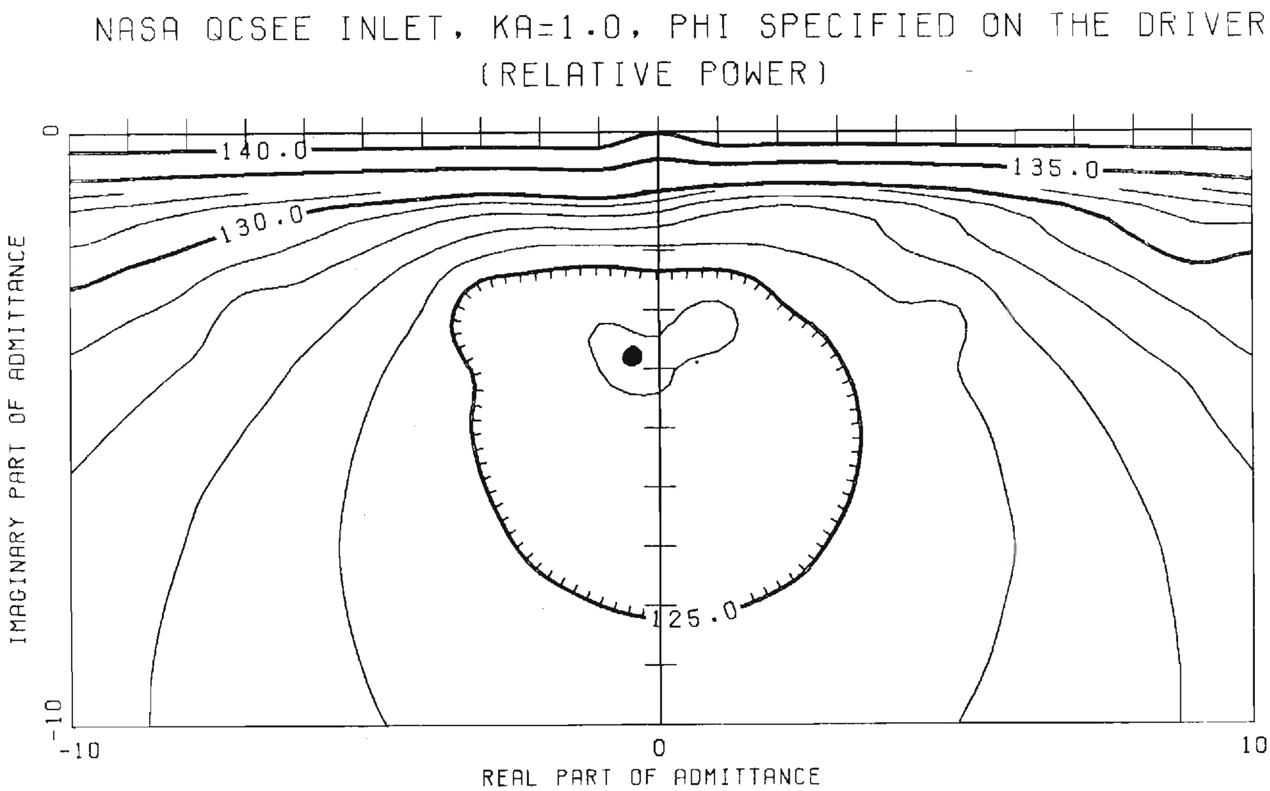

NASA QCSEE INLET, KA=1.0, PHI SPECIFIED ON THE DRIVER
(RELATIVE POWER)
140.0
135.0
130.0
125.0
0
-10
IMAGINARY PART OF ADMITTANCE
-10
0
10
REAL PART OF ADMITTANCE

Figure 14c

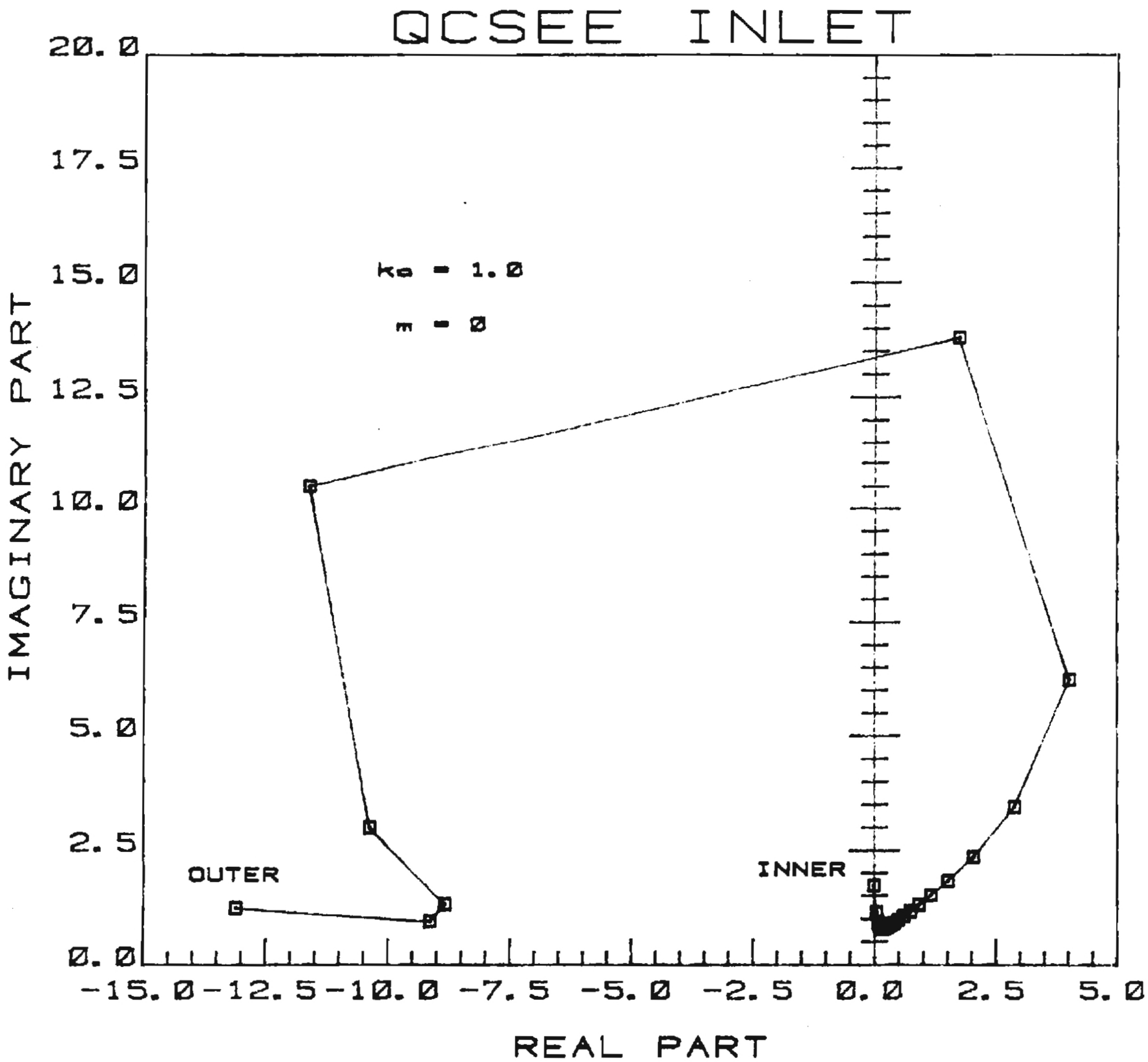

OPTIMUM ADMITTANCE DISTRIBUTION

Constant Velocity on the Driver

Figure 14d

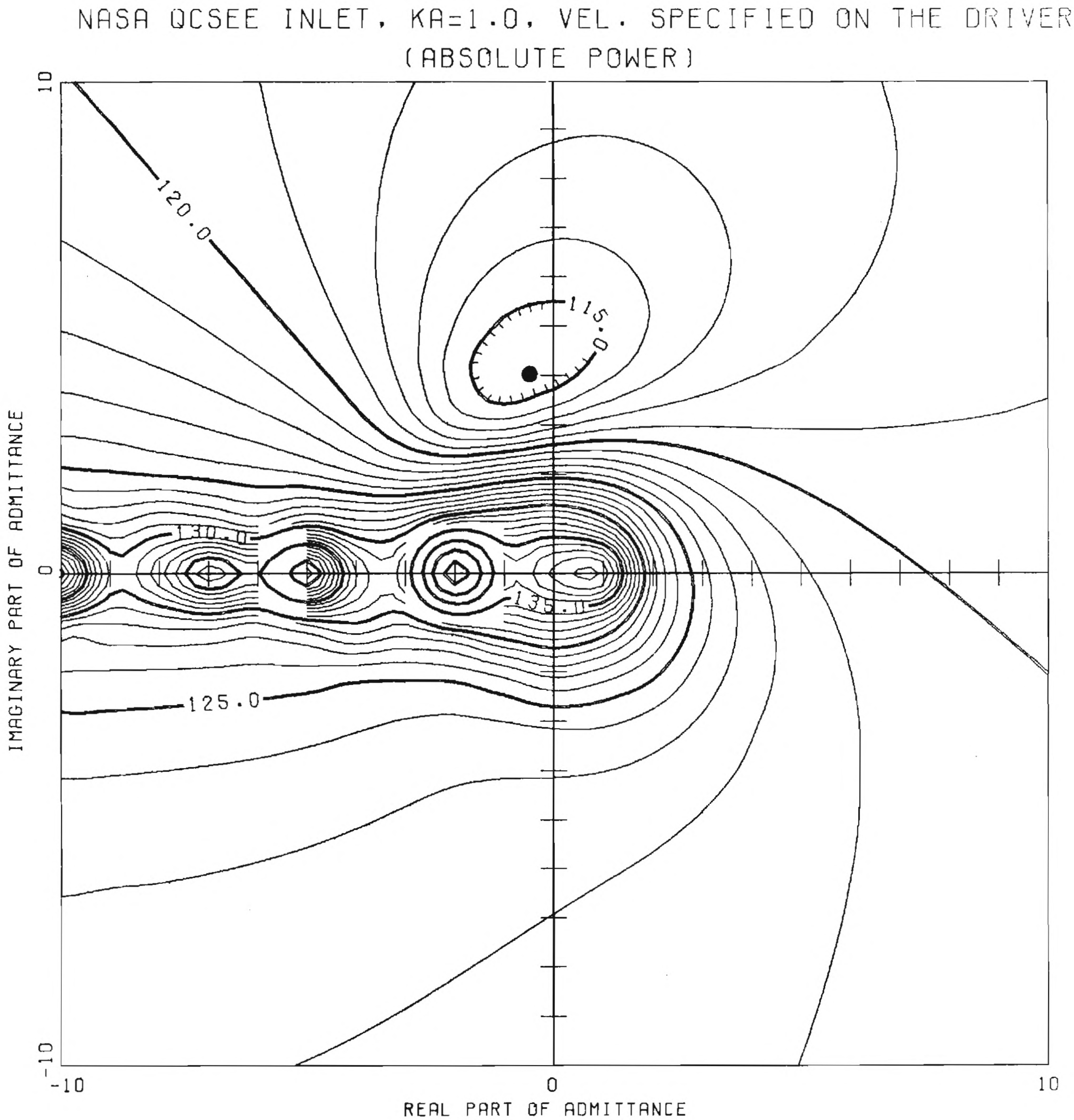

NASA QCSEE INLET, KA=1.0, VEL. SPECIFIED ON THE DRIVER
(ABSOLUTE POWER)
120.0
115.0
130.0
135.0
125.0
IMAGINARY PART OF ADMITTANCE
REAL PART OF ADMITTANCE
10
0
-10
-10
0
10

Figure 14e

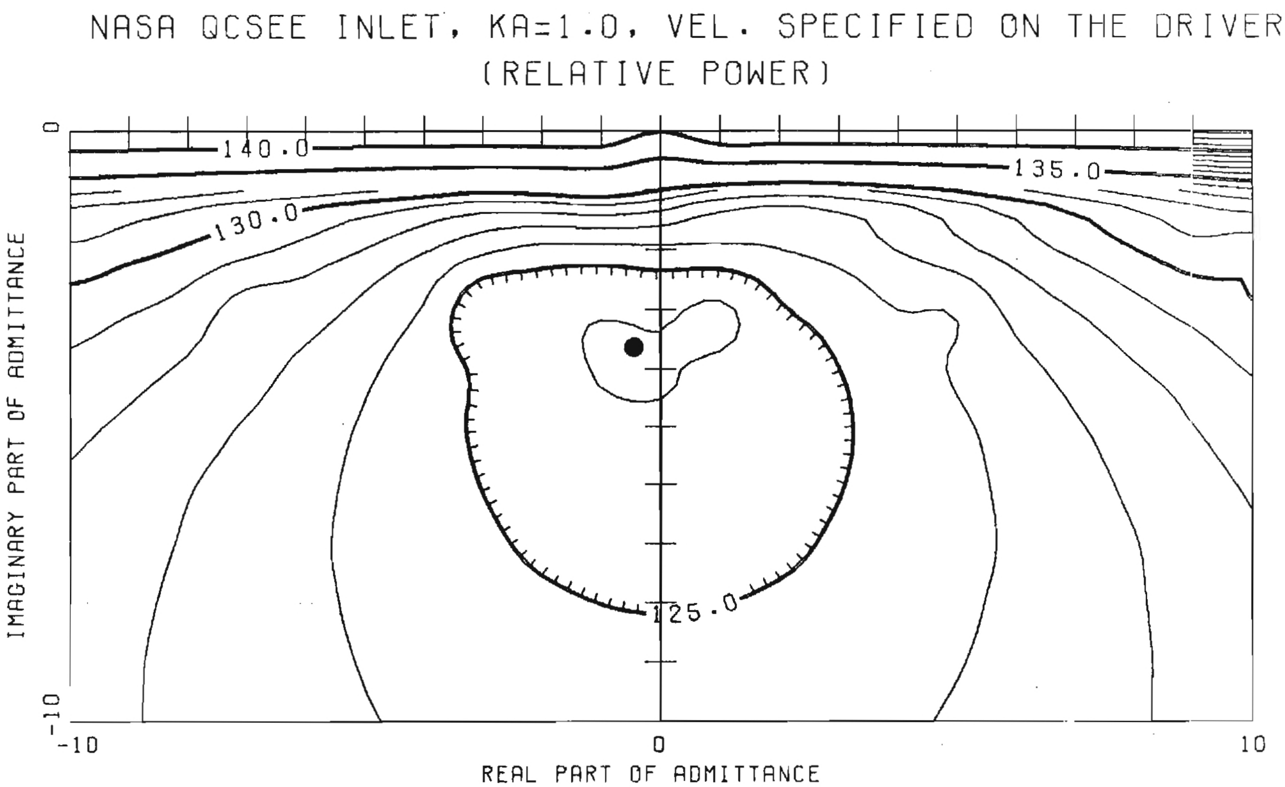
NASA QCSEE INLET, KA=1.0, VEL. SPECIFIED ON THE DRIVER
(RELATIVE POWER)
140.0
135.0
130.0
125.0
0
-10
-10
0
10
IMAGINARY PART OF ADMITTANCE
REAL PART OF ADMITTANCE

Figure 14f

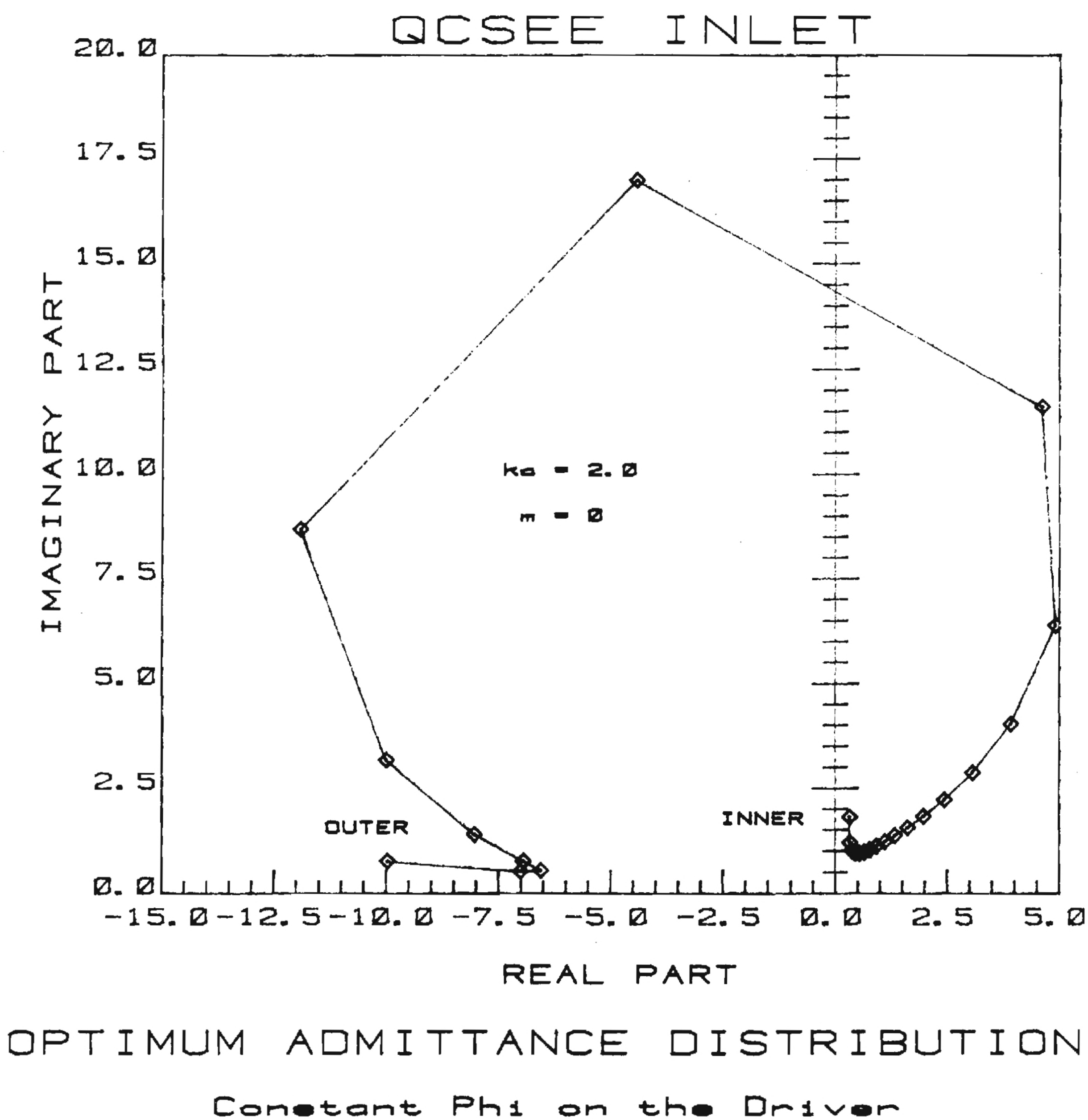
QCSEE INLET
20.0
17.5
15.0
12.5
10.0
7.5
5.0
2.5
0.0
IMAGINARY PART
ka = 2.0
m = 0
OUTER
INNER
-15.0 -12.5 -10.0 -7.5 -5.0 -2.5 0.0 2.5 5.0
REAL PART
OPTIMUM ADMITTANCE DISTRIBUTION
Constant Phi on the Driver

Figure 15a

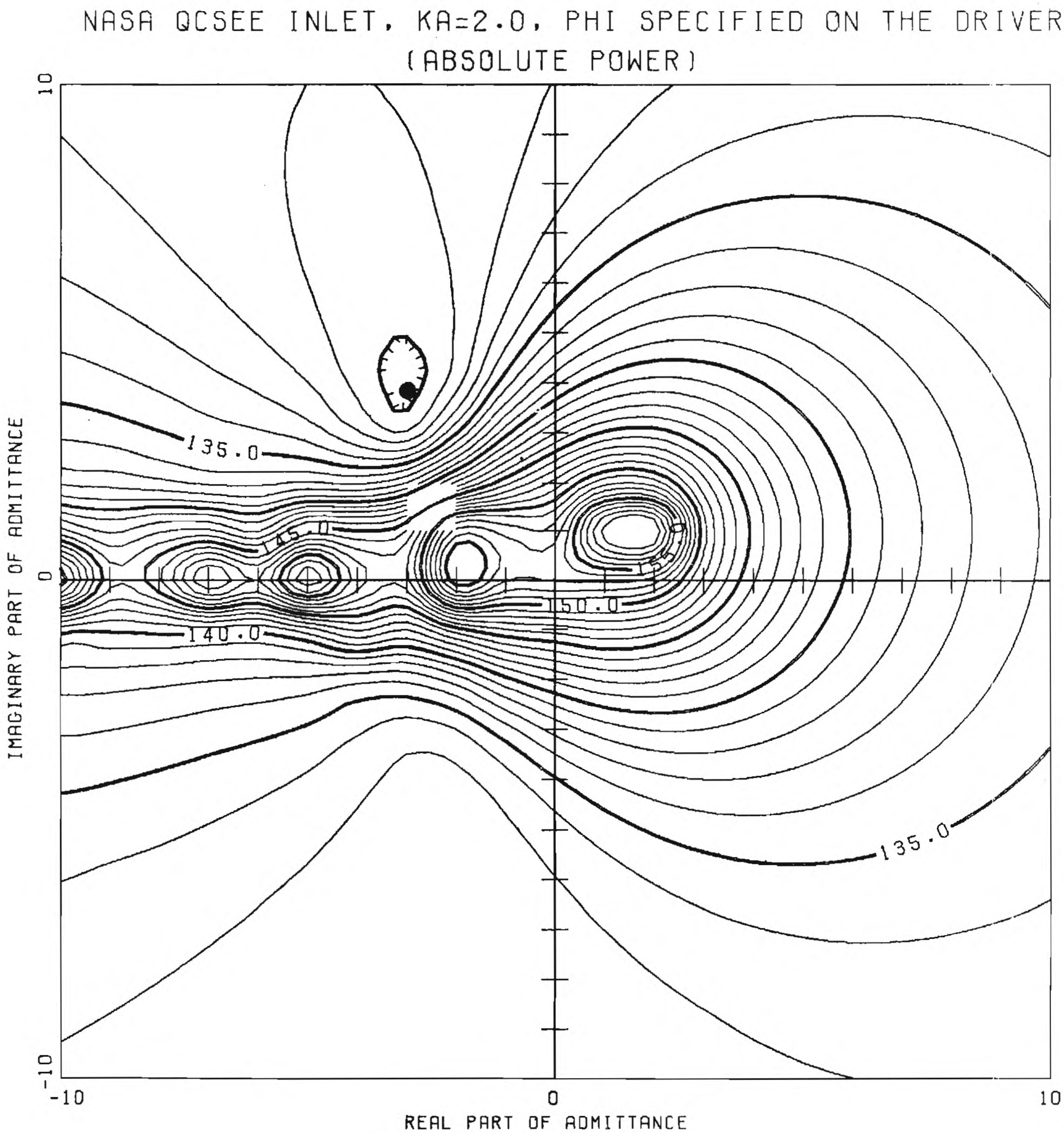
NASA QCSEE INLET, KA=2.0, PHI SPECIFIED ON THE DRIVER
(ABSOLUTE POWER)
135.0
145.0
155.0
150.0
140.0
135.0
10
0
-10
-10
0
10
IMAGINARY PART OF ADMITTANCE
REAL PART OF ADMITTANCE

Figure 15b

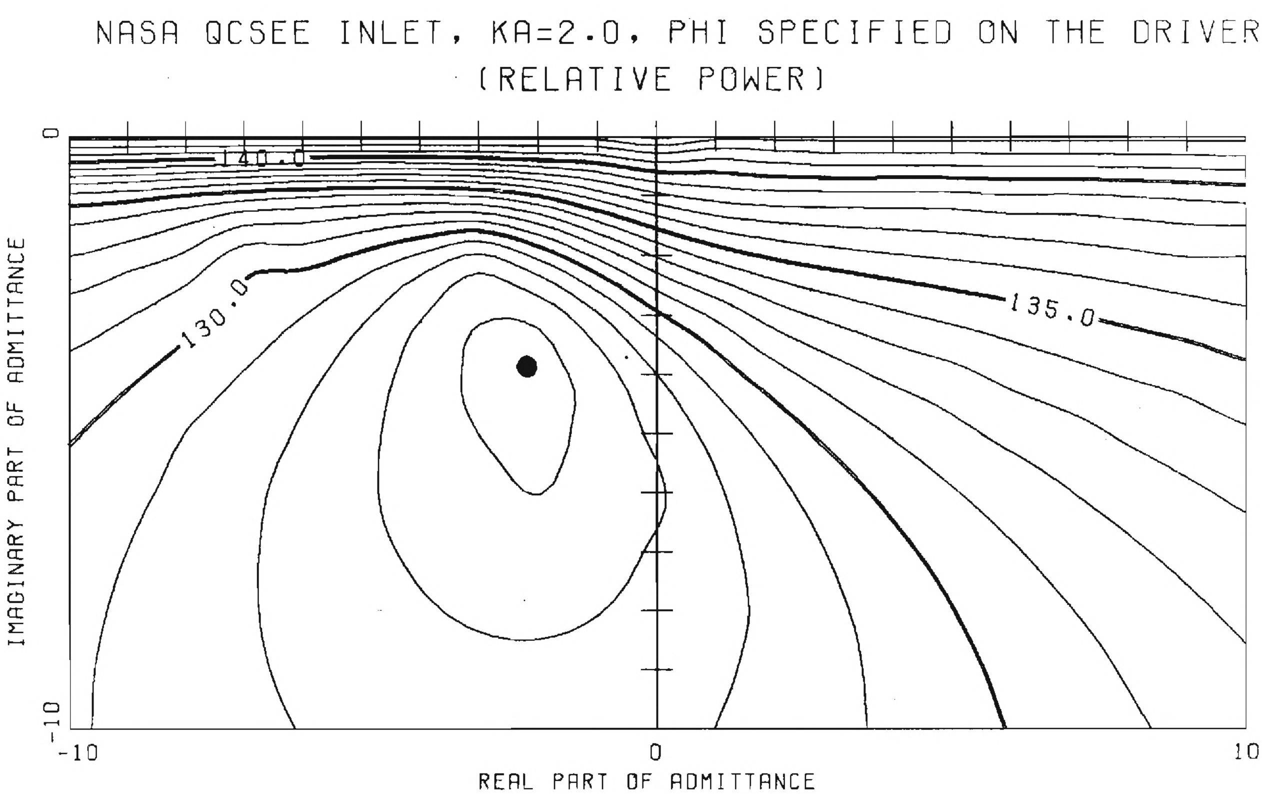
NASA QCSEE INLET, KA=2.0, PHI SPECIFIED ON THE DRIVER
(RELATIVE POWER)
140.0
130.0
135.0
0
-10
-10
0
10
IMAGINARY PART OF ADMITTANCE
REAL PART OF ADMITTANCE

Figure 15c

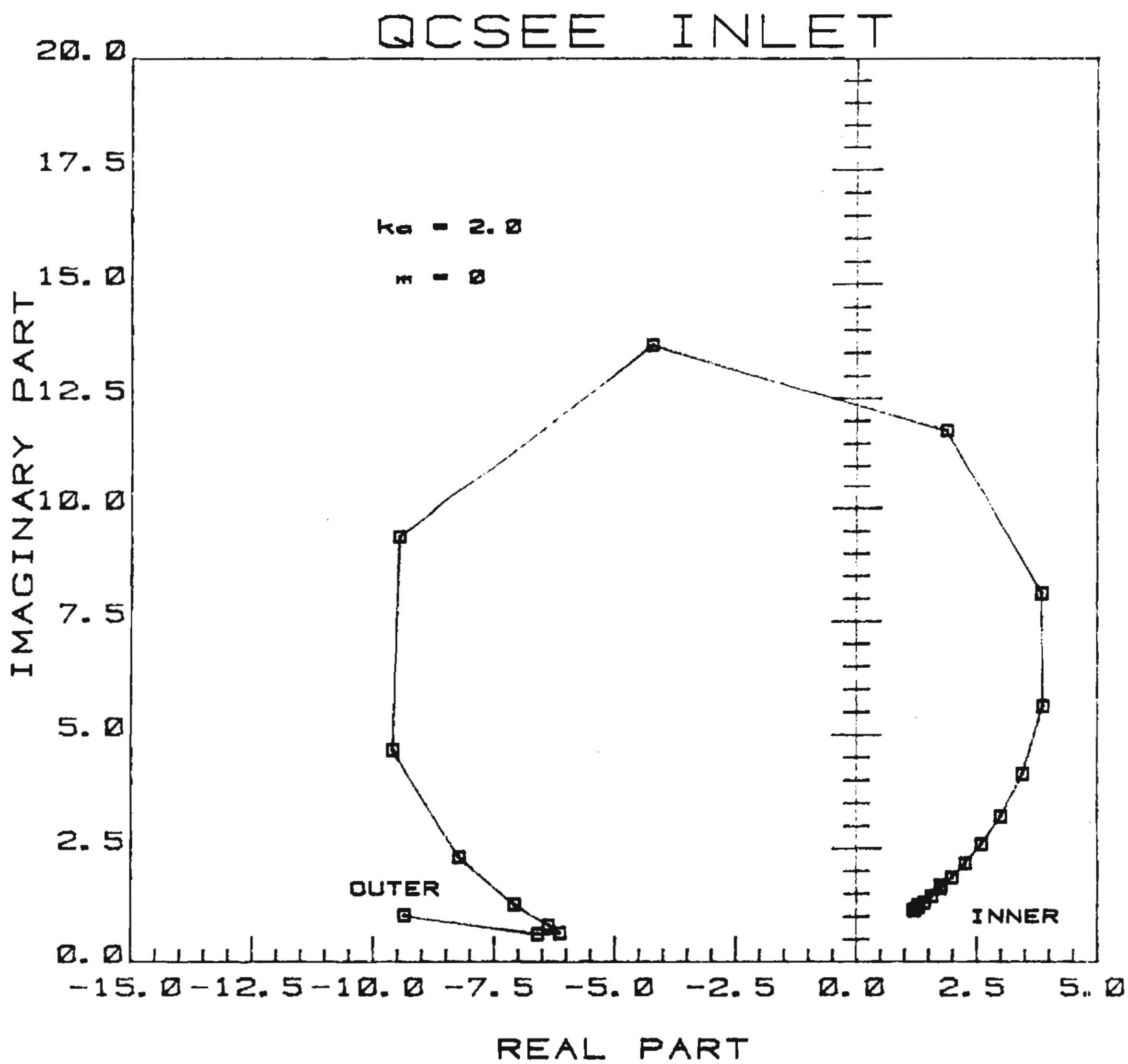

OPTIMUM ADMITTANCE DISTRIBUTION

Constant Velocity on the Driver

Figure 15d

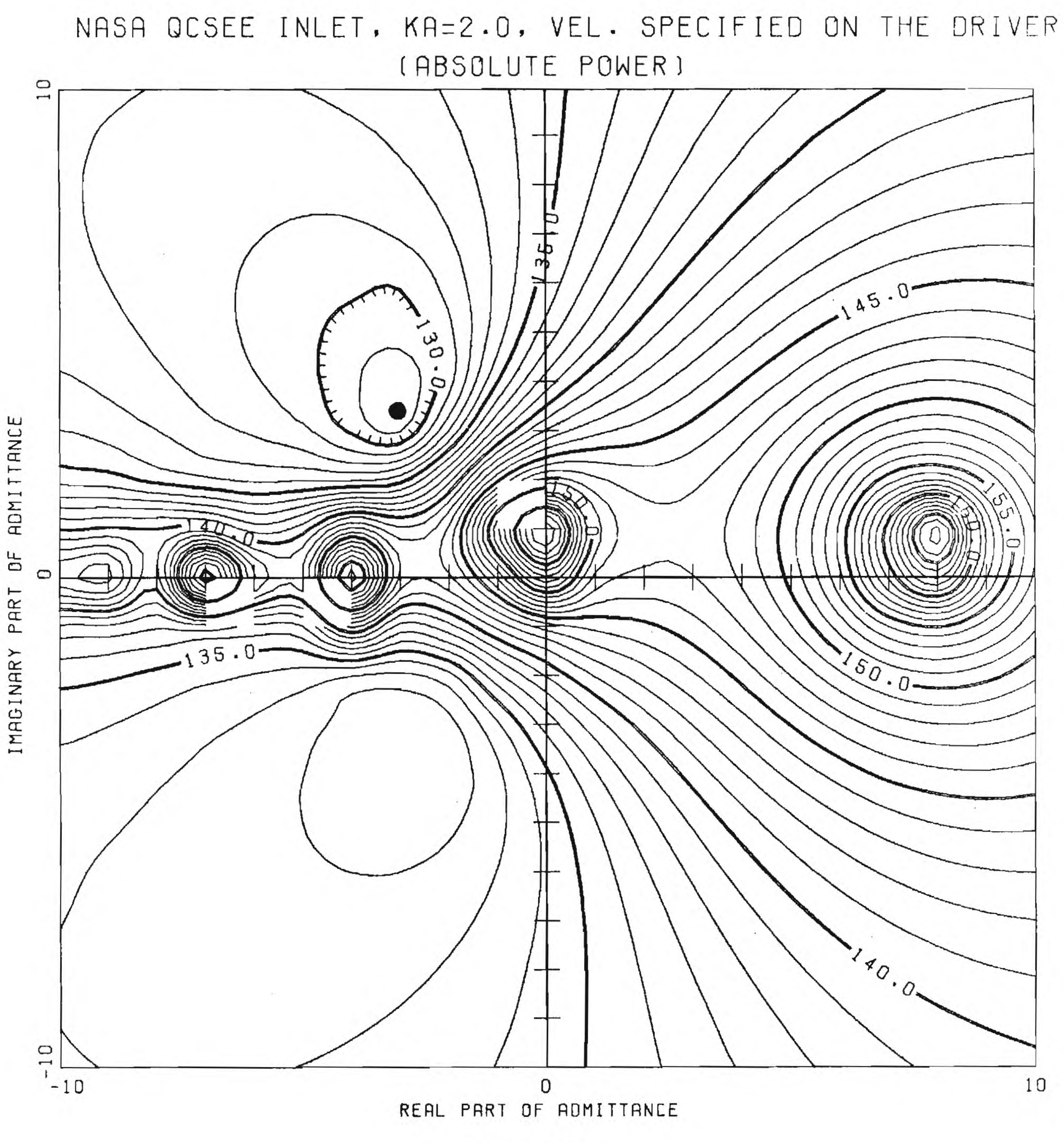

NASA QCSEE INLET, KA=2.0, VEL. SPECIFIED ON THE DRIVER
(ABSOLUTE POWER)
IMAGINARY PART OF ADMITTANCE
REAL PART OF ADMITTANCE
10
0
-10
-10
0
10
130.0
135.0
140.0
145.0
150.0
155.0
140.0
135.0
150.0
140.0

Figure 15e

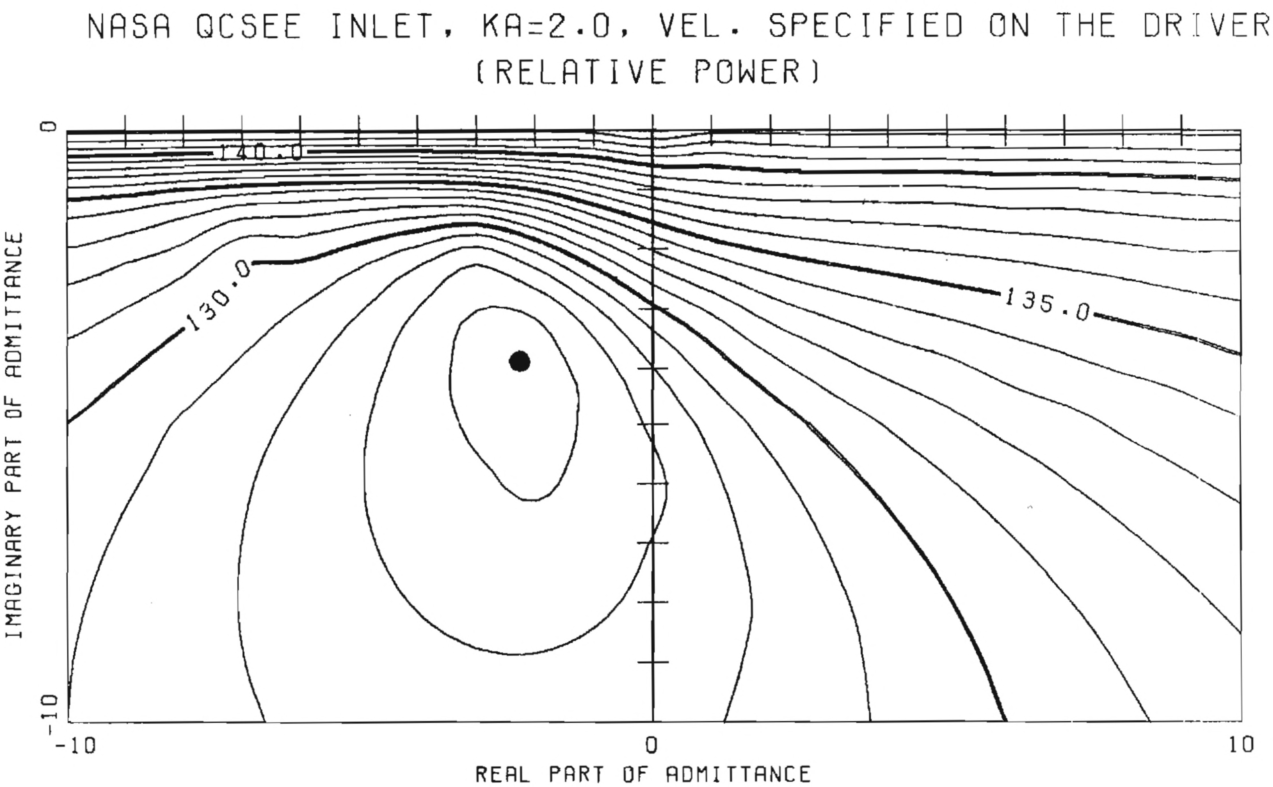
NASA QCSEE INLET, KA=2.0, VEL. SPECIFIED ON THE DRIVER
(RELATIVE POWER)
140.0
130.0
135.0
0
-10
-10
0
10
IMAGINARY PART OF ADMITTANCE
REAL PART OF ADMITTANCE

Figure 15f

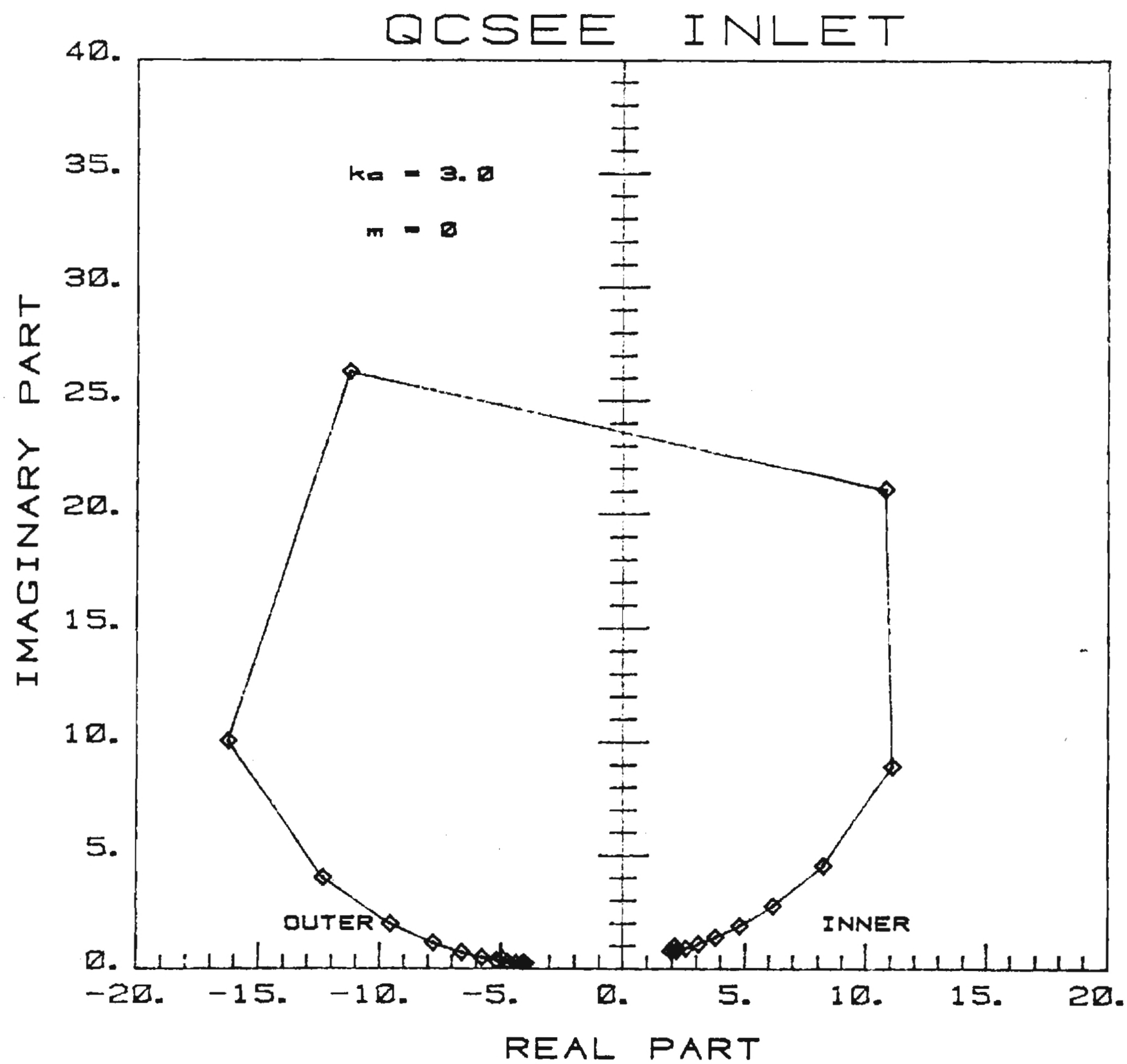

OPTIMUM ADMITTANCE DISTRIBUTION

Constant Phi on the Driver

Figure 16a

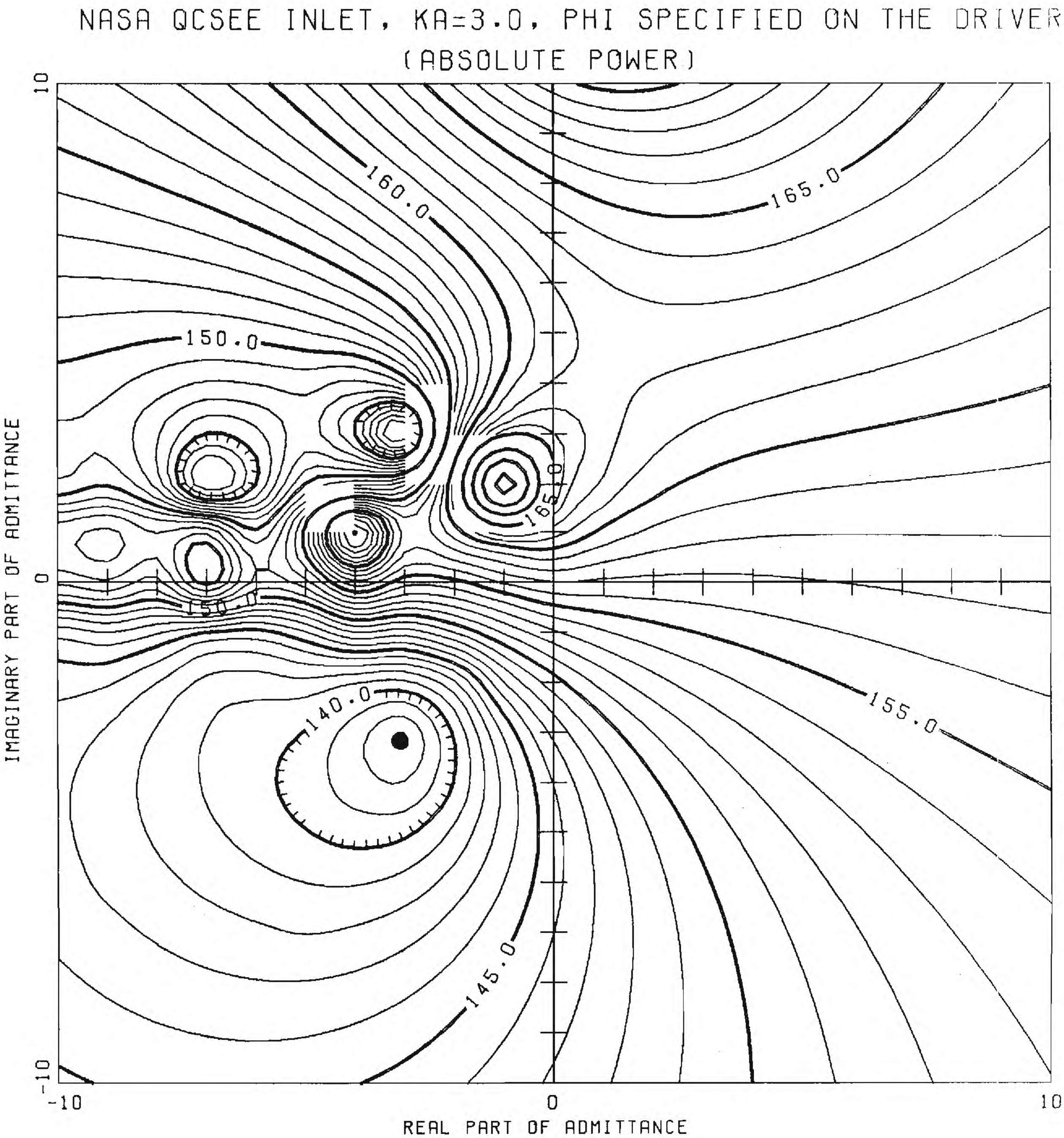
NASA QCSEE INLET, KA=3.0, PHI SPECIFIED ON THE DRIVER
(ABSOLUTE POWER)
160.0
165.0
150.0
165.0
150.0
140.0
155.0
145.0
10
0
-10
-10
0
10
IMAGINARY PART OF ADMITTANCE
REAL PART OF ADMITTANCE

Figure 16b

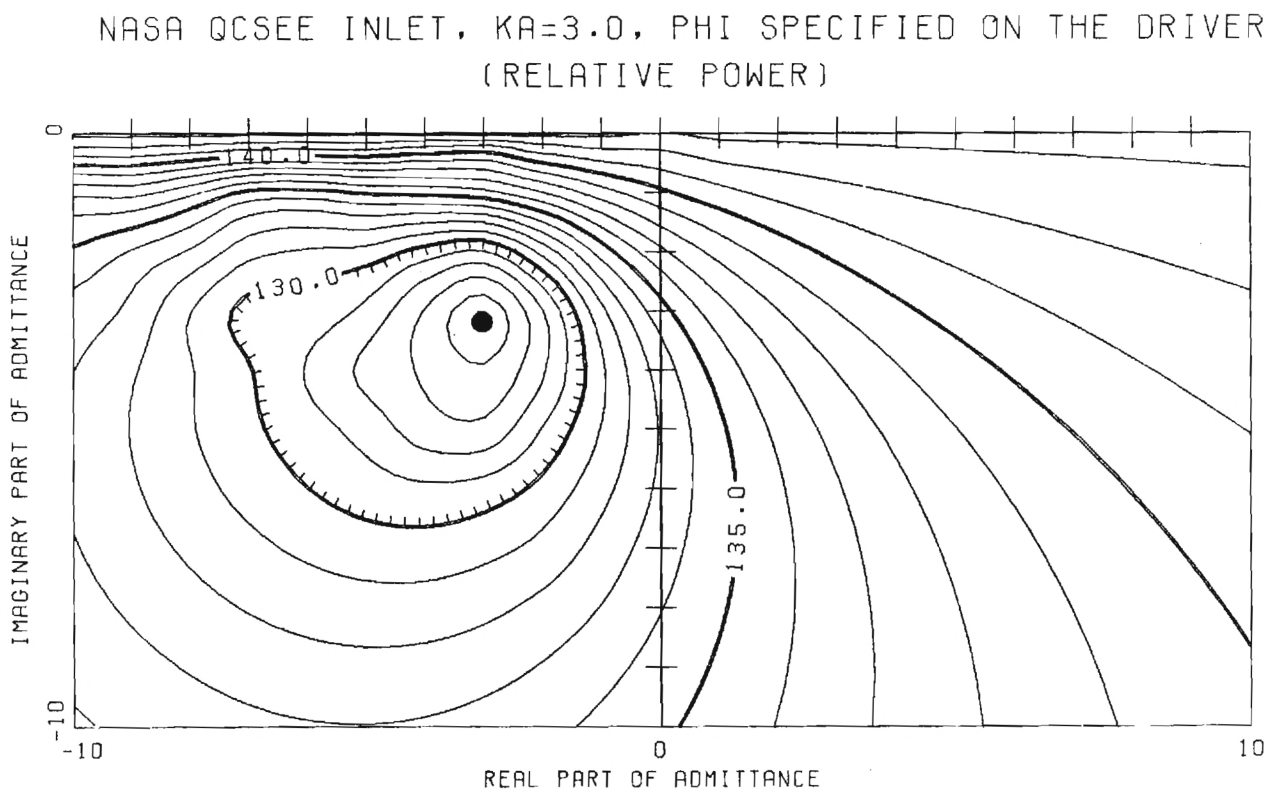
NASA QCSEE INLET, KA=3.0, PHI SPECIFIED ON THE DRIVER
(RELATIVE POWER)
140.0
130.0
135.0
0
-10
-10
0
10
IMAGINARY PART OF ADMITTANCE
REAL PART OF ADMITTANCE

Figure 16c

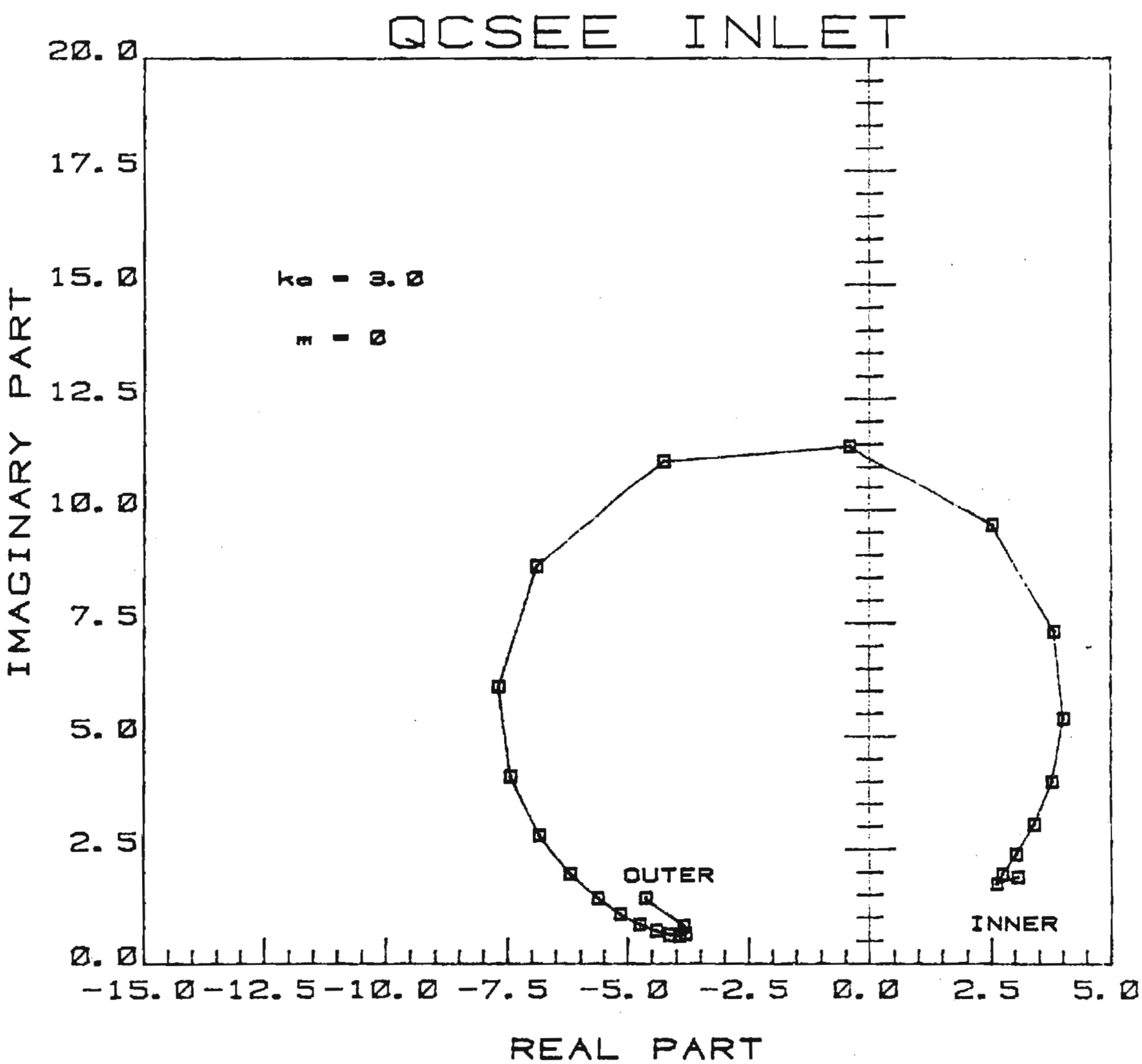

OPTIMUM ADMITTANCE DISTRIBUTION

Constant Velocity on the Driver

Figure 16d

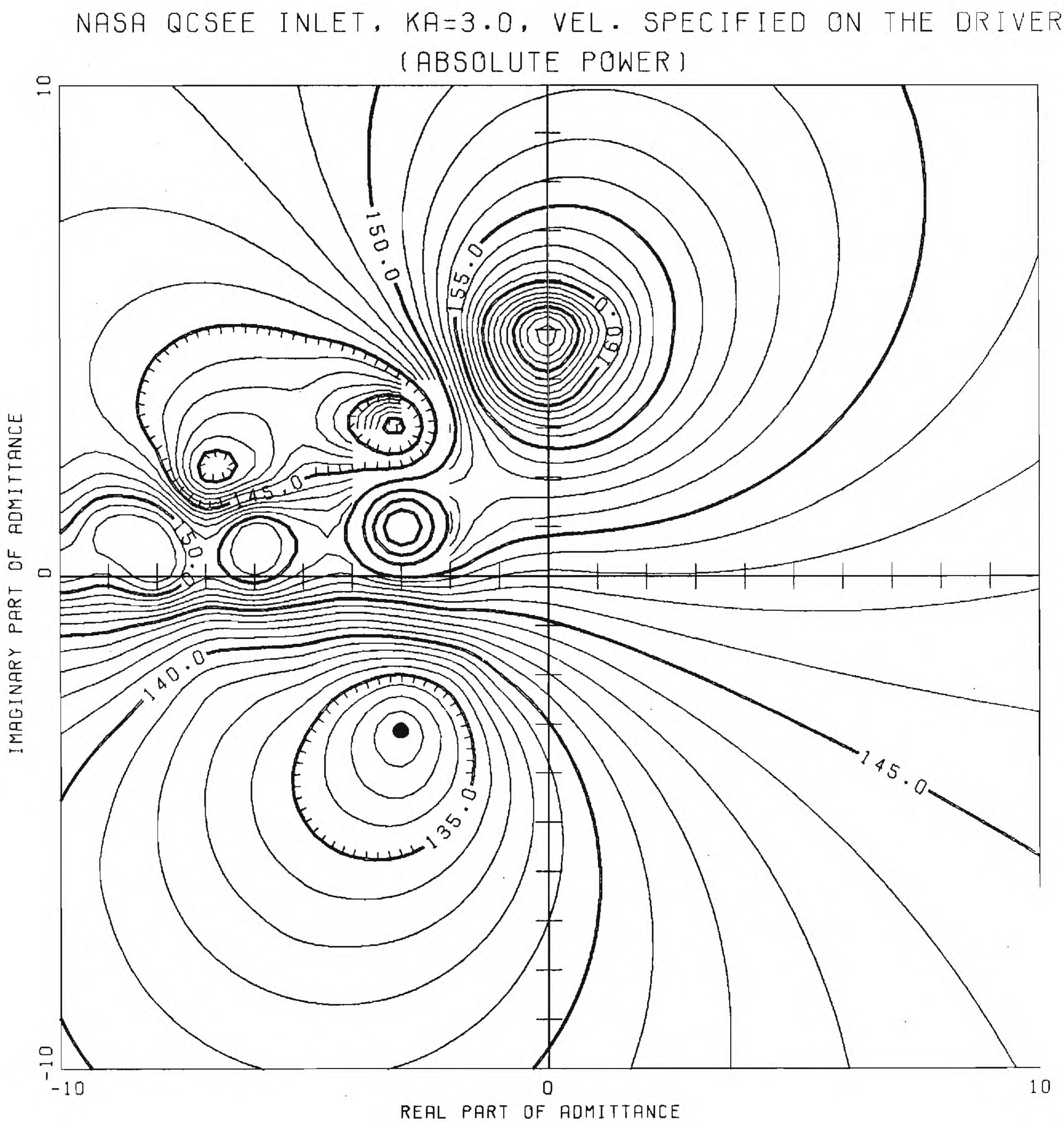
NASA QCSEE INLET, KA=3.0, VEL. SPECIFIED ON THE DRIVER
(ABSOLUTE POWER)
IMAGINARY PART OF ADMITTANCE
REAL PART OF ADMITTANCE
10
0
-10
-10
0
10
150.0
155.0
160.0
145.0
150.0
140.0
145.0
135.0

Figure 16e

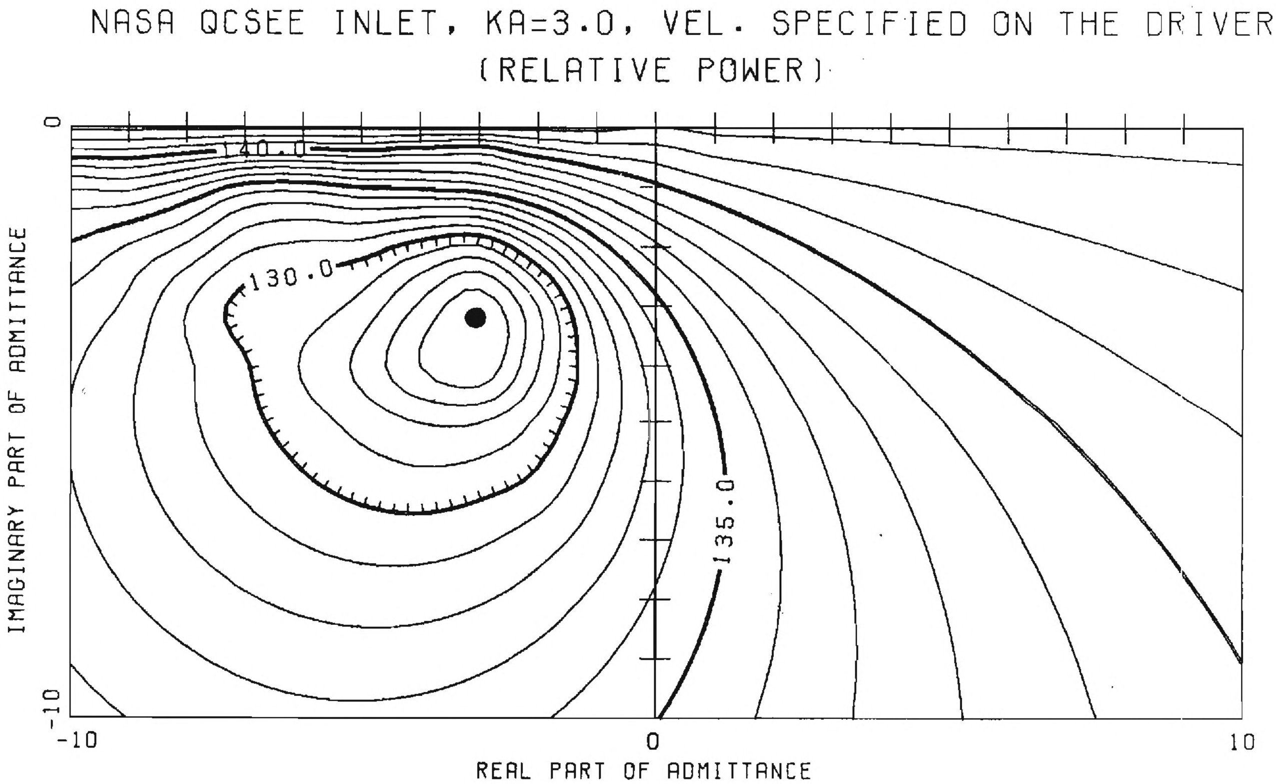
NASA QCSEE INLET, KA=3.0, VEL. SPECIFIED ON THE DRIVER
(RELATIVE POWER)
140.0
130.0
135.0
IMAGINARY PART OF ADMITTANCE
REAL PART OF ADMITTANCE
0
-10
10

Figure 16f

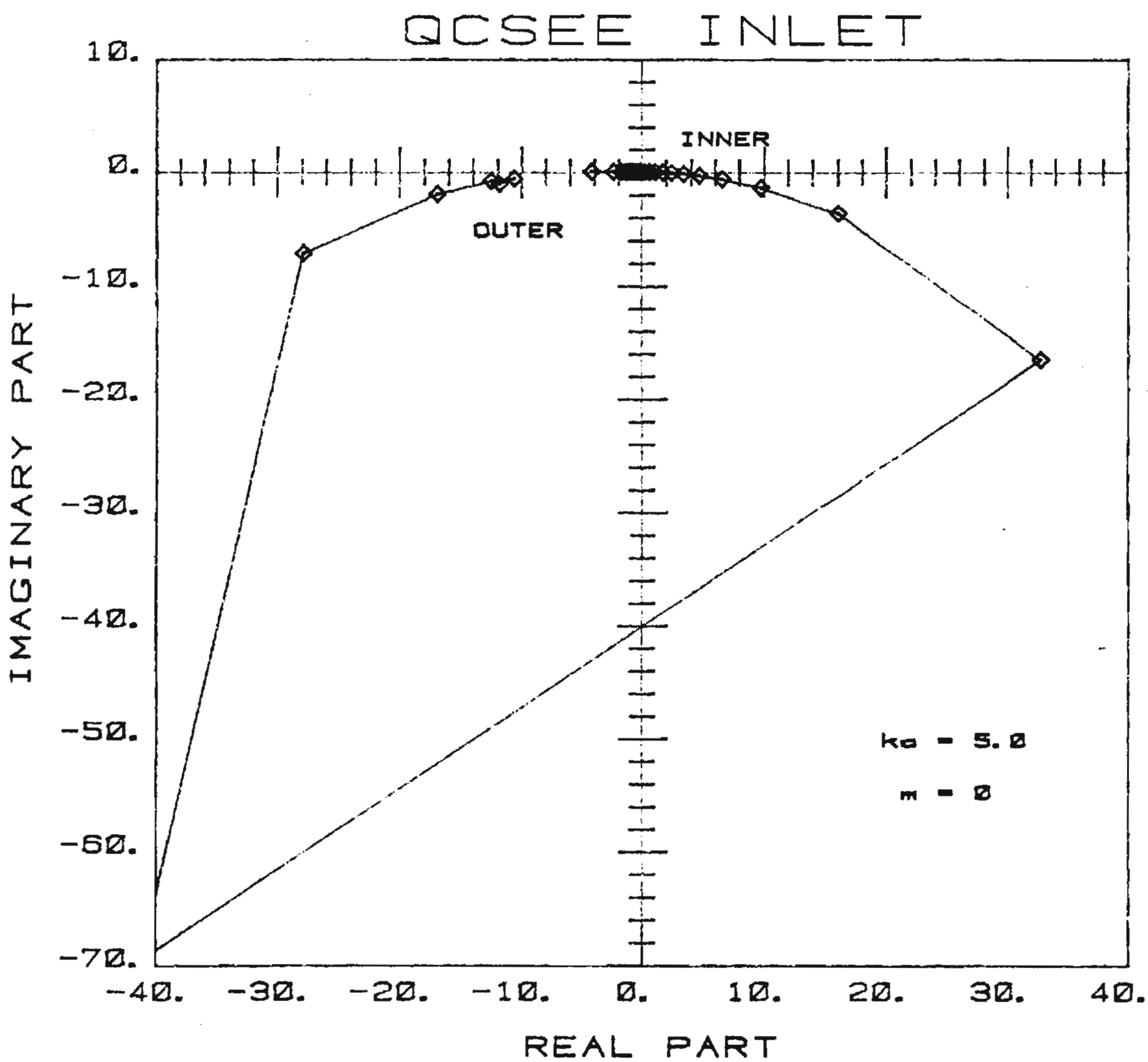

OPTIMUM ADMITTANCE DISTRIBUTION

Constant Phi on the Driver

Figure 17a

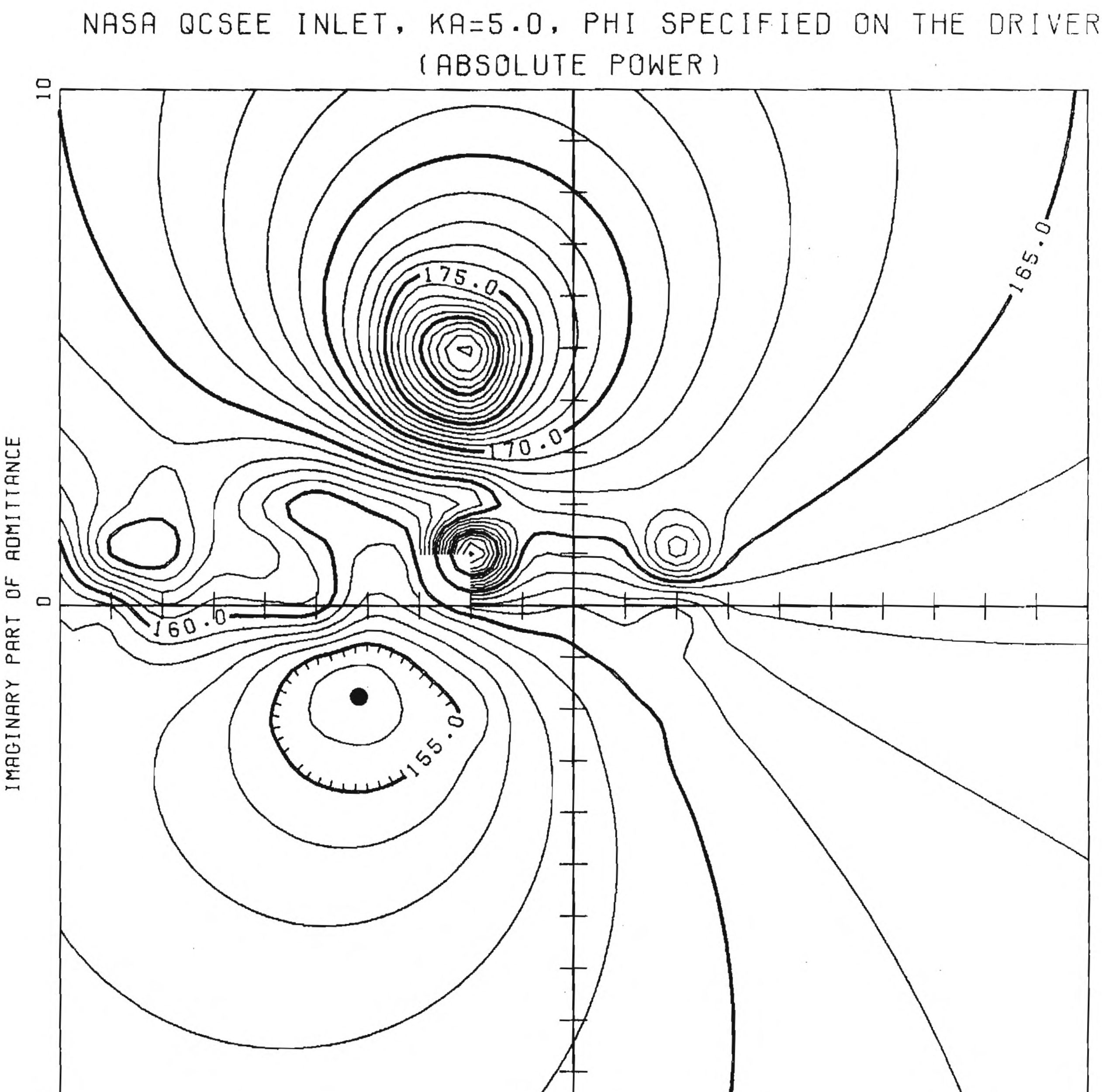
NASA QCSEE INLET, KA=5.0, PHI SPECIFIED ON THE DRIVER
(ABSOLUTE POWER)
10
0
-10
-10
0
10
IMAGINARY PART OF ADMITTANCE
REAL PART OF ADMITTANCE
175.0
170.0
165.0
160.0
155.0

Figure 17b

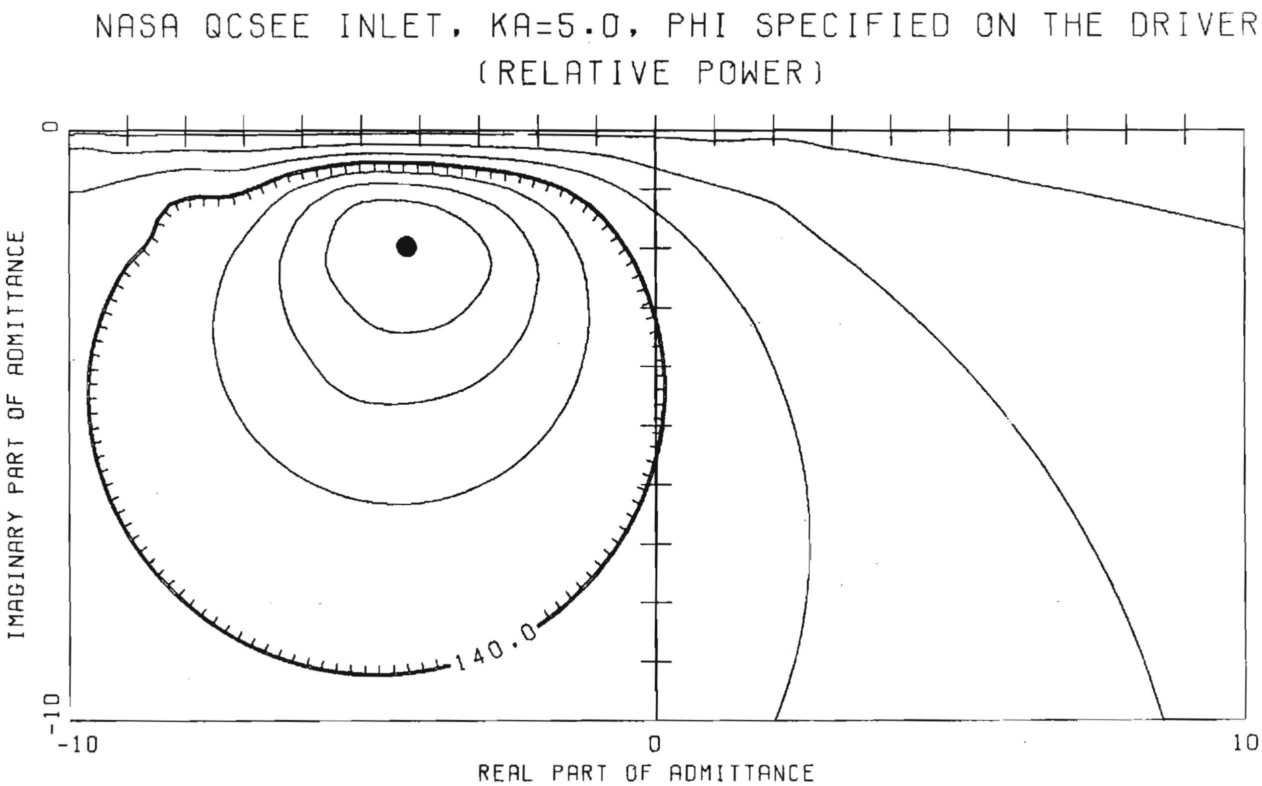

NASA QCSEE INLET, KA=5.0, PHI SPECIFIED ON THE DRIVER
(RELATIVE POWER)
0
-10
IMAGINARY PART OF ADMITTANCE
140.0
-10
0
10
REAL PART OF ADMITTANCE

Figure 17c

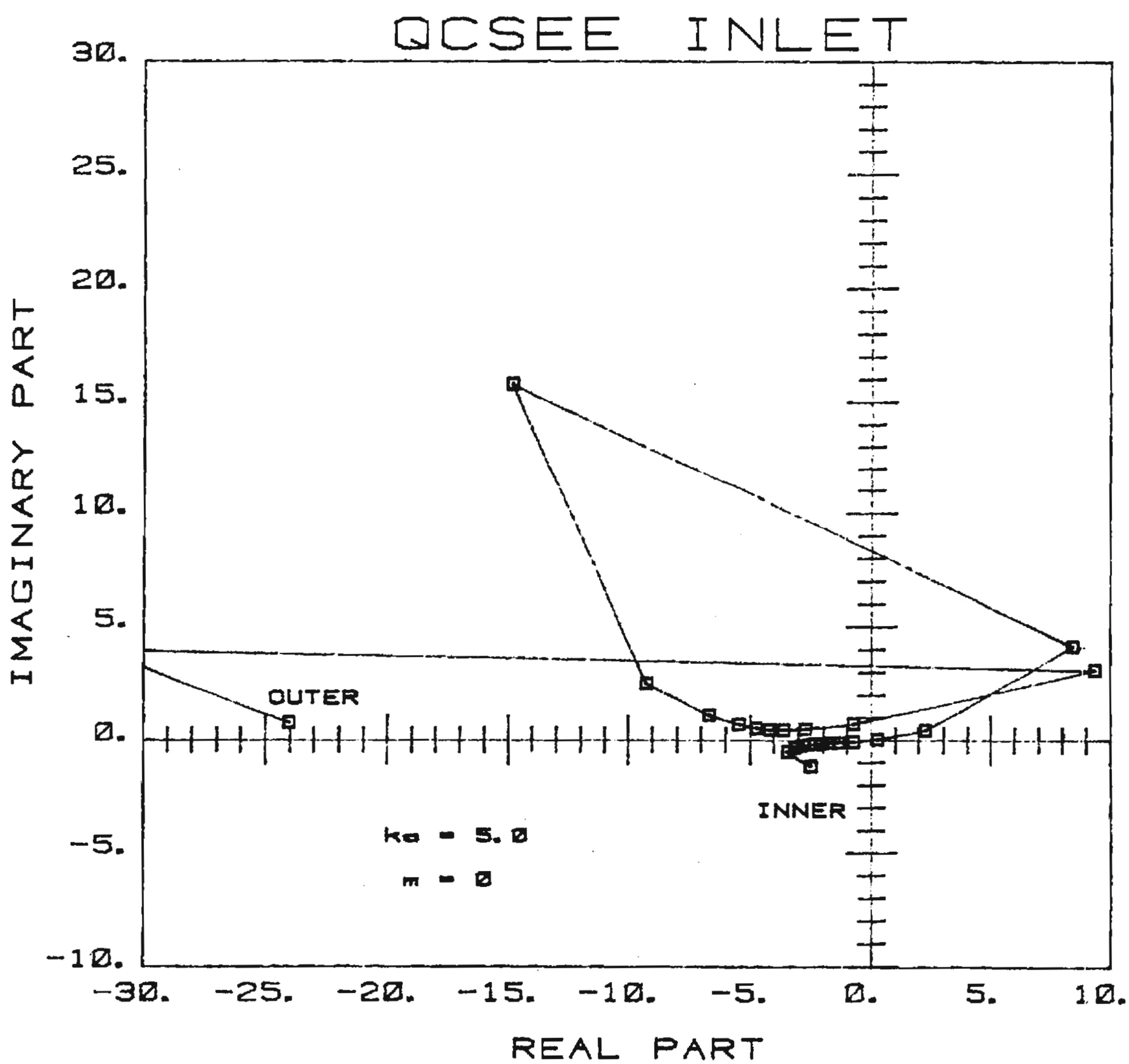

OPTIMUM ADMITTANCE DISTRIBUTION

Constant Velocity on the Driver

Figure 17d

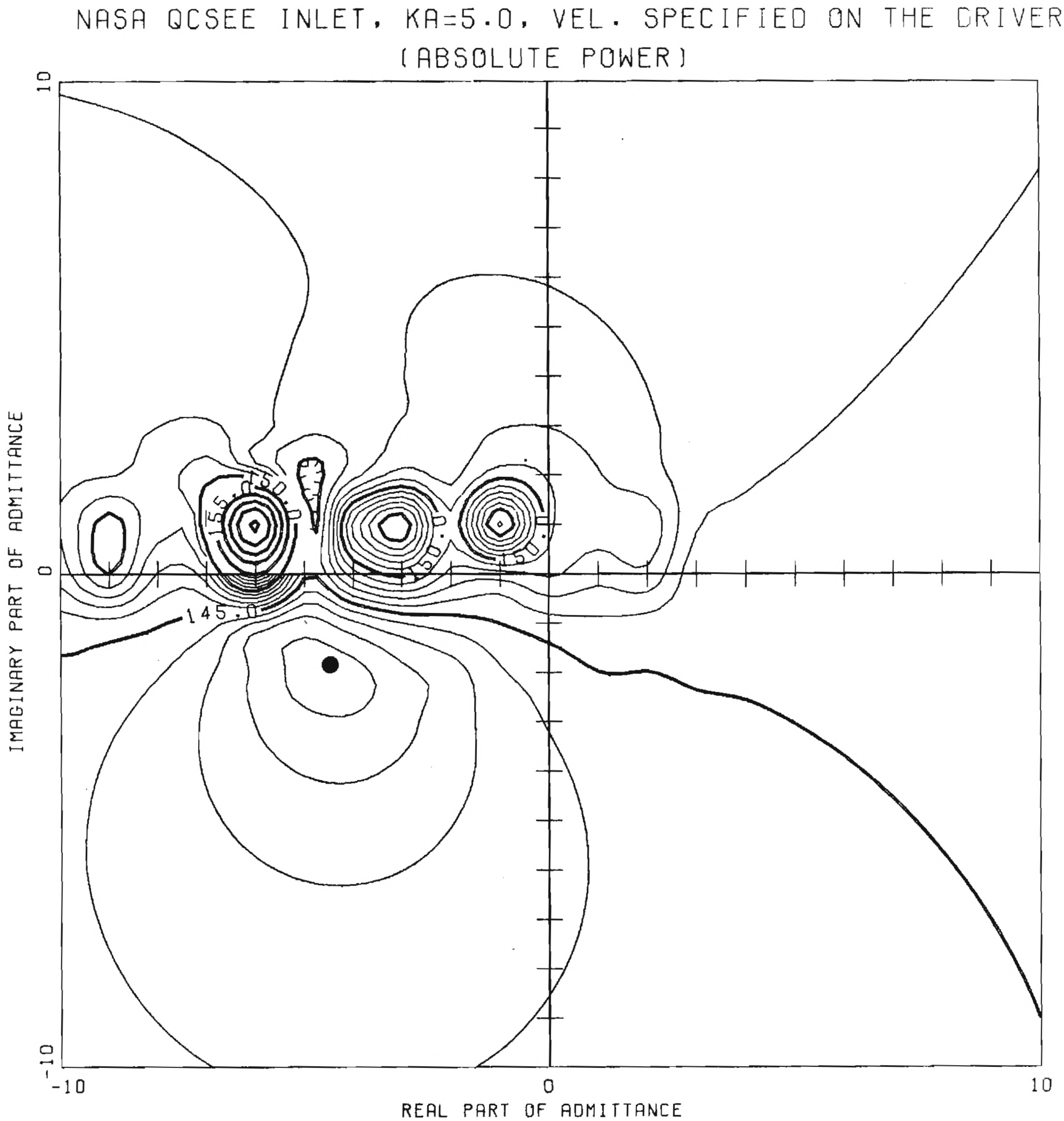

NASA QCSEE INLET, KA=5.0, VEL. SPECIFIED ON THE DRIVER
(ABSOLUTE POWER)
10
0
-10
IMAGINARY PART OF ADMITTANCE
-10
0
10
REAL PART OF ADMITTANCE
155.0
150.0
150.0
150.0
150.0
145.0

Figure 17e

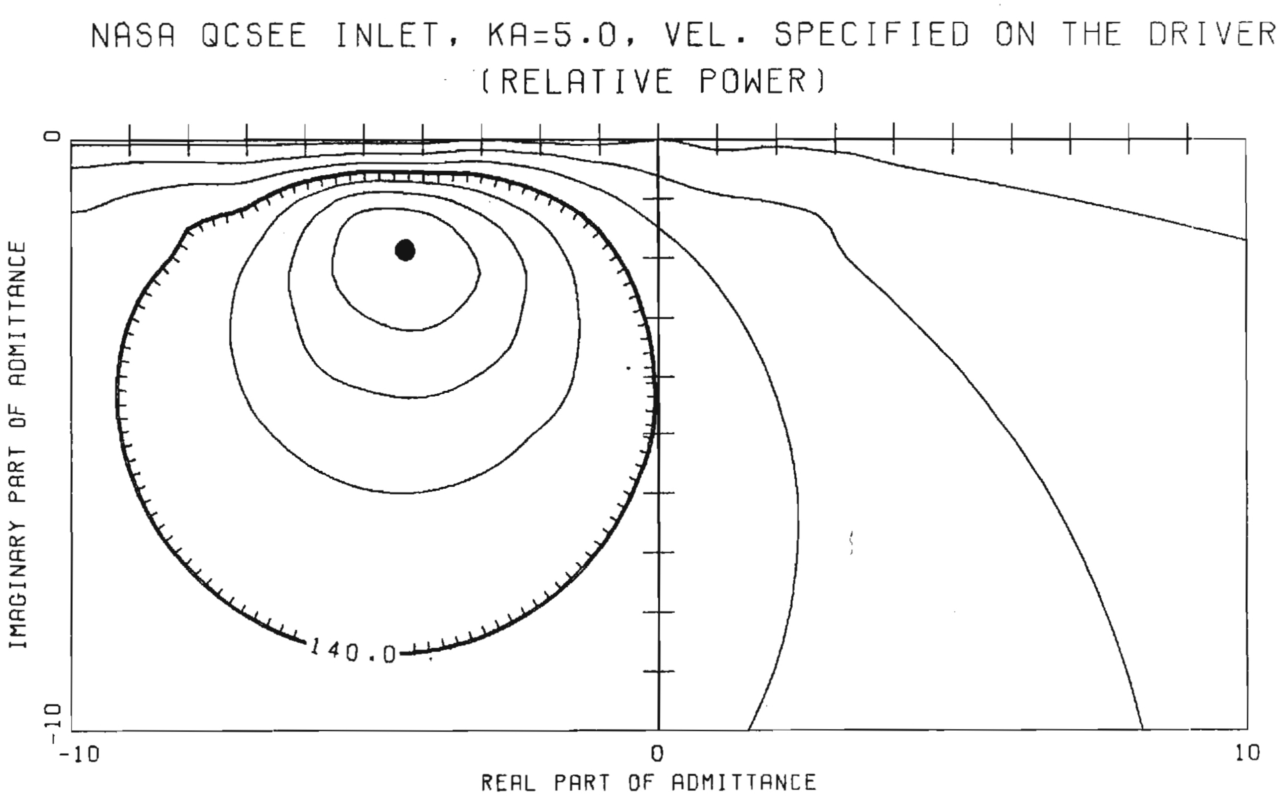
NASA QCSEE INLET, KA=5.0, VEL. SPECIFIED ON THE DRIVER
(RELATIVE POWER)
0
-10
IMAGINARY PART OF ADMITTANCE
140.0
-10
0
10
REAL PART OF ADMITTANCE

Figure 17f

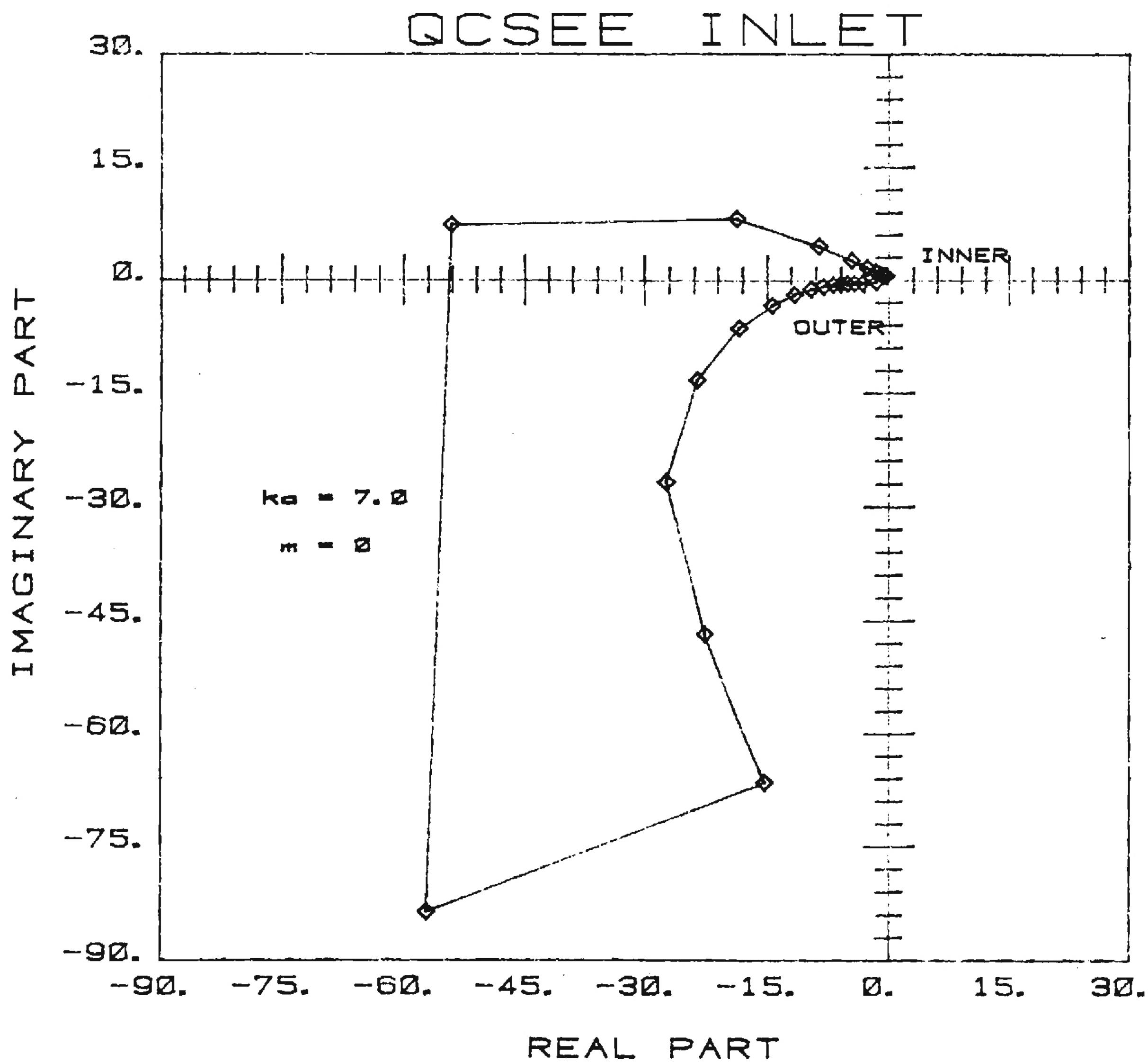

OPTIMUM ADMITTANCE DISTRIBUTION

Constant Phi on the Driver

Figure 18a

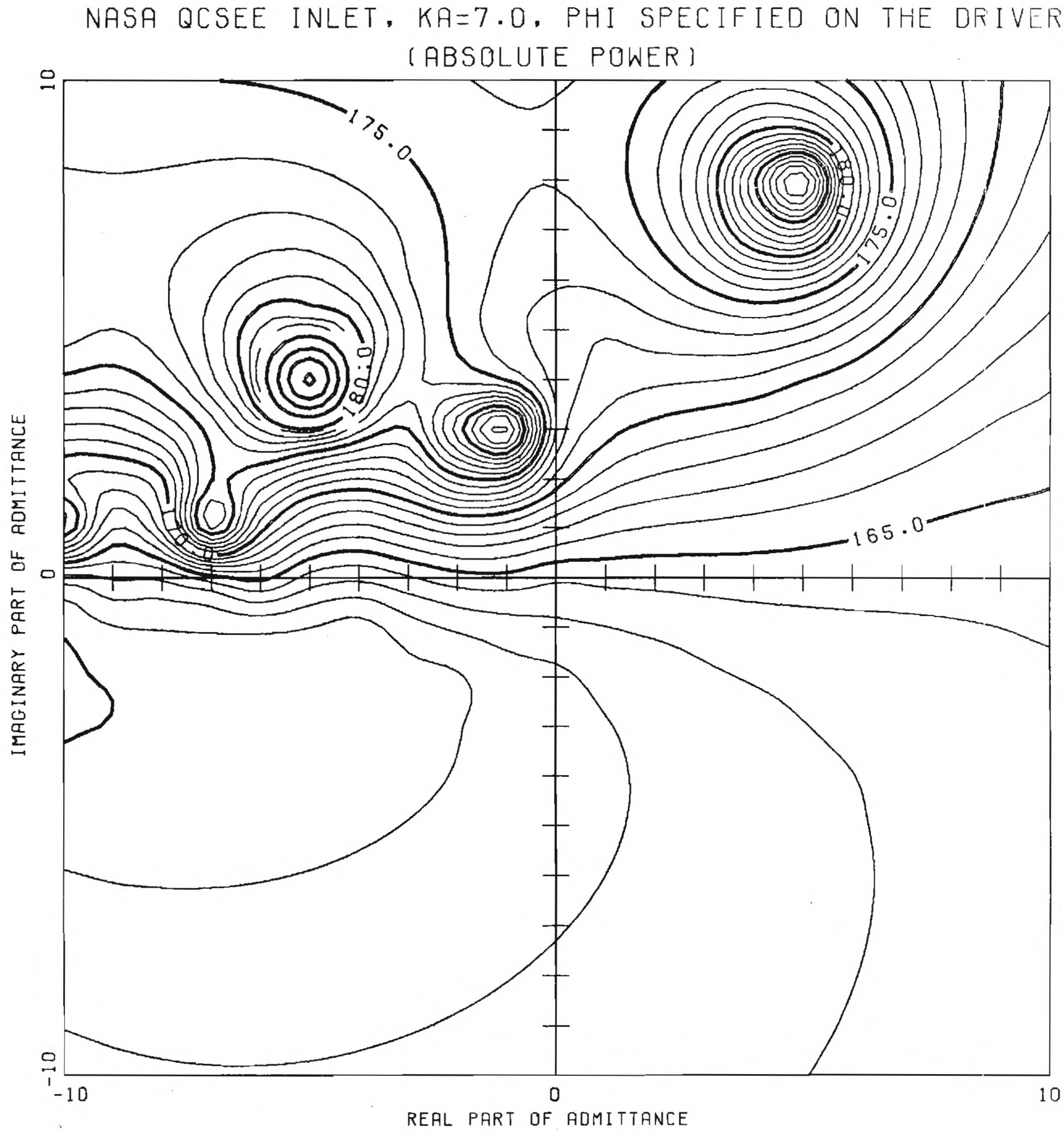
NASA QCSEE INLET, KA=7.0, PHI SPECIFIED ON THE DRIVER
(ABSOLUTE POWER)
175.0
180.0
180.0
175.0
180.0
165.0
10
0
-10
-10
0
10
IMAGINARY PART OF ADMITTANCE
REAL PART OF ADMITTANCE

Figure 18b

NASA QCSEE INLET, KA=7.0, PHI SPECIFIED ON THE DRIVER
(RELATIVE POWER)

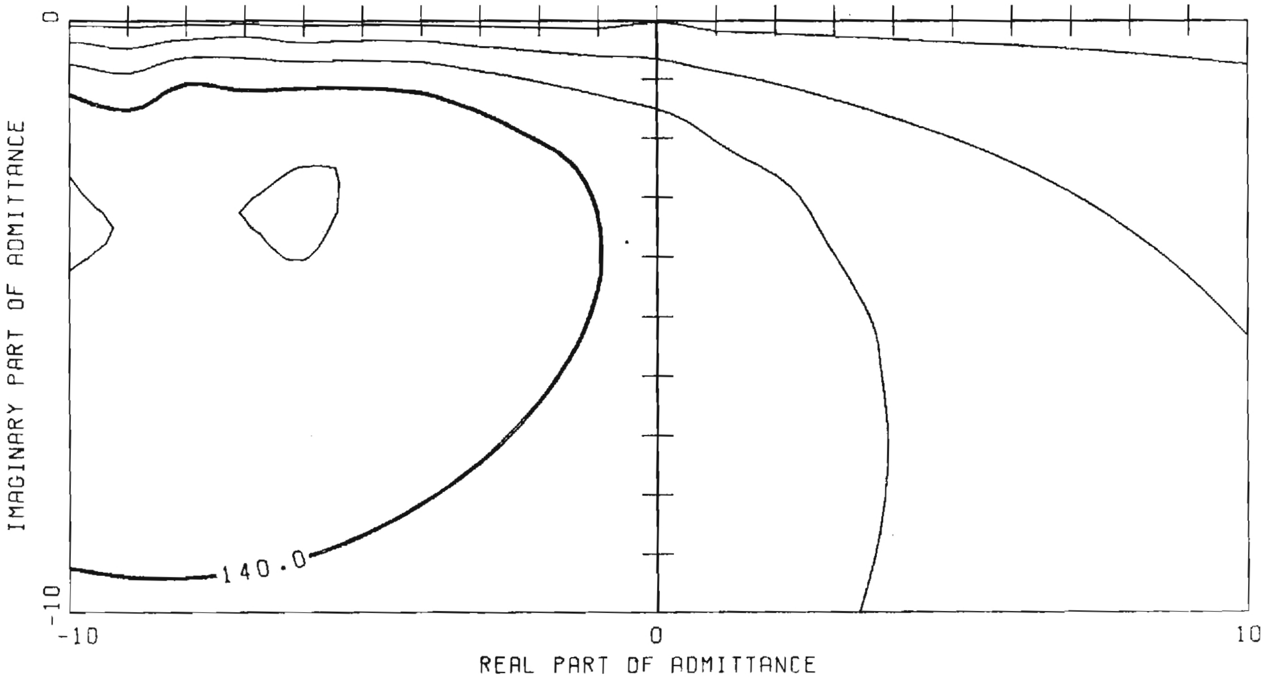

Figure 18c

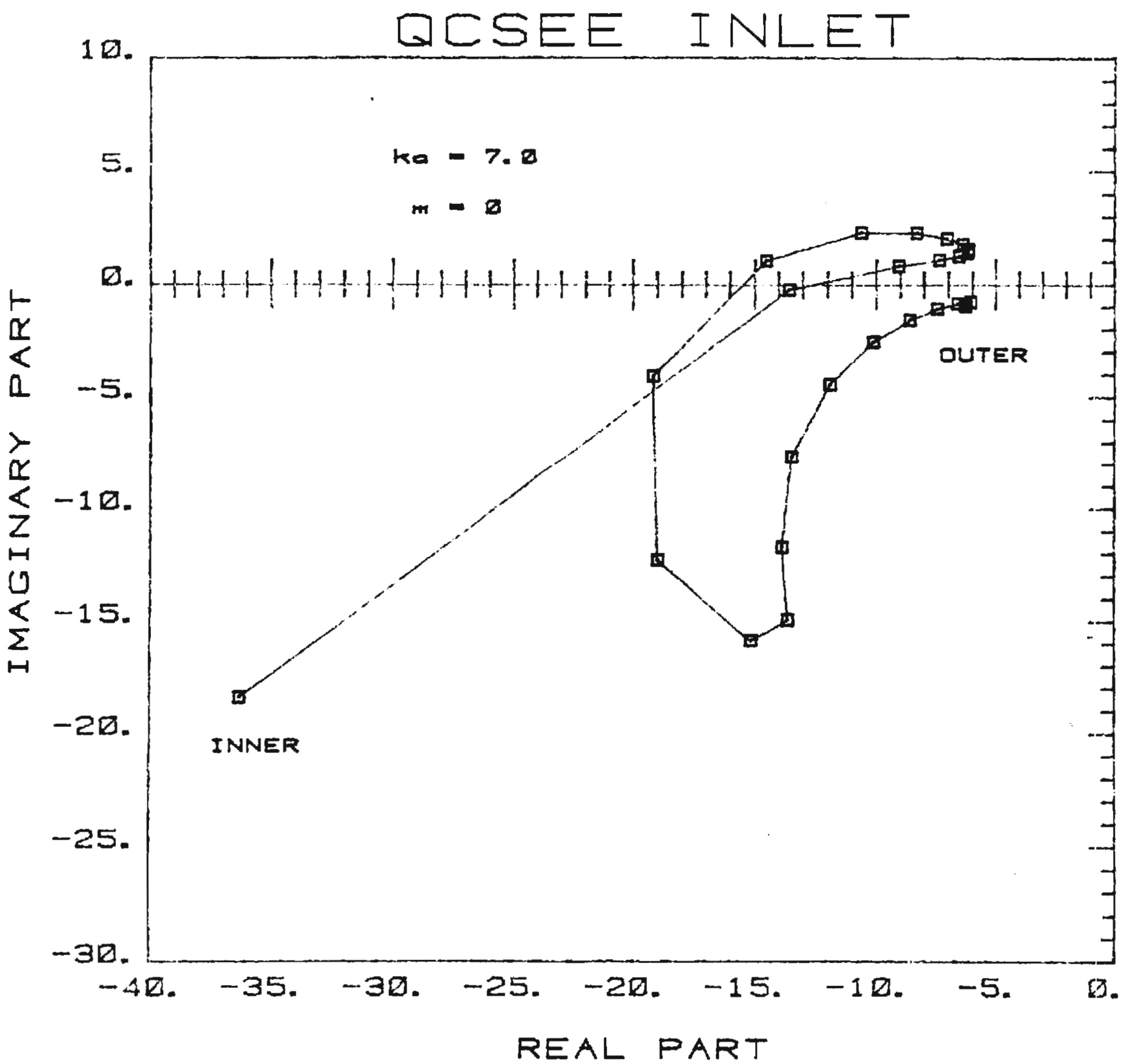

OPTIMUM ADMITTANCE DISTRIBUTION

Constant Velocity on the Driver

Figure 18d

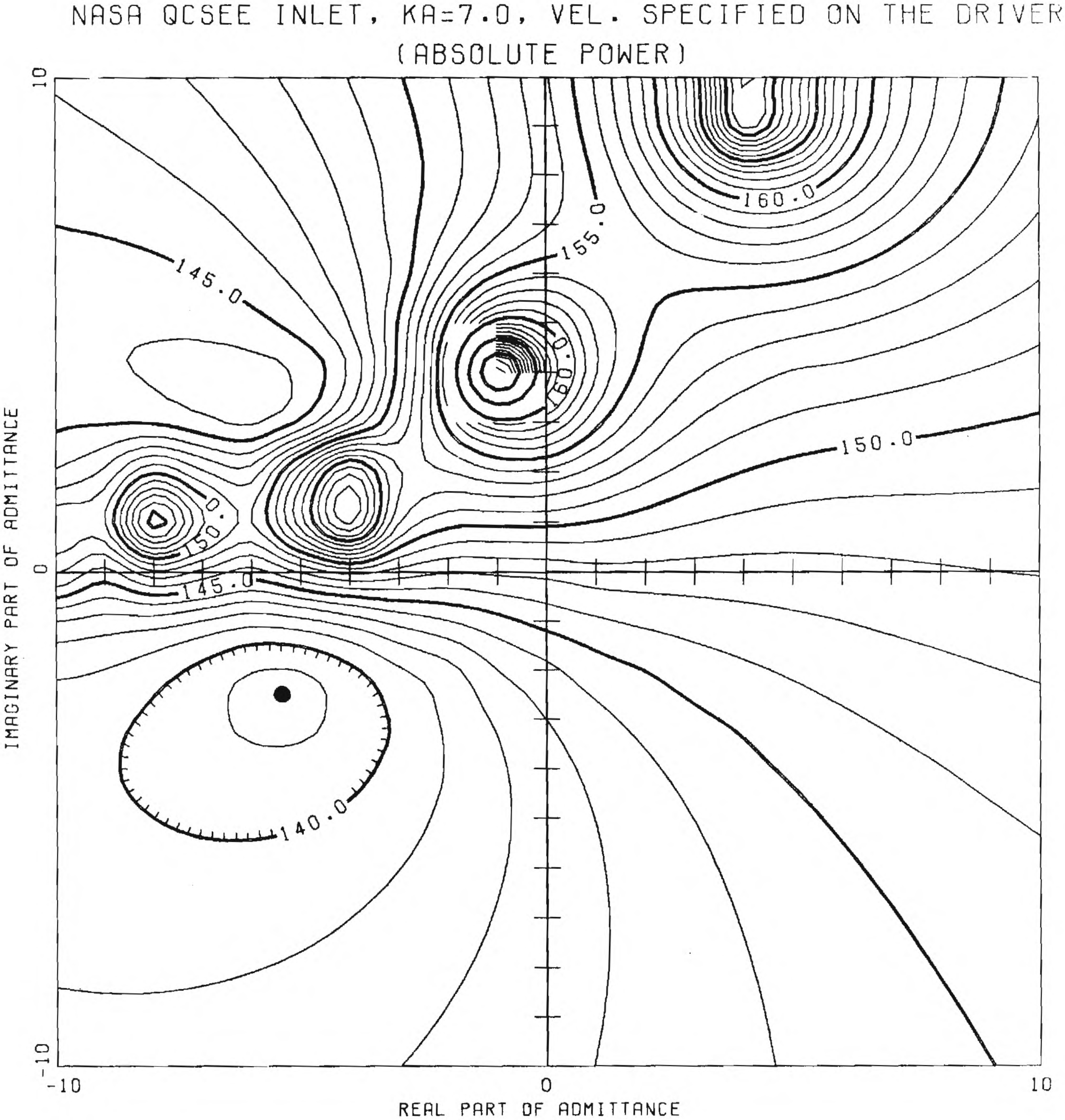
NASA QCSEE INLET, KA=7.0, VEL. SPECIFIED ON THE DRIVER
(ABSOLUTE POWER)
IMAGINARY PART OF ADMITTANCE
REAL PART OF ADMITTANCE
10
0
-10
-10
0
10
160.0
155.0
145.0
160.0
150.0
150
145.0
140.0

Figure 18e

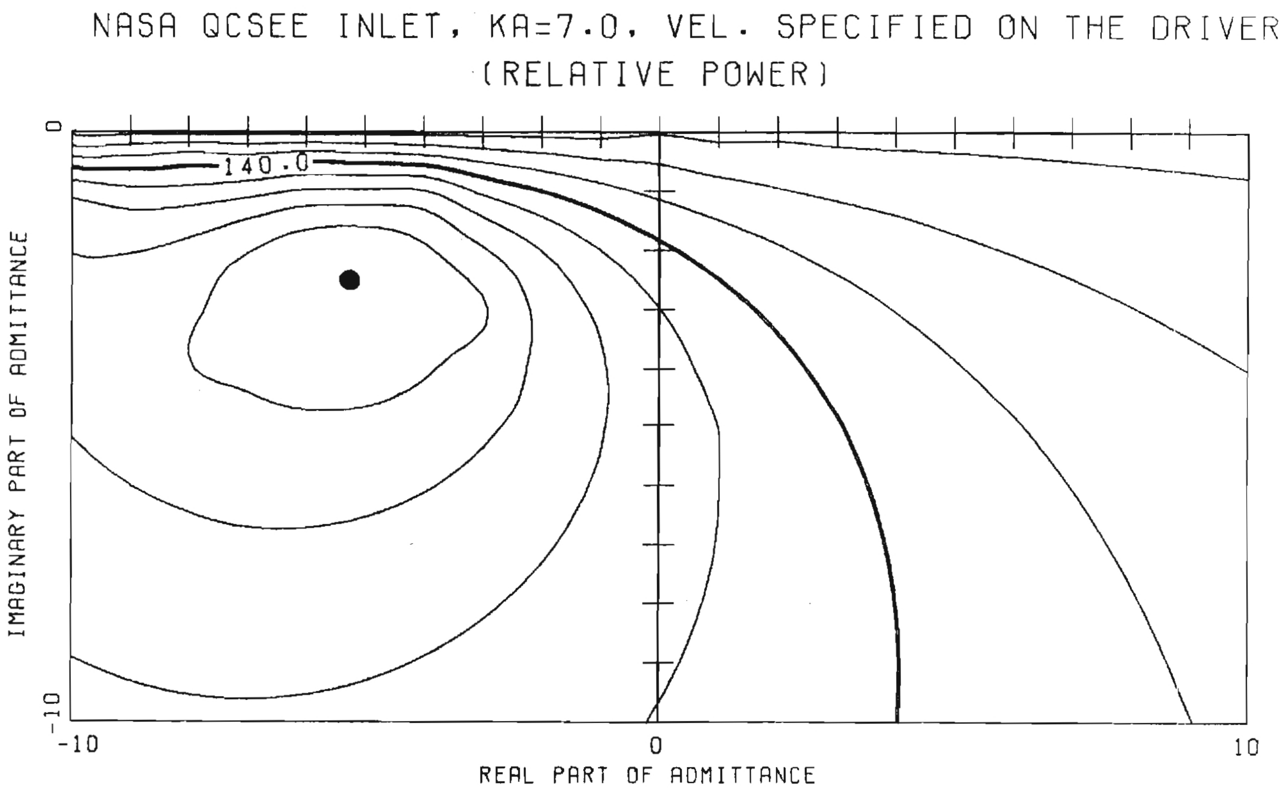

NASA QCSEE INLET, KA=7.0, VEL. SPECIFIED ON THE DRIVER
(RELATIVE POWER)
140.0
0
-10
IMAGINARY PART OF ADMITTANCE
-10
0
10
REAL PART OF ADMITTANCE

Figure 18f

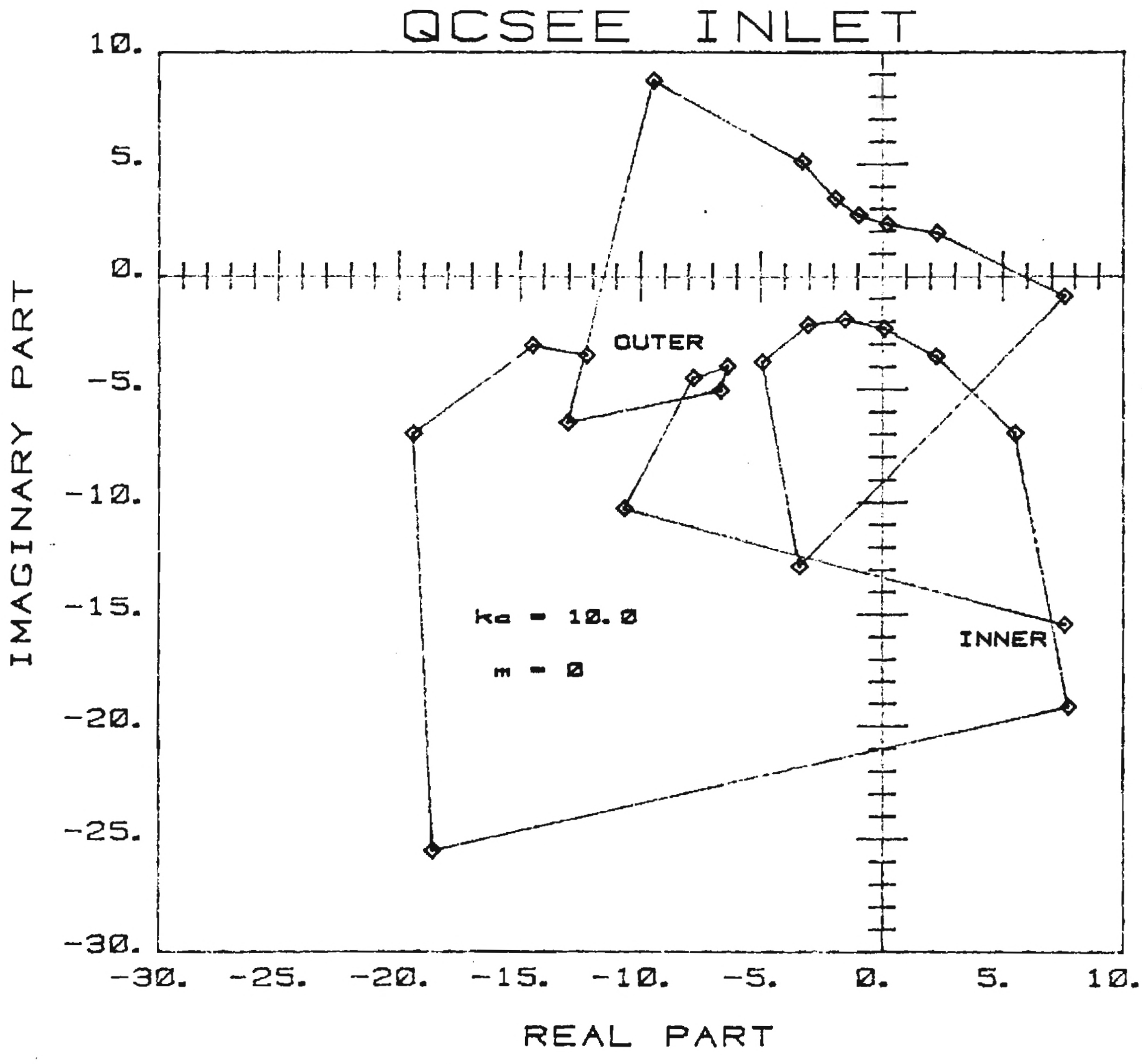

OPTIMUM ADMITTANCE DISTRIBUTION

Constant Phi on the Driver

Figure 19a

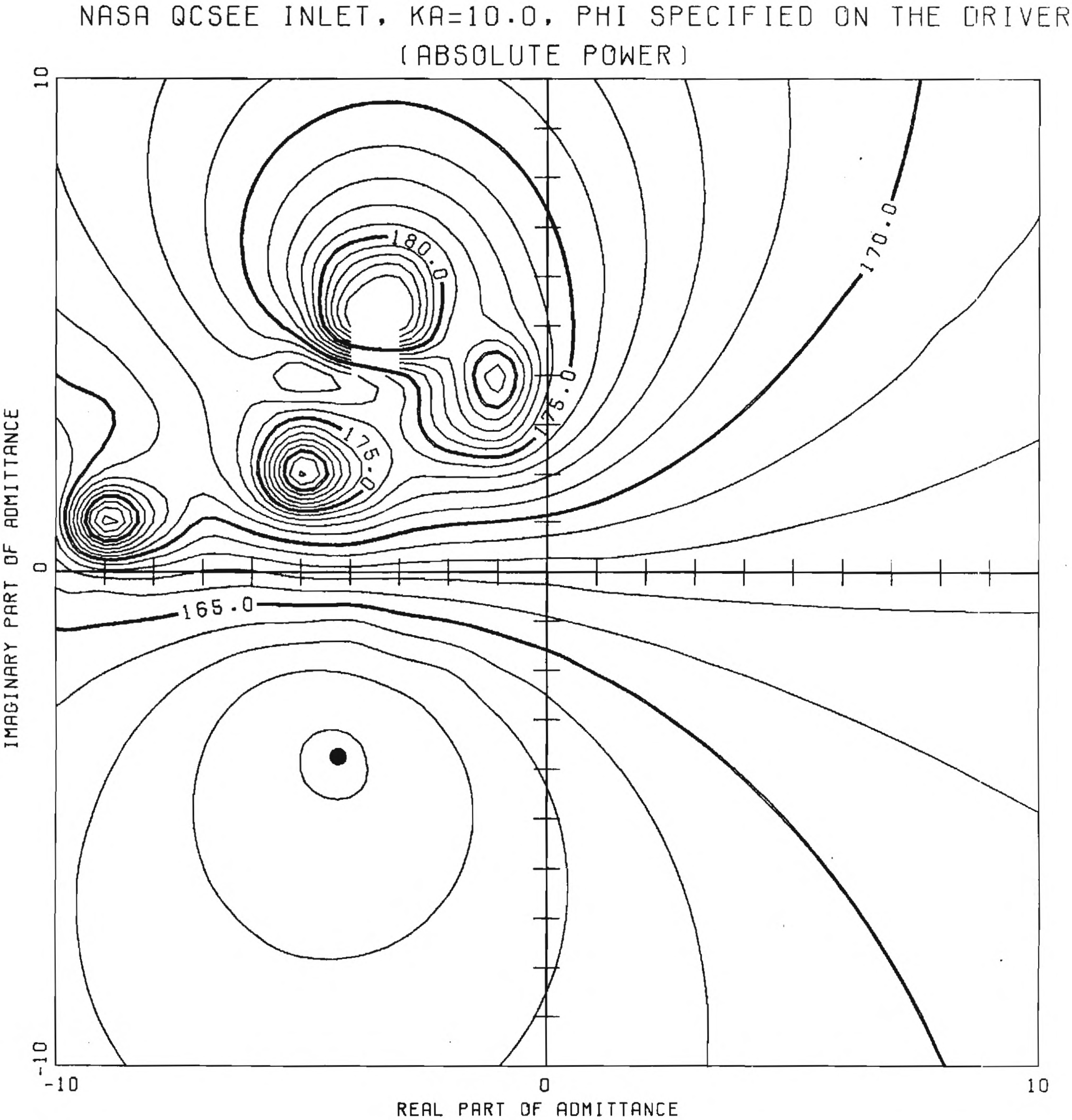
NASA QCSEE INLET, KA=10.0, PHI SPECIFIED ON THE DRIVER
(ABSOLUTE POWER)
180.0
175.0
175.0
170.0
165.0
IMAGINARY PART OF ADMITTANCE
REAL PART OF ADMITTANCE
10
0
-10
-10
0
10

Figure 19b

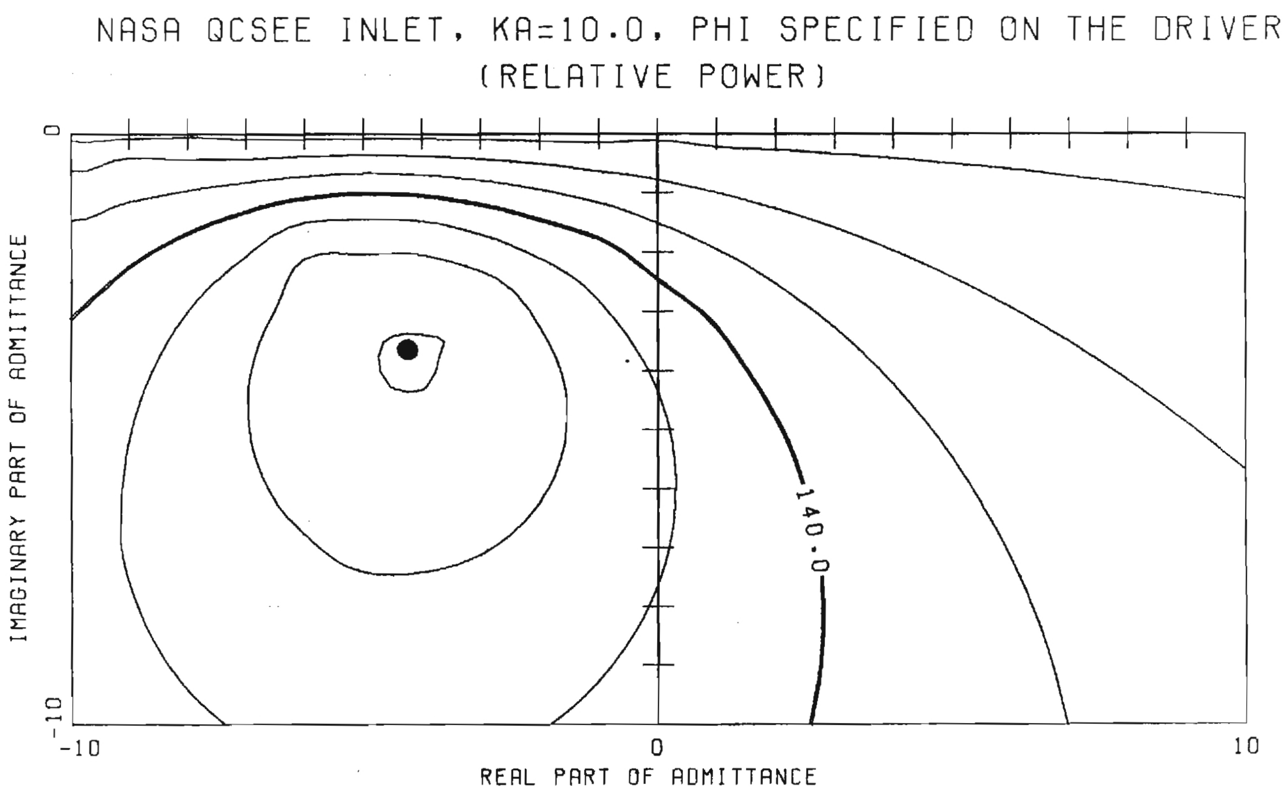
NASA QCSEE INLET, KA=10.0, PHI SPECIFIED ON THE DRIVER
(RELATIVE POWER)
0
-10
IMAGINARY PART OF ADMITTANCE
140.0
-10
0
10
REAL PART OF ADMITTANCE

Figure 19c

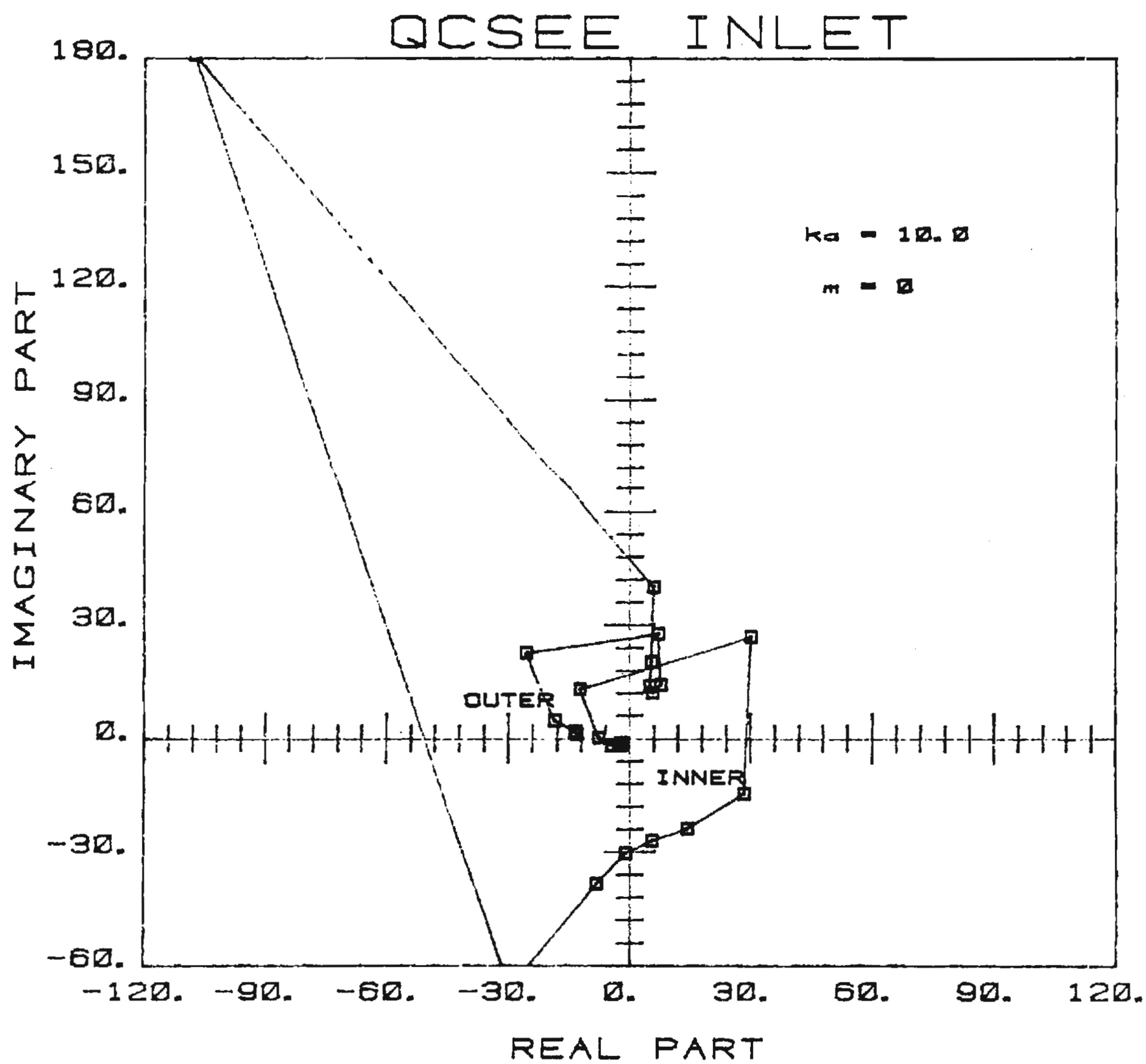

OPTIMUM ADMITTANCE DISTRIBUTION

Constant Velocity on the Driver

Figure 19d

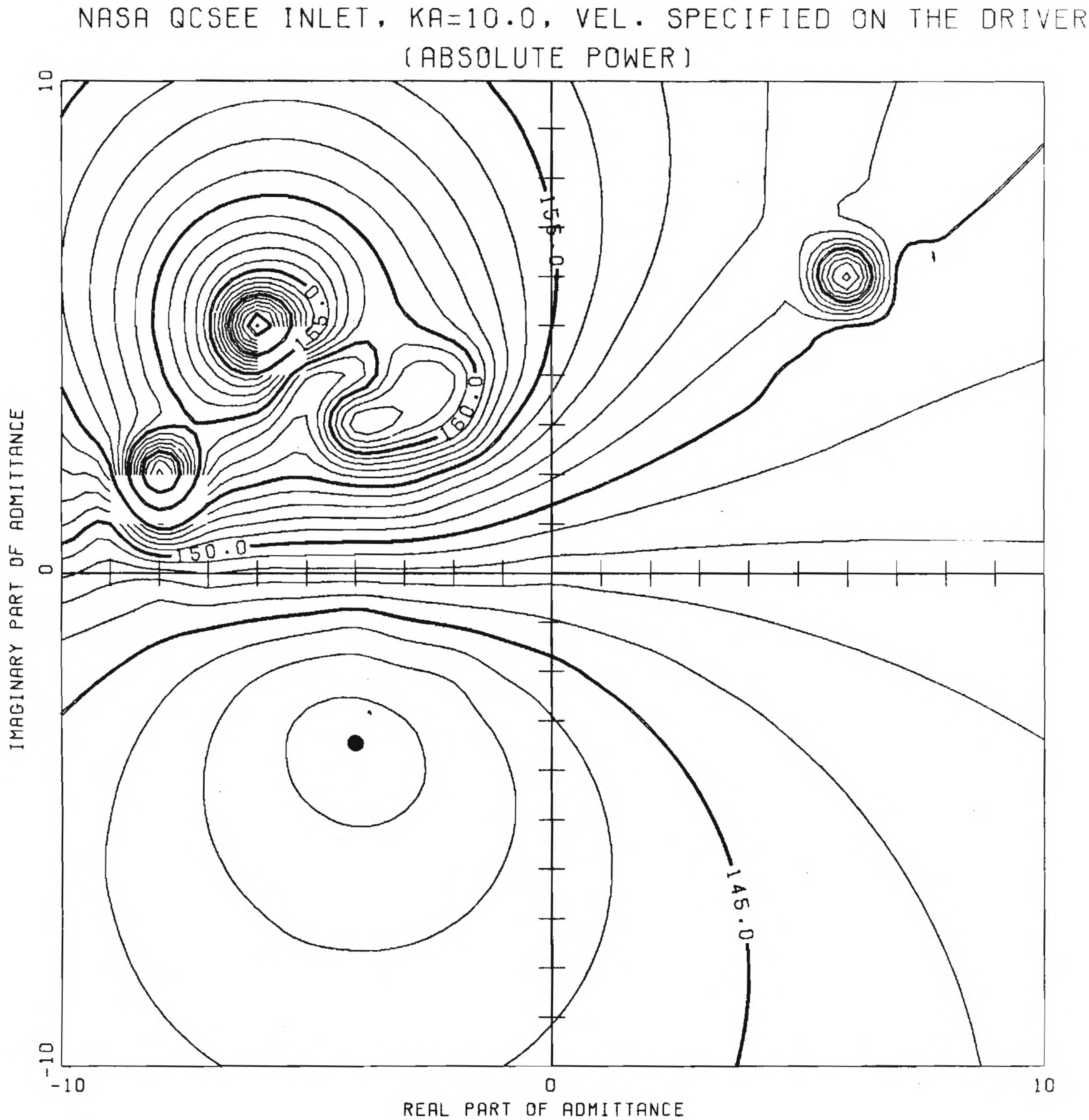
NASA QCSEE INLET, KA=10.0, VEL. SPECIFIED ON THE DRIVER
(ABSOLUTE POWER)
IMAGINARY PART OF ADMITTANCE
REAL PART OF ADMITTANCE
10
0
-10
-10
0
10
155.0
160.0
150.0
145.0

Figure 19e

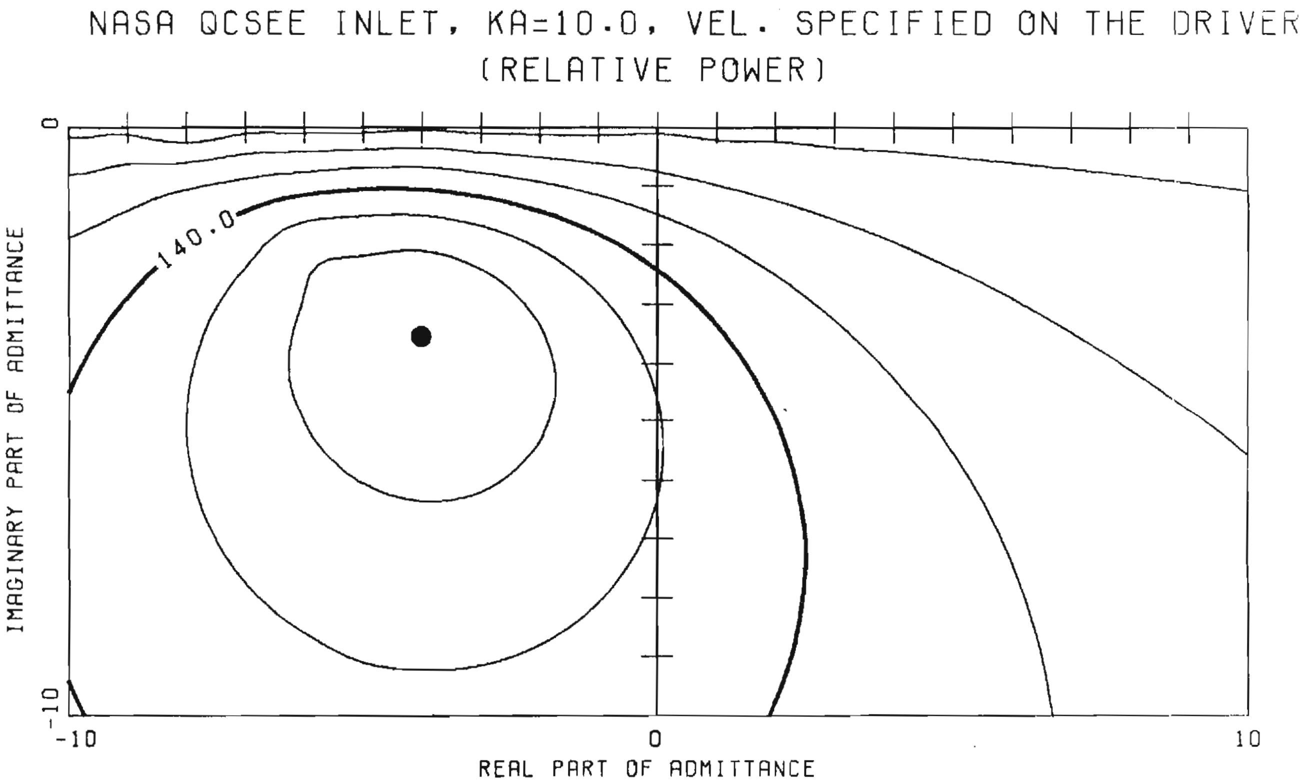

NASA QCSEE INLET, KA=10.0, VEL. SPECIFIED ON THE DRIVER
(RELATIVE POWER)
0
-10
-10
0
10
140.0
IMAGINARY PART OF ADMITTANCE
REAL PART OF ADMITTANCE

Figure 19f

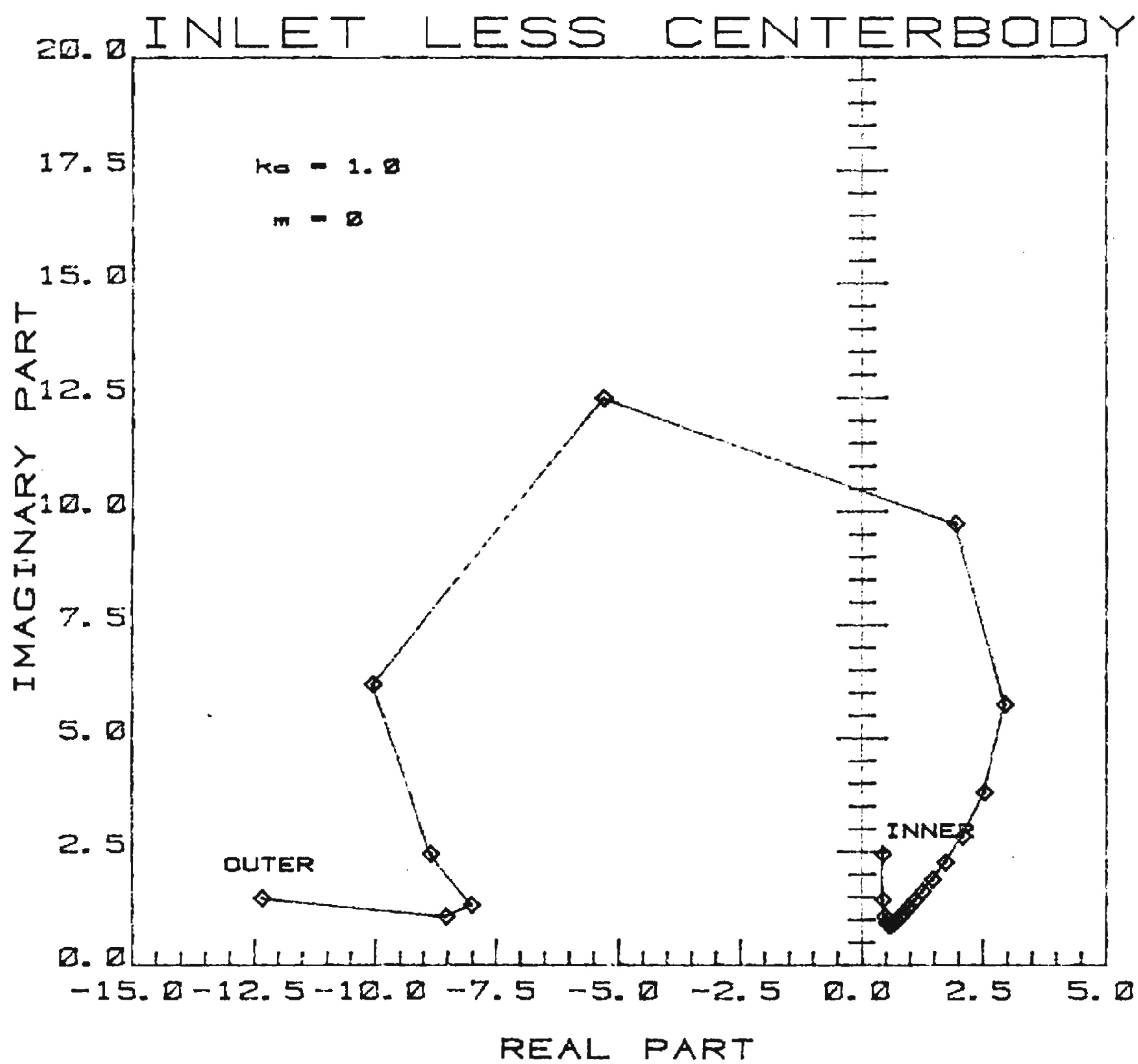

OPTIMUM ADMITTANCE DISTRIBUTION

Constant Phi on the Driver

Figure 20a

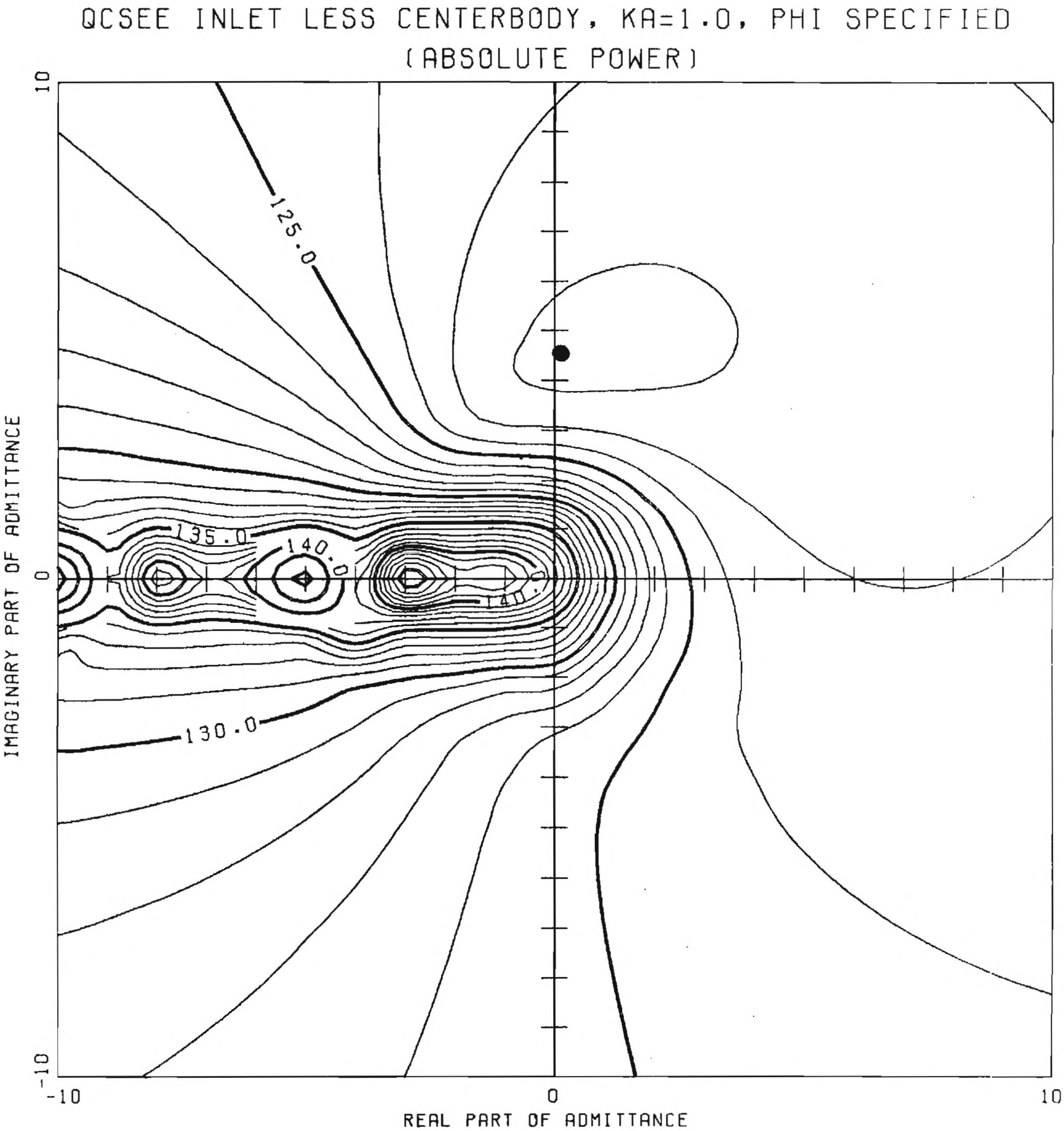

QCSEE INLET LESS CENTERBODY, KA=1.0, PHI SPECIFIED
(ABSOLUTE POWER)
IMAGINARY PART OF ADMITTANCE
REAL PART OF ADMITTANCE
10
0
-10
-10
0
10
125.0
130.0
135.0
140.0
140.0

Figure 20b

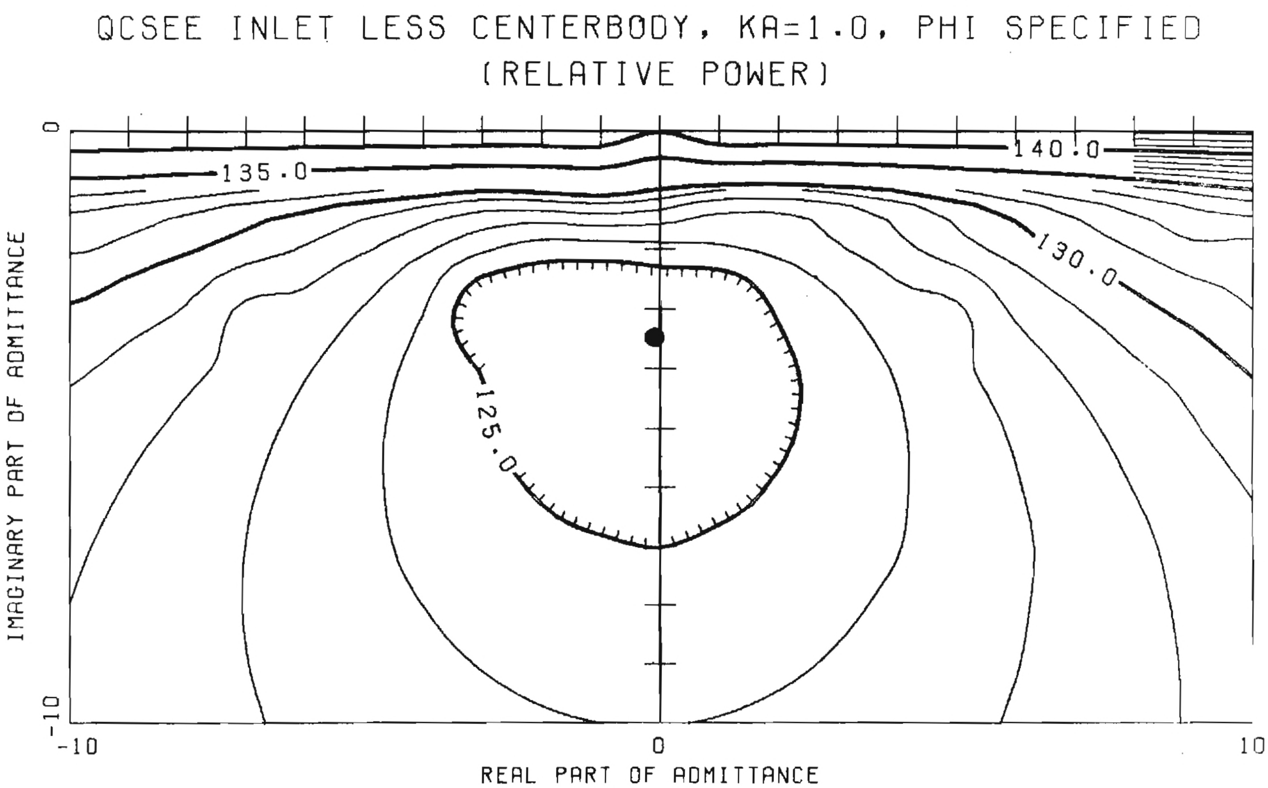
QCSEE INLET LESS CENTERBODY, KA=1.0, PHI SPECIFIED
(RELATIVE POWER)
140.0
135.0
130.0
125.0
IMAGINARY PART OF ADMITTANCE
0
-10
-10
0
10
REAL PART OF ADMITTANCE

Figure 20c

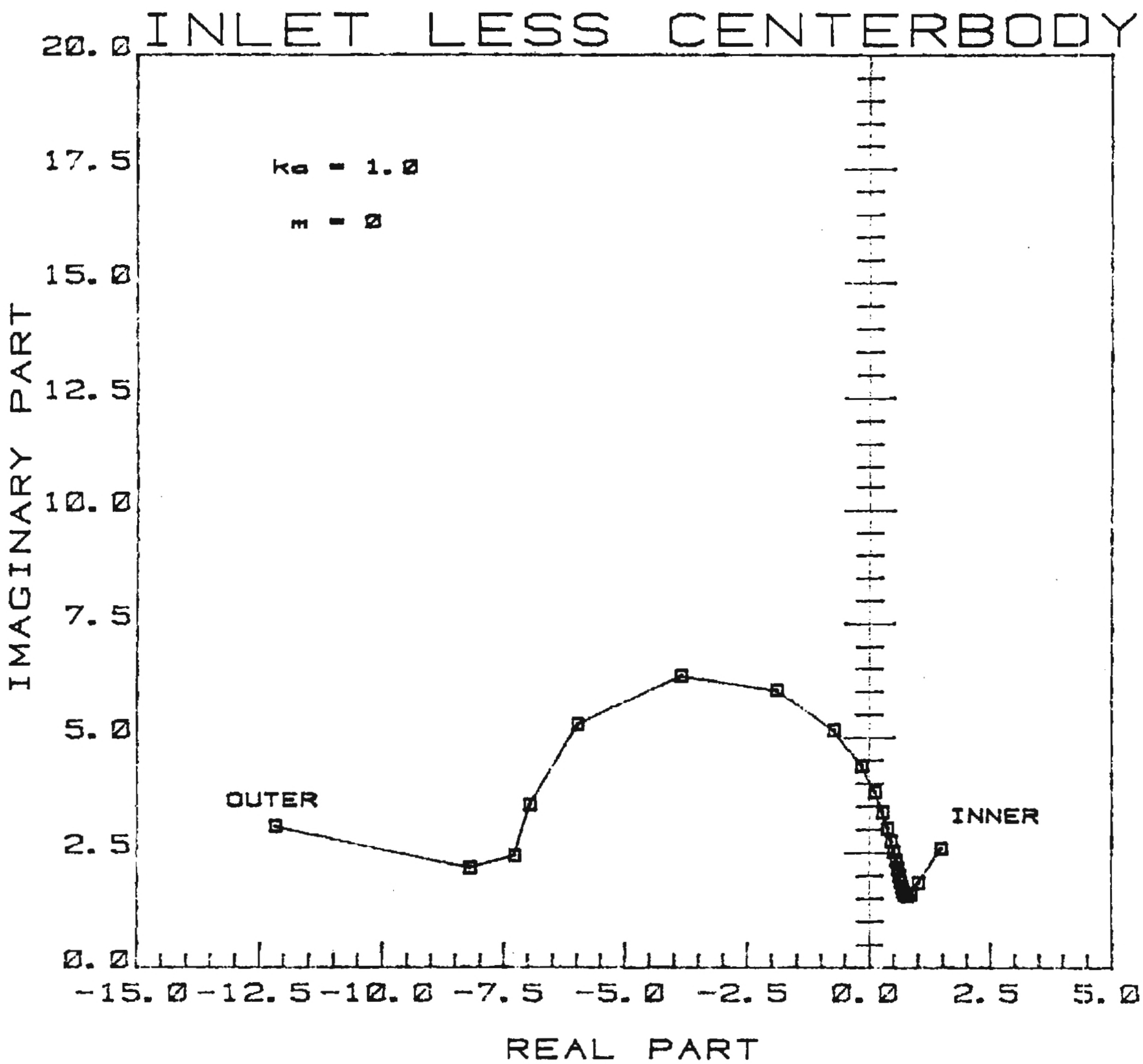

OPTIMUM ADMITTANCE DISTRIBUTION

Constant Velocity on the Driver

Figure 20d

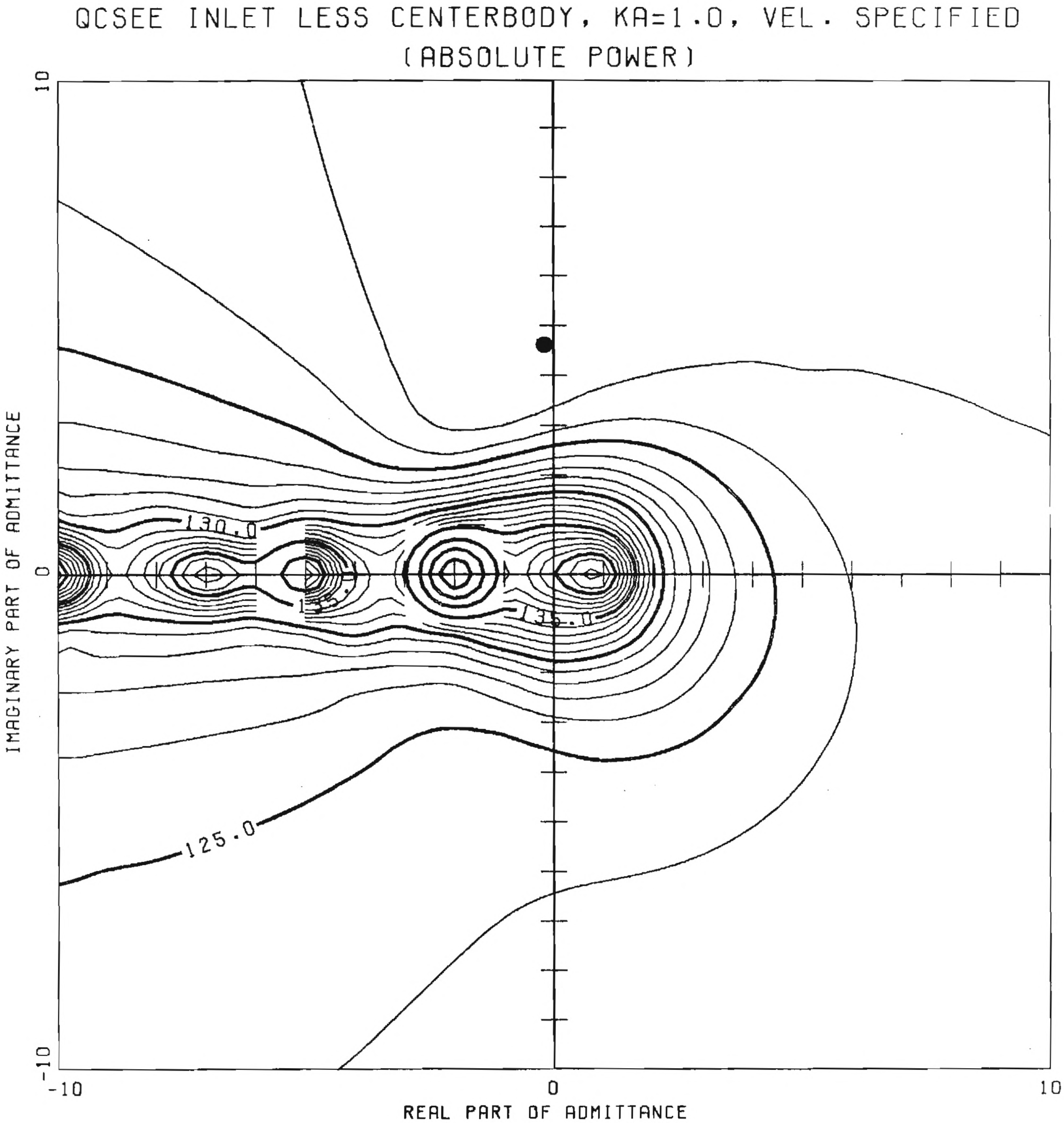
QCSEE INLET LESS CENTERBODY, KA=1.0, VEL. SPECIFIED
(ABSOLUTE POWER)
10
0
-10
IMAGINARY PART OF ADMITTANCE
-10
0
10
REAL PART OF ADMITTANCE
130.0
135.0
125.0

Figure 20e

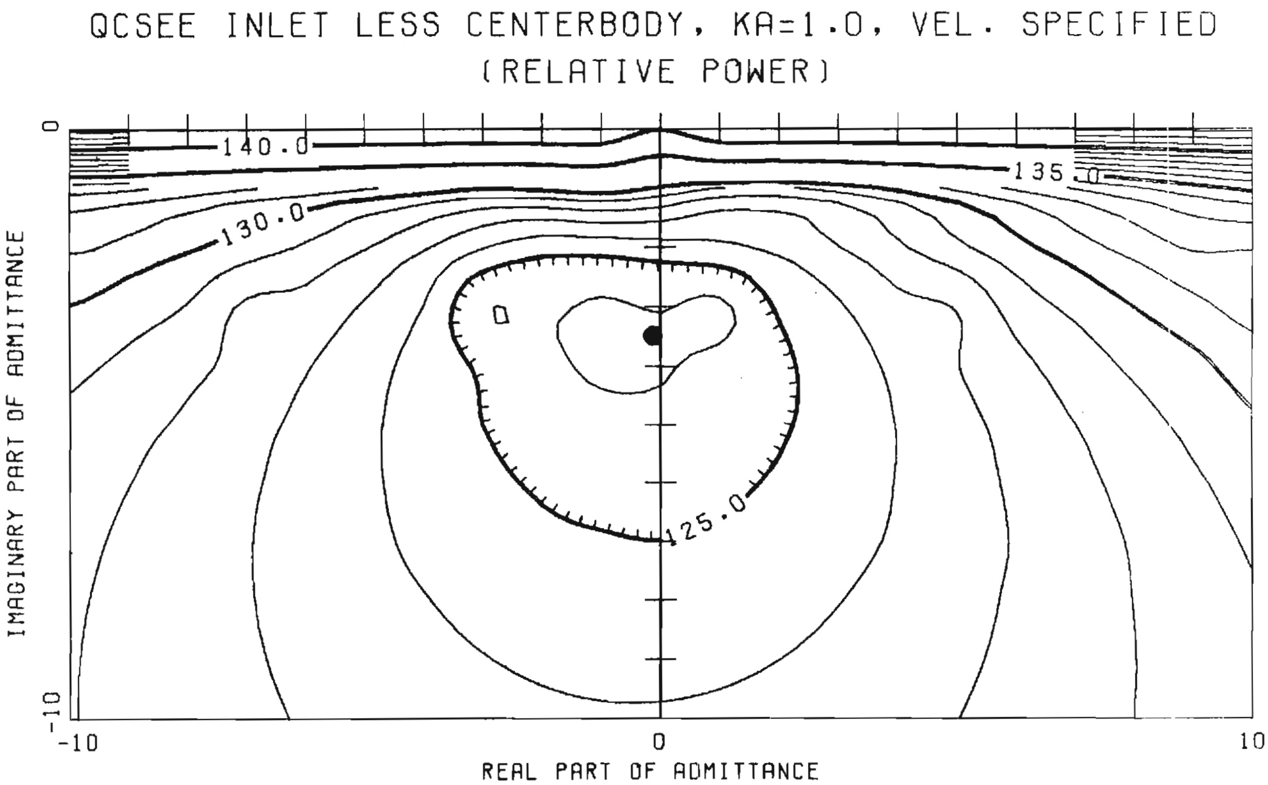
QCSEE INLET LESS CENTERBODY, KA=1.0, VEL. SPECIFIED
(RELATIVE POWER)
140.0
135.0
130.0
125.0
IMAGINARY PART OF ADMITTANCE
0
-10
-10
0
10
REAL PART OF ADMITTANCE

Figure 20f

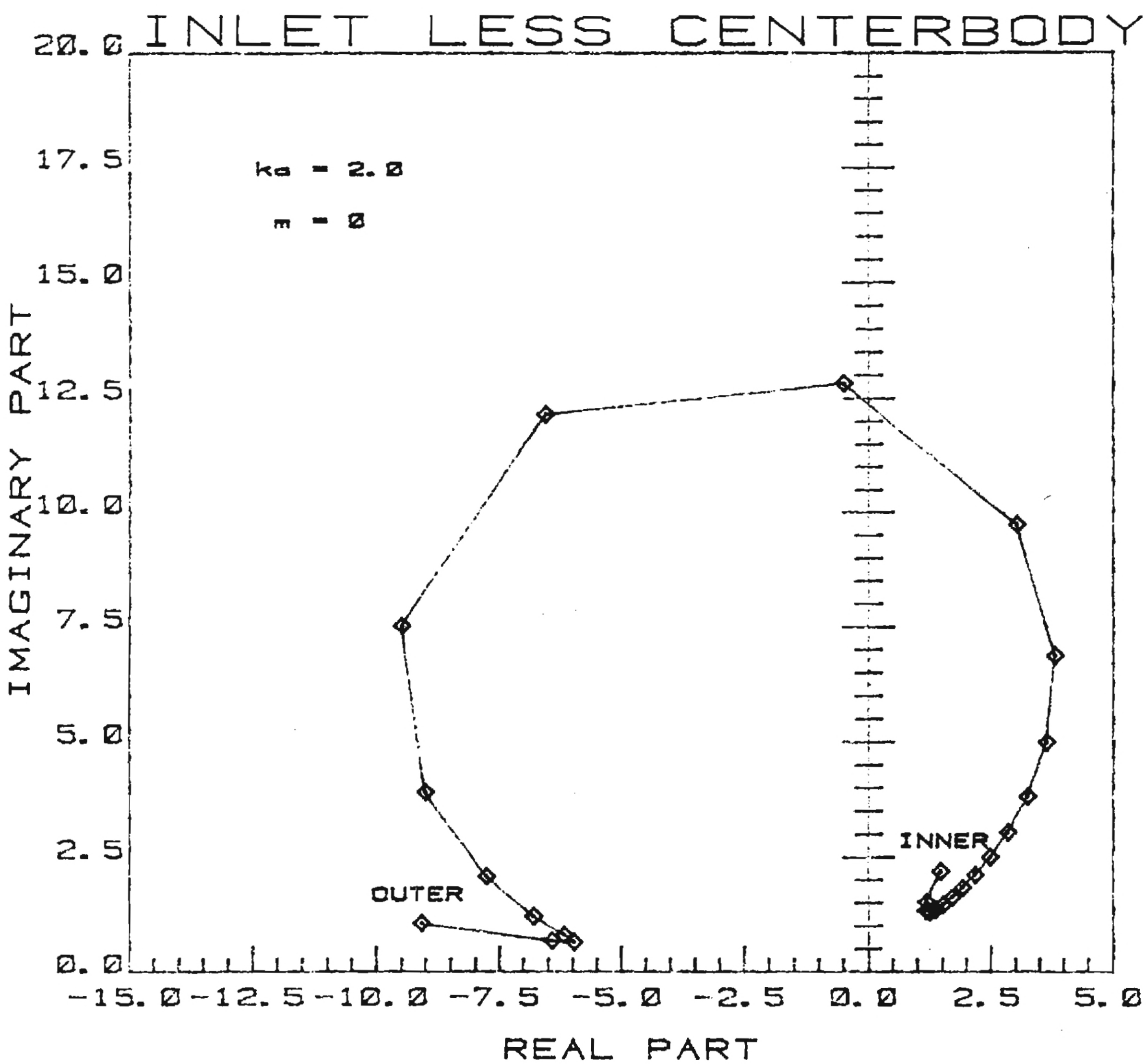

OPTIMUM ADMITTANCE DISTRIBUTION

Constant Phi on the Driver

Figure 21a

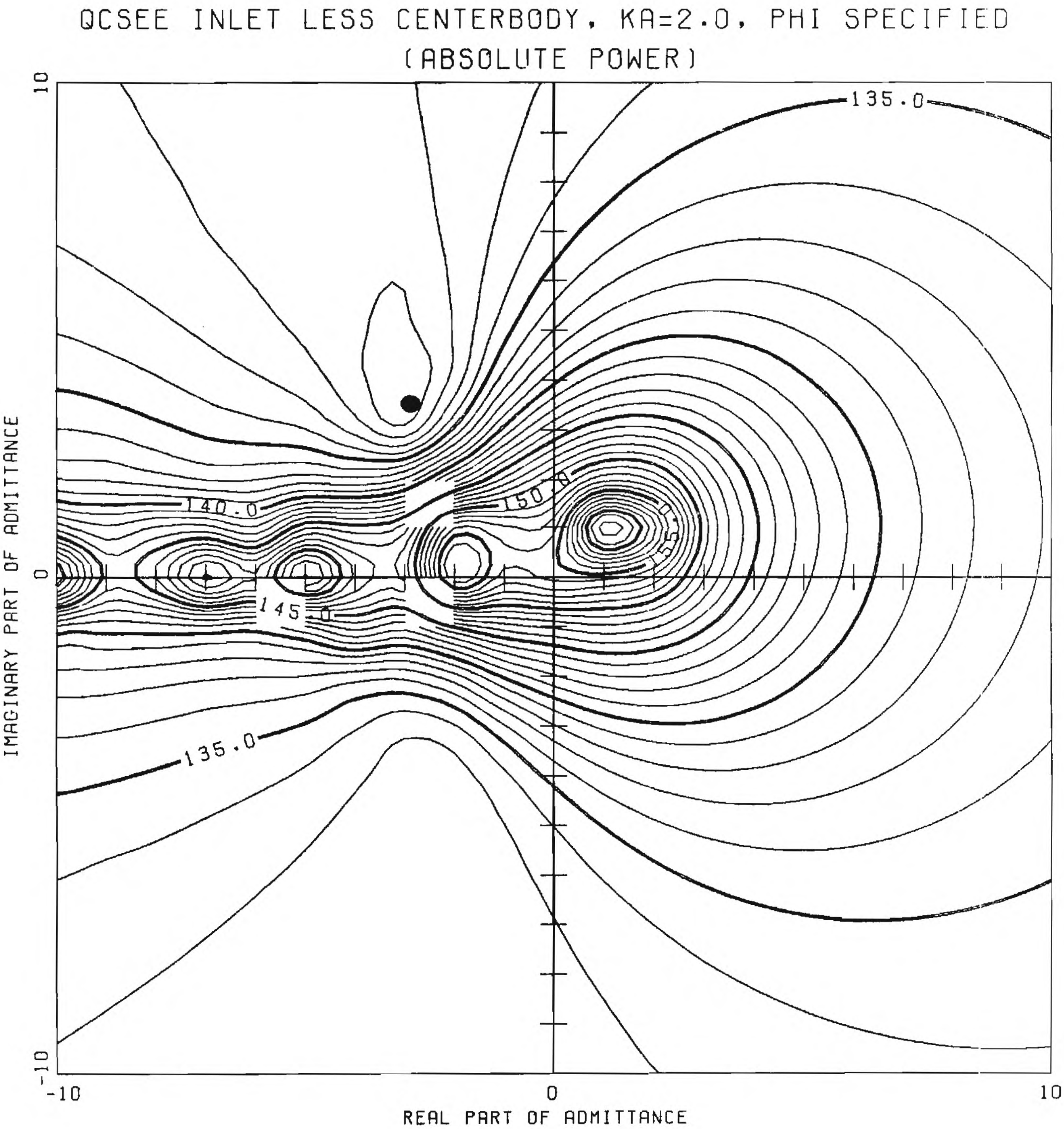
QCSEE INLET LESS CENTERBODY, KA=2.0, PHI SPECIFIED
(ABSOLUTE POWER)
135.0
140.0
150.0
155
145.0
135.0
10
0
-10
-10
0
10
IMAGINARY PART OF ADMITTANCE
REAL PART OF ADMITTANCE

Figure 21b

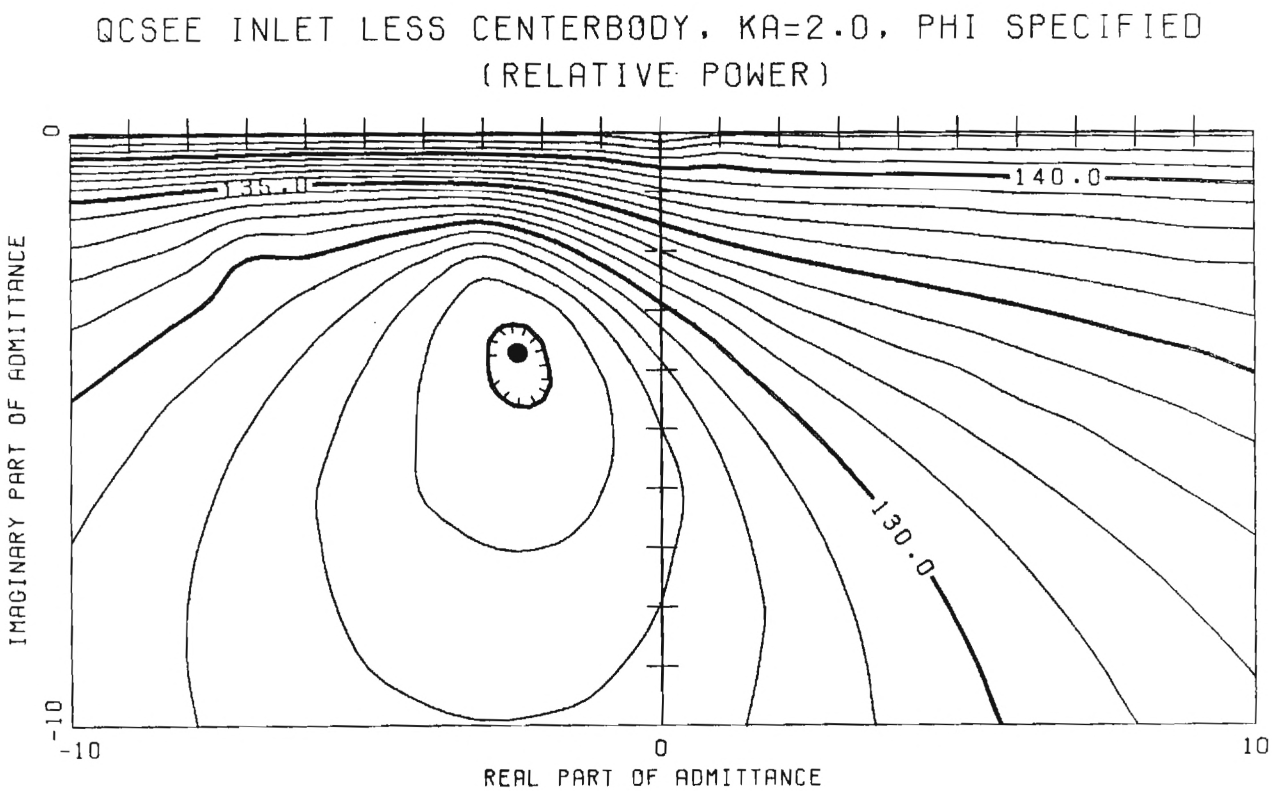
QCSEE INLET LESS CENTERBODY, KA=2.0, PHI SPECIFIED
(RELATIVE POWER)
140.0
135.0
130.0
IMAGINARY PART OF ADMITTANCE
0
-10
-10
0
10
REAL PART OF ADMITTANCE

Figure 21c

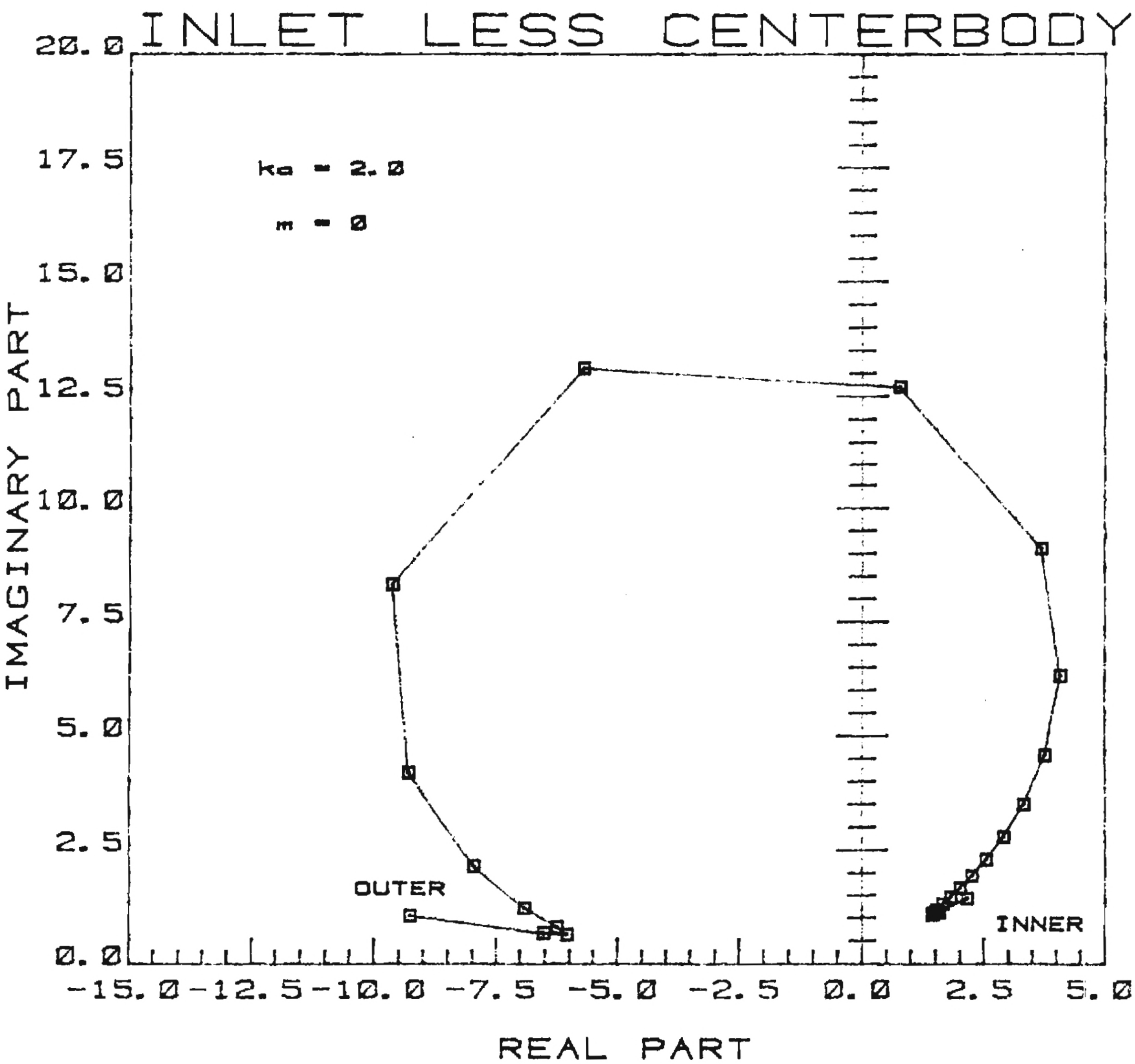

OPTIMUM ADMITTANCE DISTRIBUTION

Constant Velocity on the Driver

Figure 21d

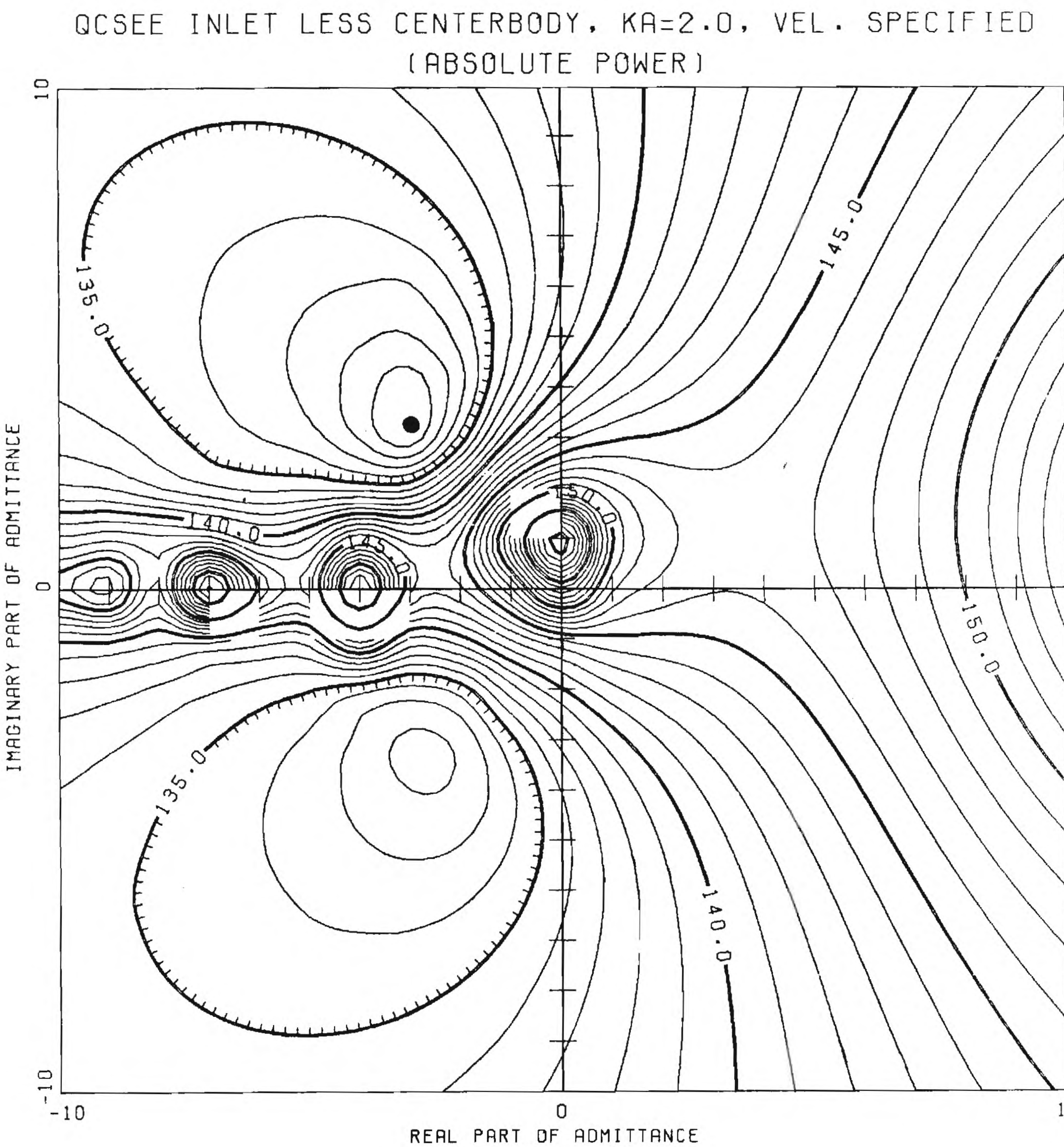
QCSEE INLET LESS CENTERBODY, KA=2.0, VEL. SPECIFIED
(ABSOLUTE POWER)
IMAGINARY PART OF ADMITTANCE
REAL PART OF ADMITTANCE
10
0
-10
-10
0
10
135.0
140.0
145.0
150.0
145.0
150.0
135.0
140.0

Figure 21e

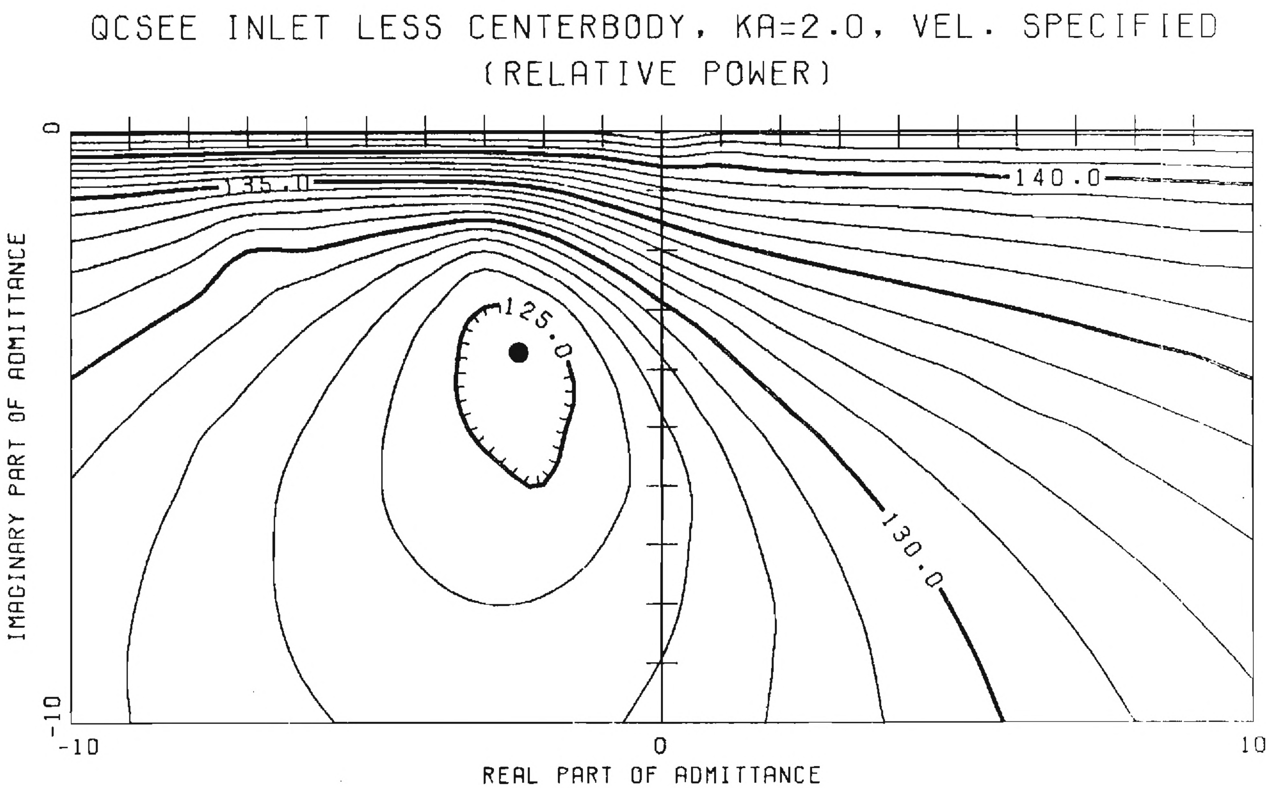
QCSEE INLET LESS CENTERBODY, KA=2.0, VEL. SPECIFIED
(RELATIVE POWER)
0
-10
IMAGINARY PART OF ADMITTANCE
-10
0
10
REAL PART OF ADMITTANCE
135.0
140.0
125.0
130.0

Figure 21f

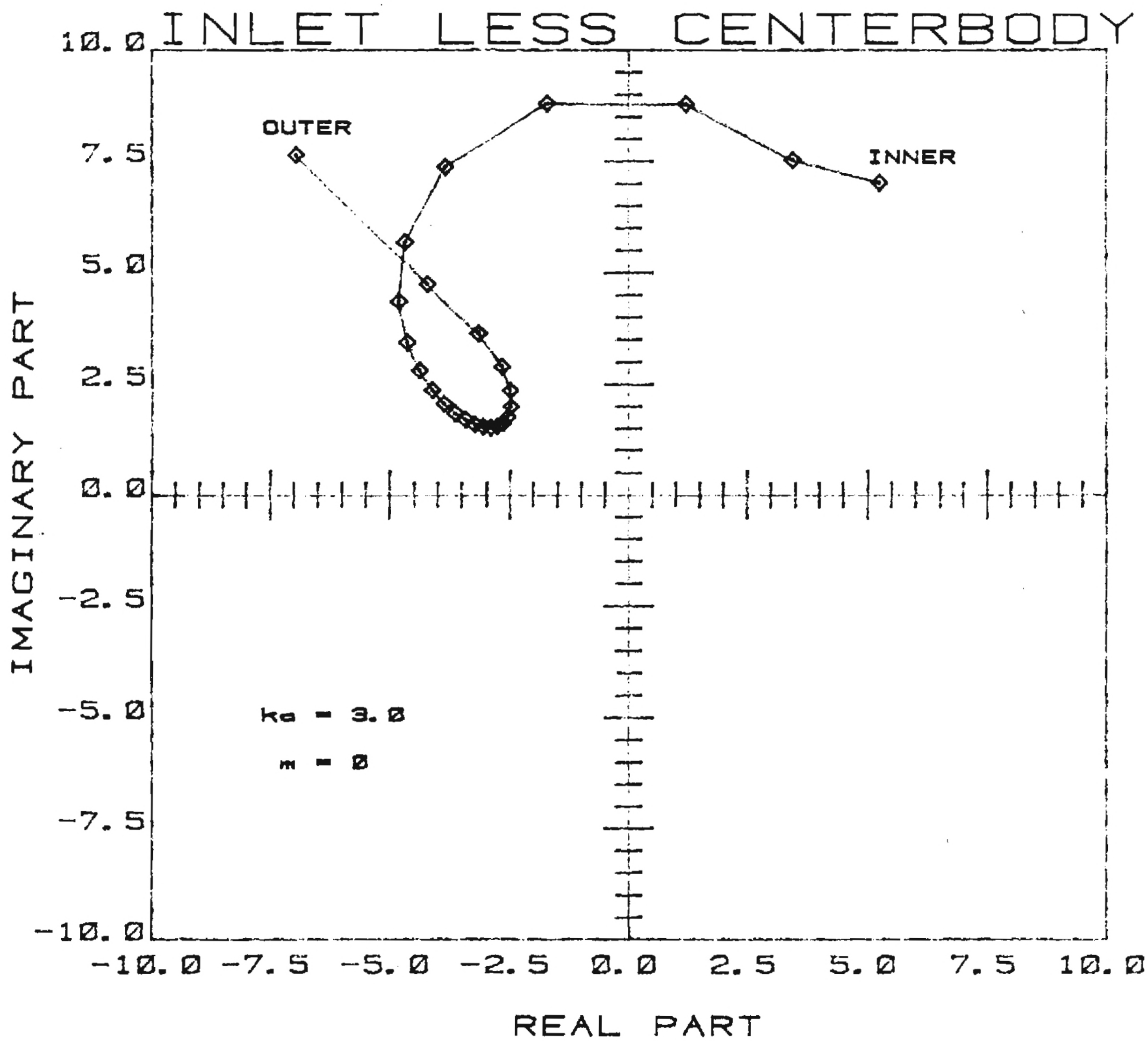

OPTIMUM ADMITTANCE DISTRIBUTION

Constant Phi on the Driver

Figure 22a

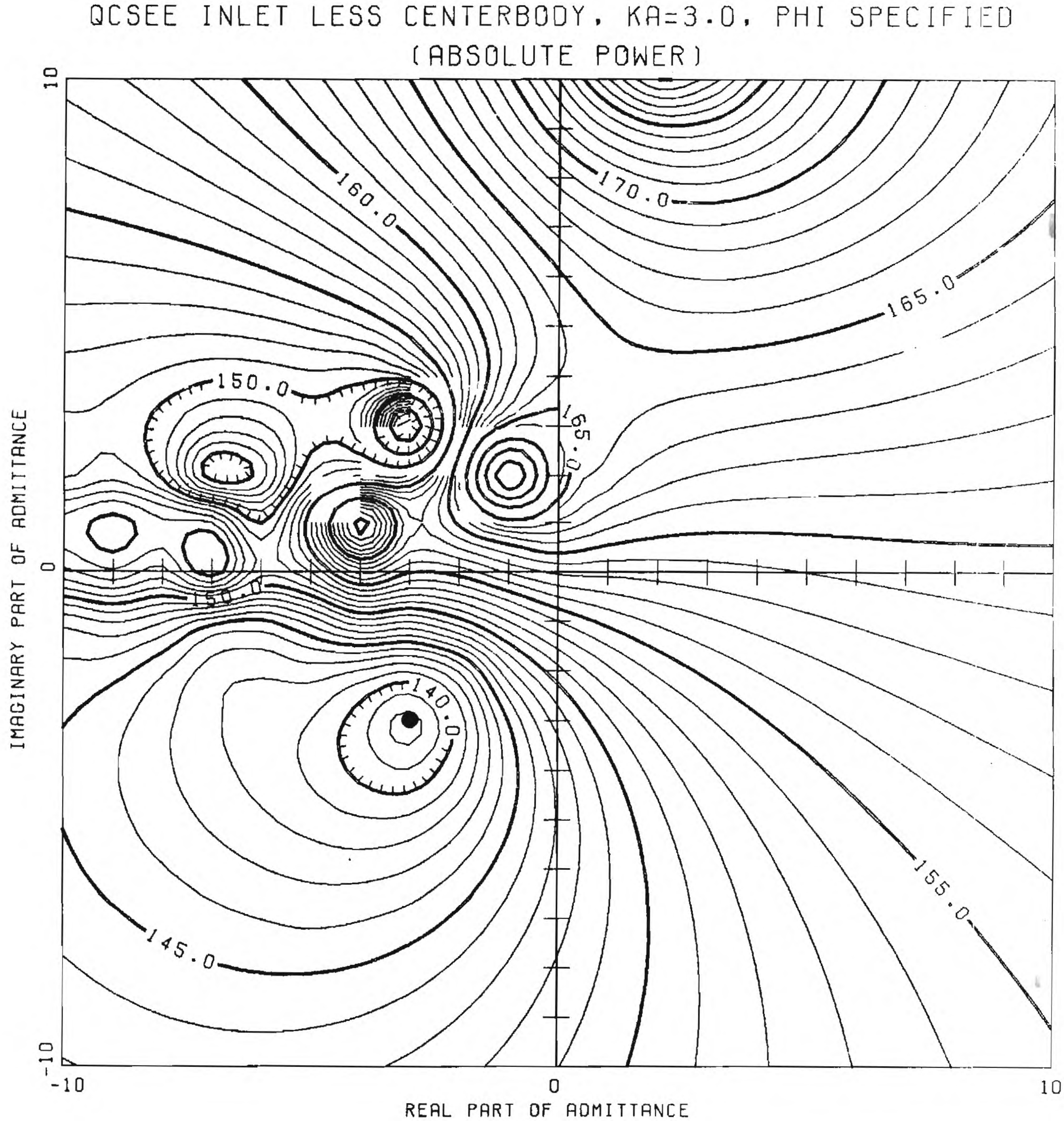
QCSEE INLET LESS CENTERBODY, KA=3.0, PHI SPECIFIED
(ABSOLUTE POWER)
IMAGINARY PART OF ADMITTANCE
REAL PART OF ADMITTANCE
10
0
-10
-10
0
10
170.0
160.0
165.0
150.0
165.0
150.0
140.0
155.0
145.0

Figure 22b

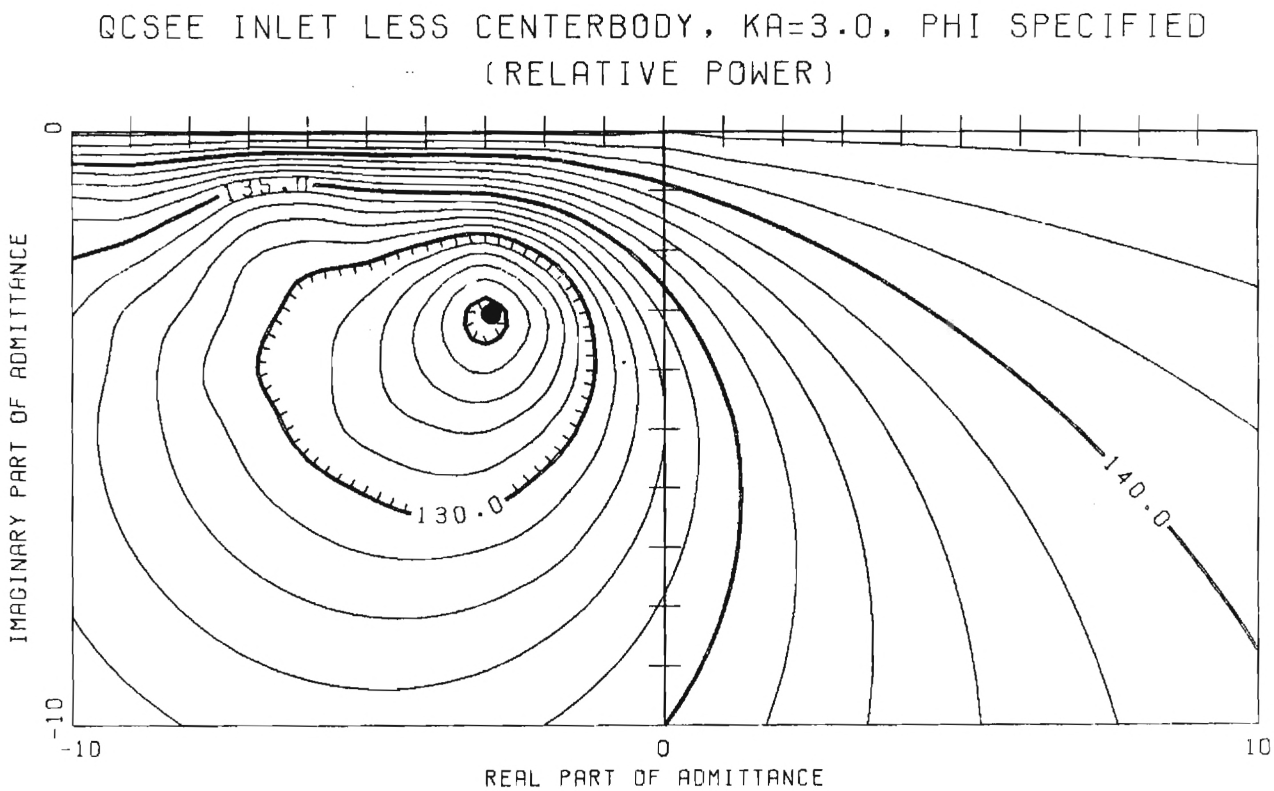
QCSEE INLET LESS CENTERBODY, KA=3.0, PHI SPECIFIED
(RELATIVE POWER)
0
-10
IMAGINARY PART OF ADMITTANCE
135.0
130.0
140.0
-10
0
10
REAL PART OF ADMITTANCE

Figure 22c

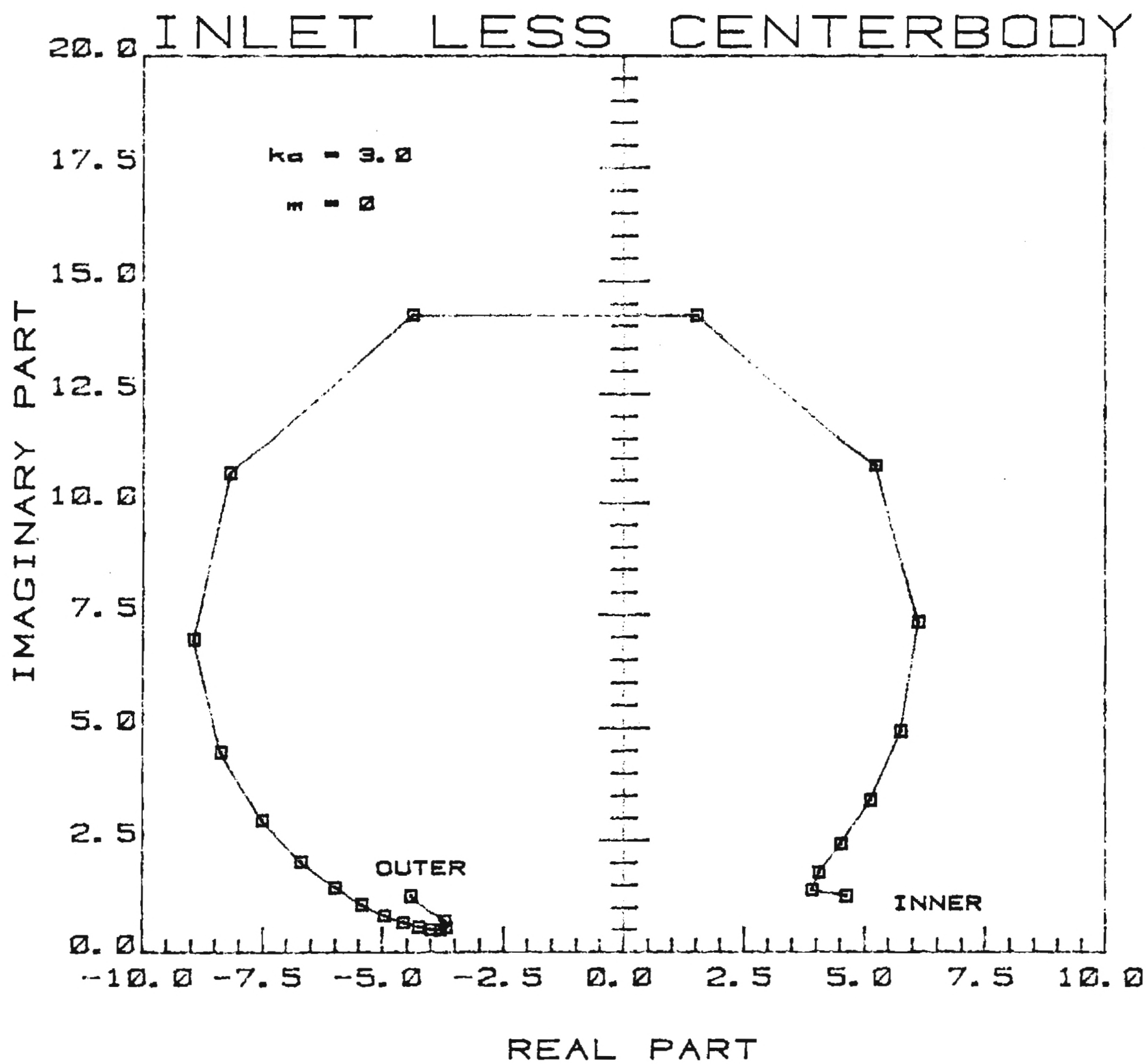

OPTIMUM ADMITTANCE DISTRIBUTION

Constant Velocity on the Driver

Figure 22d

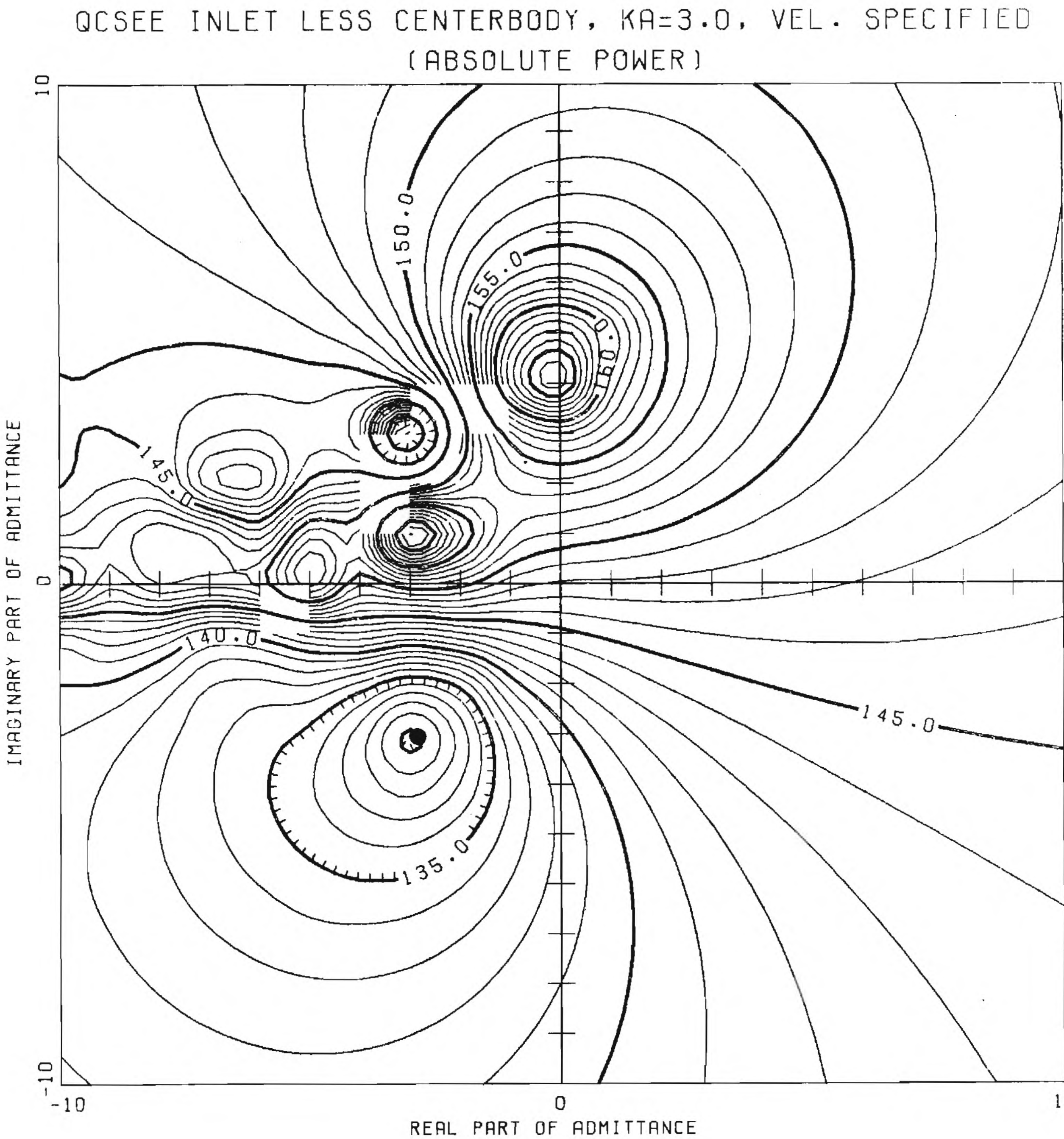
QCSEE INLET LESS CENTERBODY, KA=3.0, VEL. SPECIFIED
(ABSOLUTE POWER)
150.0
155.0
160.0
150.0
145.0
140.0
145.0
135.0
IMAGINARY PART OF ADMITTANCE
10
0
-10
-10
0
10
REAL PART OF ADMITTANCE

Figure 22e

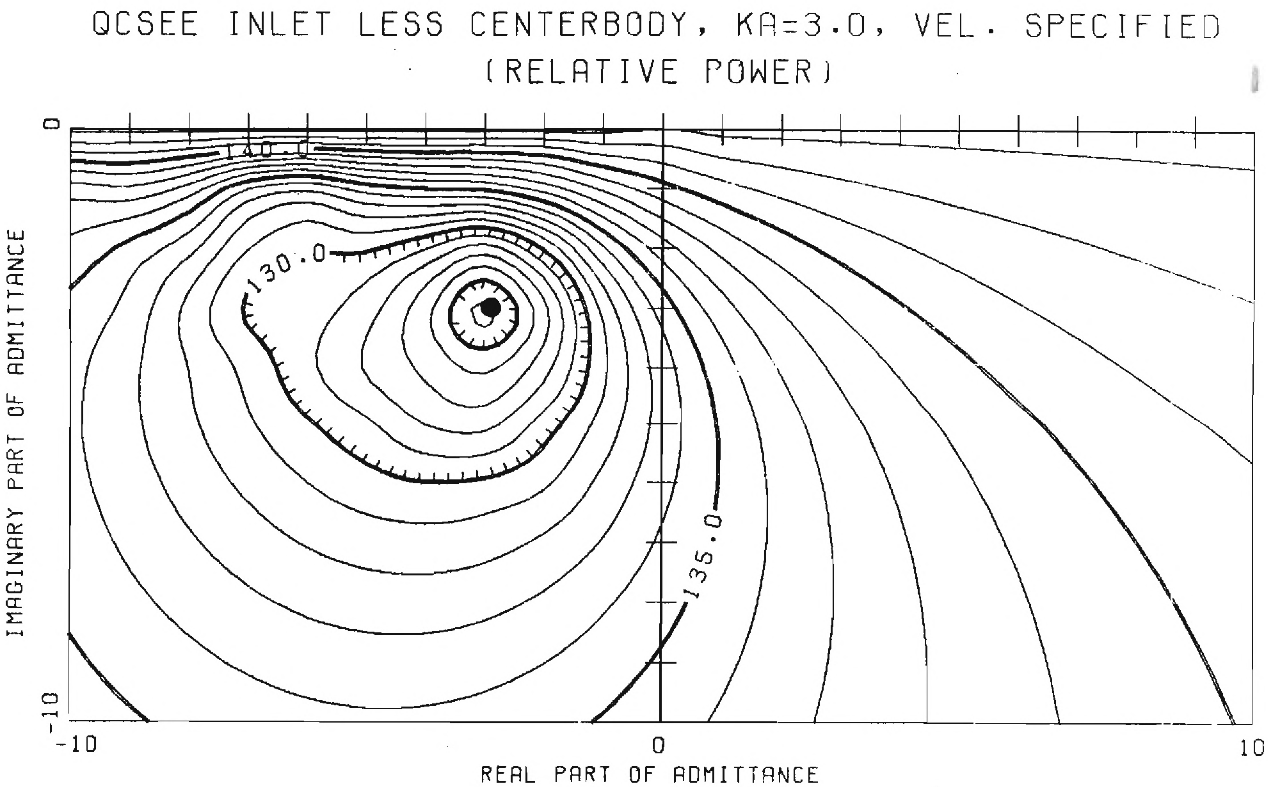
QCSEE INLET LESS CENTERBODY, KA=3.0, VEL. SPECIFIED
(RELATIVE POWER)
140.0
130.0
135.0
0
-10
-10
0
10
IMAGINARY PART OF ADMITTANCE
REAL PART OF ADMITTANCE

Figure 22f

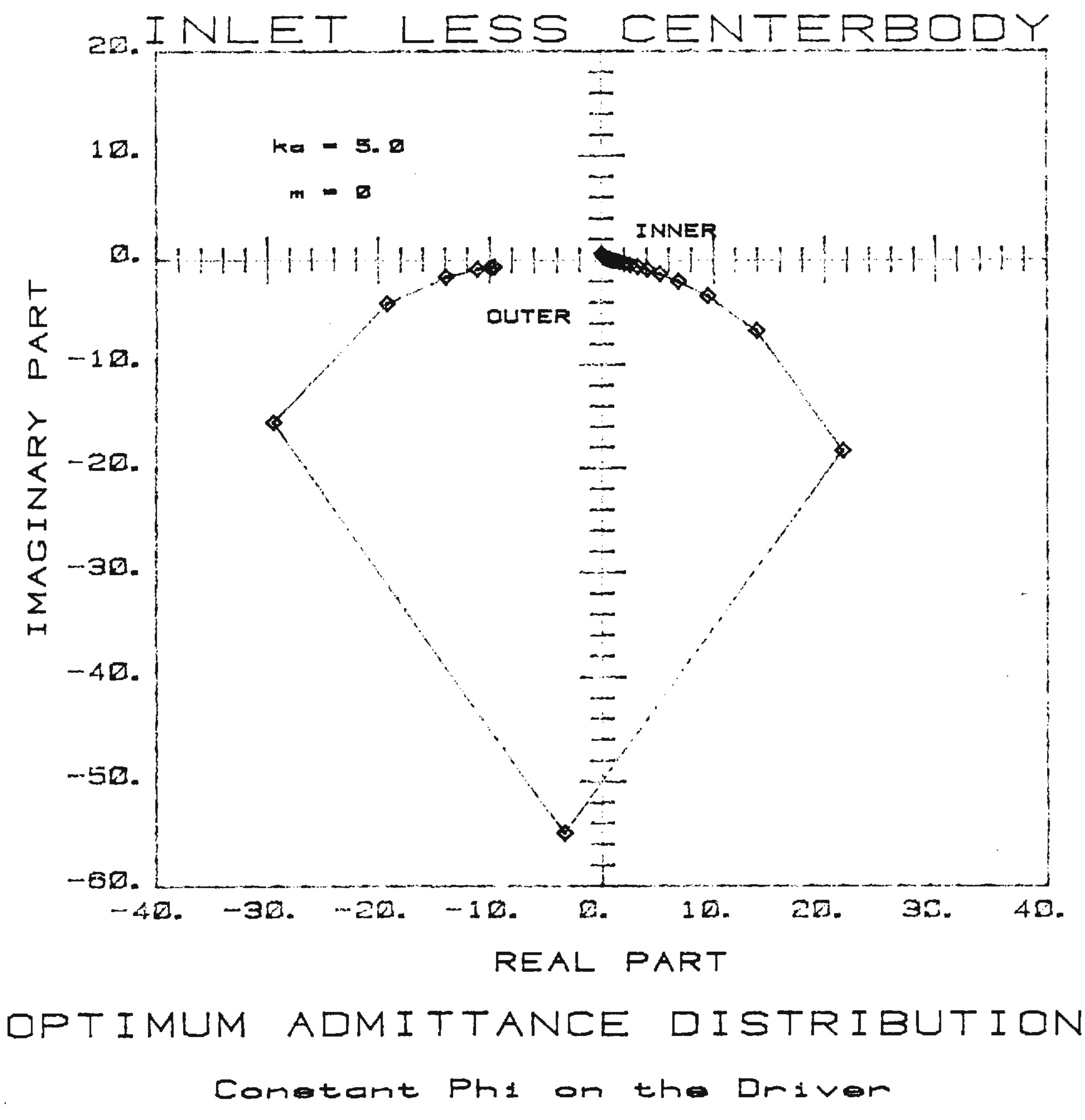
INLET LESS CENTERBODY
ka = 5.0
m = 0
INNER
OUTER
IMAGINARY PART
REAL PART
20.
10.
0.
-10.
-20.
-30.
-40.
-50.
-60.
-40.
-30.
-20.
-10.
0.
10.
20.
30.
40.
OPTIMUM ADMITTANCE DISTRIBUTION
Constant Phi on the Driver

Figure 23a

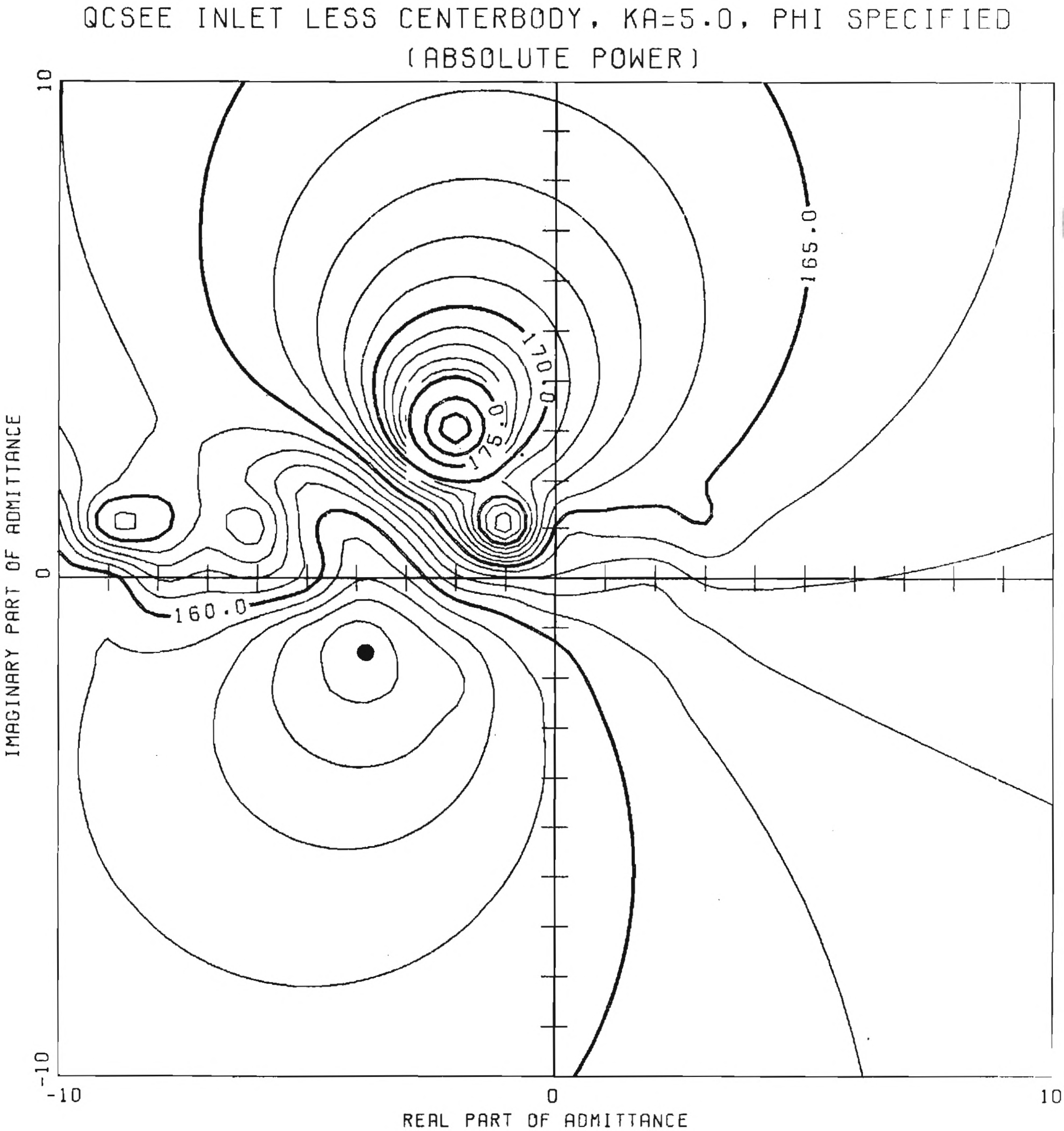

QCSEE INLET LESS CENTERBODY, KA=5.0, PHI SPECIFIED
(ABSOLUTE POWER)
IMAGINARY PART OF ADMITTANCE
REAL PART OF ADMITTANCE
10
0
-10
-10
0
10
165.0
170.0
175.0
160.0

Figure 23b

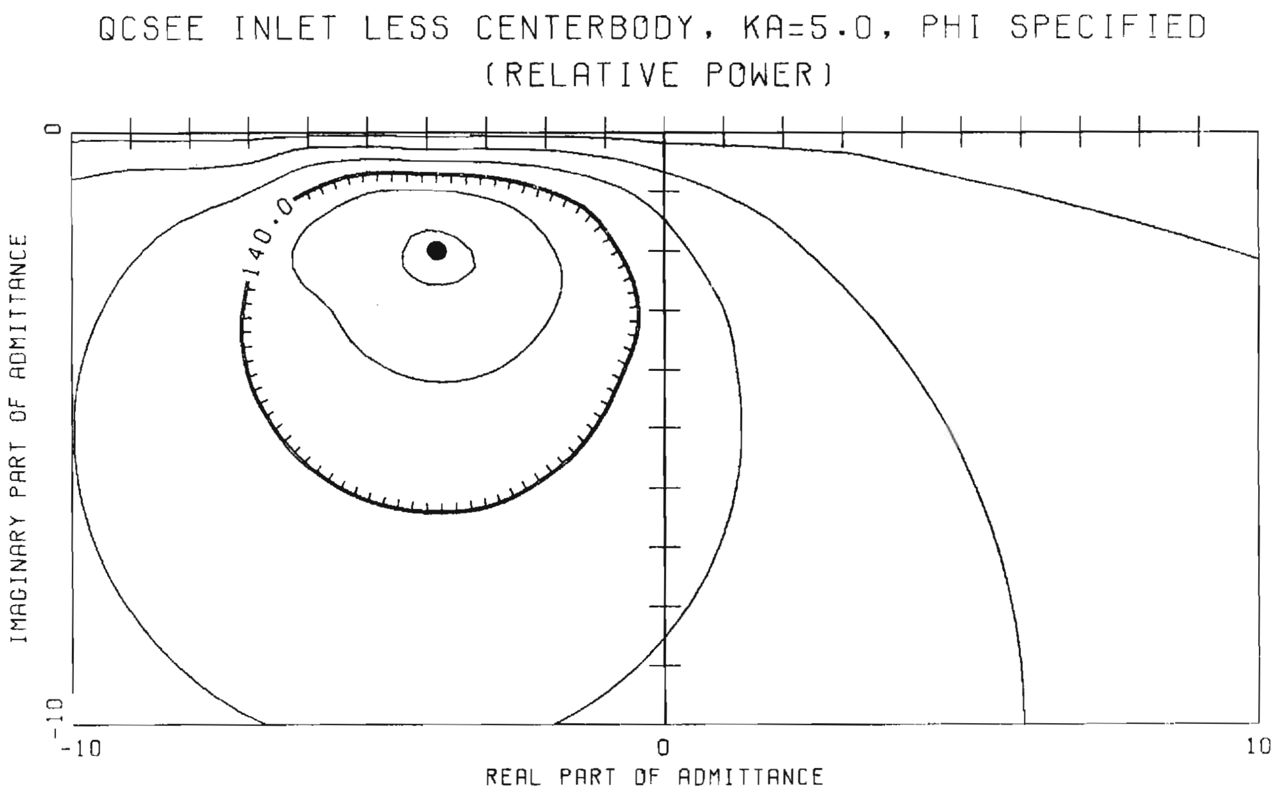

QCSEE INLET LESS CENTERBODY, KA=5.0, PHI SPECIFIED
(RELATIVE POWER)
0
-10
140.0
IMAGINARY PART OF ADMITTANCE
-10
0
10
REAL PART OF ADMITTANCE

Figure 23c

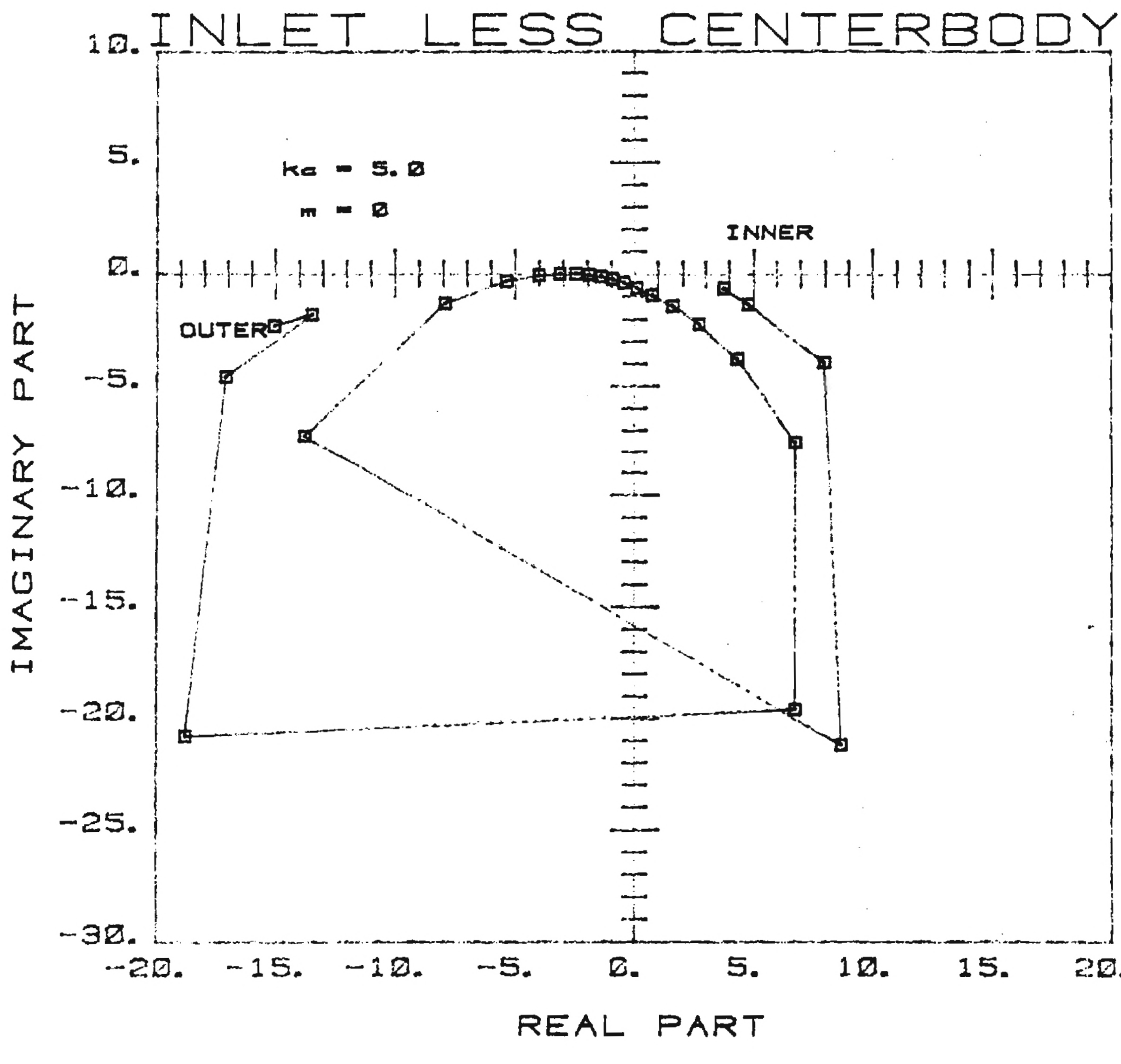

OPTIMUM ADMITTANCE DISTRIBUTION

Constant Velocity on the Driver

Figure 23d

QCSEE INLET LESS CENTERBODY, KA=5.0, VEL. SPECIFIED
(ABSOLUTE POWER)

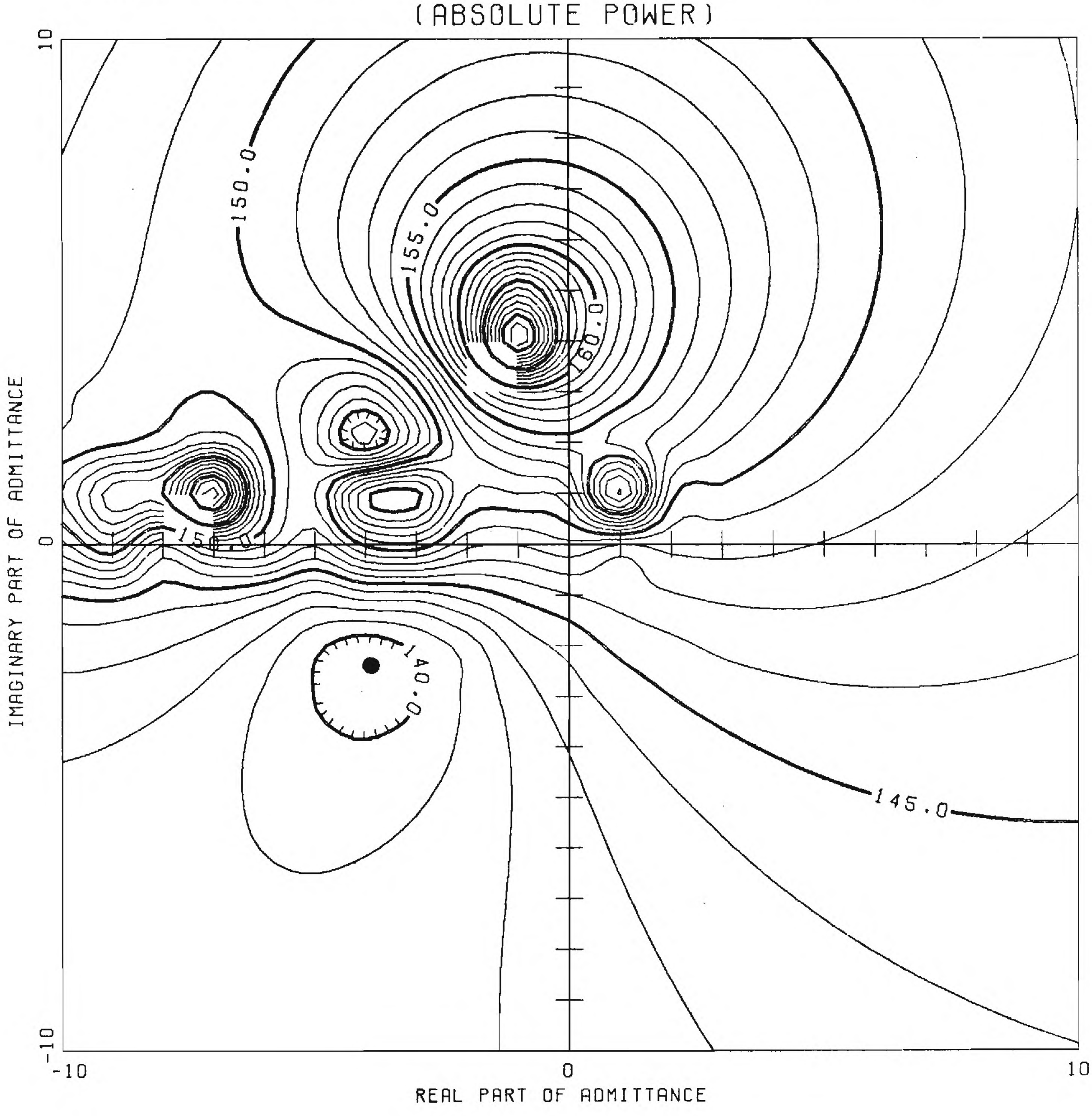

Figure 23e

QCSEE INLET LESS CENTERBODY, KA=5.0, VEL. SPECIFIED
(RELATIVE POWER)

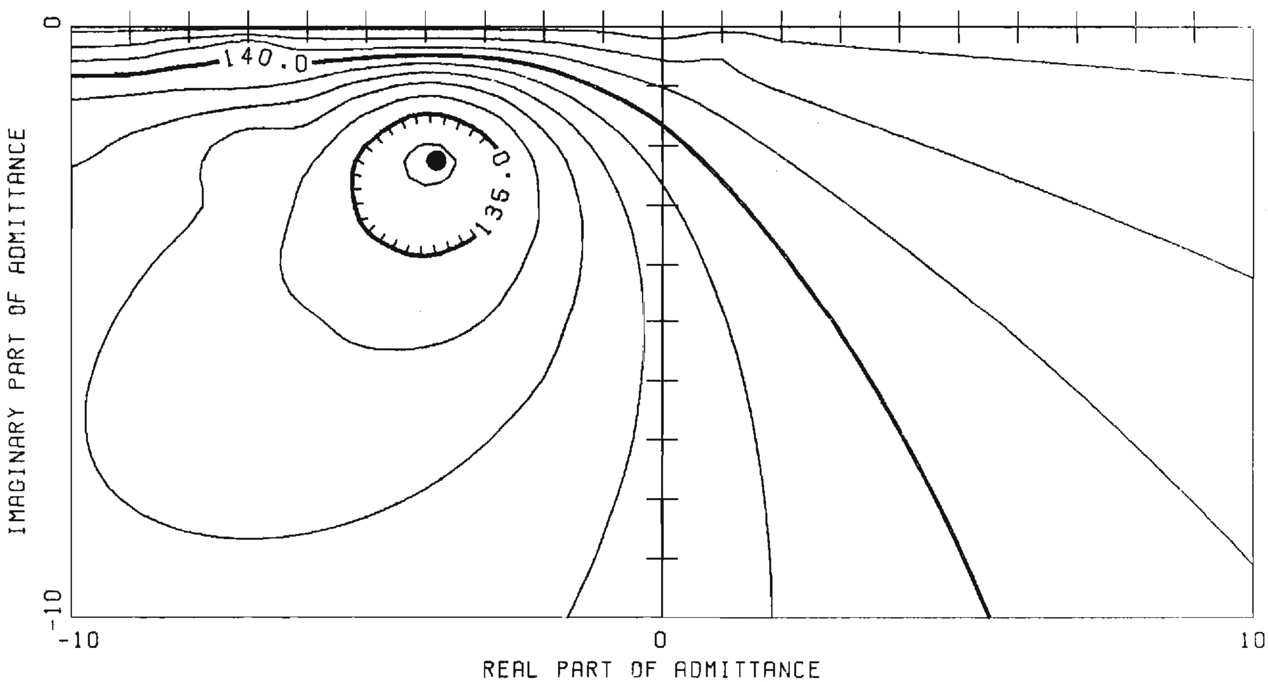

Figure 23f

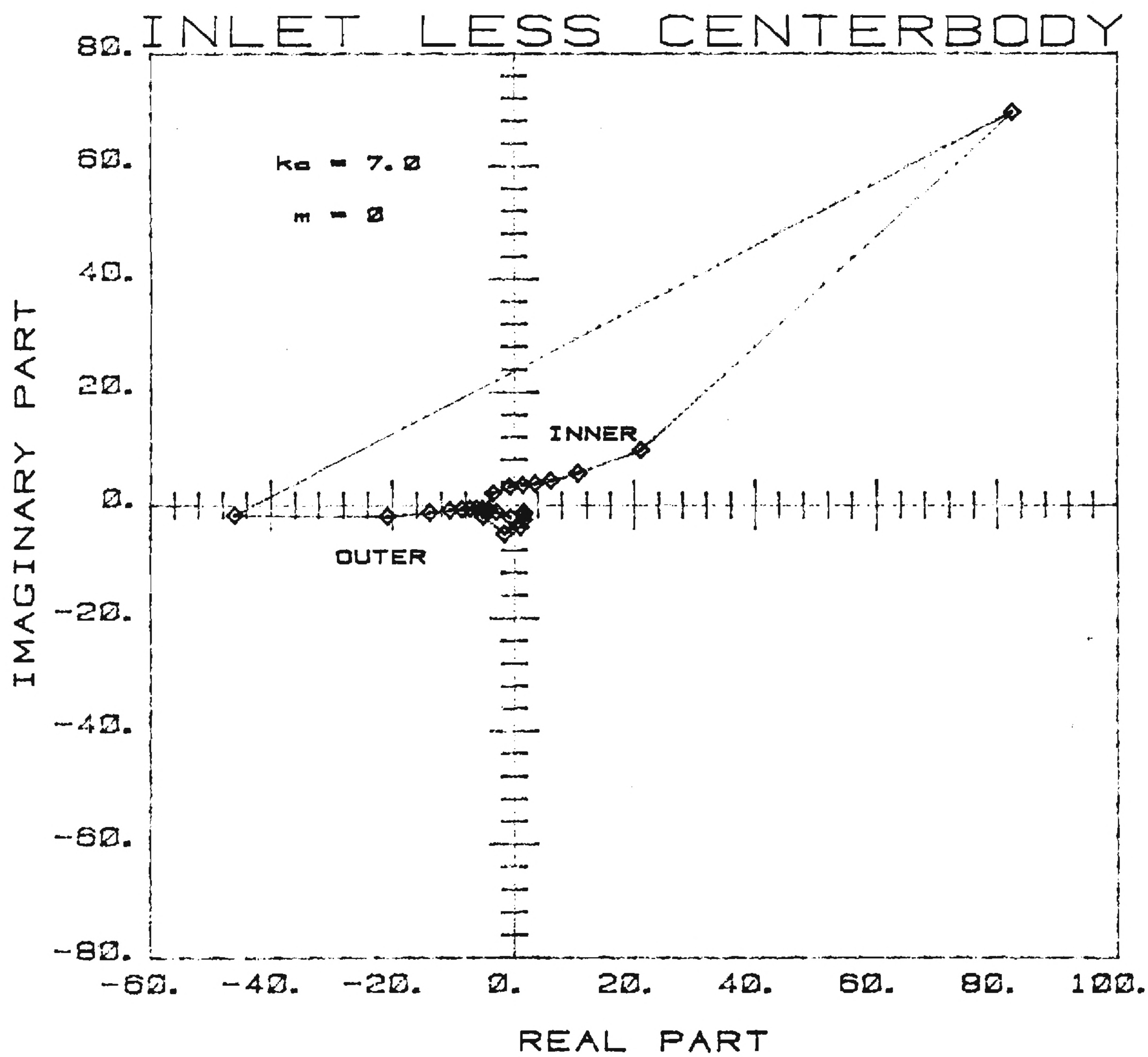

OPTIMUM ADMITTANCE DISTRIBUTION

Constant Phi on the Driver

Figure 24a

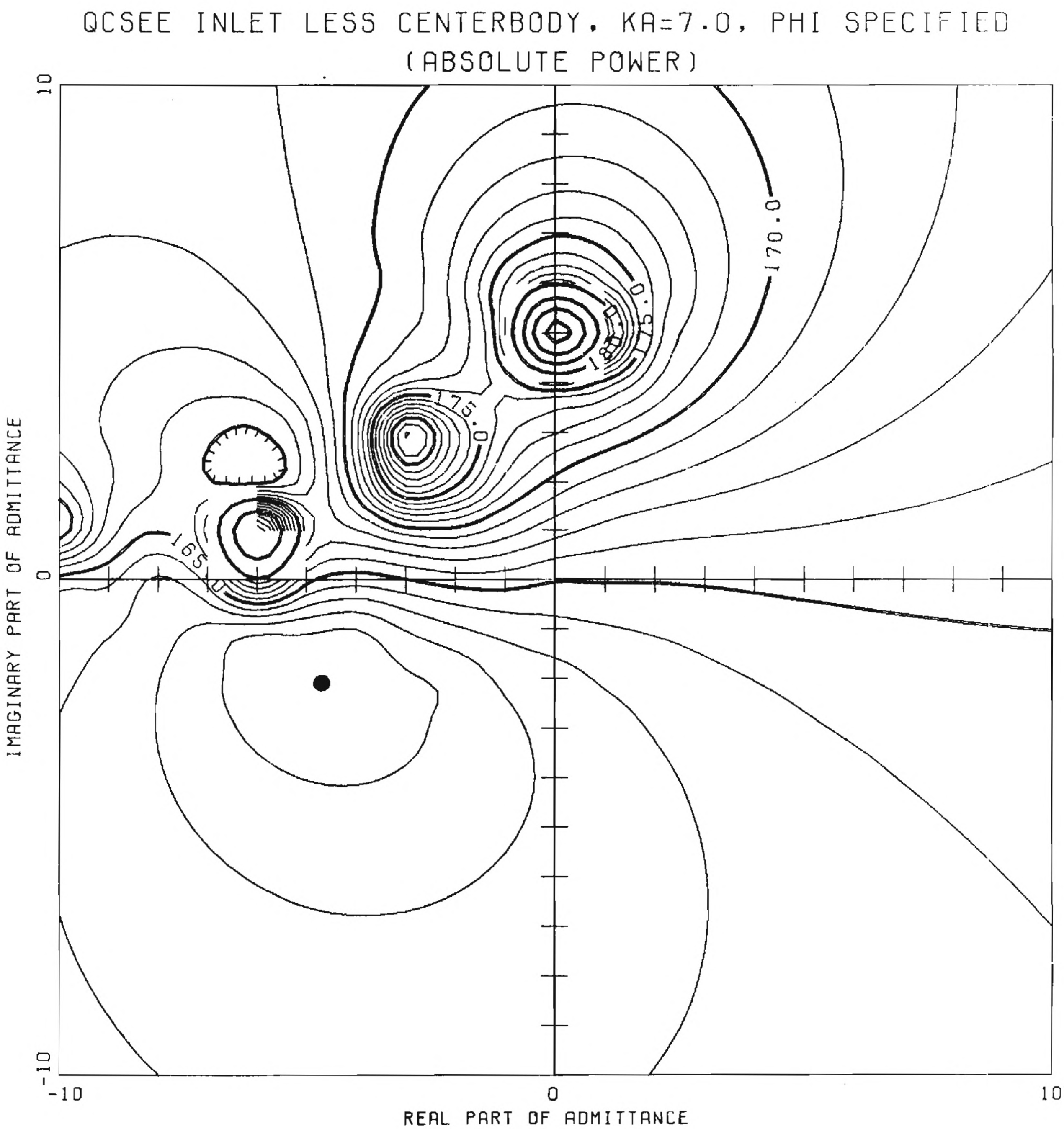
QCSEE INLET LESS CENTERBODY, KA=7.0, PHI SPECIFIED
(ABSOLUTE POWER)
IMAGINARY PART OF ADMITTANCE
REAL PART OF ADMITTANCE
10
0
-10
-10
0
10
170.0
175.0
180.0
175.0
165.0

Figure 24b

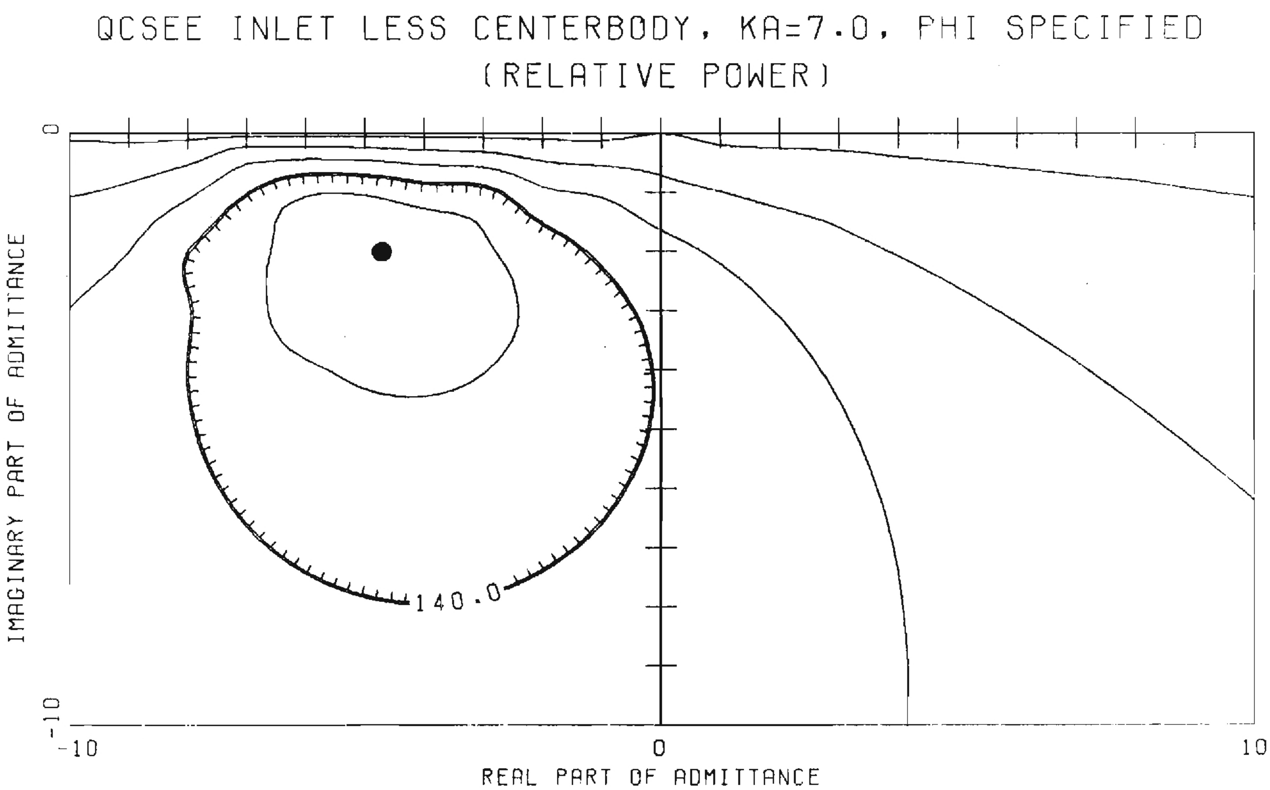
QCSEE INLET LESS CENTERBODY, KA=7.0, PHI SPECIFIED
(RELATIVE POWER)
0
-10
-10
0
10
140.0
IMAGINARY PART OF ADMITTANCE
REAL PART OF ADMITTANCE
Figure 24c

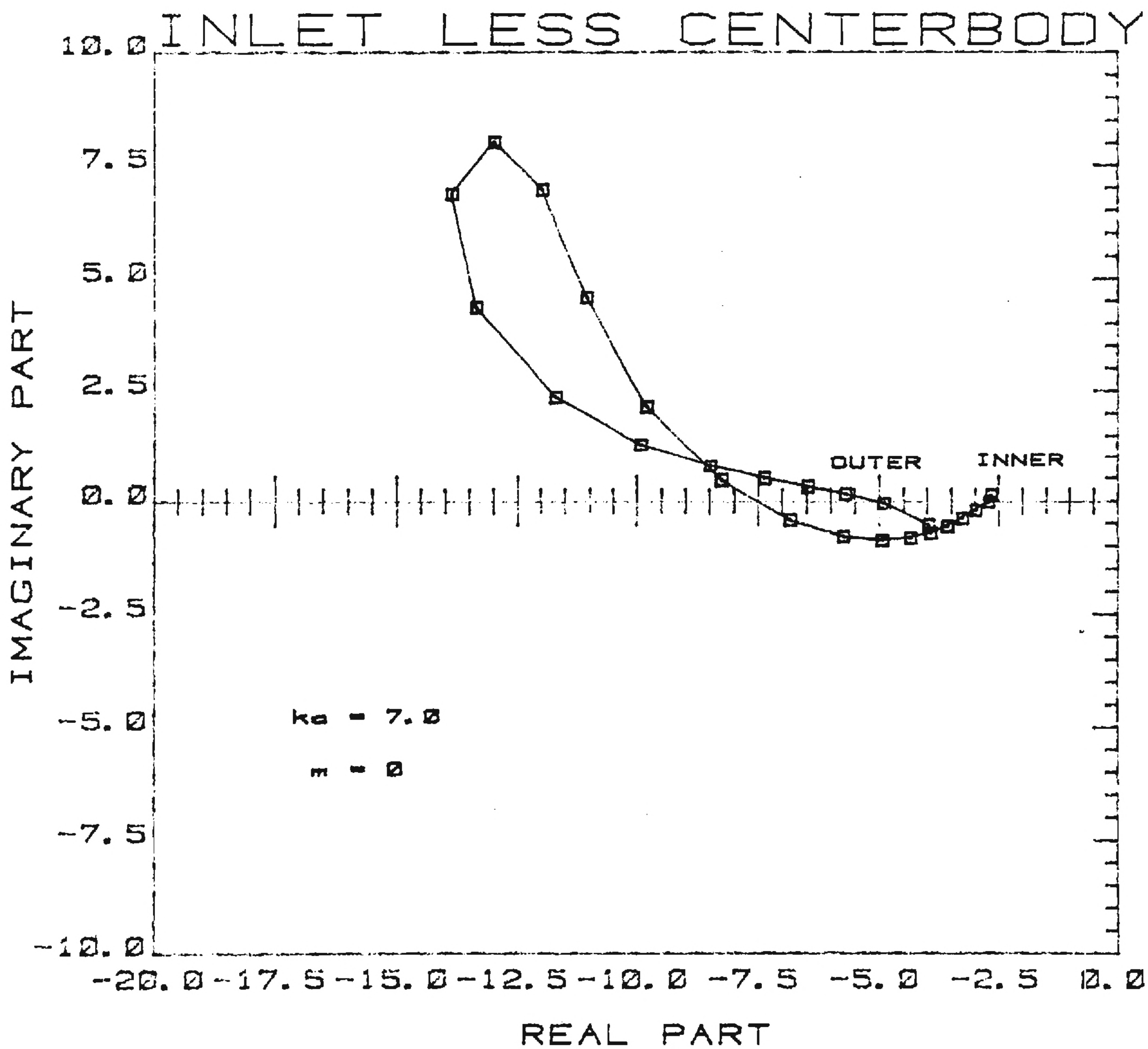

OPTIMUM ADMITTANCE DISTRIBUTION

Constant Velocity on the Driver

Figure 24d

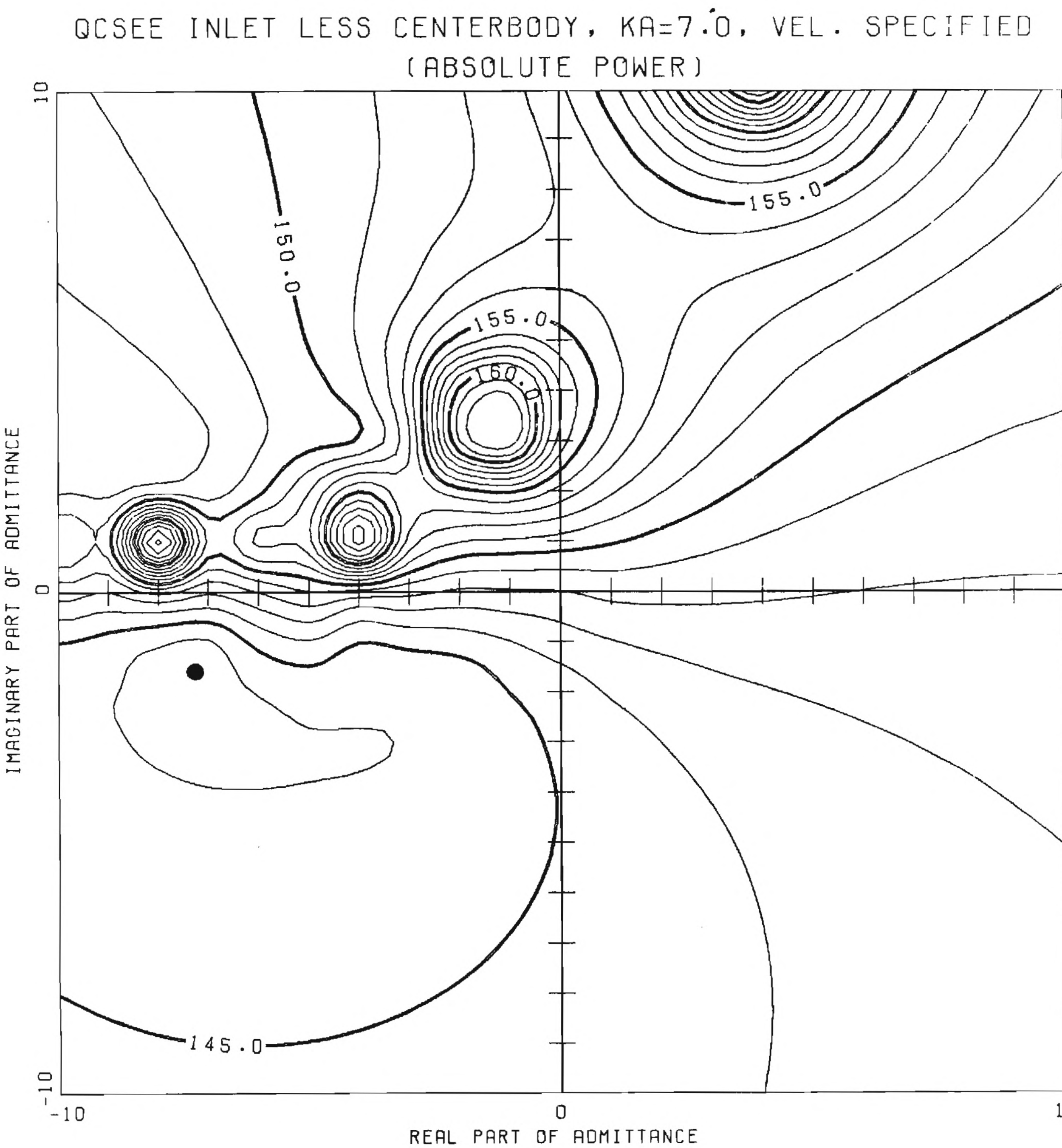
QCSEE INLET LESS CENTERBODY, KA=7.0, VEL. SPECIFIED
(ABSOLUTE POWER)
IMAGINARY PART OF ADMITTANCE
REAL PART OF ADMITTANCE
10
0
-10
-10
0
10
150.0
155.0
155.0
160.0
145.0

Figure 24e

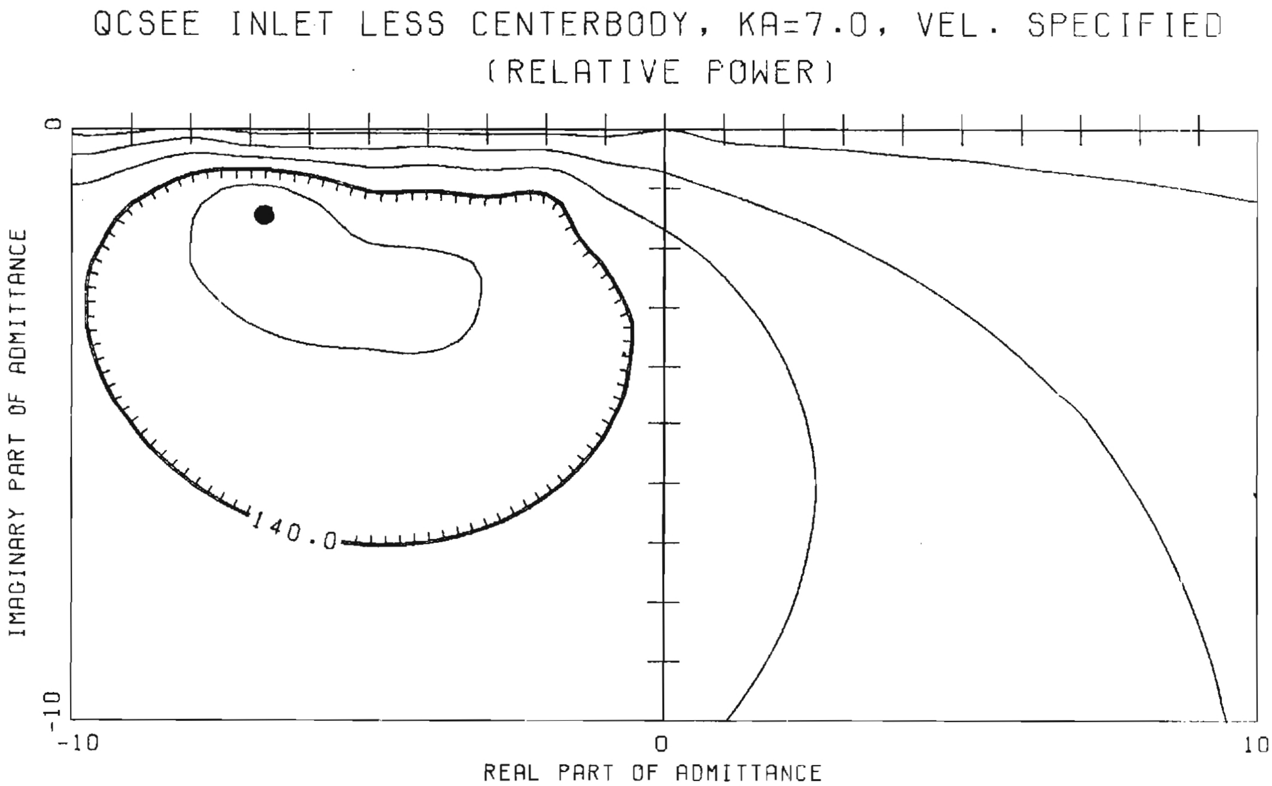

QCSEE INLET LESS CENTERBODY, KA=7.0, VEL. SPECIFIED
(RELATIVE POWER)
IMAGINARY PART OF ADMITTANCE
0
-10
140.0
-10
0
10
REAL PART OF ADMITTANCE

Figure 24f

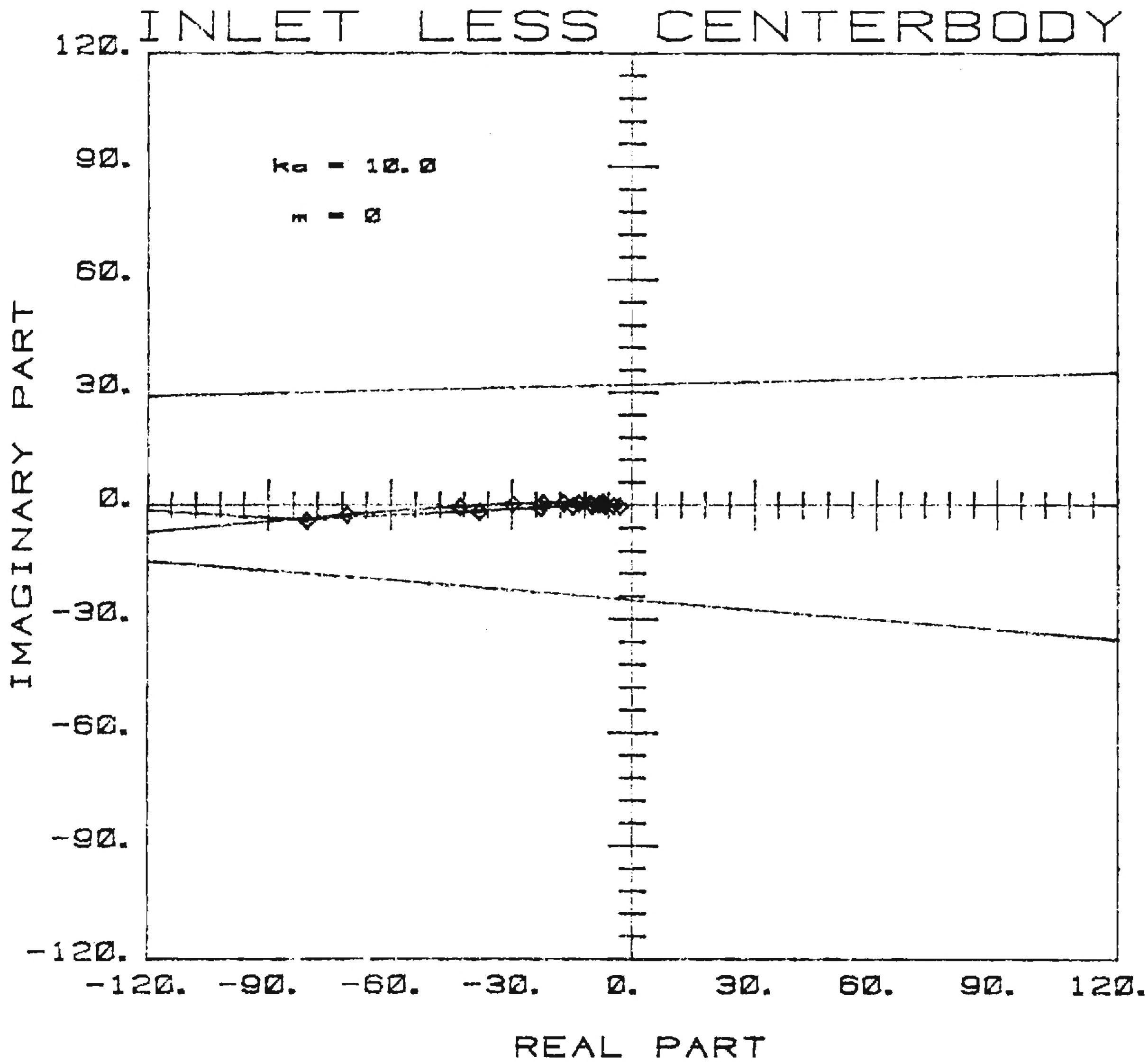

OPTIMUM ADMITTANCE DISTRIBUTION

Constant Phi on the Driver

Figure 25a

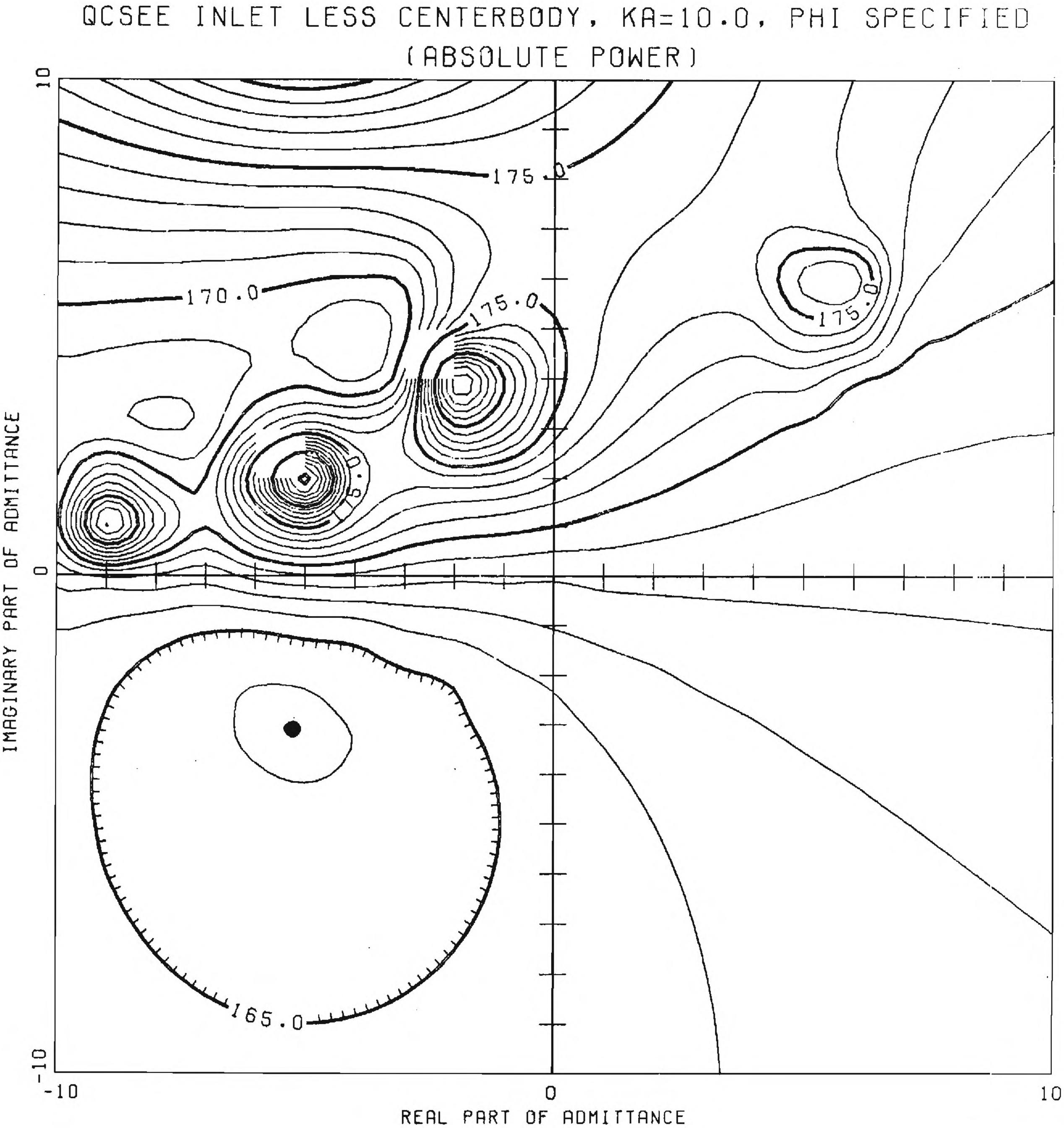
QCSEE INLET LESS CENTERBODY, KA=10.0, PHI SPECIFIED
(ABSOLUTE POWER)
IMAGINARY PART OF ADMITTANCE
REAL PART OF ADMITTANCE
10
0
-10
-10
0
10
175.0
170.0
175.0
175.0
165.0

Figure 25b

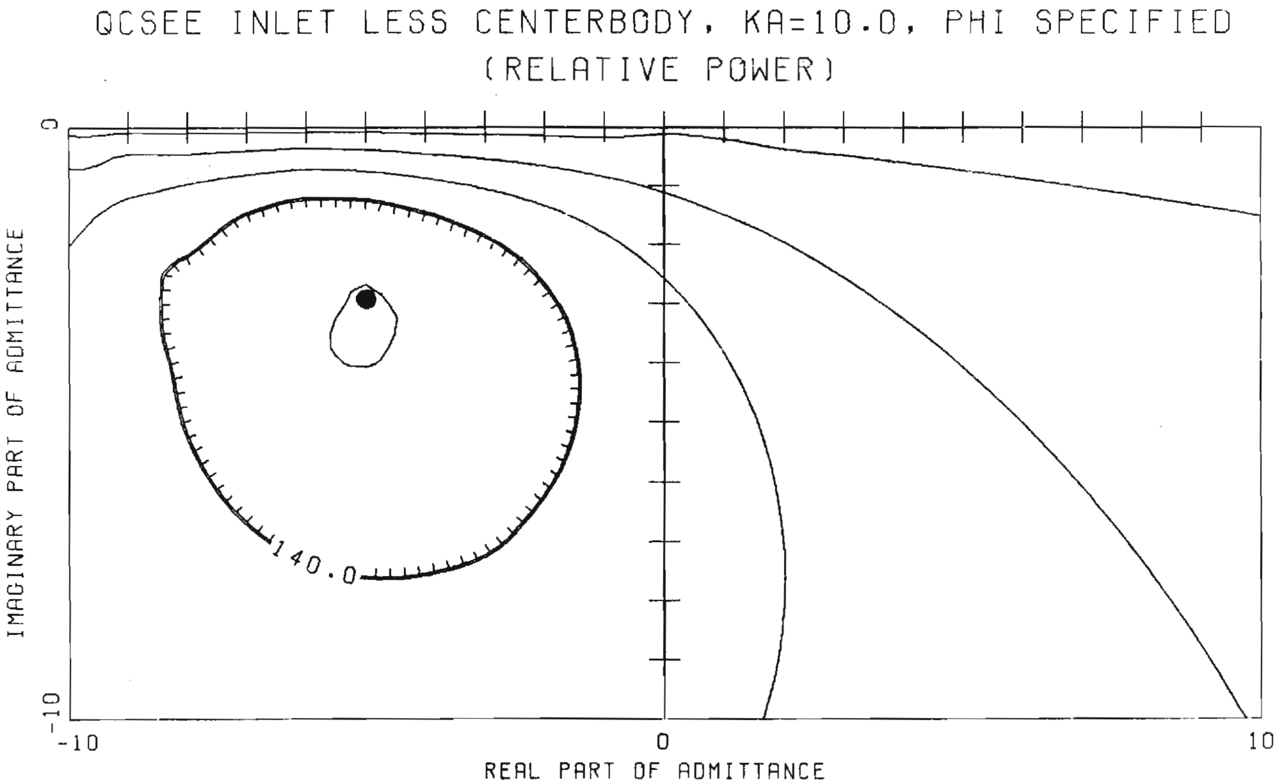
QCSEE INLET LESS CENTERBODY, KA=10.0, PHI SPECIFIED
(RELATIVE POWER)
0
-10
IMAGINARY PART OF ADMITTANCE
140.0
-10
0
10
REAL PART OF ADMITTANCE

Figure 25c

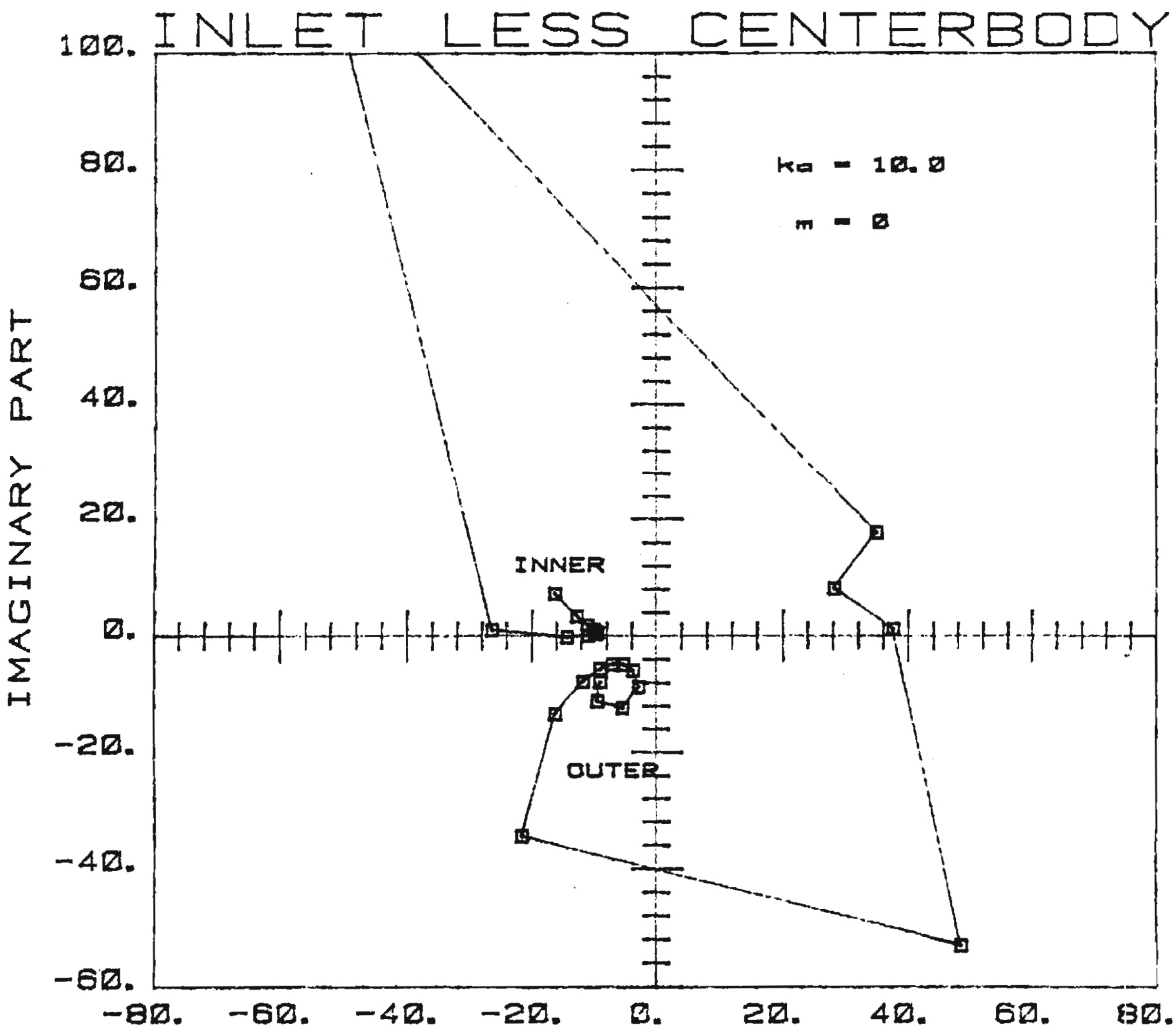

OPTIMUM ADMITTANCE DISTRIBUTION

Constant Velocity on the Driver

Figure 25d

QCSEE INLET LESS CENTERBODY, KA=10.0, VEL. SPECIFIED
(ABSOLUTE POWER)

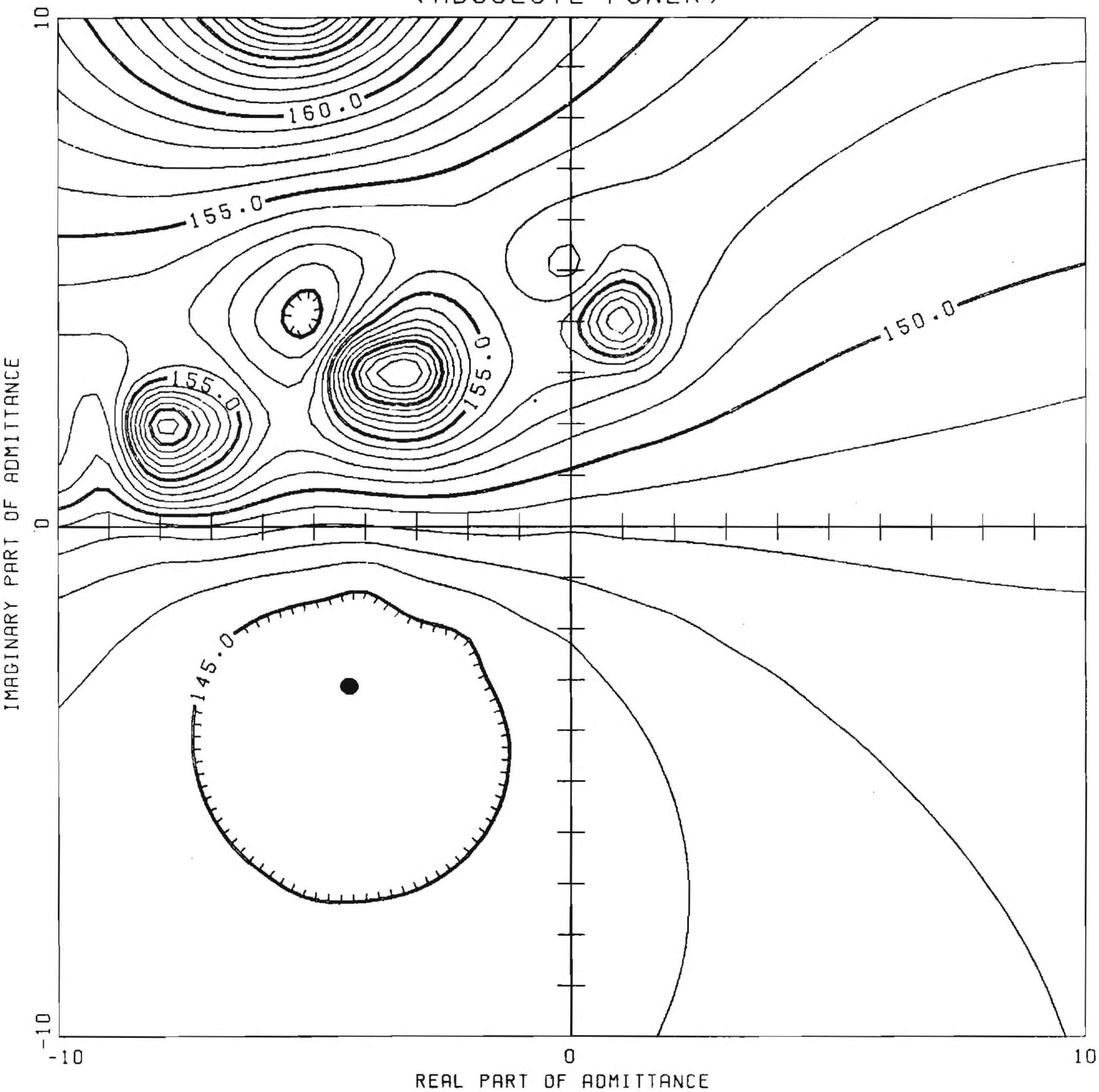

Figure 25e

QCSEE INLET LESS CENTERBODY, KA=10.0, VEL. SPECIFIED
(RELATIVE POWER)

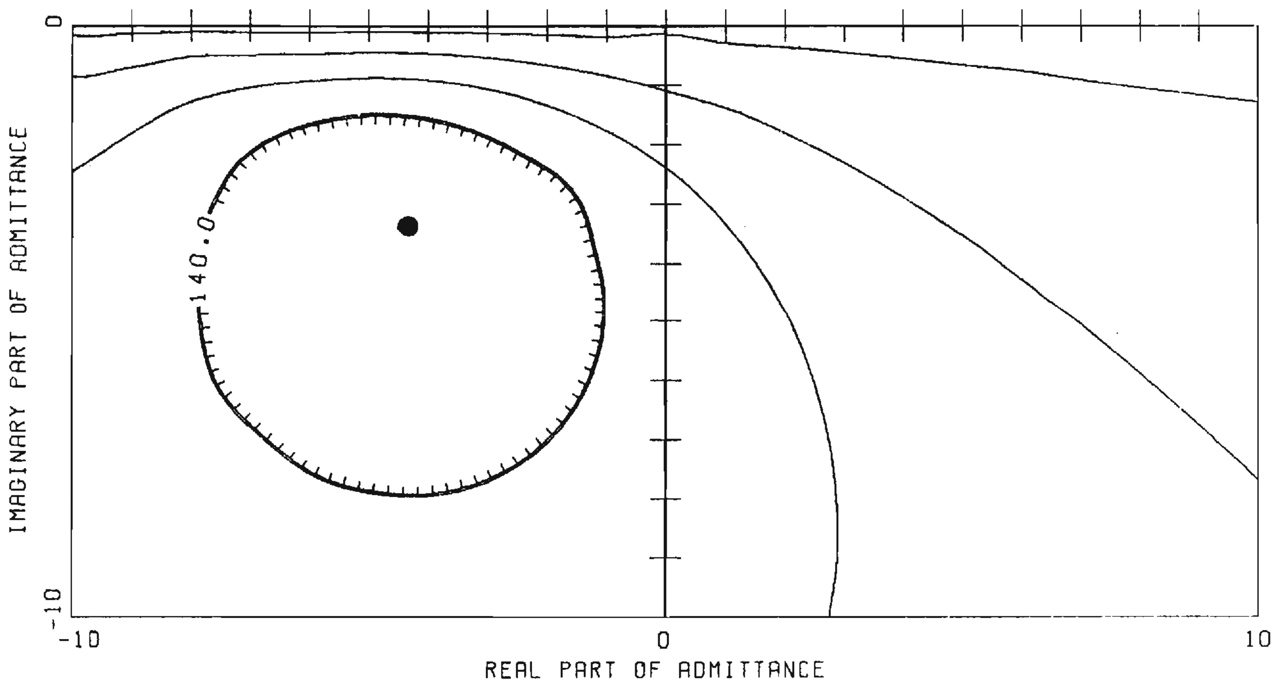

Figure 25f